Fracture and Fatigue Mechanism of Cast Iron Water Mains

By

Rui Jiang

A thesis submitted in fulfilment of the requirements for
the degree of Doctor of Philosophy

Department of Civil Engineering

February 2018

COPYRIGHT NOTICE

DECLARATION

I hereby declare that this thesis contains no material which has been accepted for the award of any other degree or diploma at any university or equivalent institution and that, to the best of my knowledge and belief, this thesis contains no material previously published or written by another person, except where due reference is made in the text of the thesis. Where sections of this thesis include the results of joint research or scholarly publication clear acknowledgement of the relative contributions of the respective authors is made in the text of the thesis.

Rui Jiang

Department of Civil Engineering

Monash University, Australia

February 2018

ABSTRACT

The ageing of water supply infrastructures has become a common challenge for the sustainability of urban water systems. Cast iron pipelines buried between the 1840s and 1980s still account for a significant proportion of water supply systems, and failures of these vital infrastructures are frequently recorded. The majority of large-diameter cast iron water mains fail by longitudinal barrel fracture, primarily due to corrosion and internal pressure, and bursts of large-diameter cast iron water mains lead to extensive financial losses and impacts on transportation and society.

In Australian cities, the manufacturing methods and corrosion mitigation techniques used in cast iron pipes are strongly correlated with the pipeline burial year. An approach is proposed to summarise the remaining in-service life of cast iron trunk mains in static and spun cast iron cohorts, in order to identify critical pipelines with high potential of longitudinal fractures in pipe barrels. A statistical analysis confirmed that spun cast pipes have higher burst rates and relatively shorter life spans than statically cast pipes, due to thinner wall thickness.

This study investigates the fatigue resistance of cast iron pipes and identifies the assets at high risk of fatigue damage predominantly caused by extensive corrosion and cyclic pressures (i.e. pressure transients). A correlation between tensile and fatigue strength (S-N curves) is established for the tested cast iron pipes. A methodology is provided to estimate the time to initiate failure considering the impact of fatigue and to compare asset life against limit state failure. A sensitivity analysis was conducted using time-driven simulations. The results of the analysis show that pipe assets subjected to frequent pressure transients may experience higher levels of fatigue damage.

Recent failures and burst tests indicate that leakages of water trunk mains tend to occur before catastrophic fracture. This study explores the cumulative damage process and fatigue properties of corroded CI pipes under the tension to tension stress range. A full-scale bursting facility has been established to simulate the varying internal water conditions and record the crack propagation in CI pipe barrels. A through-wall crack in a corrosion patch of a CI pipe barrel could propagate by cyclic pressure.

The leak-before-break time window in practice is between an occurrence of detectable leakage and a burst, and this period is mainly dependent on operating pressures and transient frequency, corrosion patch configuration and leak detection methods. In order to reduce fatigue damage, operational transients and dramatic pressure changes need to be mitigated.

ACKNOWLEDGEMENTS

I would like to express my gratitude to my supervisor, Professor Jayantha Kodikara, who encouraged me to pursue Ph.D. study and taught me the beauty of research. I am deeply grateful to him for his guidance, support, patience and encouragement during my entire candidature. I am also thankful to him for his treasured advice on achieving success in my future professional career.

I truly appreciate the valuable advice and continuous support from my co-supervisors, Professor Xiao-Ling Zhao and Professor Christopher Hutchinson. They consistently provided innovative ideas during my study. I have improved my knowledge of Structural Engineering and Microstructural analysis from them. Dr Alex McKnight assisted by proofreading the final draft for grammatical and stylistic errors.

I would like to thank my colleagues who worked with me on the Advanced Condition Assessment and Pipe Failure Prediction (ACAPFP) and Smart Water Fund (SWF) Project, including Dr. Benjamin Shannon, Dr. Suranj Rathnayaka, Dr. Chunshun Zhang, Dr. Jian Ji, Dr Derek Chan, Dr Ravin Deo and Mr. Darshana Weerasinghe. My project would never have been completed without the support of the pipeline research groups at Monash University. I must also thank the sponsors and stakeholders of pipeline research at Monash University for their generous financial support.

I would also like to thank my colleagues Daniel, Mayer, Fujia, Tharaka, Rukshan, Arunodi, Arooran, Radhika and Veljko. I sincerely thank the hardworking administrative and laboratory staff in Deportment of Civil Engineering, as well as the staff in Monash Centre for Electron Microscopy.

I truly appreciate the unconditional support and warm words of my friends: Noah Chen, Ruben Andersen, Lyndon Cantwell, Josh Williams, Jin Miao, Nathan Appleby, Darcy Bolton, Ming and Peter Eggenhuizen. Last, but not least, I owe my deepest appreciation to my beloved parents, grandparents and cousins for their priceless support and love given to me throughout my candidature.

LIST OF PUBLICATIONS

Journal articles

1. JIANG, R., ROBERT, D., HUTCHINSON, C. R., ZHAO, X. L. & KODIKARA, J. 2017a. Leak-before-break in cast iron mains: a failure analysis of a catastrophic pipe burst on Harris Street, Sydney. *Water Practice and Technology,* 12**,** 487-494.

2. JIANG, R., SHANNON, B., DEO, R. N., HUTCHINSON, C. R., ZHAO, X.-L., RATHNAYAKA, S. & KODIKARA, J. 2017b. Classification of major cohorts of Australian pressurised cast iron water mains for pipe renewal. *Australian Journal of Water Resources*, 21:2, 77-88.

3. JIANG, R., RATHNAYAKA, S., SHANNON, B., ZHAO, X.-L., JIAN, J. & KODIKARA, J. 2018d. Formation of through cracks in deteriorated cast iron pipes under cyclic pressures (under review). *Engineering Failure Analysis*.

4. JIANG, R., SHANNON, B., RATHNAYAKA, S., ZHAO, X.-L. & KODIKARA, J. 2018e. Fatigue crack growth rates in pressurised cast iron water mains under cyclic pressures (under review). *Engineering Failure Analysis*.

5. JIANG, R., RATHNAYAKA, S., SHANNON., ZHAO, X.-L. & KODIKARA, J. 2018c. Validation of leak-before-break (LBB) criteria in pressurised cast iron water mains (under review). *Structural Safety.*

6. JIANG, R., ZHANG, C., ZHAO, X.-L. & KODIKARA, J. 2018g. Evaluation of safe operating pressures for corroded cast iron trunk mains using cohesive zone models (in preparation). *Case Studies in Engineering Failure Analysis*.

7. JIANG, R., RATHNAYAKA, S., SHANNON, B., ZHAO, X.-L. & KODIKARA, J. 2018b. Failure analysis of fatigue damage in corroded cast iron mains by transient pressures: a case study (in preparation). *Journal of Failure Analysis and Prevention*.

8. JIANG, R., DEO, R. N., SHANNON, B. & KODIKARA, J. 2018a. Failure configurations of corrosion patches in pressurised cast iron water mains (in preparation). *Journal of Failure Analysis and Prevention*.

9. JIANG, R., SHANNON, B., WEERASINGHE, D., ZHANG, C., RATHNAYAKA, S. & KODIKARA, J. 2018f. Practical procedures of forensic investigation of Australian cast iron pipe failures (in preparation).

10. JIANG, R., DEO, R. N., SHANNON, B. & KODIKARA, J. 2018. Evaluation of soil corrosion effects in pressurised cast iron water mains for rehabilitation programs (in preparation). *Journal of Failure Analysis and Prevention*.

11. JIANG, R., WEERASINGHE, D., ZHANG, C. & KODIKARA, J. 2018. Failure stress of deteriorated cast iron water pipes in reactive soils (in preparation). *Journal of Vibroengineering*.

12. RATHNAYAKA, S., RATHNAYAKA, S., JIANG, R. & KODIKARA, J. 2018. New laboratory test facility to investigate the leak-before-break (LBB) window of large-diameter cast iron water pipes (accepted). *Journal of Pipeline Systems – Engineering and Practice*.

Conference articles

1. JIANG, R., WEERASINGHE, D., ZHANG, C., ZHAO, X. L., HUTCHINSON, C. R. & KODIKARA, J. Leak-before-break (LBB) analysis and failure processes for small-diameter cast iron pipes. *In:* HEIDARPOUR, A. & ZHAO, X.-L., eds. Tubular Structures XVI: Proceedings of the 16th International Symposium for Tubular Structures (ISTS 2017) December 4-6, 2017, Melbourne, Australia, 2017 Melbourne, Australia. CRC Press, 625-630.

2. JIANG, R., ROBERT, D., HUTCHINSON, C. R., ZHAO, X. L. & KODIKARA, J. 2016. Leak-before-break in cast iron mains: a failure analysis of a catastrophic pipe burst on Harris Street, Sydney. *IWA World Water Congress & Exhibition 2016.* Brisbane, Australia: IWA.

3. SHANNON, B., JIANG, R., JI, J., CHAN, D. & KODIKARA, J. 2016. Investigation of cohort properties for Australian cast iron water mains. *IWA World Water Congress & Exhibition 2016.* Brisbane, Australia IWA.

Technical reports

1. ZHANG, C., SHANNON, B., RATHNAYAKA, S., CHAN, D., JI, J., JIANG, R. & KODIKARA, J. 2017. Advanced condition assessment & pipe failure prediction project 2011 - 2017 - final technical report (under review). *In:* KODIKARA, J. (ed.). Melbourne, Victoria, Australia: Monash University.

2. KODIKARA, J., SHANNON, B., JI, J., ZHANG, C., RATHNAYAKA, S., WONG, L. & JIANG, R. 2017. Sydney water implementation phase project cohort report. Melbourne, Victoria, Australia: Monash University.

NOTATIONS

A	Crack opening area
$2a$	Length of corrosion patch in longitudinal direction
A_f	Fatigue ration coefficient
AR	Aspect ratio of corrosion patch
σ_c	Stress in the corrosion patch centre
a_e	Half of embedded crack length in longitudinal direction
a_i	Half of initial crack length induced by leak pressure
a_t	Through wall crack length
ACD	Average corrosion depth
A_p	Long-term corrosion constant
σ	Applied stress
σ_a	Alternating fatigue stress
σ_b	Soil bending stress in uncorroded pipes
σ_c	Hoop stress in the corrosion patch centre
$\sigma_{c,t}$	Stress in the age of a circular perforation
σ_E	Hoop stress from external loads
σ_E'	Longitudinal stress from external loads
σ_e	Endurance limit
σ_e'	Corrected endurance limit
σ_f'	Parameter that scales with tensile strength obtained by fitting experimental data
σ_h	Hoop stress from internal pressure
σ_h'	Longitudinal stress from internal pressure
σ_i	Stress in the crack tips of an initial crack
σ_m	Mean fatigue stress
σ_{max}	Maximum stress in a fatigue cycle
σ_{min}	Minimum stress in a fatigue cycle
$\sigma_{n,i}$	Nominal stress for the pipes with an initial crack
σ_{nt}	Nominal stress for a pressurised pipe with a longitudinal crack within a corrosion patch
σ_r	Remaining strength of a corroded pipe section
σ_u	Ultimate material strength
$\sigma_{u,s}$	Tensile strength of spun cast iron pipes
$\sigma_{u,st}$	Tensile strength of static cast iron pipes
$\Delta\sigma$	Stress difference (fatigue stress range)
ε_f'	An empirical constant known as the fatigue ductility coefficient
$\Delta\varepsilon_e/2$	Elastic strain amplitude
$\Delta\varepsilon_p/2$	Plastic strain amplitude
$\Delta\varepsilon_t/2$	Total strain amplitude
B	Beam thickness of SENB specimen
$2b$	Length of corrosion pit/patch in circumferential direction
B_f	Fatigue ration exponent
B_p	Corrosion scaling constant
β	Shape factor for calculating the stress concentration factor caused by a perforation
c	Corrosion depth
C_d	Discharge coefficient

c_e	Embedded crack depth in thickness direction
C	Paris' constant
C_p	Corrosion rate inhibition factor
C_s	Long-term corrosion intercept
D_{cr}	Critical fatigue damage factor
D_i	Internal pipe diameter
E	Modulus of elasticity
F	Geometric factor for evaluating intensity factors of pipes with a circumferential crack
f_1	Frequency of burst-refill events
f_2	Frequency of transient events
F_{max}	Maximum bending load for SENB specimen
F_{min}	Minimum bending load for SENB specimen
$F(\lambda)$	Geometric factor for evaluating intensity factors of pipes with a longitudinal crack
$f\left(\frac{a}{W}\right)$	Geometric factor for the SENB specimen
G	Energy release rate
G_c	Fracture energy
$G(\lambda)$	Geometric factor for crack opening area
k	Different stress spectrums
K	Penalty stiffness
K_b	Bending moment parameter
K_{fc}	Corrosion fatigue reduction factor
K_{fn}	Notch fatigue reduction factor
K_I	Intensity factor
K_{IC}	Fracture toughness
K_{max}	Maximum stress intensity factor
K_{min}	Minimum stress intensity factor
K_z	Deflection parameter
ΔK	Range of stress intensity factor
$\Delta \mathrm{K}_{th}$	Threshold toughness
L	Maximum allowable longitudinal extent of the corroded area
LDR	Length depth ratio of corrosion patch
m	Paris' constant
N	Number of stress cycles
N_f	Cycles to failure
N_i	Number of failure cycles for a stress amplitude to cause a fracture
n_i	Number of cycles for a stress amplitude
P	Internal water pressure
P_L	Limiting internal pressure
$P_{L,external}$	Limiting pressure for pipelines with an external surface crack
$P_{L,internal}$	Limiting pressure for pipelines with an internal surface crack
P_{leak}	Leak pressure
P_m	Maximum achieved pressures in full-scale burst tests
P_{max}	Maximum operating pressure
P_{min}	Minimum operating pressure
PF	Pitting factor
Q	Leak rate

q	Slope of the log-log curve again determined by fitting
q'	Empirical constant known as the fatigue ductility exponent
R	Fatigue stress ratio
R_e	Endurance ratio
R_f	Fatigue ration
R_i	Internal pipe radius
r_0	Initial slope of soil corrosion from the bi-linear model
r_s	Long-term corrosion rate
r_t	Radius of a circular perforation
S	Bending span of SENB specimen
SCF	Stress concentration factor induced by a corrosion patch
SCF_t	Stress concentration factor for a pipe with a circular perforation
t	Exposure period
T_f	Exposure time to form a through crack by fatigue damage
t_h	Holiday period of soil corrosion
t_i	Wall thickness in the tips of the initial crack
t_t	Wall thickness of the crack tip
t_0	Nominal wall thickness
T_o	Exposure time to form a through crack by ignoring fatigue damage
t_t	Corresponding wall thickness in the crack tips
T_u	Ultimate traction stress
ΔT	Reduced exposure period
ν	Poisson's ratio
W	Beam depth of SENB specimen
W_L	Critical external load to pipe failure
W_v	Vertical load from overburden soil and traffic load
Y	Geometric factor about crack length and structure dimensions
λ	Dimensionless factor for pressurised pipes with a through crack
λ_i	Dimensionless factor for pressurised pipes with an initial through crack
λ'	Dimensionless factor for corroded pipes with a through crack
2θ	Crack opening degree of a circumferential crack
τ	Corrosion transient time
δ	Threshold parameter
δ_f	Separation at failure
δ_0	Separation at damage initiation
γ	Threshold parameter

ABBREVIATIONS

AC	Asbestos Cement
ACAPFP	Advanced Condition Assessment and Pipe Failure Prediction
ACD	Average Corrosion Depth
AIS	Australian Iron Steel
AS	Australian Standards
ASME	American Society of Mechanical Engineers
ASTM	American Society for Testing and Materials
AWWA	American Water Works Association
BS	British Standards
CI	Cast Iron
COA	Crack opening area
CWW	City West Water
CZM	Cohesive zone model
DCV	Directional control valve
DENT	Double Edge Notched Tensile
DI	Ductile Iron
DIC	Digital image correlation
EN	European Standards
FCGR	Fatigue Crack Growth Rate
FE	Finite Element
FPPISW	Failure Probability Prediction Implementation Sydney Water
HP	Hydraulic pump
HW	Hunter Water
LBB	Leak before Break
LEFM	Linear Elastic Fracture Mechanics
NS	Natural Soil
NSW	New South Wales
NZS	New Zealand Standards
PE	Polyethylene Encased
PF	Pitting Factor
PRV	Pressure relief valve
SA	South Australia
SCF	Stress Concentration Factor
SEM	Scanning Electron Microscopy
SEW	South East Water

SENB	Single Edge Notched Beam
SOF	Shut-off valve
SW	Sydney Water
SWF	Smart Water Fund
TB	Test Bed
TBC	Transfer barrier cylinder
UK	United Kingdom
US	United States
UKWIR	UK Water Industry Research Limited
VIC	Victoria
WP	Water pump
YVW	Yarra Valley Water

TABLE OF CONTENTS

LIST OF FIGURES

LIST OF TABLES

Chapter 1 Introduction

1.1 Background

One of the challenges for the water industry is the deterioration of pipeline assets. Cast iron (CI) pipelines installed prior to 1990 still represent a significant percentage of the Australian water transportation system. These vital infrastructures are close to their ultimate service life due to continuous corrosion and the increase of service loads. Bursts of large-diameter CI pipes result in significant financial losses and severe hazards in developed urban areas (Vitanage et al., 2014). Rehabilitation programs and condition assessments for CI trunk mains are costly for Australian capital cities (Gould et al., 2013; Vitanage et al., 2014), and it has been estimated that at least 5 billion Australian dollars are required for the replacement and repair of Australian CI water pipes in the next five years (Rathnayaka, 2016).

In spite of the fact that a number of studies and investigations have been conducted worldwide in regard to the failure of CI pipes, the methods available for failure prediction and assessment management are still fairly inefficient and ineffective. One of the reasons for this situation is the lack of understanding of pipe failure processes. In order to propose appropriate solutions, more effort is required to explore the failure mechanisms of CI trunk mains.

A collaborative research project, Advanced Condition Assessment and Pipe Failure Prediction (ACAPFP), has been undertaken to improve the current procedures of condition assessment and failure prediction models for large-diameter CI pipes (diameters of 300 mm or above). Nine Australian water utilities participated in the ACAPFP project: Sydney Water (SW), Melbourne Water, Water Corporation, South East Water (SEW), City West Water (CWW), South Australian (SA) Water, Hunter Water (HW), Queensland Urban Utilities and Yarra Valley Water (YVW). This project also attracted two international partners: UK Water Industry Research Limited (UKWIR) and the Water Research Foundation. The research activities were completed by three Australian universities (led by Monash University). This project includes four major activities, which are briefly shown in Figure 1-1. The details of the ACAPFP project are summarised in Vitanage et al. (2014). Activity 1 attempted to answer "how, when and where large-diameter pipes fail within a water supply network". The study summarised in this thesis is a component of Activity 1 of the ACAPFP project.

The predominant failure mode of large-diameter CI pipes is longitudinal barrel fracture, which is caused by corrosion deterioration and hoop stress from internal operational pressures (Rajani, 2000). Soil corrosion in external pipe walls is normally considered to be the major reason for pipe deterioration (Petersen and Melchers, 2014). The corrosion pits generated by soil corrosion reduce the wall thickness and form corrosion patches that result in stress concentrations (Ji et al., 2015). Hence, the current condition assessments of water pipelines are mainly focused on the measurement of corroded depths.

This study investigates the processes and failure mechanisms of longitudinal barrel fracture in pressurised large-diameter CI pipes. The internal pressure is considered as the primary source of hoop stress, and the effects of external loads and other stresses in pipeline are evaluated and analysed. An approach is proposed to identify critical CI pipes with high potential of failure, mainly based on construction dates, pipe sizes and operation pressures. The leak-before-break (LBB) concept is verified by evidence from site observations and experimental results, and LBB criteria are proposed and verified for longitudinal barrel fractures in large-diameter CI pipes. This study also investigates the impact of fatigue mechanisms on the initiation and propagation of longitudinal cracks in corroded CI pipes under cyclic pressures. The validation of full-scale burst tests and simulations was conducted to confirm the impact of fatigue mechanisms in corroded CI pipes. The detailed thesis outline is shown in Section 1.4.

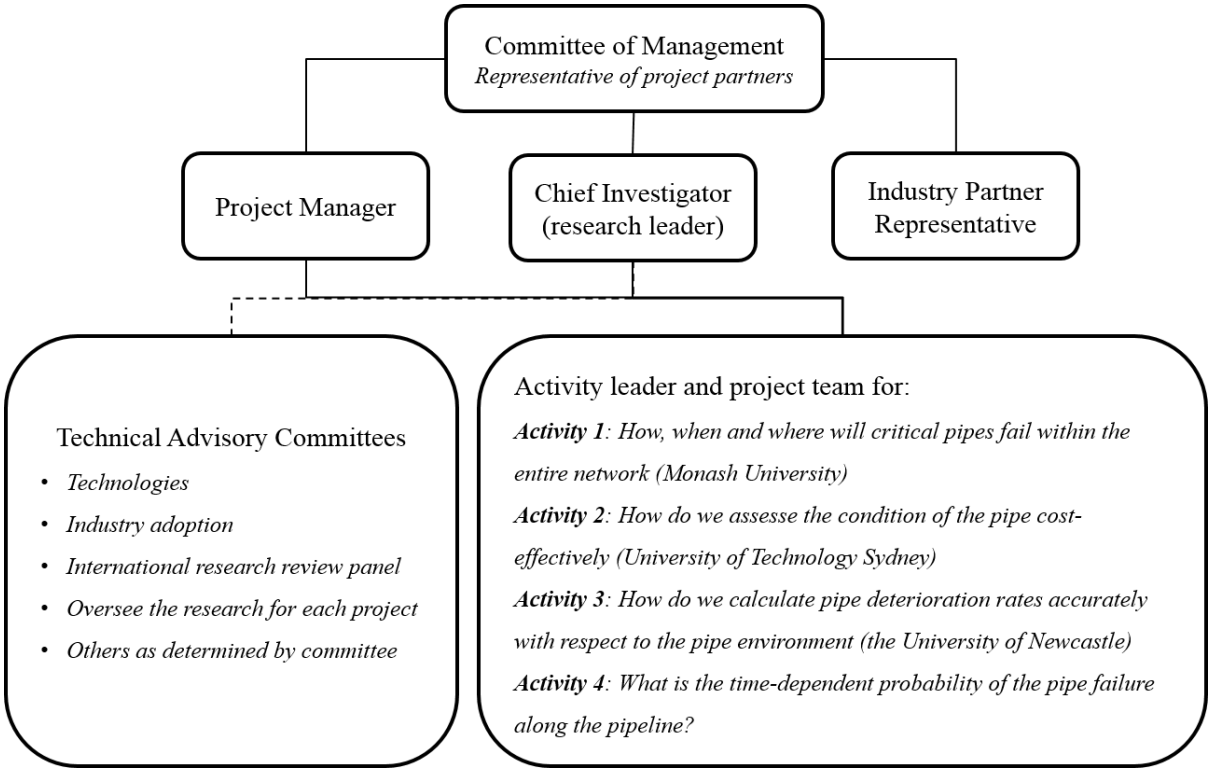

Figure 1- 1 Governance structure of the ACAPFP project

1.2 Research objectives and scope

The core hypothesis of this project is that the propagation of longitudinal cracks in large-diameter CI pipes is caused by fatigue caused by cyclic pressures. Apart from corrosion, fatigue or fatigue-related mechanisms play a vital role in the phase of crack propagation.

In this research study, the first and foremost aim is to understand the failure processes of large-diameter CI pipes prior to catastrophic bursts. There are two research questions related to this aim:

- 1. Does a through-crack generate in a corrosion patch base by a fatigue mechanism?
- 2. Does a through-crack propagate in CI pipe barrels? If the answer to question 2 is yes, how long does it take for a through-crack to grow to the critical length to cause a catastrophic burst under the fatigue mechanism?

The main objectives of this study are to explore the failure processes of the longitudinal barrel fracture of CI pipes and to provide engineering solutions to evaluate the impact of fatigue mechanisms on the deterioration of the structural capacity of CI trunk mains. An analytical approach to identifying critical CI pipes is proposed for Australian water utilities, and the validation criteria of the LBB concept are also verified based on experimental results. The objectives of this study are shown below:

- To classify CI pipe cohorts and identify critical assets with high potential of failures: see Chapter 3.
- To validate the LBB concept for longitudinal barrel fracture in corroded large-diameter CI pipes: see Chapter 4;
- To evaluate the impact of the fatigue mechanisms caused by cyclic pressures to form a through-crack in corroded large-diameter CI pipes: see Chapter 5;
- To evaluate the impact of fatigue caused by cyclic pressures to propagate a through-crack in corroded large-diameter CI pipes: see Chapter 6; and
- To verify the impact of fatigue caused by cyclic pressures on corroded CI pipes based on full-scale burst tests and finite element (FE) simulations: see Chapter 7.

This research project focuses on the deterioration mechanisms of longitudinal barrel fractures in large-diameter CI pipes. Cyclic pressures are considered as the primary source of cyclic stresses. The fatigue properties of ex-service CI trunk mains are evaluated, and models of fatigue analysis are adopted for CI trunk mains subjected to internal pressures. The significant factors for fatigue damage in CI pipes are identified on the basis of a time-dependent sensitivity analysis. A burst facility supplying cyclic pressures is established to evaluate the fatigue resistance of corroded large-diameter CI pipes. Furthermore, the results of failure analysis in small-diameter CI pipes with the failure mode of circumferential barrel fracture are summarised in this thesis. The findings from this study will assist in

modification of the current condition assessment of pressurised water pipelines, in order to prevent or predict bursts of CI trunk mains.

1.3 Contributions to the ACAPFP and the Smart Water Fund projects

Since 2011, a series of research tasks have been completed by the ACAPFP projects. The other tasks competed by Monash University are summarised below:

- 1. Historical information on large-diameter CI pipes
- 2. Pipe traffic loading tests in Sydney Water test bed
- 3. Pressure-transient monitoring and modelling
- 4. Finite element modelling of pressurised corroded CI pipes
- 5. Physical modelling for prediction of failure probability
- 6. Distributed optical fibre sensors

Task 1 provided the results of the statistical analysis of failure rates and pipe asset length based on data from five Australian water utilities and confirmed the predominant failure mode of large-diameter CI pipes is longitudinal barrel fracture. Tasks 2 and 3 found that internal pressure is the critical stress source of hoop stress contributing to longitudinal barrel fracture compared with external factors from soils and traffic loads. The patterns of pressure transient events have been simulated in Task 3. The stress concentration factors (SCFs) from corrosion patches were predicted through the FE simulations in Task 4. The outcomes of this study contributed the research scope of Task 5 and 6.

The research of the Smart Water Fund (SWF) conducted by Monash University aims to develop an innovative integrated algorithm for cost-effective management of water pipe networks for the water utilities in Melbourne, Victoria. The analysis approach summarised in Chapter 3 contributes to the evaluation methods used in the SWF.

The fatigue properties and analytical methods reported in this thesis will be used in the Failure Probability Prediction Implementation Sydney Water (FPPISW) project, which intends to validate the outcomes of the ACAPFP project using selected pipe cohorts in Sydney.

1.4 Thesis outline

The thesis outline is shown below, and the links among the chapters are illustrated in Figure 1-2.

Chapter 1 Introduction

In this chapter, the research background and the research objectives and scope are detailed. The contributions to the ACAPFP and the SMW project are summarised. A thesis outline is provided.

Chapter 2 Literature review

This chapter reviews the research on the following topics:

- Introduction
- Timeline of CI pipes and corrosion mitigation methods
- Microstructural features and mechanical properties
- Corrosion
- Pipe stress analysis and failure modes
- Pipe failure prediction models
- Fatigue mechanisms in CI pipes
- Leak-before-break (LBB) assessment

Chapter 3 Classification of major cohorts of Australian pressurised cast iron water pipes

In Australian cities, the manufacturing methods and corrosion mitigation techniques used in CI pipes depend strongly on the burial year. This chapter introduces an approach to summarising the remaining in-service CI trunk mains in several cohorts, in order to identify critical pipelines with high potential of longitudinal fracture in pipe barrels. Despite the various manufacturers and casting moulds used in Australian CI pipes, two major cohorts, static and spun CI pipes, are identified, based on manufacturing methods, material properties, microstructural analysis and wall thicknesses. A statistical analysis confirms that spun cast pipes have higher burst rates and shorter life spans than static CI pipes, due to their thinner walls.

Chapter 4 Leak-before-break (LBB) in cast iron pipes

The phenomenon of a leak occurring before a major burst (leak-before-break or LBB) within CI pipe barrels has been observed in both recent field failures and laboratory tests. In this chapter, common features of LBB in failures are illustrated. A LBB time window exists for most failures. The leak rates were verified throughout full-scale burst tests. According to the experimental results, the LBB

criterion is potentially applicable to CI water mains, and brief guidance on the LBB analysis approach is proposed for the water industry. Similarly, the LBB evidence and criteria for small-diameter pipes are also summarised.

Chapter 5 Formation of a through-crack in corroded cast iron pipes by fatigue

The majority of cast iron water trunk mains fail by the mode of longitudinal barrel fracture due to soil corrosion and internal pressure. This study investigates the fatigue resistance of cast iron pipes and identifies assets at high risk of fatigue damage caused by cyclic pressures. Stress-controlled fatigue tests were carried out on specimens from five CI pipes. A correlation between tensile strength and fatigue strength (S-N curves) was established for CI pipes. The notch effect of corrosion pits/patches on fatigue strength was found to be limited based on results from the literature and examination of corrosion patch configurations. A sensitivity analysis was conducted by time-dependent simulation. The analysis shows that assets in transient zones or with frequent failure rates may experience higher levels of fatigue damage. In addition, the long-term corrosion rates and stress ratios of transients also contribute to fatigue damage.

Chapter 6 Propagation of through cracks in cast iron pipes by fatigue

This chapter summarises the experimental results of fatigue crack growth rate (FCGR) of beam specimens taken from large-diameter CI pipes. These results are compared with data from the research literature. The fatigue crack growth model of Paris Law is adopted to evaluate the LBB time window based on the parameters from FCGR tests. The results of a fractography examination are also illustrated.

Chapter 7 Full-scale validation tests and simulation

The formation and propagation of a through-crack in a corrosion patch base are confirmed by full-scale bursting tests under cyclic pressures. A cohesive zone model is adopted to evaluate the damage processes for CI pipes with a corrosion patch using FE analysis (Abaqus). In this chapter, the results from full-scale tests and simulation are summarised. Selected case studies are also included.

Chapter 8 Conclusions and recommendations

This chapter summarises the key findings from this research project. In order to minimise fatigue damage and identify critical pipeline assets, recommendations are provided for water utilities, and some suggestions for future research to improve the efficiency of water asset management and failure prediction are made.

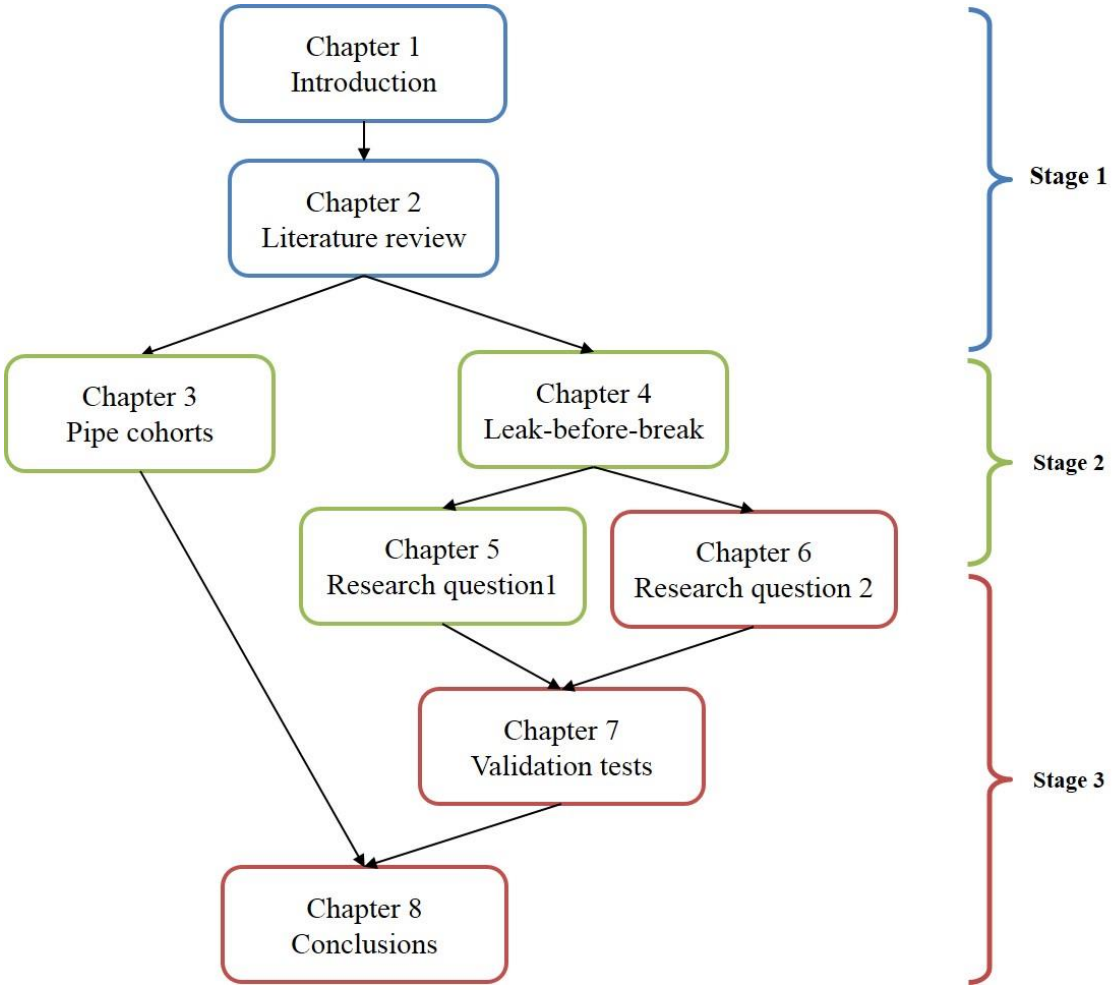

Figure 1- 2 Thesis structure and links among chapters

Chapter 2 Literature review

2.1 Introduction

This chapter provides background information and the significant outcomes from previous research on large-diameter CI water pipes. A state-of-the-art review of previous studies related to the fatigue mechanism in CI water pipes is also provided. In Section 2.2, the history of CI pipes used in Australian water networks is briefly introduced. The asset lengths and failure rates of large-diameter CI water pipes are discussed in Section 2.3. Section 2.4 outlines research studies on the microstructural features and mechanical properties of CI pipes. Research projects on corrosion deterioration in CI pipes are summarised in Section 2.5. The pipe stresses and typical failure modes of CI pipes are shown in Section 2.6, and pipe failure prediction models from previous studies are evaluated and compared in Section 2.7. Common research approaches and analytical methods are also discussed.

Section 2.8 summarises previous research on fatigue mechanisms in CI water pipes, including case studies, fatigue tests and analytical models. A thorough review of the leak-before-break (LBB) in CI pipes and relevant standards from other industries are presented in Section 2.9.

2.2 Timeline of Australian CI pipes

2.2.1 Manufacturing methods of CI pipes

As a popular historical construction material, CIs have been used worldwide in underground water transportation systems for more than 300 years (AIS, 1941). They were eventually phased out of the piping market in 1980s due to the invention of ductile iron, which has superior mechanical properties in terms of ultimate strength and fracture toughness (Nicholas and Moore, 2009). According to archived standards and documents, most of the CIs used in the piping industries are identified as Grey CI, which is characterised as an inter-notched material due to the pre-existing graphite flakes (Makar and Rajani, 2000).

There are two major types of CI pipes in Australia, depending on the manufacturing method: static and spun CI pipes. Prior to 1930, CI pipes were statically (horizontally or vertically) cast (Rajani, 2000). This casting method generally led to low material strengths and non-uniform wall thickness (Nicholas and Moore, 2009; Rajani and Kleiner, 2013b). Based on the results of previous metallurgical examinations, the graphite normally shows the pattern of flakes (Makar and Rajani, 2000).

Due to the invention of the spun (centrifugally) cast method in the 1920s, CI pipes with uniform wall thickness and higher strengths were produced throughout the worldwide piping markets after 1930 (Nicholas and Moore, 2009). Spun CI pipes and contain rosette- patterned graphite (Makar and Rajani, 2000).

In Australia, CI pipes were no longer installed in the 1980s due to the introduction of ductile iron pipes (AIS, 1941; Nicholas and Moore, 2009). Figure 2-1 shows the timeline of major manufacturing methods of CI pipes used in Australia (Nicholas and Moore, 2009; Scott, 1990; AIS, 1941).

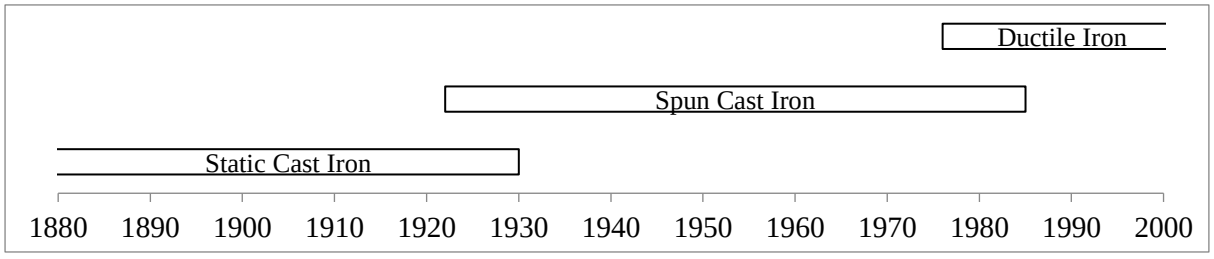

Figure 2- 1 Governance structure of the ACAPFP project

2.2.2 Internal cement lining

Cement mortar linings have been used to preserve internal pipe walls from corrosion damage since the 1920s (Bonds, 2005; AIS, 1941). Pipes laid after 1930 were internally lined with cement mortar in factories, and these pipes were designed to avoid internal corrosion (Nicholas and Moore, 2009; AIS, 1941). Most large trunk mains installed before the 1930s were relined in situ in the period between 1930 and 1960 (Nicholas and Moore, 2009; Scott, 1990). Thereafter, the growth of internal corrosion pits had been suspended in these unlined CI pipes (pipes without internal linings).

Currently, unlined metal pipes are relatively rare in Australia (Rajeev et al., 2014). To minimise internal corrosion, relevant rehabilitation programs are highly recommended for unlined mains.

2.2.3 External coating

Coatings have been designed for metallic pipes in corrosive environments. Two types of coatings have been widely used throughout the timeline of CI pipes: paint coating (tar or bitumen) and polyethylene-encased (PE) coating. Almost all CI pipes were buried with paint coating in the 20th century, but limited protection is provided by this coating type in aggressive environments (Bonds et al., 2005; Romanoff, 1957). This has been proved by site observation and experimental results (Bonds et al., 2005; Kroon et al., 2005).

PE coating has been highly recommended as the most effective coating method due to its excellent protection in extremely corrosive environments (AWWA-C105, 1972; AWWA-C105, 2010). Bonds et al. (2005) observed that even damaged polyethylene coating has better corrosion resistance than paint coating, especially in corrosive environments, as observed in long-term experiments.

2.2.4 Backfill soils

Most Australian CI pipes are buried in trenches with natural soils, and backfill sand was introduced in the process of pipeline installation in the 1960s (Nicholas and Moore, 2009). The natural soils in coastal regions consist of cohesive (clayey) soils that are more corrosive than backfill sand, CI pipes subjected to natural soils tend to experience more severe soil corrosion, if PE coatings are not installed (Rajani, 2000).

2.2.5 Transportation and installation

The methods or equipment used for the transportation and installation of CI water pipes have significant impacts on the structural integrity of these infrastructures (Rajani and Abdel-Akher, 2013; Rajani et al., 2013). CI pipes were transported using horse-driven wagons prior to the 1890s, and thereafter trucks and trailers were widely used (Rathnayaka, 2016). Collisions during the transport and unloading

processes can cause damage to CI pipe segments. The early installation method of lead-caulked bell-spigot joints also caused potential damage or even initiated cracks in CI pipe joints (Rajani and Abdel-Akher, 2013). Therefore, the failure mode of bell joint fracture in CI pipes is closely related to the methods of transportation and installation used in the network (Rajani and Abdel-Akher, 2013; Rajani et al., 2013).

2.3 Asset length and failure rates of large-diameter CI pipes in Australia

In water supply systems, the total length of large-diameter CI pipes is markedly less than the length of small-diameter CI pipes (Gould et al., 2013). The failure rate of water pipes is generally expressed as the number of failures per 100 km length per year. Recent statistical analyses conducted for Australian utilities showed that the failure rates of large-diameter (300 mm or above) CI pipes are notably lower than the failure rates of small-diameter CI pipes (Gould et al., 2013; Gould, 2011).

In comparison with other piping materials, CI water pipes tend to have higher failure rates (Gould et al., 2013). Gould et al. (2013) conducted a survey of CI pipes (with diameters from 50 to 1,000 mm) in 13 Australian water utilities and found the failure rates for CI water pipes range from 7 to 124, with an average failure rate of 40 failures/100 km/year.

Gould (2011) carried out a statistical analysis of the pipe assets of two water utilities in Melbourne, Victoria: City West Water (CWW) and South East Water (SEW). The total length of CI pipes (300 – 400 mm) is around 144.7 km installed between 1940 and 1988, and the combined failure rate of these CI pipes was about 15 failures/100 km/year (Gould, 2011).

A statistical analysis was conducted of the large-diameter water pipes by the ACAPFP project (Kodikara et al., 2012; Rajeev et al., 2014). This task analysed the asset and failure data from five Australian water utilities from New South Wales (NSW), Victoria (VIC) and South Australia (SA). The revised asset lengths and failure rates of large-diameter (300 mm or above) CI pipes for each utility are summarised in Table 2-1 with the failure rates of other piping materials, including steel, ductile iron (DI) and asbestos cement (AC). In certain utilities CI pipes are the predominant material in water supply systems, and CI pipes normally experience higher failure rates than other piping materials in Australian water utilities (Rajeev et al., 2014).

Wei et al. (2015) analysed the assets and failure rates of CI water pipes for the Water Corporation located in Perth, West Australia based on a 10-year historical failure rate statistical study. The failure rates remained high for pipes buried between the 1930s and the 1950s, and the maximum failure rate was about 35 failures/100 km/year, which was well above the average failure rate of 15 in the period (Wei et al., 2015). This finding indicates certain pipe cohorts constructed in some periods may have different material strengths or deterioration conditions. Unfortunately, the exact sizes of the CI pipes were not reported.

Table 2- 1 Asset lengths and failure rates of large-diameter CI pipes of Australian water utilities (Rajeev et al., 2014)

Utility	Length of CI pipes (*km*)	Percentage of CI pipes (%)	Failure rates (*failures/100 km/year*)			
			CI	Steel	DI	AC
A	1734	56.7	6.8	4.0	-	2.8
B	27	3.5	32.9	3.3	0.1	2.2
D	422	48.9	13.2	4.9	0.8	-
E	96	11.2	8.0	2.4	1.9	4.2
F	85	19.9	23.2	8.2	8.0	-

2.4 Microstructural features and mechanical properties

2.4.1 Microstructure

Australian water CI pipes were produced by various manufacturing methods. The microstructure of these pipes is strongly dependent on the casting methods and moulds (Makar and Rajani, 2000). The chemical compositions of CI pipes analysed in previous studies are summarised in Table 2-2.

The microstructural features of CI pipes can be observed from optical microscopic images of etched and polished specimens, and the predominant microstructural feature of CI pipes is the type of graphite flakes that directly affects the material tensile strength (Makar and Rajani, 2000). The graphite flakes of CIs can be described by the standardised approach from ASTM-A247-67 (1998). Randomly-oriented flakes (Type A) are uniformly distributed in the metallic matrices of static CI pipes, and spun CI pipes normally have fine patterns of graphite flakes (Makar and Rajani, 2000). The microstructure is relatively consistent in the wall direction for static CI pipes, and the maximum length of graphite flakes ranges from 80 to 320 μm (Makar and Rajani, 2000; Mohebbi et al., 2010). However, varying microstructures are commonly shown along the wall direction for spun CI pipes, primarily due to the different cooling rates of the centrifugal casting method (Makar and Rajani, 2000). The graphite flakes are coarser and longer in the inner surfaces than the external surfaces (Makar and Rajani, 2000).

Static CI pipes tend to contain higher amounts of pearlitic matrices than spun CI pipes, while ferritic matrices are commonly observed in spun CI pipes (Makar and Rajani, 2000).

Table 2- 2 Chemical composition of CI water pipes

Reference	Country	Casting	Element by weight (%)				
			Carbon (C)	Silicon (Si)	Manganese (Mn)	Phosphorus (P)	Sulfur (S)
Talbot (1926)	US	Static	3.38- 3.67	1.36- 2.09	0.30- 0.58	0.49- 0.84	0.05- 0.13
Yamamoto et al. (1983)	Japan	Static & Spun	3.32- 3.79	1.12- 2.98	0.36- 1.16	0.11- 0.97	0.06- 0.13
Makar and Rajani (2000)	US & Canada	Static	3.39- 3.91	1.93- 3.31	0.21- 1.13	0.69- 1.03	0.05- 0.15
		Spun	3.72- 4.20	1.39- 2.41	0.25- 0.49	0.17- 0.80	0.02- 0.11
Mohebbi et al. (2010)	UK	Static	2.75- 3.23	1.50- 2.70	0.50- 0.80	0.35- 1.20	0.08- 0.20

2.4.2 Mechanical properties

The material properties of CI pipes are greatly affected by the manufacturing methods and casting moulds (Rajani and Kleiner, 2013b). A number of standards have been developed throughout the entire timeline of CI pipes and alter in different nations, and the specified strengths and structural capacities based on archived standards are summarised in Table 2-3. Mechanical tests have been conducted to evaluate the pipe strengths and predict the remaining service life of these vital infrastructures (Conlin and Baker, 1991; Gould, 2011; Rajani, 2000; Seica and Packer, 2004; Yamamoto et al., 1983). These studies normally prepare specimens from ex-service small-diameter (< 300 mm) CI pipes, and the testing specimens contained various corrosion defects. Limited data on mechanical tests conducted on large-diameter CI pipes were reported by Yamamoto et al. (1983). Therefore, a broad range of mechanical properties have been provided in previous studies. A summary of the experimental results of mechanical properties is shown in Table 2-4.

Grey CI is a relatively brittle alloy with low tensile capacity and non-linear stress-strain characteristics (Rajani, 2012). The tensile strength of CI pipes is commonly captured by the fracture stress of tensile coupon tests. In spite of the non-linear strain-stress curves observed in the early stage of tensile tests, the values of secant modulus calculated by fracture stress and strain are commonly reported (Gould, 2011; Seica and Packer, 2004). The flexural strength based on bending tests is primarily controlled by the tensile strength of CI pipes, and therefore, bending tests are conducted to indicate the tensile strength of CI pipes (Jesson et al., 2013). CI pipes tend to have a high resistance to compression, and the compressive strength of CI pipes ranges from 519 to 1,047 MPa (Seica and Packer, 2004).

To quantify the fracture toughness of CI pipes, single-edge-notched beam (SENB) and double-edge-notched tensile (DENT) specimens are selected due to the restrictions of pipe geometry (Gould, 2011; Mohebbi et al., 2010; Rajani, 2000). The effects of fatigue pre-cracking are limited for CI pipes, and the fracture stress is generally adopted to covert the maximum values of fracture toughness (Conlin and Baker, 1991). Although a number of testing results have been reported, only a limited number of mechanical tests have been conducted on small-diameter Australian CI pipes (Gould, 2011). Table 2-5 summarises the results of fracture toughness tests of CI water pipes.

Table 2- 3 Specified minimum strength and structural capacity of CI pipes

Code	Cast	Tensile strength (MPa)	Flexural strength (MPa)	Secant modulus (GPa)	Modulus of rupture (MPa)	Crush strength (MPa)	Bursting strength (MPa)
AWWA-C100 (1908)	Horizontal	124	223	72	-	-	110
AWWA-C102 (1939)	Vertical	75	214	70	-	214	76
AWWA-C106 (1953)	Spun/ metal	124	276	83	-	276	124
AWWA-C108 (1962)	Spun/ sand	125	276	69	-	276	124
BS-78 (1938)	Vertical	124	274	90	-	-	-
BS-1211 (1958)	Spun/sand	159	-	-	-	159	-
	Spun/ metal	172	-	-	-	193	-
AIS (1941)	Spun	193	303	103	314	-	189
AS-1724 (1975)	Spun	200	400	-	-	-	-
BS/EN-877 (1999)	Spun	200	-	-	-	325	-

Table 2- 4 Comparison of mechanical properties of CI water pipes

Reference	Country	Cast	Diameter (mm)	Tensile strength (MPa)	Flexural strength (MPa)	Secant modulus (GPa)	Fracture toughness ($MPa\sqrt{m}$)
Yamamoto et al. (1983)	Japan	Static & Spun	100- 800	100 -167	-	-	-
Conlin and Baker (1991)	UK	Static	50- 100	137- 248	-	-	10.5- 17.7
Rajani (2000)	US & Canada	Static	150- 200	33- 267	165- 260	20- 70	5.7- 13.7 (10.3)
		Spun	150- 200	135- 305	240- 460	30- 98	10.3- 15.4 (13.2)
Seica and Packer (2004)	Canada	Static & Spun	100- 300	47- 297	164- 349	23- 150	-
Gould (2011)	Australia	Static	< 150	40- 230	-	15- 150	8.5- 11.9 (10.1)
		Spun	< 150	85- 250	-	10- 210	11.8- 14.3 (12.0)

Table 2- 5 Summary of fracture toughness of CI water pipes

Reference	Country	Cast	Diameter (mm)	Testing method	Fracture toughness ($MPa\sqrt{m}$)
Mohebbi et al. (2010)	UK	Static	500- 1,200	SENB	15.8- 26.4 (19.3)
Marshall (2001)	UK	Static	< 250	SENB	7.7-17.1 (11.8)
	UK	Spun	< 250	SENB	13.7- 19.3 (16.2)
Conlin and Baker (1991)	UK	Static	50- 100	SENB	10.5- 17.7 (14.0)
Rajani (2000)	US & Canada	Static	150- 200	DENT	5.7- 13.7 (10.3)
		Spun	150- 200	DENT	10.3- 15.4 (13.2)
Deb (2002)	US	Spun	100- 400	DENT	11.1- 17.8 (12.7)
Gould (2011)	Australia	Static	100- 150	DENT	8.5- 11.9 (10.4)
		Spun	100- 150	DENT	11.8- 14.3 (11.7)
Kim et al. (2007)	South Korea	Spun	150, 200	DENT	19.5- 27.7 (23.7)

2.4.3 Structural capacities

The structural capacities, including bursting strength, crush strength and modulus of rupture, can be obtained through full-scale tests. The specified minimum structural strengths listed in archived standards are shown in Table 2-3. The crushing strength and modulus of rupture of intact CI pipes are strongly dependent on the flexural strength of CI pipes, and the bursting strength is determined by the tensile strength.

In order to analyse the impact of corrosion on structural capacities, ring crushing and full-scale bending tests were conducted on corroded or as-received CI pipe segments (Atkinson et al., 2002; Marshall, 2001; Rajani, 2000; Yamamoto et al., 1983). The structural capacities reduce with the increase of corrosion depth (Atkinson et al., 2002; Marshall, 2001; Yamamoto et al., 1983). The ranges of crushing strength and modulus of rupture of ex-service CI pipes are summarised in Table 2-6.

Table 2- 6 Summary of structural capacity of CI water pipes

Reference	Country	Cast	Ring tests		Full-scale bending tests	
			Diameter (*mm*)	Crush strength (*MPa*)	Diameter (*mm*)	Modulus of rupture (*MPa*)
Yamamoto et al. (1983)	Japan	Static & Spun	100- 750	25- 310	-	-
Marshall (2001)	UK	Static	-	101- 394	75, 100	90- 380
		Spun	-	210- 420	-	-
Rajani (2000)	US & Canada	Static	150- 200	165- 260	-	-
		Spun	150- 200	130- 420	-	-
Atkinson et al. (2002)	UK	-	-	-	75, 100	42- 221

2.5 Corrosion deterioration

2.5.1 Soil corrosion

Corrosion is considered as the predominant mechanism of pipe deterioration, and a number of correlations between corrosion rate and pipe lifespan have been explored (Marshall, 2001; Petersen and Melchers, 2012; Rajani, 2000; Yamamoto et al., 1983). It has been widely accepted that corrosion reduces the thickness of the pipe wall and forms stress concentrators in the originally smooth pipe surfaces; in addition, the external pipe surfaces are more easily corroded than the internal surfaces due to the addition of internal cement lining in the early 1950s in Australia (Brevis et al., 2014; Kodikara et al., 2012; Nicholas and Moore, 2009; Yamamoto et al., 1983).

External corrosion in CI pipes is mainly caused by soil corrosion. The electrochemical reactions between metallic pipes and surrounding soils are considered the predominant reason for the deterioration of pipe integrity (Rajani, 2000; Rajani and Makar, 2000; Davis et al., 2003; Rossum, 1969; Pritchard et al., 2013; Rajani and Kleiner, 2001). In addition, microbiological corrosion may also contribute to the deterioration of external pipe surfaces, especially in the long-term phase of corrosion if some specific chemical elements and anaerobic conditions are present (Cunat, 2001; Melchers, 2013; Petersen et al., 2013; Petersen and Melchers, 2012; Petersen and Melchers, 2014).

Similar trends of corrosion depth with exposure time have been observed in both static and spun CI pipes (Doyle et al., 2003; Petersen and Melchers, 2014; Rajani, 2000; Romanoff, 1957).

2.5.2 Pitting factor

Pitting corrosion is the predominant mode of soil corrosion, which means that the pipe wall deteriorates in local areas rather than uniformly reducing wall thickness (Ahmad, 2006; Charlot and Westerman, 1981; Dorn, 1996; Mohebbi and Li, 2011; Rajani, 2000; Melchers, 2013). Pitting corrosion generates corrosion patches or localised perforations in CI pipe walls (Rajeev et al., 2014).

To evaluate the extent of pitting corrosion, the concept of the pitting factor (PF) has been widely used (Ahmad, 2006; Rajani and Makar, 2000; Lyons and Plisga, 2005). The PF is defined in Equation 2.1 and shown in Figure 2-2 (Ahmad, 2006).

$$PF = \frac{c}{ACD} \tag{2.1}$$

where, PF is pitting factor, c is maximum corrosion depth, and ACD is average corrosion depth calculated by weight loss in a pipe segment.

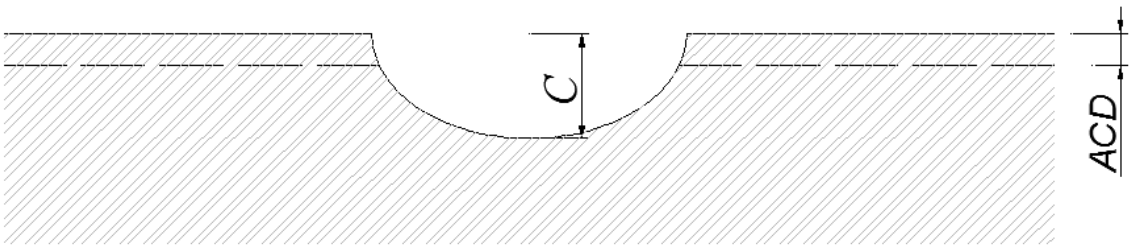

Figure 2- 2 Sketch of maximum pitting depth in a corroded pipe wall

General corrosion, an ideal deterioration form, refers to cases with uniform reduction of pipe wall thickness (Rajeev et al., 2014), which means the PF is approximately equal to 1.0 (Rajani, 2000). A pitting factor of 10.0 is suggested for CI structures in sea water conditions that represent an extremely aggressive environment for material deterioration (Ahmad, 2006). Rajani (2000) observed that the PFs of CI water pipes are above 1.0, ranging from 1.1 to 9.8 with an average value of 3.0. This observation confirms that pitting corrosion is the predominant corrosion mode for CI pipes.

Scott (1990) reported PFs for static and spun CI pipes buried in the Melbourne region. For pit CI pipes laid before 1922, the PF is up to 3.0; however, the average and maximum pitting factor for spun CI pipes are 5.0 and 10.0, respectively. These observations confirm the analytical results in Rajani (2000).

2.5.3 Corrosion depth

With regard to corrosion analysis, two types of diagrams are frequently plotted: pitting depth with buried period, and overall pitting rate with buried period. To simulate early-stage corrosion (less than 20 years), experiments can be conducted using new ferrous pipes in different soil environments (Logan, 1945; Romanoff, 1957; Romanoff, 1964). However, the analysis of long-term corrosion behaviour is heavily reliant on observations of ex-service pipes or data from condition assessments (Bonds et al., 2005; Dafter and Petersen, 2013; Doyle and Grabinsky, 2003; Doyle et al., 2003; Jakobs, 1985; McMullen, 1982; Petersen and Melchers, 2014; Rajani, 2000; Rajani and Kleiner, 2013a; Rajeev et al., 2014; Yamamoto et al., 1983). The early exposure of CI pipes shows high corrosion rates, and then the corrosion grows slowly (Doyle et al., 2003; Rajani, 2000; Romanoff, 1957; Romanoff, 1964). This trend has been verified by both site observations (Petersen and Melchers, 2014; Rajeev et al., 2014) and simulation experiments (Logan, 1945; Romanoff, 1957; Romanoff, 1964).

In site investigations, a number of corrosion pits are measured after removing graphitisation products, and the deepest corrosion depth is frequently recorded as the maximum corrosion depth in the particular soil environment. Hypothetically, a group of bare pipe specimens buried in a uniform soil layer enables to represent the corrosivity of the particular soil environment by measuring corrosion depths.

Some previous studies (detailed in Table 2-7) have reported corrosion data and surrounding soil properties for CI or DI water pipes (Doyle et al., 2003; Heathcote and Nicholas, 1998; Petersen and Melchers, 2014; Rajani, 2000; Romanoff, 1957; Wakelin and Gummow, 1993). Unfortunately, clear correlations between soil corrosion and soil properties have not been established. The corrosion rates of CI pipes may be related to soil resistivity, based on the data from site investigations or condition assessments (Doyle et al., 2003; McMullen, 1982; Rajani, 2000; Romanoff, 1957). Several studies (Doyle et al., 2003; Rajani, 2000; Scott, 1990) have summarised the ranges of soil resistivity based on soil types: cohesive soils (clay and silt) show lower resistivity than cohesionless (sand and gravel) soils. Bardet et al. (2010) observed that soils with low resistivity caused more failure incidents of CI water pipes in Los Angeles, US.

Petersen and Melchers (2014) claimed that the soil moisture (degree of saturation) is the most important factor controlling the long-term corrosion rate in CI water pipes. Using continuous measurement, the change of moisture content is reduced by the increase of soil depth, which means that the soil moisture at pipe levels is relatively consistent over years (Kodikara et al., 2013). According to AWWA-C105 (2010), the impact of moisture on pipe corrosion is evaluated by the soil drainage conditions rather than the exact values of soil moisture.

Other research projects (Marshall, 2001; Rajeev et al., 2014; Yamamoto et al., 1983) have focused on corrosion data, and only arbitrary fittings are provided by corrosion depths in networks. Figure 2-3 summarises various corrosion depths over exposure periods (Doyle et al., 2003; Petersen and Melchers, 2014; Yamamoto et al., 1983), and confirms that the long-term corrosion rate is relatively low compared to the phase of early exposure.

2.5.4 Corrosion models

Based on experimental studies and site observations, a number of attempts have been made to develop corrosion depth models (Doyle et al., 2003; Marshall, 2001; Melchers, 2013; Petersen et al., 2013; Petersen and Melchers, 2012; Petersen and Melchers, 2014; Rajani, 2000; Romanoff, 1957; Romanoff, 1964; Rossum, 1969; Yamamoto et al., 1983). For example, Rajani (2000) proposed an exponential equation to evaluate the corrosion depth with exposure time (Equation 2.2). The corrosion curve calculated by Equation 2.2 with the average soil corrosion parameters proposed by Rajani (2000) is plotted in Figure 2-3.

$$c = A_p\, t + B_p\, (1 - e^{-C_p\, t}) \tag{2.2}$$

where, c is the corrosion depth, t is the exposure period (year), A_p is the long-term corrosion constant (mm/year), B_p is the corrosion scaling constant (mm), and C_p is the corrosion rate inhibition factor (year^{-1}).

Petersen and Melchers (2014) established a bilinear model (Equation 2.3) to evaluate the long-term corrosion rate of CI water pipes. Figure 2-4 describes the corrosion growth in CI members. This model is relatively simple to describe the corrosion depth, which is applicable for predicting the remaining life of corroded CI pipes, and the key parameters in this model have actual physical meanings for defining corrosion deterioration.

$$c = C_s + r_s\, t \tag{2.3}$$

where, C_s is long-term corrosion intercept (mm), and r_s is long-term rate (mm/year).

2.5.5 Internal corrosion

Internal corrosion caused severe loss of pipe thickness of CI pipes laid before the 1920s, due to the absence of internal mortar lining (Rajani and Kleiner, 2013a). Rehabilitation projects were widely conducted to install cement lining in these unlined pipes (Nicholas and Moore, 2009; Scott, 1990). These internal corrosion pits are preserved in the cement lining.

Table 2- 7 Summary of sampling information in CI water pipes

Reference	Country	Cast	Exposure (*year*)	Soil properties
Romanoff (1957)	US	CI/DI	17	Resistivity, pH, Moisture content, Redox potential, Chloride ions, Suphide ions
Rajani (2000)	Canada & US	Static/S pun CI	114	Resistivity, pH, Redox potential, Chloride ions, Suphide ions
Rajani and Kleiner (2013a)	UK	CI	169	NSRI system
Marshall (2001)	UK	Static/S pun CI	129	-
Doyle et al. (2003)	Canada	CI/DI	122	Resistivity, pH, Suphide ions, Moisture content
Wakelin and Gummow (1993)	Canada	CI/DI	110	Resistivity, pH, Chloride ions
Yamamoto et al. (1983)	Japan	CI	67	-
Heathcote and Nicholas (1998)	Australia	CI	57	Linear Polarisation Resistance (LPR)
Petersen and Melchers (2014)	Australia	CI	129	Saturation, moisture content
Rajeev et al. (2014)	Australia	CI/DI	113	-

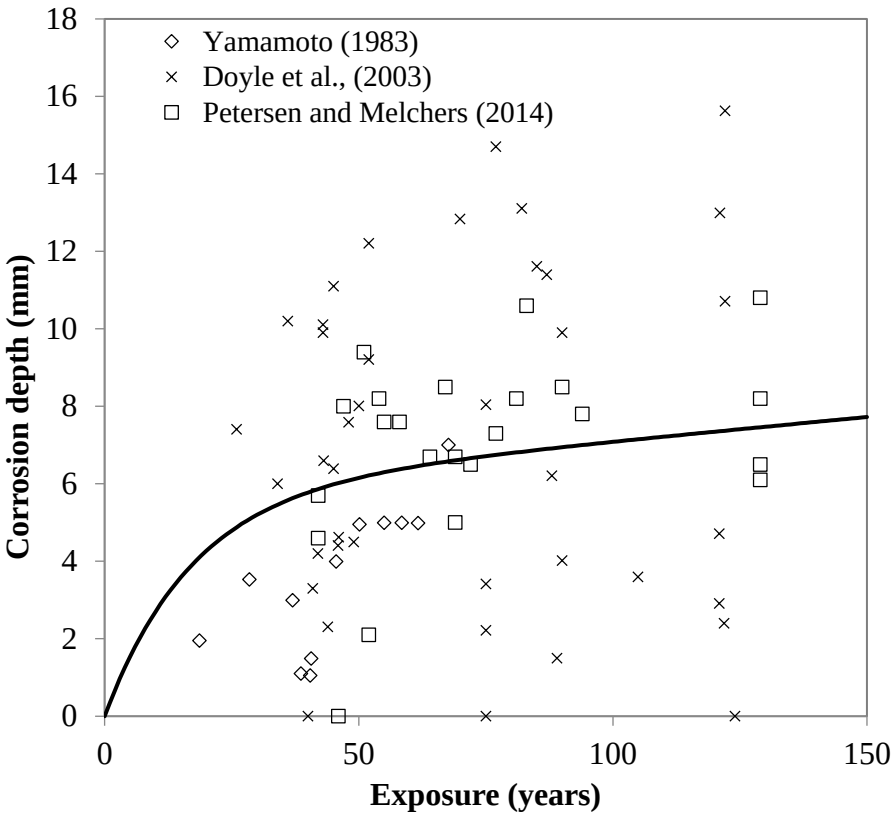

Figure 2- 3 Corrosion depths with exposure of CI water pipes

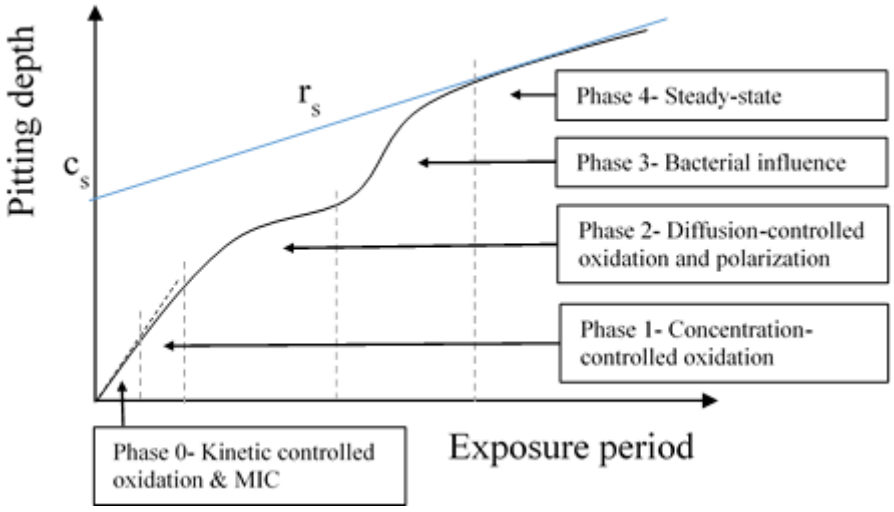

Figure 2- 4 Bilinear model for corrosion behaviour in CI pipes, based on Petersen and Melchers (2014)

Internal corrosion is directly controlled by local water properties, such as pH, dissolved oxygen, alkalinity, calcium, silica, chlorine and sulfate (Sarin et al., 2003). Analysis of corrosion pits has been completed based on pipe sizes (Rajani and Kleiner, 2013a), but no significant patterns were observed.

Marshall (2001) and Yamamoto et al. (1983) proposed internal corrosion rate curves based on a series of corrosion examinations. Similarly, the internal corrosion rate is also significantly reduced by the increase of exposure period (Rajani and Kleiner, 2013a). In comparison with external corrosion, internal corrosion pits show flatter bases and larger areas (Marshall, 2001).

Internal corrosion only occurs in unlined pipes. The in-situ lining programs that have been undertaken have minimised the number of unlined water trunk mains in urban networks. Therefore, the analysis of internal corrosion is less critical than that of external corrosion for CI lined water pipes.

2.6 Pipe stress analysis and failure modes

2.6.1 External loads

Pressurised water pipelines are subjected to different external loads: earth, traffic and thermal loads (Rajani and Kleiner, 2013b). External loads on CI water pipes are mainly from backfill soils and traffic loads, due to the absence of a frost season and lower ranges of underground temperature changes in most of Australia (Chan et al., 2015a; Chan et al., 2016b).

Traffic loading tests were conducted at the Test Bed (TB) site prepared for simulating field conditions by Sydney Water (Chan et al., 2016b). Ex-service vertically cast iron pipe with 600 mm internal diameter laid in 1922 was reburied under the bitumen surface and low-plasticity silty clay (Chan et al., 2016b). The average wall thickness of the pipe section under traffic loads was about 30 mm, the thickness of the bitumen road surface was approximately 92 mm, and the pipe burial depth from the surface was about 960 mm (Chan et al., 2016b; Rathnayaka, 2016). The layout of the TB site is shown in Figure 2-5.

The traffic loading tests were carried out using five trucks (weighing up to 39 tons) on three road surfaces (road base, bitumen and concrete), and strain gauges were installed to record strain changes during the tests. A number of traffic loading behaviours were tested, including passing (15 and 50 km/h), braking (15 and 50 km/h), passing speed hump (40 km/h), cornering (20 km/h) and at rest. These tests were undertaken under both non-pressurised and pressurised (up to about 500 kPa water pressure) pipe conditions.

The preliminary results showed that the trucks did not cause significant strains in the target pipe sections, and the maximum strain of non-pressurized cases occurred at the pipe crown was less than 33 micro strain (0.0033%) when the pipe was under road base only (Chan et al., 2016a; Chan et al., 2016b). The strains in the spring-lines were generally lower than the strains measured at the crown. The impact of traffic loads and soils is relatively insignificant on pressurised large-diameter CI water mains, in comparison with internal pressures.

Corrosion pits or patches alter the stress distribution from traffic loads. The capacity of deteriorated CI pipes under compression loads was analysed using FE simulations (Robert et al., 2016b). Probabilistic physical modelling (Ji et al., 2017) and sensitivity simulation (Wilson et al., 2016) also show that external loads from soil and traffic have limited impact on corroded CI pipes.

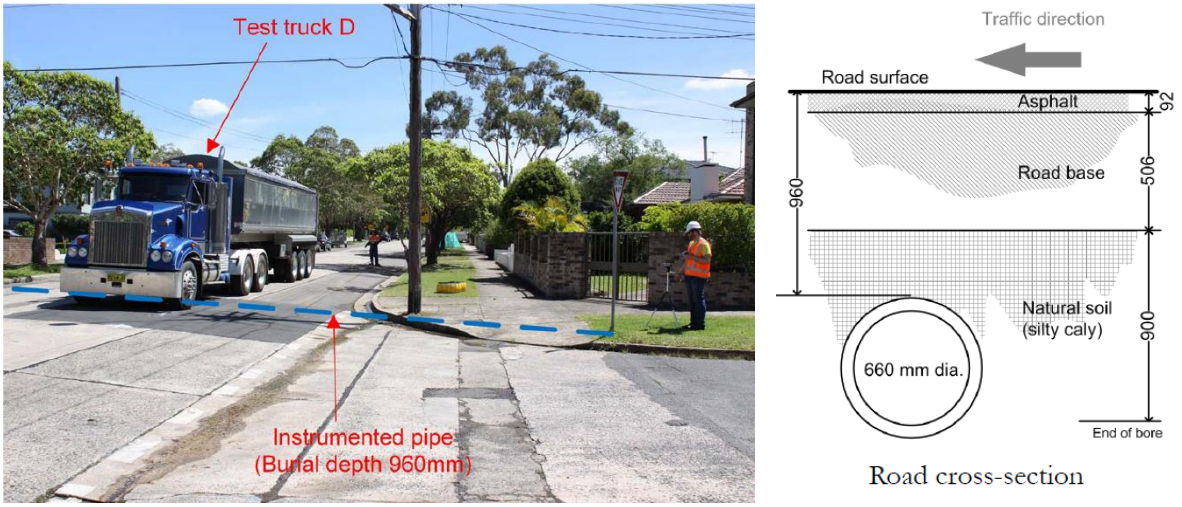

(a) (b)

Figure 2- 5 (a) Layout of truck tests; (b) Road cross-section of trunk tests (Chan et al., 2016b)

2.6.2 Internal loads

Internal pressure is a major source of hoop stress in CI water pipes, and at least three classes of pipe wall thickness have been designed for different operational pressures (AIS, 1941). The results of bursting tests have been evaluated for the design purposes, as reported in archived standards, and the bursting pressures determined by the pipe diameter, thickness and tensile strength of intact CI pipes (AIS, 1941; AWWA-C100, 1908; AWWA-C102, 1939; AWWA-C108, 1962).

Both full-scale experiments (Rathnayaka, 2016) and analytical simulations (Ji et al., 2017; Rathnayaka et al., 2017a) confirm that internal pressure has a dominant influence on the structural integrity of large-diameter corroded CI trunk mains.

The transient pressures from pump and valve operations have been analysed, and failures of CI water pipes have been observed after transient pressure events (Rathnayaka et al., 2016a; Rathnayaka et al., 2016b).

2.6.3 Hoop and longitudinal stress

The internal and external loads in CI pipes can generate pipe stress in hoop and longitudinal (axial) directions. The hoop and longitudinal stress on intact CI pipes from internal pressure are expressed in Equations 2.4 and 2.5, respectively (Robert et al., 2016b).

$$\sigma_h = \frac{PD_i}{2t_0} \tag{2.4}$$

$$\sigma_h' = \nu \frac{PD_i}{2t_0} \tag{2.5}$$

where, σ_h is the hoop stress from internal pressure, P is the internal pressure, D_i is the nominal (internal) pipe diameter, t_0 is the nominal wall thickness, σ_h' is the longitudinal stress from internal pressure, and ν is the Poisson's ratio of the pipe material.

The pipe stresses from external loads are generally converted by the elastic ring theory (Robert et al., 2016b; Wilson et al., 2016). The pipe hoop and longitudinal stress from external (soil and traffic) loads are shown in Equations 2.6 and 2.7, respectively (Robert et al., 2016b).

$$\sigma_E = \frac{3K_b W_v E t_0 D_i}{E t_0^3 + 8K_z P D_i^3} \tag{2.6}$$

$$\sigma_E' = \nu \frac{3K_b W_v E t_0 D_i}{E t_0^3 + 8K_z P D_i^3} \tag{2.7}$$

where, σ_E is the hoop stress from external loads, W_v is the vertical load from overburden soil and traffic load, E is the modulus of elasticity, K_b is the bending moment parameter, K_z is the deflection parameter, and σ_E' is the longitudinal stress from external loads.

2.6.4 Pipe failure

The failure of CI water pipes is defined by either localised fracture or the loss of structural capacity (Rathnayaka et al., 2017b). Localised failure occurs when a crack initiates in an area with stress concentrations produced by corrosion patches or manufacturing defects (Brevis et al., 2015; Rathnayaka et al., 2017b). It has been shown that localised failure initiates water leaks in CI pipes (Brevis et al., 2015; Rathnayaka et al., 2017b).

The loss of structural capacity of CI pipes normally refers to catastrophic pipe bursts (Rathnayaka et al., 2017b; Shannon et al., 2016b). Leaking CI pipes may eventually lose their structural capacity through a major fracture normally referred to as a burst (Bardet et al., 2010; Rathnayaka et al., 2017b).

2.6.5 Failure modes

The modes of CI pipe failures can be summarised into the locations of failure at the pipe barrel and the joint. Based on the fracture orientations, CI barrel pipe failures normally include longitudinal and circumferential barrel fractures. For large-diameter CI pipes, the predominant failure mode is longitudinal barrel fracture rather than circumferential barrel fracture, due to the higher resistant capacity against bending (Makar, 2000).

Longitudinal barrel fracture is normally caused by the hoop stress from internal pressures and stress concentrations corrosion and manufacturing defects (Makar, 2000). Circumferential barrel fractures commonly occur in small-diameter CI pipes induced by soil bending stress and corrosion deterioration (Atkinson et al., 2002; Makar, 2000).

Pipes with joint fractures normally contain pre-cracks or damage caused by transportation or installation, and the propagation of pre-existing cracks under certain crack growth mechanisms may lead to a leak or a burst (Makar, 2000). Furthermore, for large-diameter pipes, the joints can attract significant stresses due to ground movement, since pipes undergo mostly rigid body movement.

2.7 Pipe failure prediction models

A number of pipe failure prediction models have been established worldwide to attempt to address the challenges of ageing water infrastructures (St. Clair and Sinha, 2012; Wilson et al., 2017). Due to the lack of historical failure data, physical mechanism-based models are normally proposed to predict the failures of large-diameter CI water pipes (Rajani and Kleiner, 2001; Wilson et al., 2017).

Schlick (1940) conducted full-scale tests on intact CI water pipes ranging from 150 to 1200 mm. Both internal pressures and external loads were provided on these pipe sections, and the failure criterion based on experimental results is shown in Equation 2.8 (Schlick, 1940). This failure criterion has been adopted as the design method for CI water pipes, and a combination of external loads and internal pressure is considered for pipeline stress analysis.

$$(\frac{W_v}{W_L})^2 + \frac{P}{P_L} \leq 1 \tag{2.8}$$

where, W_v is the vertical load from overburden soil and traffic load, W_L is the critical external load to pipe failure, and P_L is the limiting internal pressure (bursting pressure).

Rajani (2000) proposed an empirical equation to quantify the residual yield strength of CI water pipes based on the growth of corrosion pits. This method attempted to use linear elastic fracture mechanics (LEFM) to estimate the remaining strength of corroded CI pipes. However, pitting corrosion tends to produce graphitization and reduce the wall thickness in CI water pipes rather than create cracks in external surfaces. Hence, the LEFM equation may not be applicable to corroded CI pipes until a crack has initiated.

The dimensions of corrosion patches or defects in pressurised pipelines are evaluated in ASME-B31G (1991). The maximum allowable longitudinal defect length is expressed in Equation 2.9. The pipeline needs to be repaired or removed if the defect is above 80% of the original wall thickness. However, this method of analysis is too conservative for CI water pipes, since operational water pressures are generally smaller than those in the petroleum industry for which the above standard was mostly developed (Rathnayaka et al., 2017a).

$$L = \begin{cases} 4.48\sqrt{D_i t_0}, & 0.1 \leq \dfrac{c}{t_0} < 0.175 \\ 1.12\sqrt{D_i t_0}\sqrt{(\dfrac{c/t_0}{1.1c/t_0 - 0.15})^2 - 1}, & 0.175 \leq \dfrac{c}{t_0} < 0.8 \end{cases} \tag{2.9}$$

where, L is the maximum allowable longitudinal extent of the corroded area.

Robert et al. (2016b) proposed methods to evaluate the impact of internal pressure and external loads on uniformly corroded CI water pipes, based on three-dimensional (3-D) FE simulations validated against the results of traffic loading tests. In addition, physical probabilistic models have been developed to predict the remaining life and failure rates of large-diameter CI water pipes experiencing soil corrosion (Ji et al., 2017). The pipe dimensions (diameter and thickness), corrosion parameters and operational pressures have significant impacts on the probability of CI pipe failure, based on time-based sensitivity analysis and probabilistic physical modelling (Ji et al., 2017). These results were confirmed by a statistical analysis of the failure data from two Australian water utilities (Ji et al., 2017).

2.8 Fatigue mechanism in CI pipes

2.8.1 Failure cases related to fatigue mechanism

To explore the reasons for crack propagation within cast iron pipes, alternative mechanisms of crack growth have been considered and analysed. Fatigue is a common failure mode for metal infrastructures, including bridges and building structures (Anderson, 2005; Schijve, 2001). In some recent failure cases, some pipes were in a slightly corroded condition, and hence, they were investigated for fatigue damage features before catastrophic failure and likely fatigue failure (Bardet et al., 2010; Cullin et al., 2014; Rajani and Kleiner, 2010; Rajani et al., 2012).

Bardet et al. (2010) investigated the increase of the number of CI water pipe failures in Los Angeles in 2009 and observed the consistent ratios of leaks to breaks for the period between 2001 and 2009. Bardet et al. (2010) claimed that additional fatigue damage caused by water fluctuations from a water-rationing program was responsible for the increase of CI water pipe failures. Brevis et al. (2015) proposed a conceptual approach to analyse the fatigue damage of the CI pipes which failed in Los Angeles in 2009. The S-N curves adopted from the empirical correlations and a two-phase corrosion model were used to evaluate the fatigue damage in CI water pipes. Brevis et al. (2015) claimed that the fatigue mechanism shortens the service life of CI water pipes.

Rajani and Kleiner (2010) conducted a conceptual study of fatigue analysis on the failure of a 1,200 mm diameter CI trunk main without severe corrosion. The mechanical properties and load spectra were taken from the literature, and the Paris' law was adopted to predict fatigue crack growth in CI pipes (Rajani and Kleiner, 2010). The initial crack length was found to be crucial for the fatigue life of CI water pipes (Rajani and Kleiner, 2010).

A failure analysis was conducted on a 750 mm diameter CI pipe in Cleveland with the features of multiple failure phases (Rajani et al., 2012). The CI pipe buried in 1880 failed in bell joint fracture mode, and dual corrosion phases were observed in the major fracture surface (Rajani et al., 2012). Based on the analysis, it was suggested that fatigue propagated the pre-crack in the bell joint until catastrophic fracture, and a concrete vault located on the bell joint was responsible for transferring the fatigue stresses of traffic loads to the target pipe joint (Rajani et al., 2012).

Cullin et al. (2014) evaluated the failure mechanisms of a 300 mm CI pipe in Anchorage, Alaska. Due to the observation of dual corrosion phases in the major fracture surface, fatigue was considered as the possible mechanism of pipe failure. A 400 mm sub-critical crack was observed in the fracture surface, and corrosion fatigue was assumed to be the failure mechanism due to the absence of extra high operational pressure data (up to 450 kPa).

2.8.2 General analysis approaches and fatigue tests

2.8.2.1 S-N curves

Stress-controlled fatigue tests have been widely used in the fields of structural fatigue design and prediction, especially in the range of high-cycle fatigue (Bannantine et al., 1990).The fatigue endurance limit (σ_e) for a certain material is defined as the amplitude of cyclic stress that produces infinite fatigue life, and this stress amplitude was observed based on specimens which survived 10 million cycles.

Yamamoto et al. (1983) evaluated the bending fatigue strength of CI pipes based on smooth and corroded beam specimens taken from two large-diameter CI pipes. The fatigue stress ratios of fatigue tests are defined in Equation 2.10 by the minimum and maximum fatigue stress. The fatigue stress ratio of 0.0 was used, and the bending fatigue specimens were taken from two CI pipes (690 mm buried in 1958 and 750 mm buried in 1901). The endurance limit under bending fatigue stresses was approximately 60% of the material flexural strength, and the corrosion pits lowered the fatigue strength and shifted the S-N curves (Yamamoto et al., 1983). Unfortunately, the corrosion pits in bending specimens were not measured or reported in this study.

$$R = \frac{\sigma_{min}}{\sigma_{max}} \tag{2.10}$$

where, R is fatigue stress ratio, σ_{min} is minimum fatigue stress, and σ_{max} is maximum fatigue stress.

Belmonte et al. (2009) conducted fatigue tests on small-diameter pipes (up to 125 mm in diameter). Although three pipe specimens were used in the fatigue tests, only one data set was capable of sketching an S-N curve (Belmonte et al., 2009). The fatigue stress ratio of 0.1 was used, and as-received specimens containing corrosion pits were taken from pipe rings (Belmonte et al., 2009). The S-N curves from bending fatigue tests are plotted in Figure 2-6 (Belmonte et al., 2009; Yamamoto et al., 1983). The surviving specimens are plotted with hollow labels in Figure 2-6.

Gould (2011) reported a series data of fatigue tests based on DENT specimens obtained from gas CI pipes; however, the results may not be valid for further analysis due to the different stress ratios (0.17, 0.5 and 0.83) used to form S-N curves. Crack propagation was not recorded during the fatigue test, and these reported data therefore cannot provide any design parameters or fatigue properties for CI pipes.

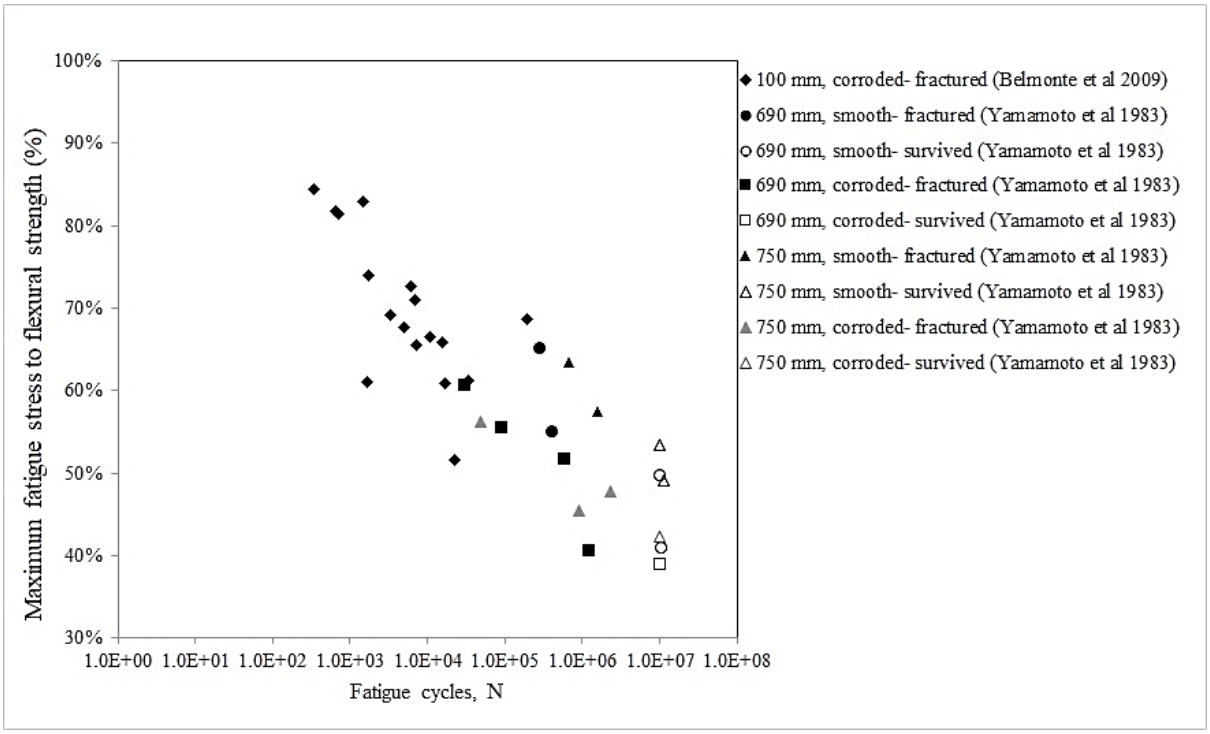

Figure 2- 6 S-N curves of CI water pipes from bending fatigue tests

2.8.2.2 ε-N curves

Strain-controlled tests tend to provide trustworthy curves (ε-N) to predict the low-cycle fatigue behaviour due to the availability of elastic and plastic strain values from hysteresis loops (Schijve, 2001). The Coffin-Manson relation (Equation 2.11) is generally used in low-cycle fatigue analysis:

$$\frac{\Delta\varepsilon_t}{2} = \frac{\Delta\varepsilon_e}{2} + \frac{\Delta\varepsilon_p}{2} = \frac{\sigma_f'}{E}(2N_f)^q + \varepsilon_f'(2N_f)^{q'} \qquad (2.11)$$

where, $\Delta\varepsilon_t/2$ is total strain amplitude, $\Delta\varepsilon_e/2$ is elastic strain amplitude, $\Delta\varepsilon_p/2$ is plastic strain amplitude, E is modulus of elasticity, N_f is the cycles to failure, σ_f' is a parameter that scales with tensile strength obtained by fitting experimental data, q is the slope of the log-log curve again determined by fitting, q' is an empirical constant known as the fatigue ductility exponent, and ε_f' is an empirical constant known as the fatigue ductility coefficient, the failure strain for a single reversal, detailed in Schijve (2001).

Since CI water pipes are normally subjected to stress-controlled fatigue stresses (Rathnayaka et al., 2016b), ε-N curves are inapplicable for evaluating fatigue damage in CI pipes.

2.8.2.3 Fatigue crack growth rate (FCGR)

Fatigue crack growth properties have been successfully used to predict fatigue crack propagation using the empirical equation Paris' laws (Equations 2.12 and 2.13). Typically, fatigue crack growth can be divided into three phases: crack initiation, propagation and final fracture. The stage of crack propagation is of particular concern due to its potential of failure prevention. Equation 2.10 can be rewritten as Equation 2.14:

$$\Delta K_I = K_{max} - K_{min} = Y\ \sigma_{max}\sqrt{\pi a} - Y\ \sigma_{min}\sqrt{\pi a} = \ Y\ \ \Delta\sigma\sqrt{\pi a_t} \tag{2.12}$$

$$\frac{da}{dN} = C\ \Delta K^m \tag{2.13}$$

$$R = \frac{K_{min}}{K_{max}} = \frac{\sigma_{min}}{\sigma_{max}} \tag{2.14}$$

where, a_t is through-wall crack length, N is the number of stress cycles, C and m are Paris' constants, σ_{max} is maximum nominal stress, σ_{min} is minimum nominal stress $\Delta\sigma$, is the stress difference, K_{max} is maximum stress intensity factor, K_{min} is minimum stress intensity factor, and ΔK_I is the range of stress intensity factor.

Mohebbi et al. (2010) reported the crack growth properties (*C* and *m*) of four large-diameter CI pipes, based on single-edged beam bending tests. The fatigue crack growth data are plotted in Figure 2-7. The background information and Paris constants are summarised in Table 2-8.

Table 2- 8 Pipe data used for FCGR tests and Paris constants, summarised from Mohebbi et al. (2010)

Pipe	Pipe dimensions (*mm*)		Paris constants	
	t_0	Diameter	m	C ($\times 10^{-16} m/cycle$)
A	28	1070	7.5	46
B	32	760	8.0	28
C	22	1220	7.4	9.5
D	28	530	7.7	2.1

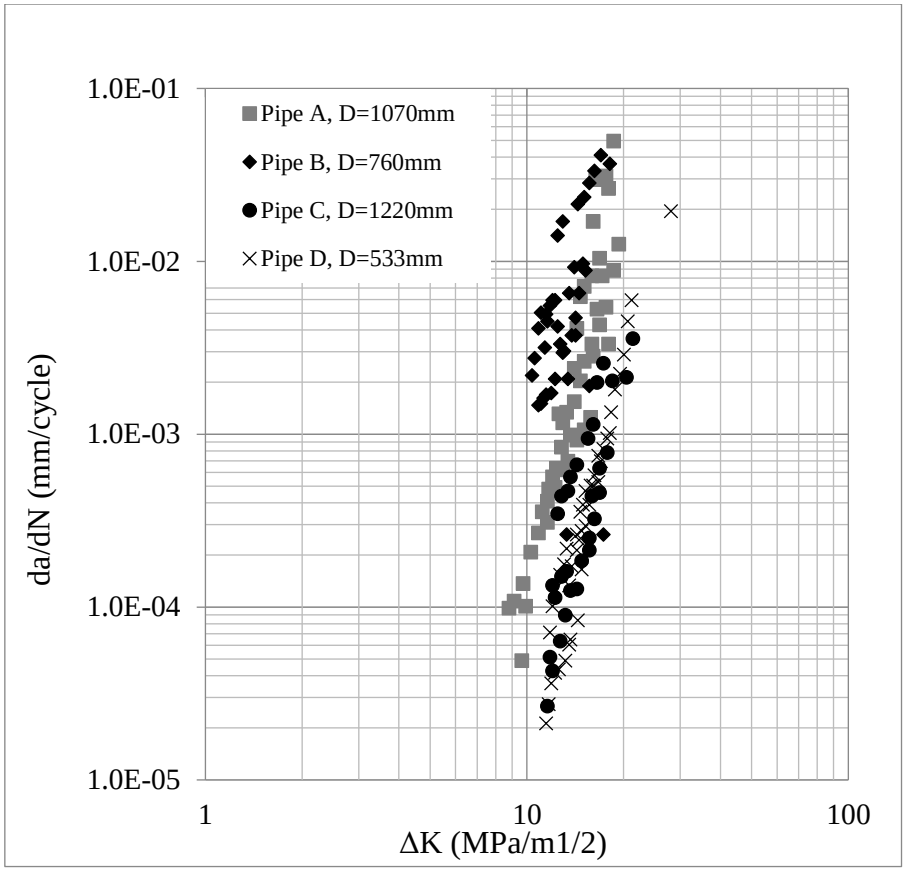

Figure 2- 7 Fatigue crack growth rate of four cast iron pipes, summarised from Mohebbi et al. (2010)

2.8.3 Full-scale fatigue tests

Full-scale steel pipes and aluminium tubes have been previously tested under cyclic internal pressure (Alexander et al., 1997; Erdogan et al., 1969). Erdogan et al. (1969) proposed crack propagation growth models for thin-walled aluminium tubes with a diameter of 88 mm and 0.56 mm thick. The cyclic internal pressures propagate the pre-existing cracks in the tube, and the fatigue growth rates can be simulated by Paris' law.

Alexander et al. (1997) used steel pipes 324 mm in diameter and with 4.8 mm nominal wall thickness to conduct fatigue tests. The pipe samples had the ultimate tensile strength of 497 MPa and various dented scratches on the external surfaces. Based on observations during the fatigue tests, leaks were generated from the notched areas throughout the changeable water pressures ranging from 0.7 to 8.3 MPa.

2.9 Leak-before-break (LBB) assessment

2.9.1 LBB in CI water pipes

The leak-before-break (LBB) concept has been adopted by other piping industries, with the aim of preventing catastrophic fractures by detecting leakages in pressurized structures (Wilkowski, 2000). In standardised LBB assessments (BS-7910, 2005; API-579, 2016), a postulated surface crack is required in accordance with the geometry of manufacturing defects. The surface crack may grow in wall and longitudinal directions under fatigue mechanism of cyclic pressures, and a through-crack must be generated to allow a substantial leak before catastrophic failure. Furthermore, a sufficient LBB window between the detectable leak and break must be allowed for taking action. The prerequisites of the LBB criterion in API-579 (2016) include: (1) Evaluate the initial flaw size and ensure break will not occur under operating situations; (2) Estimate the critical crack length to cause a break; (3) Calculate the crack opening area (COA) for critical crack lengths; (4) Predict the leakage rates for critical cracks and ensure the leakage is detectable by detection systems.

Bardet et al. (2010) reported the ratios of breaks to leaks of CI water pipes in Los Angeles. These failures were summarised into different groups based on soil resistivity, which is a common indicator of corrosivity (Rajani, 2000). The ratios of breaks to leaks range from 0.09 to 0.15 for all groups of soil corrosivity (Bardet et al., 2010), which indicates that certain crack growth mechanisms unrelated to soil corrosion may contribute to the growth of though-wall cracks in CI water pipes.

Rathnayaka et al. (2017b) introduced the LBB concept for large-diameter CI pipes based on full-scale laboratory bursting tests. A leak through a localised fracture in the corrosion patch was observed at a relatively lower pressure level than the maximum pressure achieved in the test, and CI pipes containing a longitudinal barrel crack can still resist a certain level of pressure before bursting (Rathnayaka et al., 2017b). Therefore, the LBB concept may be applicable to pressurised CI water pipes.

2.9.2 Leak detection methods

Two types of leak detection methods, global and local, have been invented and validated for water supply networks and specific pipe components, respectively (BS-7910, 2005). The analysis of artificial transient pressures can be used in leak detection based on changes of pressure signals (Misiunas et al., 2005). Similarly, the acoustic detection method which monitors the noise and vibration generated the water operation is also a common global leak detection method (Fuchs and Riehle, 1991). Moreover, pattern recognition approaches inspect the water supply patterns and identify abnormal events, such as leaks or breaks (De Silva et al., 2011).

Local leak detection methods, the Smartball and Sahara systems, are commonly used, which are able to locate the leaking component in a water network (Fletcher and Chandrasekaran, 2008; Liu and Kleiner, 2013). Table 2-9 summarises the sensitivities of typical leak detection methods.

Table 2- 9 Comparison of leak detection methods

Method	Sensitivity (*L/min*)	Type	Reference
Sahara (acoustic)	0.12	Local detection	Bond et al. (2004)
Smartball (acoustic)	0.38	Local detection	Fletcher and Chandrasekaran (2008)
Leak reflection (transient)	2.4	Local detection	Jönsson (2001)
Pattern recognition	60	Global detection	Zhang (1997)
Inverse transient analysis	180	Global detection	Covas et al. (2005)

2.10 Conclusion

This chapter summarises the research progress on CI water pipes and indicates the predominant failure mode of CI pipe failures and relevant deterioration mechanisms. Research gaps are defined following a thorough literature survey. Background information on CI water pipes, including servicing timelines, corrosion mitigation techniques and statistical analysis results were reviewed and tabulated. Such information supports the time-driven failure analyses detailed in Chapter 3.

Some research data on mechanical and fatigue testing results are summarised for comparison with the mechanical testing results from this project (detailed in Chapter 5 and 6).

Research outcomes from the ACAPFP project provide the methods of analysis of stress concentration in corroded CI pipelines, and the LBB concept developed through full-scale bursting tests is verified by analytical solutions and site observations in Chapter 4.

Chapter 3 Classification of Major Cohorts of Australian Pressurised Cast Iron Water Mains for Pipe Renewal

3.1 Introduction

Australian water supply networks have a significant proportion of cast iron (CI) pipes installed before 1990 (Rajeev et al., 2014). Various manufacturing methods and corrosion mitigation techniques were used to produce the CI pipes that were laid between 1860 and 1990 (Nicholas and Moore, 2009; Rajani, 2000; Shannon et al., 2016a). In Australia, CI pipe manufacturing methods and corrosion mitigation techniques are strongly correlated with the manufacturing and burial dates (Davis et al., 2003; Nicholas and Moore, 2009; Scott, 1990). Due to corrosion deterioration and demanding service conditions and loads, some of these pipes are approaching their ultimate service life (Robert et al., 2016b). Failure rates of CI pipes are higher than both steel and ductile iron pipes (Rajeev et al., 2014) and special attention is required to avoid destructive failures in CI pipes. A failure in a pressurised trunk main may have severe consequences for the public water supply, and the substantial financial losses in some cases can amount to millions of dollars (Jiang et al., 2017a; Vitanage et al., 2014). Therefore, efforts must be made to improve the condition assessment and rehabilitation programs of aged CI pipelines owned by Australian water utilities.

The predominant failure mode in large-diameter pipe (nominal diameter ≥300 mm) is longitudinal barrel fracture, and this is driven by internal pressure and pipe corrosion (Makar, 2000). In Western Australia, Wei et al. (2015) found that CI pipes laid between the 1930s and 1950s have higher burst rates than other CI pipes, indicating that certain pipe batches laid after 1930 may have shorter service lives. Therefore, it is important to determine which CI pipe cohort groups are more susceptible to failure.

In the present study, a strategy for evaluating pipe structural integrity and deterioration condition is proposed for Australian CI pipes, taking into account the range of pipe properties and construction practices based on pipe cohorts. This approach is able to provide important data on CI pipelines and estimate the residual strength, based on the burial date and nominal diameter. Pipe classes and the corresponding safe operating pressures were analysed for different cohorts (i.e., groups of pipes that have similar properties) using handbooks and standards. Metallurgical analyses and mechanical tests were conducted on fractured or decommissioned large-diameter CI pipes in order to confirm the manufacturing method and construction date. The cohort data and some pipe failures in Australian water utilities were analysed to estimate the remaining structural capacity and this information was used to identify critical cohorts.

3.2 Factors important for determination of pipe cohort groups

The following sections provide the background on each of the factors important for large-diameter CI pipe cohort analysis, including pipe manufacturing methods, pipe dimensions, pipe class and safe operating pressures, corrosion mitigation systems and material strength.

3.2.1 Pipe manufacturing methods

Two major types of CI pipes (i.e., static and spun cast) were buried in Australian cities in the 19th and 20th centuries. Prior to 1920 in Australia, all CI pipes were statically (vertically and horizontally) cast, which could result in non-uniform thickness and low material strength if the moulds were off-centre or defects were present in the casting. Spun CI pipes were widely installed after 1930 due to their improved strength and relatively uniform thickness compared with static CI pipes. The relevant standards and handbooks were reviewed to extract the manufacturing methods used for large-diameter CI pipes in Australian water utilities and these are summarised in Table 3-1.

CI pipes were imported to Australia from the UK prior to about 1890 to build water supply networks. From the 1890s, local manufacturers in Australia started to produce small-diameter CI pipes using static casting methods, but imported pipes were still common. In 1904, large-diameter vertical moulds were produced in Australia. The casting process involved either horizontal or vertical casting in sand moulds. From the 1920s, spun CI pipe production in Australia was initiated and advanced manufacturing methods including improved casting processes and moulds were introduced in the AIS (1941). The use of CI pipes in the water industry was eventually phased out in the 1980s due to the use of ductile iron pipes (Nicholas and Moore, 2009).

3.2.2 Pipe dimensions, classes and safe operating pressures

The dimensions of CI pipelines were restricted by manufacturing methods and local demands. The pipe nominal diameter and thickness are shown in Figure 3-1. Pipe lengths were 3.7 m prior to 1961 and 5.5 m thereafter. For CI trunk mains of nominal diameter ≥300 mm, the typical operating pressures range from 300 to 1,000 kPa (Rathnayaka et al., 2016a). CI water distribution pipes were designed in three classes (the wall thickness increases with higher pipe class) for each pipe nominal diameter, to cope with different operating pressures (AIS, 1941; AWWA-C100, 1908; BS-78, 1938). For a specific casting method, the bursting pressure is determined by the nominal pipe diameter and the wall thickness. High-pressure zones require thicker pipe walls, and therefore the operating pressures may indicate the servicing CI pipe classes. Servicing CI trunk mains can be summarised into three classes, and the corresponding safe operating pressures (P_s) are summarised in Table 3-2 in accordance with the archived standards (AIS, 1941; AWWA-C100, 1908; BS-78, 1938).

Table 3- 1 Manufacturing standards of CI water pipes

Casting method	Production	Pipe ID	Standards and Handbooks			Installation period
			Australia	UK	US	
Horizontal- Static (sand mould)	UK	1	-	-	AWWA-C100 (1908)[1]	≤1921
Vertical- Static (sand mould)	Australia and imported	2	-	BS-78 (1938)[1]	AWWA-C102 (1939)	1885–1930s
De Lavaud process- Spun (metal mould)	Australia and imported	3	-	BS-1211 (1958); BS/EN-877 (1999)	AWWA-C106 (1953)	1926 –1980
Super De Lavaud process- Spun (sand mould)	Australia	4, 5	AIS (1941)[1]; AIS (1953)[1]	-	AWWA-C108 (1962)	
Spun (metal mould)	Australia	6, 7	AS-1724 (1975) [1]	-	-	

[1] Standards primarily used in Australian pipes and the present study.

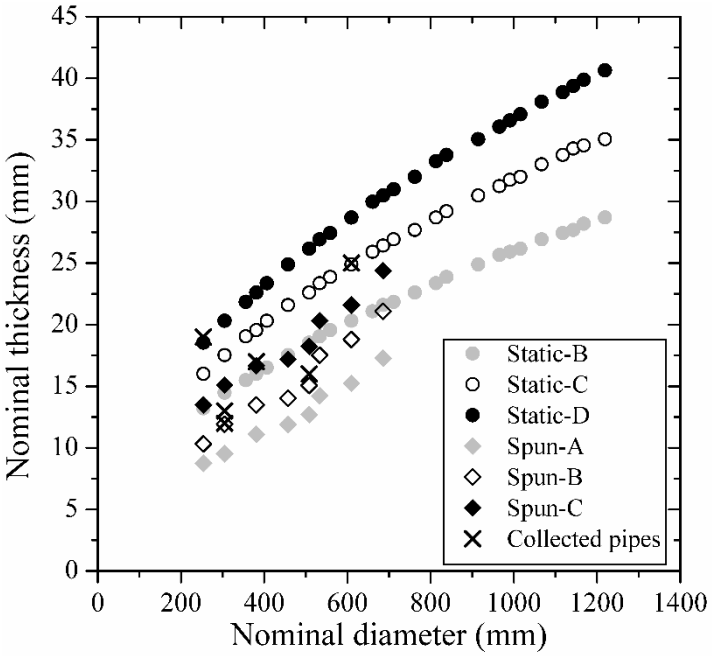

Figure 3- 1 Pipe thicknesses (mm) and nominal diameter (mm) listed in BS 78 (1938), AIS (1941) and AS1724 (1975)

With the increase of material strength from static cast to spun cast, the pipe thickness was reduced in spun CI pipes. The hoop stress (σ_h) of a pipe barrel is dependent on the pipe inner diameter (D_i), initial thickness (t_0) and internal water pressure (P) (Equation 2.4). The thicknesses in different pipe sizes are plotted in Figure 3-1 based on the dimensions listed in the standards (AIS, 1941; AIS, 1953; BS-78,

1938; BS-1211, 1958). For a particular pipe size and class, spun CI pipes are under higher hoop stresses than static CI pipes, due to the thinner wall thickness, when corrosion damage is negligible.

3.2.3 Corrosion mitigation systems

In the CI water network, pitting corrosion (where pipe walls deteriorate in localised areas rather than uniformly) is identified as the most common corrosion mode (Rajani, 2000). To reduce pitting corrosion in CI pipes, external and internal corrosion mitigation systems were used as described next.

3.2.3.1 External corrosion: coating and backfills

Two types of coatings have been widely used for metallic pipes throughout the timeline of CI pipes: paint coating (tar or bitumen) and polyethylene-encased coating. Almost all the CI pipes were buried with paint coating in the 20th century. However, limited protection is provided by this coating type in aggressive environments (Bonds et al., 2005; Romanoff, 1957). Consequently, CI pipes with paint coating in natural soils may be prone to more severe corrosion than pipes buried in backfill sand (Rajani, 2000).

To prevent soil corrosion on external pipe surfaces, polyethylene external coatings and sand backfill were introduced for CI pipes in the 1960s (Nicholas and Moore 2009; Scott 1990). Polyethylene encasement was highly recommended as an effective coating method, owing to its excellent protection in extremely corrosive environments (AWWA-C105, 1972). Bonds et al. (2005) observed that even damaged polyethylene coating has better resistance than paint coating, especially in corrosive environments. However, only a limited number of Australian CI pipes were coated by polyethylene encasement in the 1970s, implying that the majority of the CI pipes underwent corrosion deterioration in soil.

3.2.3.2 Internal corrosion: cement lining

In the late 1920s, the internal surfaces of CI pipes were factory lined using cement mortar to prevent internal corrosion and improve water flow. Consequently, internal corrosion caused wall loss in unlined CI pipes laid before the 1920s (Rajani and Kleiner, 2013a). To minimise internal corrosion, the majority of unlined pipes went through in situ lining rehabilitation programs (1930–1960s), depending on the individual water utilities (Nicholas and Moore, 2009; Rajeev et al., 2014). Due to the rehabilitation programs for in situ lining in Australia, internal corrosion pits were preserved in cement lining (Robert et al., 2016a). The in-situ lining programs have minimised the number of unlined CI water trunk mains in the Australian urban network. Therefore, the analysis of internal corrosion damage is less critical in comparison with external soil corrosion for aged water mains.

3.2.4 Material Strength

The tensile strength and fracture toughness of CI are important parameters for determining safety, failure probability and remaining pipe life. Recent research has highlighted that CI pipes tend to fail by developing cracks within a corrosion patch in the pipe barrel, which can lead to water leakage (leak-before-break) (Rathnayaka et al., 2017b). Subsequent repetitive stress changes, such as transient water pressures and traffic loads, can lead to the propagation of cracks until such time that the cracks become critical and generate spontaneous fracture propagation, causing a break. Rathnayaka et al. (2017b) also highlighted that the tensile strength of in situ CI pipe material is responsible for initiating water leakage caused by a fracture, and the fracture toughness is responsible for final spontaneous fracture propagation/break. Therefore, tensile strength and fracture toughness are essential material properties for the identification of pipe cohorts. Table 3-3 shows the specific tensile strengths that were required based on various standards and moulding types. Although the minimum values of fracture toughness for CI pipes were not specified in archived standards, test results from the literature are shown in Figure 3-3(b).

Table 3- 2 Classes and safe operating pressures for CI pipe cohorts

Spun (AIS, 1941; 1953)		Static vertically-cast (BS-78, 1938)		Static horizontally-cast (AWWA-C100, 1908)	
Class	P_s (kPa)[1]	Class[2]	P_s (kPa)	Class	P_s (kPa)
A	790	B	600	B	600
B	940	C	900	C	900
C	1150	D	1200	D	1200

[1] Safe operating pressure for spun CI pipes was determined by 500 mm diameter pipes.
[2] Class A of static vertically-cast pipes was designed for gas pipelines only.

Table 3- 3 Specified minimum strength of CI pipes in standards and handbooks

Standards and handbook codes	Year	Country	Material	Minimum tensile strength (MPa)
AWWA C100	1908	US	Static-horizontal	124
AWWA C102	1953	US	Static-vertical	75
AWWA C106	1953	US	Spun (metal)	124
AWWA C108	1962	US	Spun (sand)	125
BS 78	1938	UK	Static-vertical	124
BS 1211	1958	UK	Spun (metal)	172
			Spun (sand)	159
AIS	1941, 1953	AUS	Spun	193
AS 1724	1975	AUS	Spun (metal)	200
BS EN 877	1999	UK/Europe	Spun	200

3.3 Specific properties of cohorts

3.3.1 Collection of representative pipe samples for microstructural and mechanical strength testing

Seven ex-service CI pipes were examined from Australian water utilities (see Table 3-4), of which five pipes (pipes 2–6 in Table 3-4) were analysed for their microstructural and mechanical strength properties. All the selected pipes failed by longitudinal fracture, with the exception of pipe 2, which was decommissioned in 2011 after ~90 years in service (see Table 3-4). The chemical composition was determined using inductively-coupled plasma atomic emission spectroscopy (ICP-AES), optical emission spectroscopy (OES) and the Leco combustion technique. The microstructural features of the pipe samples were examined using metallographically polished and etched CI samples. The description of graphite flakes in each sample was based on ASTM-A247-67 (1998). Tensile tests were conducted using an Instron-4402 loading frame with a load cell of 50 kN and the specimens were tested at 0.5 mm/min. Test specimens were prepared in accordance with ASTM-E8 (2009). Two strain gauges were installed vertically at the centre of the test specimen to obtain the stress-strain curve. Scanning electron microscopy (SEM) was used to examine the fracture surfaces of the tensile coupon specimens. Fracture toughness tests were conducted using an Instron-4402 loading machine and single-edged-notched-beam (SENB) specimens, which were prepared according to ASTM-E1820 (2013). A minimum of four tests were conducted for each of the five Australian pipe samples in this study.

Table 3- 4 Background of pipe samples used in this study

Pipe ID	Location	Casting method	Burial year	Failure year	Nominal diameter (*mm*)	Nominal thickness (*mm*)	Lining
1[1]	Melbourne, Victoria	Static (horizontal)	1868	2014	250	19	In situ
2	Sydney, NSW	Static (vertical)	1922	2011[2]	600	25	In situ
3	Melbourne, Victoria	Spun	1938	2014	380	17	Factory
4	Newcastle, NSW	Spun	1957	2013	300	13	Factory
5	Sydney, NSW	Spun	1961	2014	500	16	Factory
6	Melbourne, Victoria	Spun	1976	2015	300	12	Factory
7[1]	Melbourne, Victoria	Spun	1976	2014	300	12	Factory

[1] Used in corrosion modelling only
[2] Pipe 2 was decommissioned in 2011.

3.3.2 Chemical and metallurgical analysis

The chemical compositions of the selected samples are summarised in Table 3-5. The results are compared with the typical ranges applicable to CI pipes in North America (Makar and Rajani, 2000).

The metallurgy microstructure description for graphite flakes found in each sample is shown in Table 3-6. Static CI pipes contained larger graphite flake lengths than spun CI pipes (Figure 3-2). For spun CI pipes, different graphite types and sizes were observed through the wall-thickness: inner surfaces tend to have longer graphite flakes than outer surfaces, due to the slower cooling rates at the inner surface during the centrifugal casting process. This observation is consistent with the spun CI pipes in the UK and US (Longmuir, 1939; Makar and Rajani, 2000). Both ferritic and pearlitic matrices were observed. However, more ferritic matrices were observed in spun than static CI pipes, and the distribution of pearlitic matrices in static CI pipe was higher than that in spun CI pipes.

Table 3- 5 Chemical compositions of pipe samples in % w/w

Pipe ID	C	Mn	Si	S	P	Ni	Cr	Cu	V	Ti
2	3.52	0.43	1.83	0.10	0.57	<0.001	0.01	0.20	0.01	0.05
3	3.71	0.86	2.07	0.05	1.42	0.03	0.04	0.02	0.11	0.08
4	3.60	0.51	1.52	0.05	0.49	0.01	0.01	0.01	0.01	0.06
5	3.65	0.50	1.69	0.05	0.49	0.01	0.01	0.01	0.01	0.11
6	3.64	0.44	1.88	0.10	0.23	0.09	0.11	0.23	0.01	0.03
Static[1]	3.39–3.91	0.21–1.13	1.93–3.31	0.05–0.15	0.69–1.03	-	-	-	-	-
Spun[1]	3.72–4.2	0.25–0.52	1.39–2.41	0.02–0.11	0.06–0.80	-	-	-	-	-

[1] Range of values reported by Makar and Rajani (2000).

Table 3- 6 Microstructural features of cast iron pipe samples based on ASTM A247-67 (1998)

Pipe ID	Graphite flake type[1]			Graphite size[2]			Graphite form[3]		
	Inner surface	Centre	Outer surface	Inner surface	Centre	Outer surface	Inner surface	Centre	Outer surface
2	A	A	A	2	2	2	VII	VII	VII
3	A	D & A	D	3	3	4	VII	VII	VII
4	A & D	D	D	5	5	7	VII & V	V	V
5	A & D	D	D	4	5	6	VII & V	V	V
6	B	B & D	E	6	6	6	VII & V	V	V

[1] Type A- Uniform distribution and random orientation; B- Rosette pattern and random orientation; D- Inner-dendritic segregation and random orientation; E- Inner-dendritic segregation and preferred orientation.
[2] Size 2 (0.32–0.64mm); Size 3 (0.16–0.32 mm); Size 4 (0.08–0.16 mm); Size 5 (0.04–0.08 mm); Size 6 (0.02–0.04 mm); Size 7 (0.01–0.02 mm).
[3] Form V Crab graphite; Form VII Flake graphite.

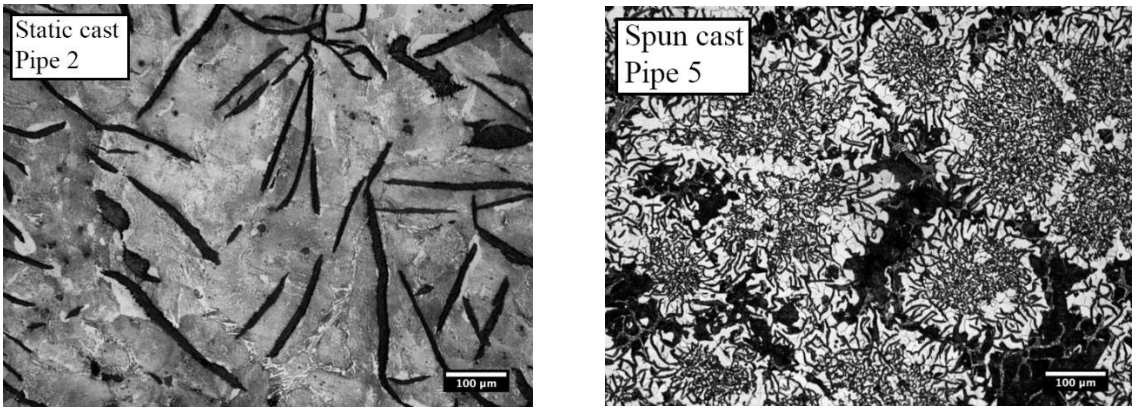

(a) (b)

Figure 3- 2 Typical microstructure of CI pipes: (a) Static cast; (b) Spun cast

3.3.3 Mechanical properties

Previous research on CI pipes used corroded specimens to obtain the remaining strength of corroded pipes (Gould, 2011; Rajani, 2000; Seica and Packer, 2004), and specimens were generally obtained from small-diameter pipes (<300 mm diameter). This study utilised CI specimens extracted from large-diameter CI pipes with corrosion products removed for the purpose of testing the mechanical response of CI. The tensile strength and the construction date of each pipe sample are shown in Figure 3-3(a), together with the tensile strength data from the literature for small-diameter pipes (<300 mm) (Gould, 2011; Makar and Rajani, 2000; Seica and Packer, 2004). The tensile strengths of the large-diameter CI pipes tested in this study were generally lower than those of the small-diameter pipes manufactured at a similar period (Figure 3-3(a)). The tensile strengths of CI pipes 2, 3, 4 and 5 were below the nominal tensile strength (193 MPa for spun, 124 MPa for static) listed in the Australian Standards (AIS 1941; AIS 1953; AS-1724 1975) for pipes 3–5 and the British Standard (BS-78 1938) for pipe 2. In this study, there was a limited increase of material strength throughout the spun CI pipes constructed between 1930 and 1960 (pipes 2, 3 and 4), compared to the higher strength observed in pipe 6 (buried in 1976). Conservatively, tensile strengths of 100 and 150 MPa may be adopted for stress analysis in Australian static and spun large-diameter CI water mains, respectively.

The fracture toughness test results and literature data are plotted against construction date in Figure 3(b) (Cullin et al., 2014; Deb, 2002; Gould, 2011; Kim et al., 2007; Mohebbi et al., 2010; Rajani, 2000) and the average fracture toughness values tested in this study were similar to those recorded in the literature.

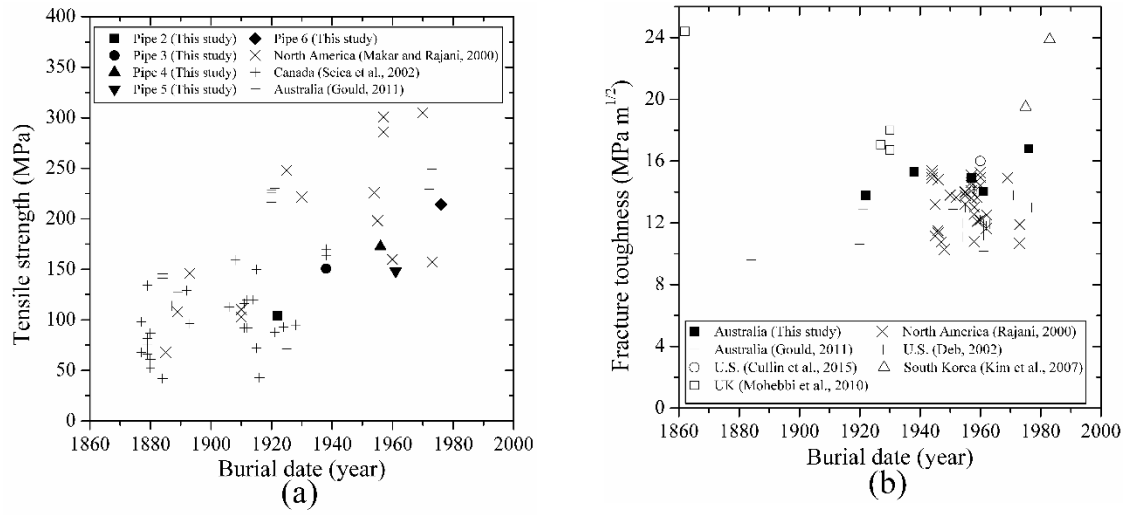

Figure 3- 3 (a) Tensile strengths (MPa) of CI pipes with burial date (year). (b) Fracture toughness (MPa $m^{1/2}$) of CI pipes with burial date (year)

3.3.4 Micro-cracking modes

Trans-granular fracture is the predominant micro-cracking mode due to the existence of large graphite flakes (Figure 3-4(a)). The graphite flakes can be considered as internal notches that may grow fractures in the surrounding metallic matrices when specimens are loaded (Castillo and Baker, 1984; Glover and Pollard, 1969). Inter-granular fracture was observed only in areas with relatively high amounts of ferrite (Figure 3-4(b)).

A correlation was observed between graphite flake length and material fracture tensile strength (Figure 3-5), which indicates that the size of graphite flakes has a direct influence on the material strength of the CI pipes tested in this study. The correlation between the fracture tensile strength and maximum graphite flake length ($1/\sqrt{2a}$) is shown in Figure 3-5. The reasoning for this representation can be explained based on how the stress relates to the stress intensity factor expression of linear elastic fracture mechanics (Equation 3.1). Assuming the graphite flakes act as inherent cracks, the stress within iron matrix may be expressed as:

$$\sigma = \frac{K_I}{Y\sqrt{\pi\, a_t}} \tag{3.1}$$

where, σ is the applied stress, K_I is the intensity factor, Y is a geometric factor about crack length and structure dimensions, and a_t is crack length (the half of the graphite flake length).

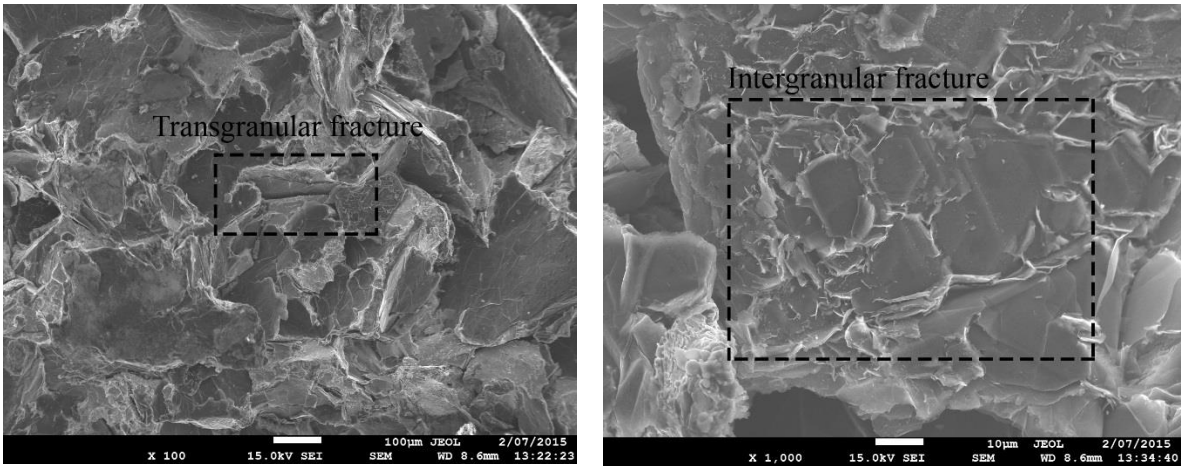

(a) (b)

Figure 3- 4 Micro-cracking modes in cast iron pipes (pipe 2): (a) transgranular; (b) intergranular fracture

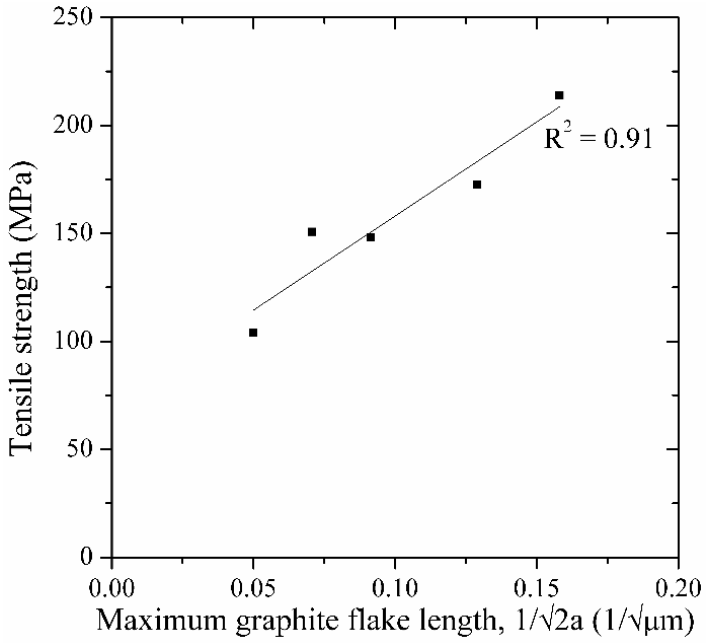

Figure 3- 5 Average tensile strength (MPa) vs. maximum graphite flake length (1/√µm)

3.4 Pit depth propagation model and analysis

3.4.1 Measurement of external corrosion depth

Laboratory examinations of the seven exhumed CI pipes (Table 3-4) were conducted to measure the pit depths, patch sizes, and wall thicknesses. The graphitised layer was removed by low-speed grit-blasting. The exhumed pipe sections were scanned using a Creaform 3-D laser scanner on the external surfaces to obtain the corrosion configuration profiles, consisting of the pit depth and patch dimensions.

Internal corrosion pit depths were also measured, albeit only for the two pipes that commenced service unlined and were later lined in-situ. There were no perforations caused by internal corrosion in these two pipes. Internal corrosion was not observed in any received factory-lined CI pipes, and the received conditions of in situ cement linings in static CI pipes were generally intact.

3.4.2 Pit depth propagation models

The extent of damage inflicted by corrosion is usually quantified in terms of the maximum pit depth. Several empirical models have been proposed (Rajani, 2000; Romanoff, 1957; Rossum, 1969), which can be used to describe the propagation of maximum pit depth with time. A model based on analysis of an extensive database for CI pipes is by Rajani (2000) and is given by Equation 2.2.

$$c = A_p\, t + B_p\, (1 - e^{-C_p\, t}) \qquad (2.2)$$

According to Equation 2.2, the minimum corrosion rate attained after a long period is equal to A_p mm year^{-1}, while the maximum corrosion rates present during early times is given by $A_p + B_p C_p$ mm year^{-1}. For simplicity, the model by Rajani (2000) will be hereafter referred to as the exponential model. Alternatively, Petersen and Melchers (2014) have proposed a bi-modal trend that approximates the maximum pit depth propagation, whereby different reaction mechanisms dominate the corrosion process at different times. The bi-modal characteristic is illustrated in Figure 3-6, which shows that the instantaneous corrosion rate (dc/dt) starts steep initially (r_o), and after a large exposure time attenuates to a steady-state value (r_s). The time taken for the steady-state corrosion rate of r_s is variable. The c_s is directly connected to the difference between the initial and long-term corrosion rate and the time of their transitions. Moreover, it is obvious that $r_o > r_s$.

The bi-modal trend is a scientific development from observations in atmospheric and marine environments, which are detailed in Melchers (2003), Melchers (2014) and Melchers (2015). For applications in underground corrosion, the model is still in the development phase within the ACAPFP project and its mathematical form is not fully yet published.

With regard to Figure 3-6, it is noted that the exponential and the bi-modal model for CI pipes exhibit similar features during the early and late exposure periods. Both models are bounded by tangents described by $c = r_0\, t$ and $c = r_s\, t + c_s$ at shorter and longer times respectively (the limiting cases given in Equations 3.2 and 3.3). Consequently, the exponential model is restated in terms of the parameters characterising the bi-modal trend as per Equation 3.4:

$$\left.\frac{dc}{dt}\right|_{t\to 0} = A_p + B_p C_p = r_0 \tag{3.2}$$

$$\left.\frac{dc}{dt}\right|_{t\to \infty} = A_p = r_s \tag{3.3}$$

$$c = r_s(t - t_0) + c_s\,(1 - e^{-\frac{(t-t_h)}{\tau}}) \tag{3.4}$$

where, t_h is the holiday period (year) corresponding to the onset of corrosion after a delay period due to the breakdown of any protective coating.

3.4.3 Pit depth propagation parameters

The data on maximum pit depth measured in this study, as well as the pit depth propagation curves calculated using Equation 3.4 from the corrosion related parameters (r_s, c_s, τ) suggested by Rajani (2000) and Rajani and Tesfamariam (2007), summarised in Table 3-7, are shown in Figure 3-7.

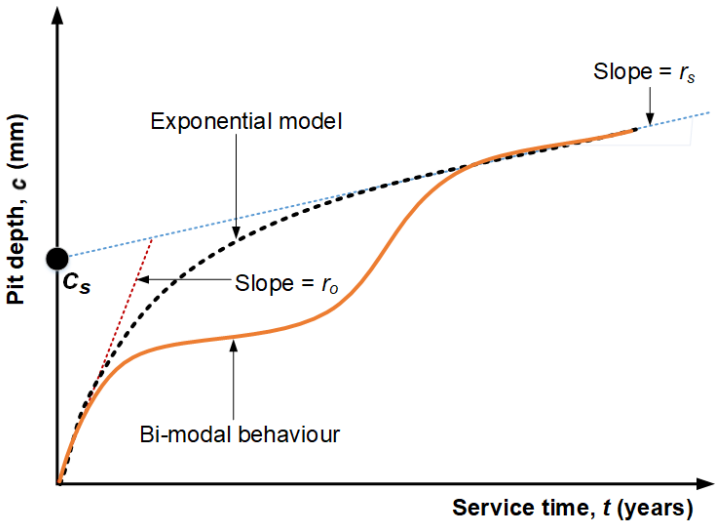

Figure 3- 6 Bimodal trend (solid line) and exponential model (dashed line) for cast iron maximum pit depth (c) propagation

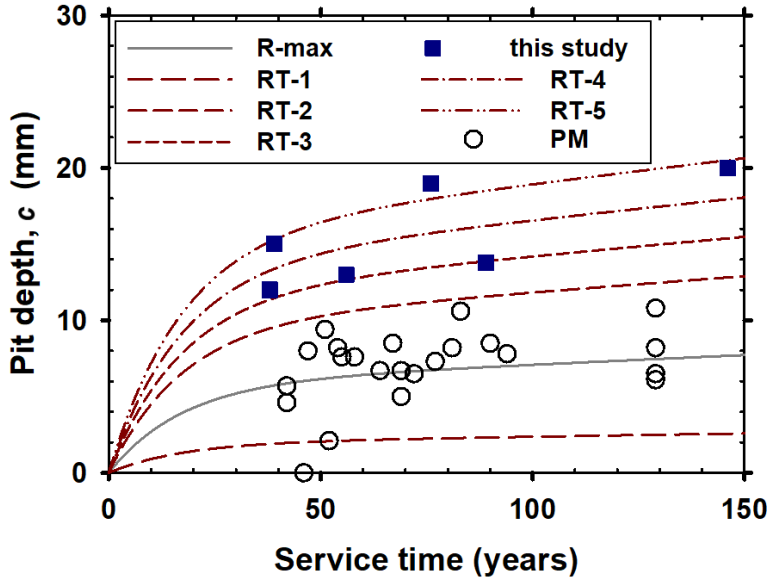

Figure 3- 7 External corrosion pit propagation curves (assuming $t_o = 0$) and data from research literature with the data from present study

Table 3- 7 Comparison of corrosion-related parameters of exponential models

	Label	r_s ($mm\ year^{-1}$)	c_s (mm)	τ ($year$)	Soil corrosivity
Rajani (2000)	R-max	0.0125	5.85	17.24	
Rajani and Tesfamariam (2007)	RT-1	0.0042	1.95	17.24	very low
	RT-2	0.021	9.75	17.24	low
	RT-3	0.0252	11.7	17.24	moderate
	RT-4	0.0294	13.65	17.24	high
	RT-5	0.0336	15.6	17.24	very high
Present work		0.0294	13.65	17.24	

Rajani (2000) determined the corrosion-related parameters using data on maximum pit depths for static and spun CI pipes. Furthermore, Rajani and Tesfamariam (2007) provided a range of corrosion- related parameters that can manifest in soils with corrosivity ranging from very low to very high based on physical observations of through-hole corrosion pits. These parameters serve as baseline values for comparison purposes. The inspection data from Petersen and Melchers (2014) are also plotted in Figure 3-7. Petersen and Melchers (2014) collected data mostly from in-service pipelines and developed a method for predicting r_s and c_s values through linearisation of the long-term features of the bi-model. These data are well bounded within the propagation curves expected in very low to low corrosive soils by Rajani and Tesfamariam (2007), consistent with the fact that these data were from in-service pipelines. In contrast, the data in the present study were mainly from failed pipes, and these are reasonably confined within the pit depth propagation curves anticipated in moderate to very high corrosive soils. Therefore, a set of pit depth propagation parameters (shown in Table 3-7) proposed by

Rajani and Tesfamariam (2007) is adopted here to describe the external pit depth propagation in CI water pipes.

3.4.4 Internal corrosion

As discussed in Section 3.2.3.2, most of the pipes were cement lined in-situ to mitigate corrosion. It is assumed that the internal corrosion for most of the unlined CI pipes progressed for less than 50 years.

Marshall (2001) observed that the growth of internal pit depths significantly reduces with the increase of exposure time for CI water pipes, and an average internal corrosion rate of 0.04 mm $year^{-1}$ was proposed for unlined CI pipes exposed over 30 years. Due to the limited data available on CI pipes, the rate of 0.04 mm/year is adopted in the present study. This corresponds to an average internal wall loss of 2 mm for an exposure period of 50 years. It is noted that a detailed investigation of the propagation characteristics of internal pit corrosion for unlined CI pipes would be highly beneficial.

3.5 Determining priority pipe cohort for replacement

To determine the CI cohort group with greatest need of replacement, statistical analyses of data from major water utilities and corrosion modelling were conducted. The pipe burst rates of six major water utilities in three states in Australia were calculated for CI pressurised water mains (pipe diameter ≥ 300 mm) and the results are shown in Figure 3-8. Longitudinal fracture failure was selected for the analysis as this failure mode is predominantly driven by corrosion and internal water pressure. The total asset lengths of CI pipes laid in each decade were calculated separately. The burst rates were expressed as failure numbers per 100 km per year. The participating utility in New South Wales had failure data from 2000 to 2012 and had their CI pipes installed between the 1900s and 1979. The participating utility in South Australia had failure data from 1976 to 2010 and had their CI pipes installed between the 1880s and 1975. Three participating utilities in Victoria had failure data from 1994 to 2012 and their CI pipes were installed between the 1840s and 1988.

The results indicate that the period from 1960 to 1980 had the highest burst rate. This suggests that the newer pipes are not outperforming the older static cast pipes. The variations in the remaining wall thickness of 500 mm static and spun CI pipes with exposure time were computed and are illustrated in Figure 3-9, based on the average external corrosion parameters (r_s, c_s, τ) shown in Table 3-7. As discussed in Section 3.4 above, static CI pipes are assumed to experience 50 years of internal corrosion damage with an average rate of 0.04 mm per year^{-1}.

According to Figure 3-9, the perforations were expected to occur earlier in spun CI pipes than in static CI pipes due to the thinner initial wall thickness of the former. In Figure 3-9, pipes in the Static-C and D classes as well as Spun-C still have sufficient minimum remaining wall thickness. If corrosion progresses at the rates characterised by the (r_s, c_s, τ) parameters adopted, the 500 mm diameter pipes from the Static-B, Spun-A and Spun-B classes would most likely have thinner remaining wall thickness and fail by longitudinal fracture. This may account for the Western Australian spun CI pipes laid between 1930 to 1950 having higher failure rates than some of the older CI pipes, as reported by Wei et al. (2015). Therefore, pipes laid during this period (or belonging to this cohort) can be considered one of the priority pipe groups that needs attention during pipe renewal planning.

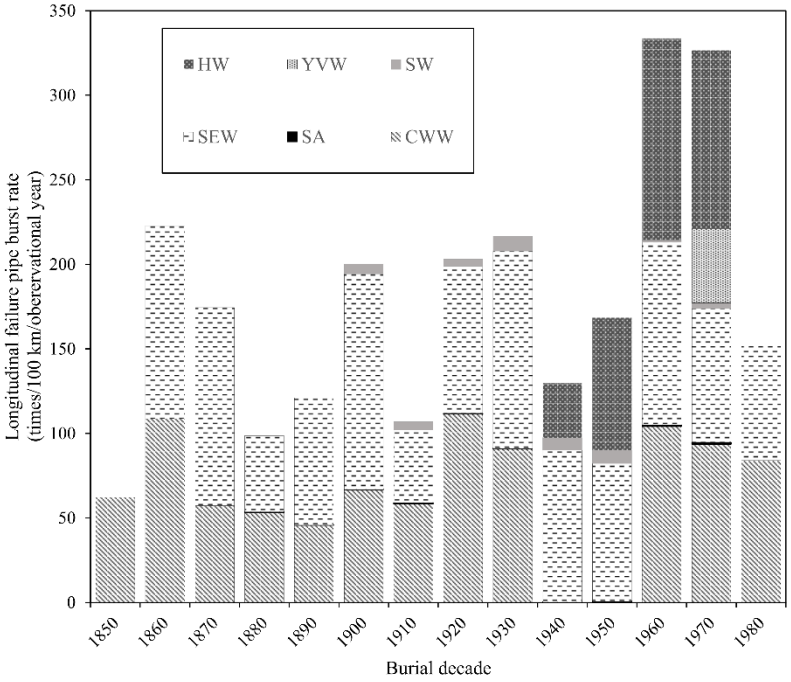

Figure 3- 8 Results of longitudinal pipe failure rate analysis against burial decade for six different water utilities

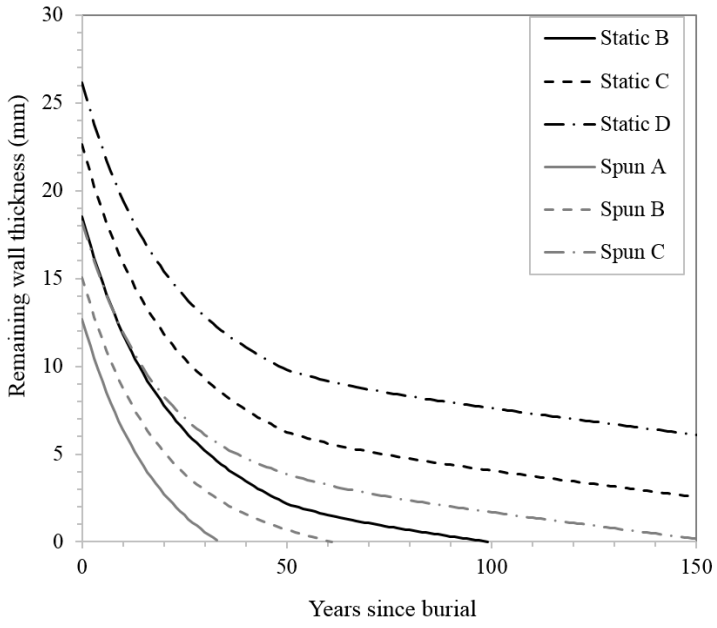

Figure 3- 9 Remaining wall thickness for 500 mm diameter static and spun CI pipes in extremely corrosive soils vs. service time (in years)

3.6 Discussion

A major proportion of buried metallic water mains in Australia contains a large proportion of ageing CI water mains. As some relevant information on these pipe properties has not been recorded in pipe utilities, it is difficult to analyse the remaining capacity of these pipelines. Therefore, a number of factors (i.e., pipe manufacturing methods, pipe dimensions, pipe class and safe operation pressures, corrosion mitigation systems, material strength and microstructure) were identified and analysed to understand changes that occur in these factors with servicing time. This analysis enables the classification of pipes into a limited number of cohorts in such a way that all necessary pipe properties can be assigned to selected pipe cohorts by conducting limited laboratory tests. In this way, the essential material properties (i.e., tensile strength and fracture toughness) required for failure analysis are assigned to each pipe cohort.

As the failure capacity of a CI pipeline is strongly affected by the manufacturing method and pipe wall thickness (many failures in pipe barrel are driven by external corrosion), the cohorts were determined by the casting method and the changes in corrosion mitigation strategies. The timeline of the changes in corrosion mitigation systems used in Australia is summarised in Table 3-8 (AIS, 1941; Davis et al., 2003; Nicholas and Moore, 2009; Scott, 1990).

Table 3-8 presents the utility-dependent cohort methods used in casting, the recommended material properties, the corrosion mitigation systems and exposure in each decade for Australian CI water trunk mains laid between 1860 and 1980. It is worth noting that Table 3-8 was devised based on standards and information from six Australian water utility networks and these may vary depending on individual Australian water utilities. Table 3-8 can be used as a guide if the buried period data are available for CI pipes in a network.

A flow chart is shown in Figure 3-10 for the determination of Australian pipe cohorts. The burial dates of water pipes were typically recorded by water utilities. Determining the mechanical properties for large numbers of pipes can be costly. If the construction or burial date is known, the lining, coating, backfill and recommended material properties can be found using Table 3-8. If the available network information includes nominal diameter and operational pressure, a nominal thickness (class) can be obtained using Table 3-2. The flow chart and the summary of cohort properties may be efficient tools for water asset management and renewal plans. The pipe cohorts with high failure potential can be identified using the approach introduced in this thesis, and preliminary renewal decisions can be made based on the limited data available and targeted data collection can be directed to fill data gaps.

Table 3- 8 Summary of cohort properties of CI trunk mains in Australia

Buried period	Casting[3, 4]	Tensile strength (*MPa*)[5]	Recommended material properties		Corrosion mitigation system			Exposure (*years*)
			Tensile strength (*MPa*)	Fracture toughness ($MPa\sqrt{m}$)	Cement lining	Coating [1]	Backfill[2]	
1860s	Static H	75–124	100	12	In situ	Paint	NS	>150
1870s	Static H	75–124	100	12	In situ	Paint	NS	>140
1880s	Static H	75–124	100	12	In situ	Paint	NS	>130
1890s	Static H	75–124	100	12	In situ	Paint	NS	>120
1900s	Static V	75–124	100	12	In situ	Paint	NS	>110
1910s	Static V	75–124	100	12	In situ	Paint	NS	>100
1920s	Static V/ Spun	75–159	100/150	12	In situ	Paint	NS	>90
1930s	Spun	124–159	150	14	Factory	Paint	NS	>80
1940s	Spun	124–200	150	14	Factory	Paint	NS	>70
1950s	Spun	124–200	150	14	Factory	Paint	NS	>60
1960s	Spun	124–200	150	14	Factory	Paint/PE	NS/Sand	>50
1970s	Spun	124–200	150	14	Factory	Paint/PE	NS /Sand	>40

[1] PE-Polyethylene coating
[2] NS-Natural soil
[3] H-Horizontal
[4] V-Vertical
[5] Minimum tensile strength required based on standards

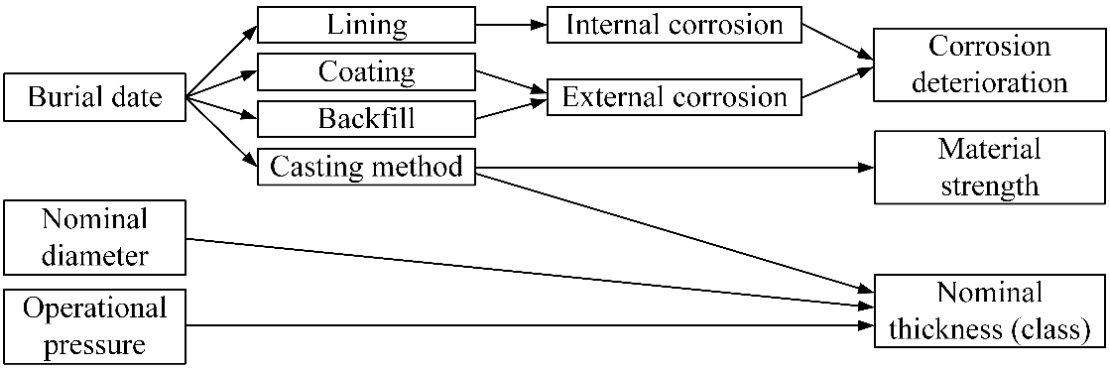

Figure 3- 10 Flow chart for determination of Australian pipe cohorts

3.7 Conclusion

In this study, CI pipes used in Australian water utilities have been grouped into cohorts based a series of factors affecting pipe performance. The large-diameter CI pipes in this study were generally found to have lower material strength than the smaller diameter CI pipes tested in previous studies. Spun CI pipes may have shorter life spans due to the low pipe wall thickness compared with static CI pipes. This is evident by the CI pipes laid between 1960 and 1980 suffering higher burst rates, as determined by statistical analysis. Such high failure rates are potentially caused by the reduction in wall thickness, when manufacturing methods changed from static pit cast to spun cast. The shorter lifespan is primarily due to the rapid corrosion progression during the early part of the corrosion process. Therefore, it is argued that spun CI pipes with thinner original wall thickness should be placed on the priority list for renewal. However, higher pipe strength in spun cast pipe must be taken into account, based on systematic analysis before making final renewal decisions.

Chapter 4 Leak-before-break (LBB) in cast iron pipes

4.1 Introduction

Leak-before-break (LBB) is a design approach to the operation of pressurised vessels and pipelines, which aims to ensure a detectable leak occurs before catastrophic fracture in pressurised pipelines (Wilkowski, 2000). The LBB concept has altered design and operational guidelines and safety assessments in different industries, including gas and petroleum transportation, pressure vessels and nuclear power plants (IAEA-TECDOC-710, 1993). The applications of LBB have been verified for ductile metallic materials, such as high-strength steels, based on practice and experiments (Bartholome and Wellein, 1995; Kannan et al., 2015; Nam et al., 1992).

Cast irons (CIs) are brittle with low fracture toughness relative to steels and ductile irons, and cast iron pipe failures are therefore generally assumed to be brittle fractures with limited warning (Seica and Packer, 2004). As a result, LBB was considered to be inapplicable for CI pipes.

The ACAPFP project investigated the influences of corrosion patches on the pressure-bearing capacity of CI pipes in full-scale laboratory bursting tests and observed that localised failure generates a through-crack in the corrosion patch and causes a leak under lower pressures than burst pressures (Rathnayaka

et al., 2017b). Based on the observations of bursting tests, the LBB concept was introduced for corroded CI water pipes (Rathnayaka et al., 2017b).

This chapter summarises and analyses the recent LBB evidence on CI pipes based on site observations and experiments. The stress concentrations for longitudinal barrel fractures produced by soil corrosion or defects are discussed separately. LBB criteria are proposed for large-diameter CI pipes using limit stress and linear elastic fracture mechanics (LEFM). These criteria are verified by experimental results from the static bursting tests conducted by the ACAPFP. The procedures of LBB assessment are proposed in accordance with the standardised approaches used in other industries. In addition, the findings of failure analyses conducted on small-diameter pipes are summarised, which indicate that the LBB concept is also applicable to pipelines failing by the mode of circumferential fracture. A reason for considering smaller diameter pipes (< 300 mm in diameter) was that evidence is easier to gather than for larger diameter pipes, where failures are not common.

4.2 Field observations of LBB in cast iron pipes

4.2.1 Recent failures of large-diameter cast iron pipes

Seven recent failures of CI trunk mains with the major failure mode of longitudinal barrel fracture were investigated. In these pipe specimens, limited corrosion damage was observed in the internal pipe surfaces due to the installation of cement lining. Substantial corrosion patches were observed in external pipe surfaces, and these corrosion patches act as stress concentrators in pipe barrels.

Most of these cases showed certain evidence of LBB, and the background information of the failures is summarised in Table 4-1.

4.2.2 Detectable leaks

In some failure cases, the evidence of water leakage prior to catastrophic bursting was reported to the local utilities. In Case 4, a leak event with a leak rate of 50 litters per minute was found 12 days before the burst, on the basis of water flow pattern analysis. Similarly, a water leak in Case 2 was reported about one month before the burst event. Therefore, a water leak is likely to be detectable several weeks before the pipe bursts, dependent on the resolution of leak detection techniques.

4.2.3 Dual corrosion phases

Different corrosion products generated in the major fracture surface can indicate the occurrence of multiple failure processes in CI pipes, which have been documented in recent case studies (Cullin et al., 2014; Makar, 2000; Rajani et al., 2012). Areas with black or brown corrosion products are likely to indicate the locations of through-wall crack initiation. Orange-coloured products tend to appear on fresh fracture surfaces, which are normally generated after a catastrophic burst. The position of through-wall crack initiation and propagation stages can be revealed from the dual-corrosion phases along with the change of corrosion patch configuration.

4.2.4 Extensive transient event before burst

The occurrence of extensive transients may result in a direct catastrophic failure; however, a time gap between the extensive transient and final burst was recorded in some failure cases. For example, a dramatic transient event (pressures ranging from 50 to 1,100 kPa) in Case 3 was recorded two weeks prior to the subsequent burst event. A sub-critical crack may have been initiated by the transient event, and then the crack may have propagated to a critical length during the time window before the burst. This dramatic transient event is considered to have been caused by uncontrolled pump or valve operation in nearby high-rise buildings. The time gap between the extensive transient and burst also indicated the existence of an LBB time window.

Table 4- 1 Failure cases of CI trunk mains with longitudinal fractures

Case	City	Burial	Failure	Diameter, (*mm*)	Thick -ness, (*mm*)	Burial depth, (*m*)	Cement lining	Backfill	Traffic
1	Newcastle	1957	2013	300	15	0.6	Factory	Clay	No
2	Sydney	1961	2013	500	15	1.6	Factory	Sand	Arterial
3	Melbourne	1868	2014	250	16	0.9	In-situ	Natural soil	High- way
4	Melbourne	1976	2014	300	13	0.8	Factory	Natural soil	Foot path
5	Melbourne	1938	2014	375	20	3.0	Factory	Natural soil	Minor road
6	Melbourne	1976	2015	300	15	1.0	Factory	Natural soil	Arterial
7	Sydney	1954	2015	500	17	1.5	Factory	Natural soil	Minor road

4.2.5 Evidence of LBB in recent failures

The relevant evidence of LBB from recent large-diameter CI pipe bursts is summarised in Table 4-2. The evidence of a detectable leak before a burst is able to directly prove the existence of a LBB time window in CI pipes. Nonetheless, leak detection techniques are not widely adopted by these water utilities. Indirect LBB evidence, such as dual corrosion phases and extensive transient before burst, can also confirm in some cases that the burst event is a result of crack propagation.

Table 4- 2 Summary of field evidence of LBB in cast iron pipes based on forensic analyses

Case	Detectable/observed leak	Dual corrosion phases	Extensive transient before burst	Corrosion patch in barrel
1				✓
2[1]	✓	✓		
3		✓	✓	✓
4		✓	✓	✓
5	✓			✓
6				✓
7				✓

1. Case 2 pipe contained a pre-crack in the barrel socket previously covered by the adjacent bell joint.

4.3 Stress concentration in cast iron pipes

4.3.1 Corrosion patch

CI pipes were designed with sufficient safety factors to allow any future corrosion damage and uncertainties in estimated design parameters (Rajani and Abdel-Akher, 2012), which means that the original wall thickness is adequate to resist operating pressures at the design stage. A substantial corrosion patch might be formed by coalesced corrosion pits caused by soil corrosion, and the significant stress concentration generated in such patches (Rajeev et al., 2014). As shown in Table 4-2, the presence of a corrosion patch is the most common and most critical stress concentration mode in CI water pipe barrels.

According to ASME-B31G (2009) and API-579 (2016), corrosion patch configurations can be approximated by an elliptical geometry with three basic parameters: *2a* (patch length in longitudinal direction), *2b* (patch length in hoop direction) and *c* (depth of corrosion), as shown in Figure 4-1. The nominal hoop stress and maximum stress in the centre of the patch base are expressed in Equations 2.4 and 4.1, respectively (Ji et al., 2015). The stress concentration factors (SCFs) were obtained from Zhang et al. (2017), based on finite element (FE) simulations verified by full-scale bursting tests. The present project focuses on pipe barrel failure induced by corrosion patches, and an explanation of other failure modes and mechanisms is briefly discussed in Chapter 2.

$$\sigma_c = SCF\ \sigma_h \tag{4.1}$$

where, σ_h is the nominal hoop stress, SCF is the stress concentration factor, which depends on corrosion patch geometry and pipe dimensions, and σ_c is the hoop stress in the corrosion patch centre.

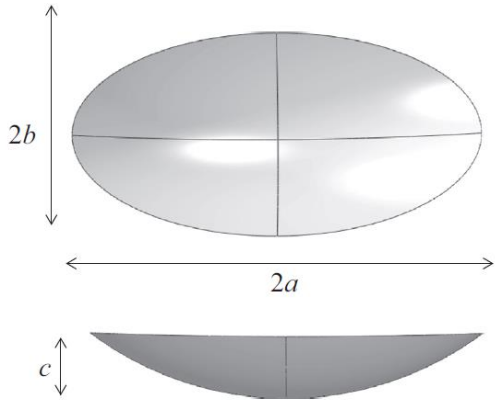

Figure 4- 1 Conceptual diagram of pipe section containing circular perforation

4.3.2 Corrosion perforation

Corrosion perforations are commonly observed in ageing CI pipes caused by soil pitting corrosion. These perforations, which normally have a circular shape and a relatively small through-wall diameter, are plugged by corrosion graphitization and cement lining (Robert et al., 2016a; Romanoff, 1957). The stress concentration factor for the edge of a through-wall hole in a pressurised pipe is expressed in Equations 4.2- 4.4 (Pilkey and Pilkey, 2008). Figure 4-2 shows a conceptual diagram of a pipe section containing a circular perforation.

$$\sigma_{c,t} = SCF_t \, P \frac{D_i}{2t_o} \tag{4.2}$$

$$SCF_t = \begin{cases} 2.5899 + 0.8002\beta + 4.0112\beta^2 - 1.8235\beta^3 + 0.3751\beta^4 \ (0 \le \beta \le 2) \\ 8.3065 - 7.1716\beta + 6.7\beta^2 - 1.35\beta^3 + 0.1056\beta^4 \ (2 < \beta \le 4) \end{cases} \tag{4.3}$$

$$\beta = \sqrt[4]{\frac{3(1-\nu^2)}{2}} \left(\frac{r_t}{\sqrt{R_i t_o}}\right) \tag{4.4}$$

where, SCF_t is the stress concentration factor for a pipe with a circular perforation, $\sigma_{c,t}$ is the stress around the perforation, ν is the Poisson's ratio, β is a shape factor, R_i is internal pipe radius, and r_t is perforation radius.

Corrosion perforations were revealed in the pipe barrels of Case 3 and Case 5 after sand-blasting. The through-wall corrosion pits were previously preserved in corrosion products (graphitization), and these perforations did not cause major longitudinal fractures. Water leaks did not occur in these perforations due to the integrity of the internal cement lining and graphitization.

As shown in Figure 4-3, four perforations were observed in Case 3. The largest perforation has a diameter of 20 mm, which causes a stress of 24 MPa under the internal pressure of 1.1 MPa based on Equations 4.2 – 4.4. These results indicate that corrosion perforations with a diameter of 20 mm or less in CI pipe barrels are unlikely to result in catastrophic fracture or even a leak.

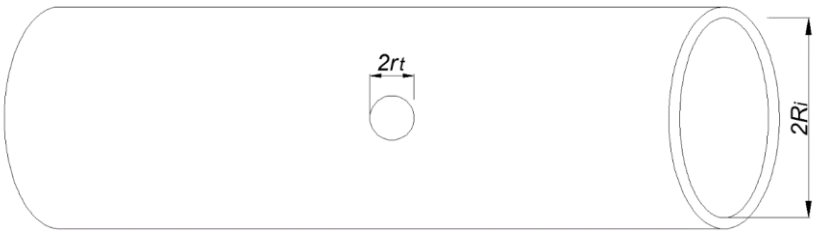

Figure 4- 2 Conceptual diagram of pipe section containing circular perforation

(a)

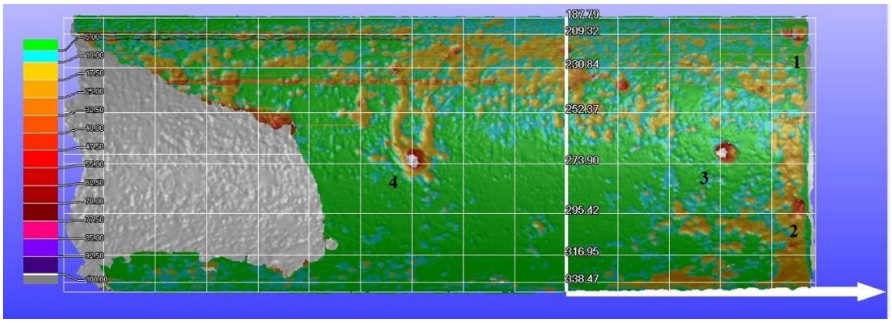

(b)

(c)

(d)

Figure 4- 3 CI water main (Case 3) containing corrosion perforations: (a) after sand-blasting; (b) scanning image; (c) Perforation 3; (d) Perforation 4

4.3.3 Pre-cracks

For large-diameter CI pipes, pre-cracks commonly located in the areas of bell-spigot joints are generated during construction, transportation, handling and installation processes (Rajani and Abdel-Akher, 2013; Rajani et al., 2013). These pre-cracks may propagate over the entire servicing period, depending on the initial crack length and the crack-driven mechanisms in the local network. Furthermore, in large diameter pipes, any ground movement can translate to joints due to the high moment of inertia against bending of the pipe barrel. However, leakage can occur when joints become loose or cracks become significant. A case study of a 500 mm diameter CI failure (Case 2) due to a pre-crack is presented in Chapter 7.

4.3.4 Defects

Manufacturing defects are not uncommon in CI pipes produced by early casting methods due to poor cooling control. These defects causing inherent voids or de-bonding interfaces are shown in Figures 4-4 (a) and (b), respectively.

The dimensions of these defects can be described as elliptical embedded cracks with the following parameters: length in longitudinal direction ($2a_e$), and depth in wall thickness direction (c_e). The maximum dimensions of defects recorded in this study are 32 × 6 mm in Case 5, as shown in Figure 4-2 (b).

The analytical solutions of critical pipe pressures for CI pipe barrels with external and internal surface cracks are expressed in Equations 4.5 and 4.6, respectively (Al Laham, 1998). The critical pressure for the largest defect is 9.2 MPa, which is much higher than the maximum operational pressure of 0.9 MPa recorded in Case 5. The measured dimensions of the pipeline from Case 5 were adopted.

$$P_{L,external} = \sigma_u \frac{2t_0}{D_i}\left(1 - \frac{2a_e c_e}{t_0(2a + 2t_0)}\right) \tag{4.5}$$

$$P_{L,internal} = \sigma_u \left(\frac{2c_e}{D_i\sqrt{1 + \frac{3.22\, a_e^2}{D_i c_e}}} + \left(\frac{D_i}{2\left(\frac{D_i}{2} + c_e\right)}\right)\ln\left(\frac{D_i + 2t_0}{D_i + 2c_e}\right)\right) \tag{4.6}$$

where, $P_{L,external}$ is the limiting pressure for pipelines with an external surface crack, σ_u is the ultimate tensile strength of piping material, a_e is half of the embedded crack length in longitudinal direction, c_e is the embedded crack depth in thickness direction, and $P_{L,internal}$ is the limiting pressure for pipeline with an internal surface crack.

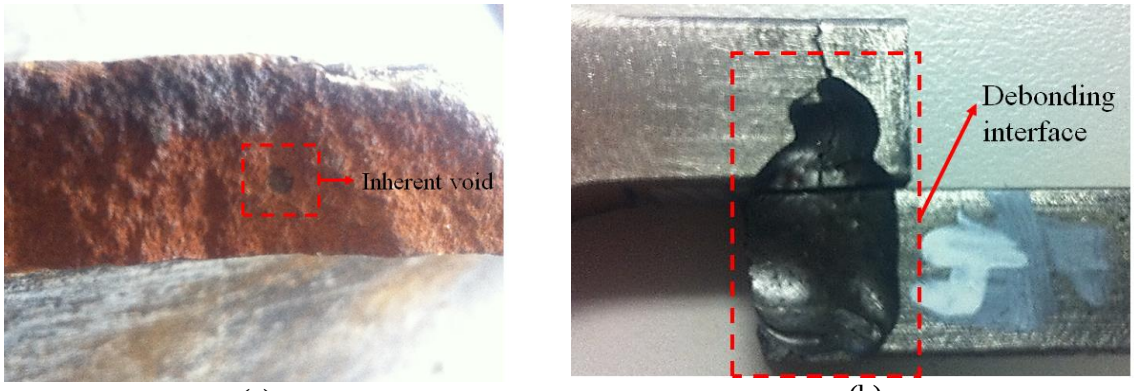

(a) (b)

Figure 4- 4 Manufacturing defects in CI pipe (Case 5): (a) inherent void; (b) de-bonding interface in metallic piping material

4.4 Experimental evidence and LBB criteria for cast iron pipes

4.4.1 Full-scale burst tests under static pressure

A pipe bursting facility (Figure 4-5) was established to evaluate the remaining strength of corroded CI trunk mains under static pressure. The static bursting set-up has three major components: a pipe containment system with steel plates and tension bars; a pumping system including a high-pressure hose, a pressure regulator and a pressure amplifier; and an instrumentation system to measure the pressure and strain changes. The pressure is gradually supplied to each pipe specimen, and the leak pressure (P_{leak}) and maximum achieved pressures (P_m) are recorded for each test. Detailed information on the bursting facility and experimental approach is presented in Rathnayaka (2016). The testing results are summarised in Table 4-3. The data on initial crack length ($2a_i$) generated by the leak pressure are shown in Table 4-3 with the corresponding wall thickness in the initial crack tips (t_i). The crack length on the external pipe surface is measured using a portable Dino-Lite digital microscope.

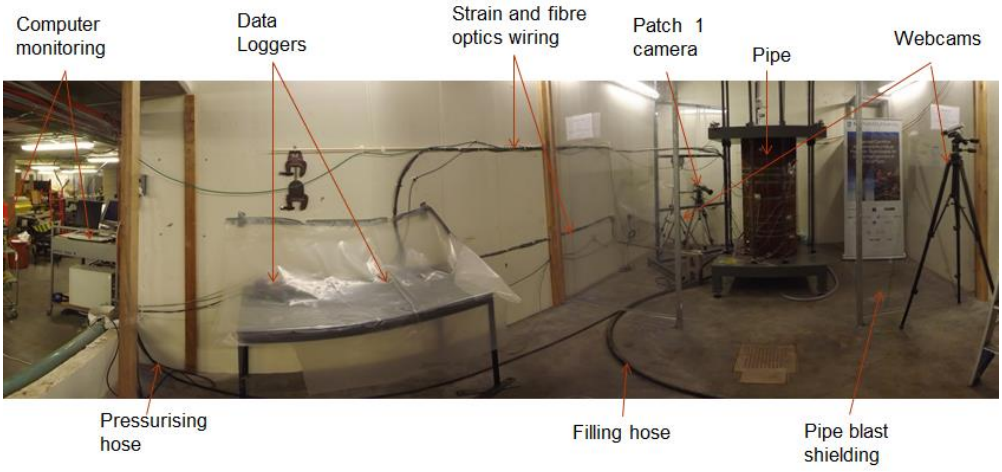

Figure 4- 5 Full-scale burst facility for CI trunk mains

Table 4- 3 Summary of bursting test results

Pipe	Patch	t_o (mm)	2a (mm)	2b (mm)	c (mm)	P_{leak} (MPa)	$2a_i$ (mm)	t_i (mm)	P_m (MPa)
1	Natural-1	25	125	93	17.9	3.5	24	11	3.6
1	Natural-2	25	300	370	18.5	3.3	15	12	3.6
2	Circular	25	190	190	19.9	3.2	90[1]	10.5	3.7
3	Elliptical	17	330	100	13	1.3	-	-	1.4
4	Elliptical	18	400	160	14.5	1.2	4	4.5	1.3

1. Crack length was measured under a pressure of 2.85 MPa.

4.4.2 Leak criterion

4.4.2.1 Initiation of a through-wall crack

A through-wall crack is considered to initiate when the localised stress in the patch base exceeds the material tensile strength (Equation 4.8). The stress solution (Equations 4.1, 4.2, 4.8) can predict the initiation of a leak in the corrosion patch base. The initial leak may occur at lower pressures than the pressure estimated by Equations 4.1, 4.2 and 4.8 in the presence of manufacturing defects or small deep pits in large corrosion patches. Alternatively, a through-crack may also be generated under cyclic pressures with a lower pressure level. This hypothesis of fatigue-induced leaks is detailed in Chapter 5.

$$\sigma_c \geq \sigma_u \tag{4.8}$$

where, σ_c is the stress in the corrosion patch centre, and σ_u is the material tensile strength.

4.4.2.2 Estimation of through-wall crack length

Localised failure typically occurs in a corrosion patch base. The crack tips can be arrested within the thicker ligaments of the corrosion patch, due to the significantly varying stress distribution in the corrosion patch and stress reducing below the tensile strength at the crack tip. The approximate initial crack length ($2a_i$) in the corrosion patch is shown in Figure 4-6. The stress solution for uniform-walled pressurised tubes with axial through-cracks is adopted to estimate the initial crack length. This solution is given in Equations 4.9- 4.11 (Al Laham, 1998). If the stress at the crack tips is above the material strength, a through-crack can generate further extension of the crack. This explanation is based on the cohesive crack model of crack extension, where tensile strength is used as the limiting criterion for crack extension (Anderson, 2005). In LEFM however, fracture toughness will be used to detect crack extension.

$$\lambda_i = \frac{a_i}{\sqrt{R_i\, t_i}} \tag{4.9}$$

$$\sigma_{n,i} = P\ \frac{R_i}{t_i} \tag{4.10}$$

$$\sigma_i = \sigma_{n,i}\sqrt{1 + 1.05\lambda_i^2} \leq \sigma_u \tag{4.11}$$

where, a_i is half of the initial through crack, t_i is the wall thickness in the tips of the initial crack, λ_i is a geometric parameter for pressurised pipes with an initial through crack, $\sigma_{n,i}$ is the nominal stress for pipes with an initial crack, and σ_i is the stress in the crack tips of an initial crack.

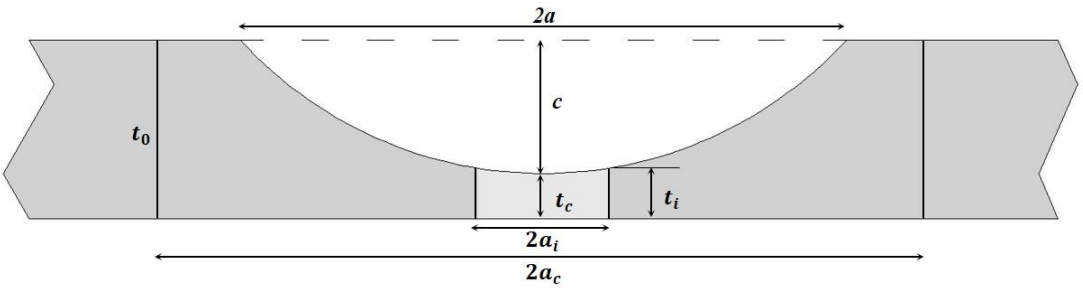

(a)

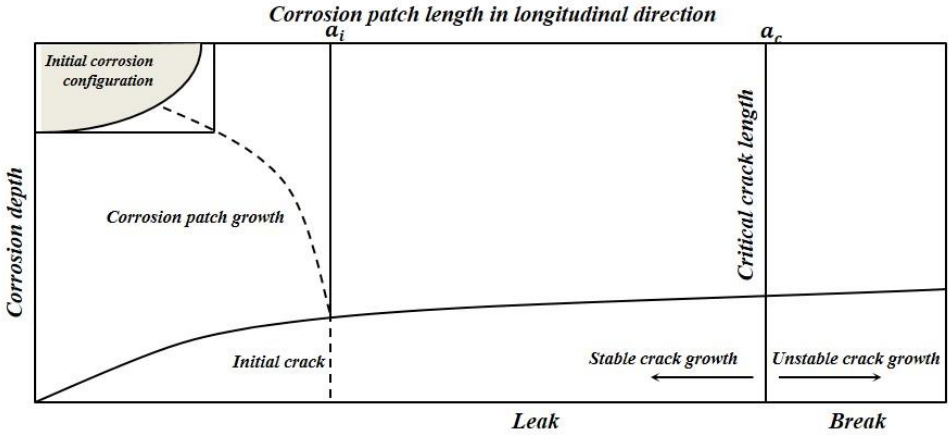

(b)

Figure 4- 6 (a) Sketch of elliptical corrosion patch (b) LBB conceptual diagram for cast iron water trunk mains with an external corrosion patch

4.4.3 Break criterion: critical crack length using LEFM

According to linear elastic fracture mechanics (LEFM), the stress intensity factor in a pressurised pipe (K_I) with a longitudinal crack (see Figure 4-7) can be calculated using Equations 4.12- 4.15 (Tada et al., 2000). Stress intensity rises with crack growth until the crack reaches the critical length ($2a_c$). For pressurised large-diameter pipes, a break occurs when the stress intensity (K_I) reaches the material fracture toughness (K_{IC}) as shown in Equation 4.15. For corroded CI pipes, the upper limit of critical crack length can be determined by the equations established for uniform-walled pipes (Equations 4.12-4.15). The values of fracture toughness are based on mechanical tests and full-scale tests in the research literature. Hence, the critical crack length is mainly controlled by the fracture toughness of the material, the pipe dimensions and the internal pressure. However, this analysis does not consider the presence of a patch. Nonetheless, it gives an upper bound estimate of the critical length required for break occurrence, since if the fracture could grow spontaneously in a pipe with nominal wall thickness it would certainly grow in a patch area with reduced wall thickness. Furthermore, in some cases, the critical crack length would be larger than the corrosion patch length and the crack would need to grow in a pipe section with nominal thickness and this in this situation, this solution is directly applicable.

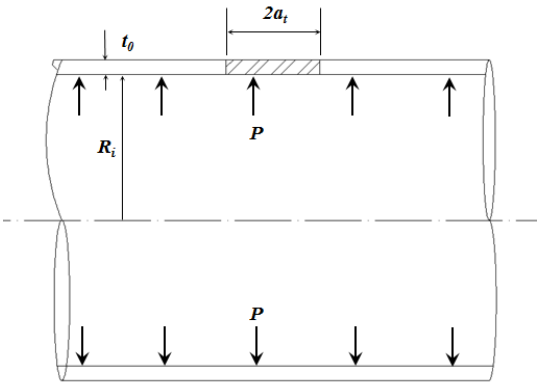

Figure 4- 7 Pressurised tube structures containing longitudinal crack (Tada et al., 2000)

$$\lambda = \frac{a_t}{\sqrt{R_i\, t_0}} \tag{4.12}$$

$$F(\lambda) = \begin{cases} \sqrt{(1 + 1.25\lambda^2)} & 0 < \lambda \leq 1 \\ 0.6 + 0.9\lambda & 1 < \lambda \leq 5 \end{cases} \tag{4.13}$$

$$K_I = \sigma_n \sqrt{\pi a_t}\, F(\lambda) \tag{4.14}$$

$$K_I \geq K_{IC} \tag{4.15}$$

where, a_t is the half of the total through-wall crack length, R_i is internal radius, λ is a geometric parameter for pressurised pipes with a through crack, $F(\lambda)$ is a geometric factor for evaluating intensity factors in cracked pipes, K_I is intensity factor, and K_{IC} is fracture toughness.

4.4.4 Leak rates

The crack opening area (A_c) and leak rate (Q_c) can be estimated for the corresponding critical crack length ($2a_c$). LBB analysis is only applicable when the critical leak rate is above a threshold detectable leak flow rate (API-579, 2016; BS-7910, 2005).

The leak rate is strongly affected by crack length and internal pressure. An analytical solution is proposed to calculate the leakage rates. The crack opening area for different crack lengths can be estimated by linear elastic correlations, as shown in Equations 4.16 and 4.17 (Tada et al., 2000). The leak rates can be calculated by the simplified formula given in Equation 4.18 (Cassa et al., 2010).

$$G(\lambda) = \begin{cases} \lambda^2 + 0.625\lambda^4 & 0 < \lambda \leq 1 \\ 0.14\lambda + 0.36\lambda^2 + 0.72\lambda^3 + 0.405\lambda^4 & 1 \leq \lambda \leq 5 \end{cases} \tag{4.16}$$

$$A = \frac{2\pi R_i^2 P\, G(\lambda)}{E} \tag{4.17}$$

$$Q = C_d A\sqrt{2P} \tag{4.18}$$

where, t_t is the corresponding wall thickness in the crack tips, $G(\lambda)$ is the geometric factor for crack opening area, A is the crack opening area, P is the internal pressure, E is the modulus of elasticity, Q is the leak rate, and C_d is the discharge coefficient, 0.67 is used for a longitudinal crack in CI pipes (Cassa et al., 2010).

4.4.5 Validation of LBB criteria for large-diameter cast iron pipes

4.4.5.1 Validation of leak criterion

The experimental results and analytical solutions for burst tests are summarised in Table 4-4. The leak criterion is verified by the results of analytical solutions based on Equations 4.1, 4.2 and 4.8, which indicate that the actual stress in the corrosion patch centre is above the material tensile strength measured by direct tension mechanical tests (detailed in Chapter 3).

The stress solution (Equations 4.9- 4.11) was used to estimate the approximate length of the initial crack ($2a_i$) in pressurised CI pipes. The results of dimensional analysis are plotted in Figure 4-8, on the basis of the measured crack lengths and the corresponding water pressures (Table 4-3). The tensile strength of 110 MPa was used to calculate the curve of the limit load solution in Figure 4-8.

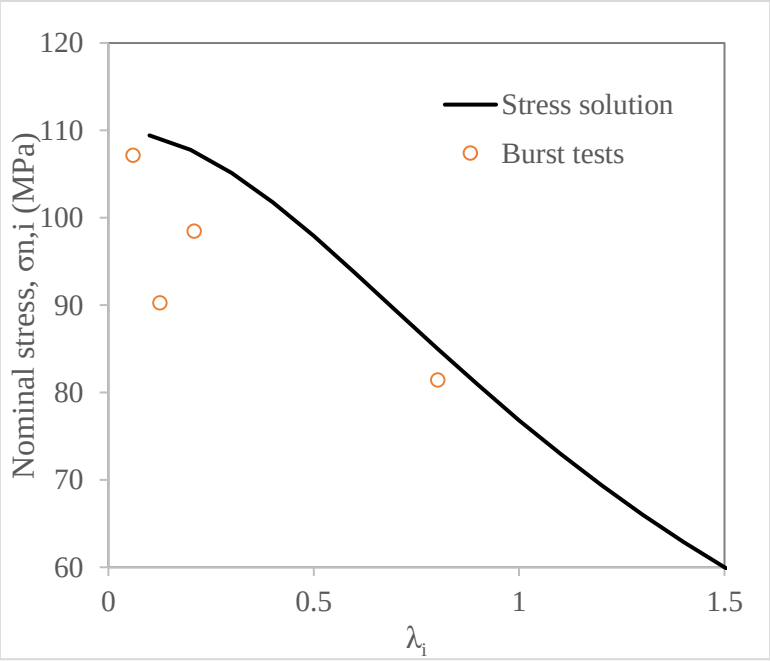

Figure 4- 8 Dimensionless analysis of crack tip stress of pressurised pipe with longitudinal crack

4.4.5.2 Validation of break criterion

The LEFM solution, expressed in Equations 4.12- 4.14, was adopted to evaluate the burst pressures of pipes containing a longitudinal crack, and the fracture toughness of 15 MPa m was selected to determine the break criterion. Figure 4-9 shows the burst pressures for a 600 mm diameter CI pipe with different crack lengths. As shown in Table 4-3, the nominal wall thickness of pipe specimens is either 18 (17) or 25 mm. Following the BS-78 (1938) pipe class classifications, Class A (18 mm) and C (25 mm) were analysed for pit-cast CI pipes 600 mm in diameter. Leaking CI pipes can withstand substantial pressure, mainly dependent on the crack length. The break criterion is also affected by the corrosion patch configuration in the longitudinal direction, when the length of corrosion patch (*2a*) is equal to the critical crack length calculated by the nominal wall thickness and fracture toughness.

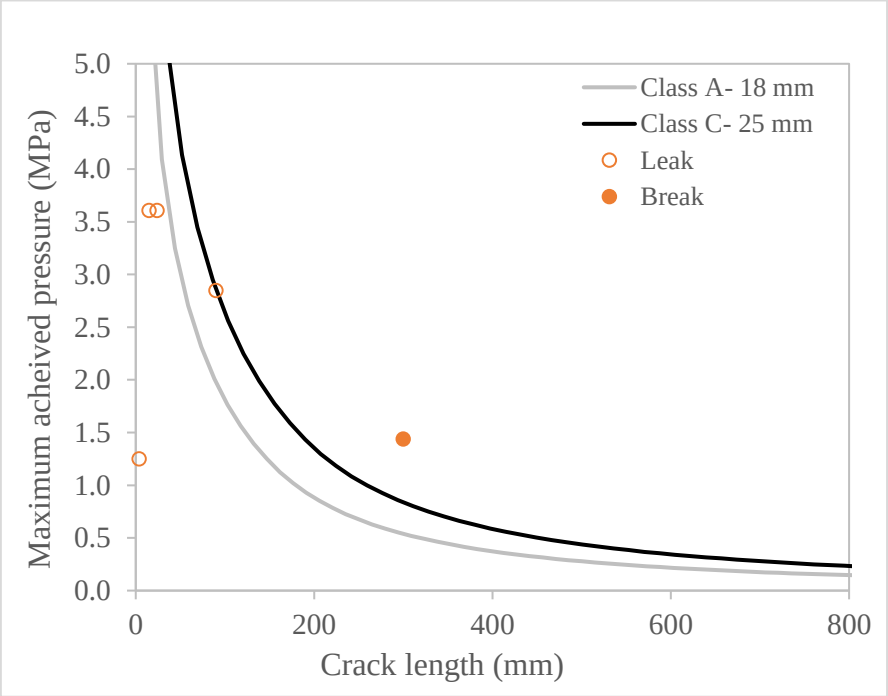

Figure 4- 9 Burst pressures for 600 mm CI pipes containing a longitudinal crack

Table 4- 4 Summary of testing results and comparisons with analytical solutions

Pipe	Test result	Leak criterion		Break criterion			Analytical solution
		Stress (*MPa*)	Solution	Measured crack (*mm*)	Critical crack (*mm*)	Solution	
1[1]	Leak	130	Leak	24	65	Leak	Leak
1[2]	Leak	164	Leak	15	65	Leak	Leak
2	Leak	161	Leak	90	91	Leak	Leak
3	LBB	110	Leak	330*	122	Break	LBB
4	Leak	107	Leak	4	141	Leak	Leak

1. Natural patch 1
2. Natural patch 2

4.4.5.3 Analytical solution of leak rates

The leak rates were evaluated using Equations 4.16- 4.18 and the results plotted in Figure 4-10. A modulus of elasticity of 100 GPa and a discharge coefficient of 0.67 were used for leak rate analysis (Cassa et al., 2010). The selected value for the modulus of elasticity matches the common range of CI properties (see Figure 3-3(b)). The leak rates for critical crack lengths were evaluated to validate the LBB concept using Equations 4.1 and 4.12- 4.15. The fracture toughness of 15 MPa m was used to estimate the critical crack length, and the corresponding critical crack opening area and critical leak rates were calculated using Equations 4.16- 4.18 for 600 mm-diameter CI pipes with different wall thicknesses. The critical leak rates under different pressures (300 to 1,200 kPa) are plotted in Figure 4-10 for the four wall classes listed in the BS-78 (1938). The relevant design pressures are also shown in Figure 4-10. Since the operating pressures in aged water networks might have been altered due to the development and rearrangement of urban water supply systems, the designation of wall thickness on the pressure class may not always be applicable. The critical leak rates plotted in Figure 4-10 appear to conservatively predict the actual leak rates. However, the minimal critical leak rate is still over 20 L/min for Class A pipe under a pressure of 1.2 MPa, which indicates the critical leak rate is generally detectable using the general leak detection methods listed in Table 2-9.

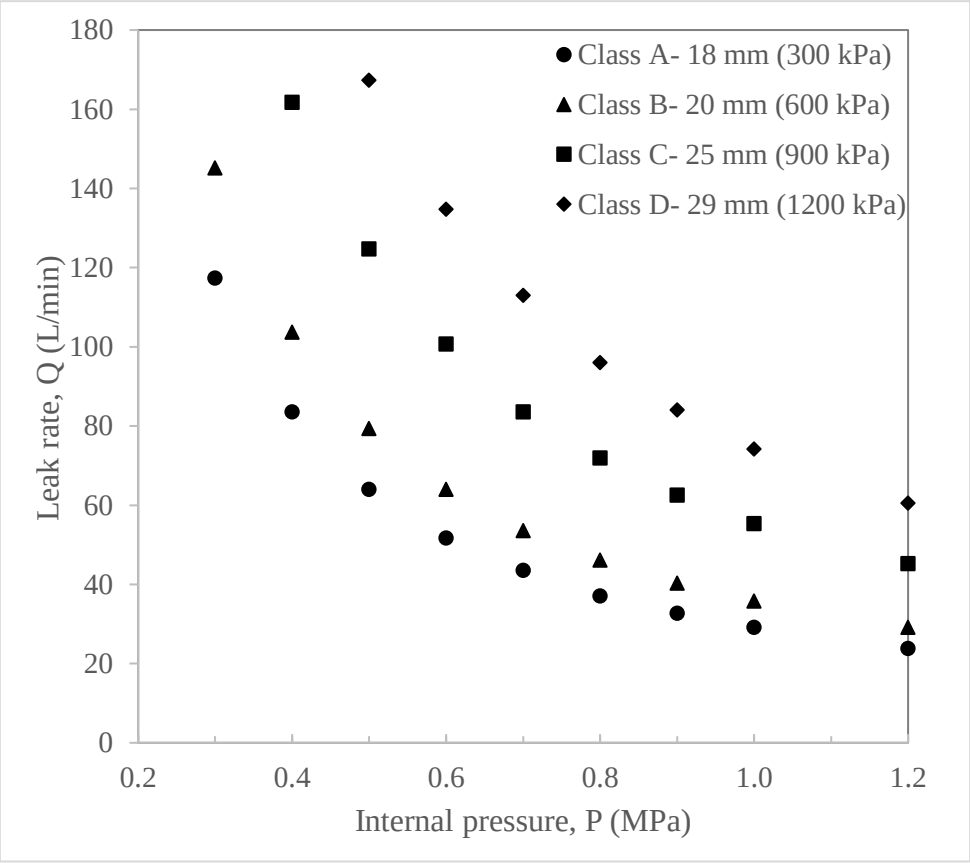

Figure 4- 10 Minimum leak rates for critical crack lengths under normal operating pressures

4.5 LBB assessment procedures for large-diameter cast iron pipes

The standard procedure for using the typical LBB concept involves the presence of longitudinally-oriented surface cracks in pipes or vessels (API-579, 2016; BS-7910, 2005). The surface crack may grow both across the pipe wall and in pipe longitudinal directions following relevant crack growth mechanisms (i.e. fatigue by cyclic pressure) until a through-wall crack is generated to allow a substantial leak before catastrophic failure. A sufficient LBB time window between the detectable leak and the break is required in order to use the LBB concept for failure prevention. The prerequisites of the LBB criterion in API-579 (2016) include: (1) Evaluation of initial flaw size and ensuring that the break will not occur under operating situations, (2) Estimation of the critical crack length that causes a break; (3) Calculation of crack opening area (COA) for critical crack lengths; (4) Prediction of leak rates for critical cracks and ensuring that the leak is detectable by detection tools.

Based on field and experimental observations, longitudinal barrel fractures in large-diameter CI pipes show a leak tends to occur before catastrophic burst, mainly due to the stress concentrations from coalesced pitting or patch corrosion that occurs in underground metallic corrosion. The LBB criterion verified by experimental results and analytical solutions is proposed for large-diameter CI pipes. Table 4-5 summarises the differences of the LBB concept in the standard approach and in large-diameter CI water pipes. In comparison with the existing LBB standards (API-579, 2016; BS-7910, 2005), a series of LBB assessment procedures are illustrated in Figure 4-11.

Table 4- 5 Comparison of LBB assessment procedures in CI water pipes and standardised approach for ductile metals

Phases	Standardised LBB approach	LBB in CI pipes
Initial deterioration	Postulated surface flaws	Coalesced pitting or patch corrosion
Leak initiation	Surface flaws grow to a critical depth in thickness direction	Corrosion progression and stress-induced localised failure
Initial crack length	Flaw length after breakthrough	Length of corrosion patch base
Propagation of a through-crack	Increase of intensity factor	Change of intensity factor
Break- critical crack length	Dependent on fracture toughness and nominal hoop stress	Dependent on fracture toughness and local stress distribution
LBB time window	Crack growth mechanisms	Crack growth mechanisms and stress distribution in a corrosion patch

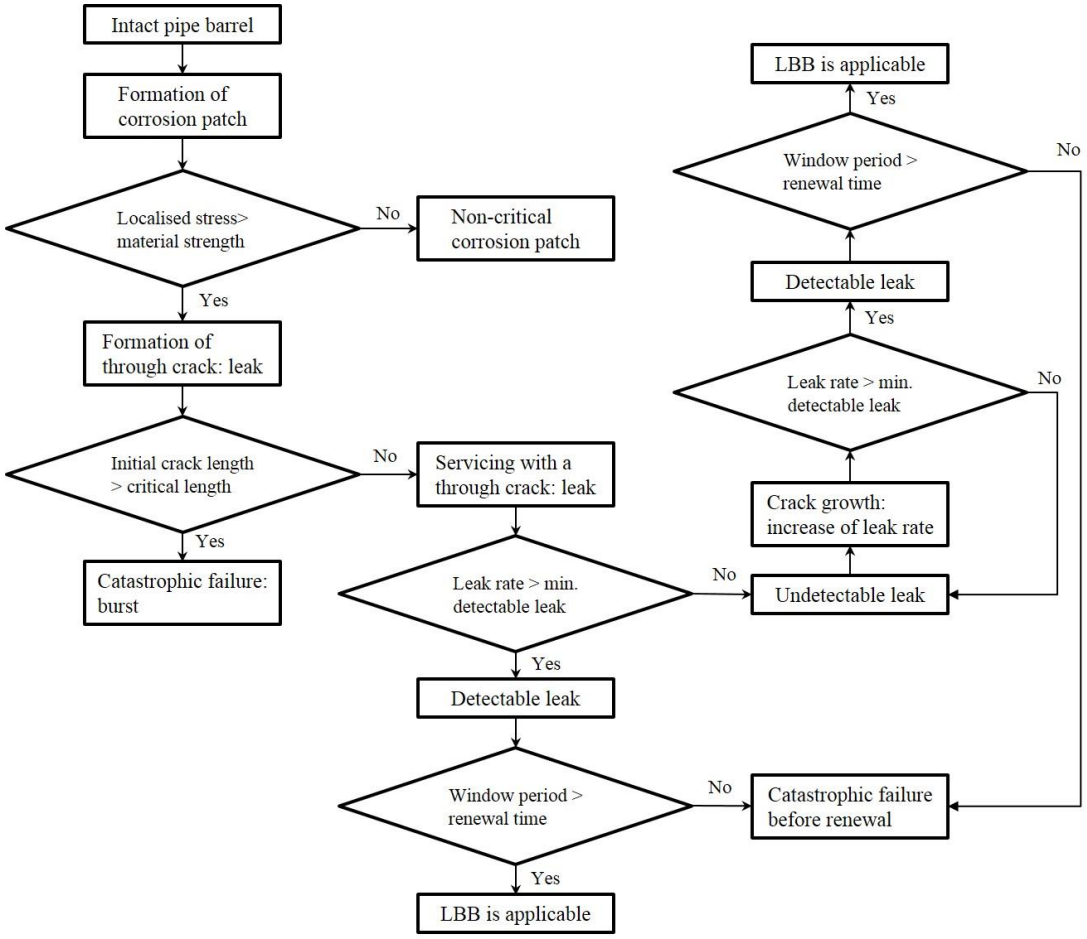

Figure 4- 11 Proposed leak-before-break procedure for cast iron trunk mains failed by a longitudinal fracture based on Rathnayaka et al. (2017b))

4.6 LBB analysis and failure processes in small-diameter cast iron pipes

4.6.1 Background

One of the key issues in LBB analysis is the investigation of the corrosion condition of CI pipes. Most CI water pipes were buried in natural soils without effective coatings, and the common soil corrosion mode, pitting corrosion, tends to produce local metal losses and reduce structural capacity (Rajani, 2000). Correlations between corrosion depths and fracture stresses have been investigated for both static and spun CI pipe specimens (Antaki, 2003; Atkinson et al., 2002; Gould, 2011; Rajani, 2000; Yamamoto et al., 1983).

Bending loads, another important contribution to circumferential fracture failures, are mainly induced by external factors, including ground movements, traffic loads and temperature changes (Rajani, 2000). Of these factors, thermal stress is generally insignificant for Australian cities, due to the moderate changes of underground temperatures (Chan et al., 2015b), and traffic loading tests indicate a relatively minor effect of traffic loads in CI pipes (Chan et al., 2016b). Hence, the seasonal swelling/shrinking behaviour of reactive soils and different ground conditions in pipe trenches are the predominant causes of bending loads for CI pipes (Gould, 2011; Weerasinghe et al., 2015). The nominal (without corrosion pits or patches) bending soil stresses range from 20 to 30 MPa obtained from site measurements (Chan et al., 2015b) and simulation models developed under the Smart Water Fund (SMF) in the Melbourne region (SWF, 2017). The bending stresses in pipe barrels are located in either the pipe crown or base due to seasonal ground movements. An example of typical pipe bending stress variations in a selected suburb is presented in Figure 4-12 (SWF, 2017).

This section evaluates the failure processes of circumferential fractures in CI pipes for recent failures. A crack initiation criterion is proposed using the limit stress method, and the residual strength of pipes containing a circumferential crack is evaluated using linear-elastic fracture mechanics (LEFM). The applicability of the LBB concept for maintaining and replacing small-diameter CI pipes is proposed.

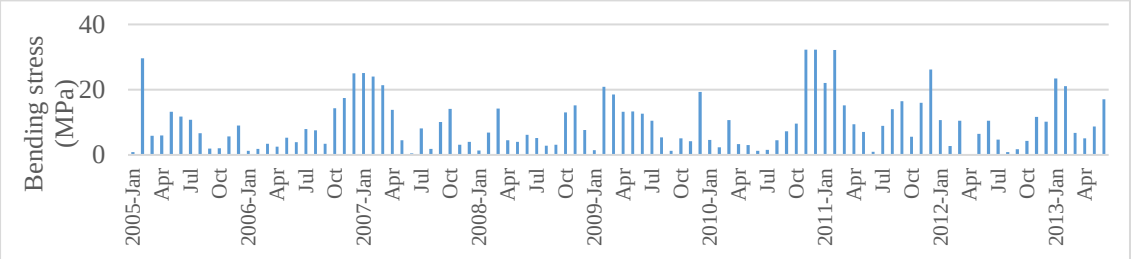

Figure 4- 12 Typical pipe bending stresses due to ground movement in Altona North, Melbourne (SWF, 2017)

4.6.2 Methods and materials

4.6.2.1 Circumferential barrel fracture

Between 2014 and 2017, ten failure cases of CI pipes were collected for failure analysis. Most of these pipes had previously leaked (Figure 4-13 (a)) and were repaired using tightened clamps (Figure 4-13(b)). The background information is shown in Table 4-6.

The nominal thickness (t_0) and diameter (D_i) were measured, and the corrosion products were removed by low-speed sand blasting. The corroded metallic surfaces were recorded using a three-dimensional (3-D) Creaform laser scanner. The wall thickness changes along the major fracture surface were analysed based on 3-D scanning data. The circumferential crack opening angles (2θ, shown in Figure 4-14) were obtained by measurement or site pictures.

Table 4- 6 Summary of CI pipe failures

ID	D_i (mm)	Location	Depth (m)	Construct-ion	Leak[1]	Replacing [2]	Failure mode	2θ
1	100	Driveway	0.95	1973	05/2016	-	Leak	180
2	100	Natural strip	0.90	1966	05/2016	-	Leak	160
3	100	Natural strip	0.95	1973	08/2006	03/2017	LBB	-
4	150	Minor road	0.85	1958	03/2017	-	Leak	140
5	100	Driveway	0.45	1960	03/2017	-	Leak	150
6	100	Driveway	0.85	1960	03/2017	-	Leak	70
7	100	Minor road	0.60	1958	03/2017	-	Leak	85
8	150	Driveway	0.90	1967	05/2014	06/2014	Leak	220
9	100	Driveway	0.90	1959	12/2009	06/2014	Leak	300
10	100	Driveway	0.75	1929	02/2003	06/2014	LBB	-

1. Leaking time refers to the first site inspection or installation of tightened clamps.
2. Some repaired pipes are still in service.

(a) (b)

Figure 4- 13 (a) Leakage of a 100 mm-diameter CI pipe through a circumferential crack; (b) Tightened clamp in a leaking CI pipe

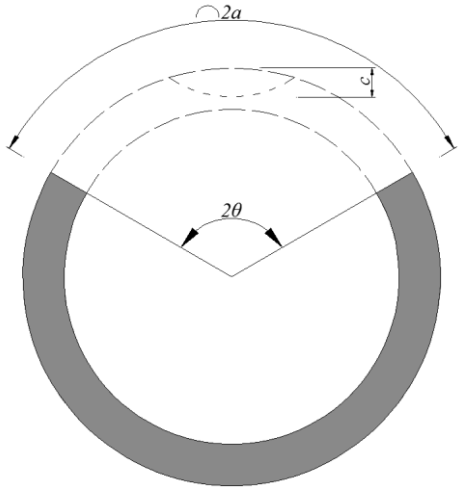

Figure 4- 14 Pipe containing a circumferential crack

4.6.2.2 Leak criterion

Leakage in corrosion pits is controlled to a large extent by the corrosion depth. The linear relationship between corrosion depth and remaining strength (Equation 4.19) was investigated using mechanical tests of corroded specimens (Rajani, 2000; Yamamoto et al., 1983). The minimum specified tensile strengths for static and spun CI pipes listed in BS-78 (1938) and AS-1724 (1975) are used in this analysis. The remaining strengths and corrosion depths are plotted in Figure 4-15(a).

The hoop stress induced by internal pressure for intact pipes is expressed in Equation 4.1. Equation 4.21 presents the condition when the circumferential crack is generated, i.e., the bending stress is equal to or higher than the hoop stress and the tensile strength of the CI pipe (Equations 4.20 and 4.21). For corroded pipes, a circumferential crack initiates when pipe stress is above the residual strength allowing for corrosion (Equation 4.21). The crack orientation is determined by the magnitudes of hoop and bending stresses.

Figure 4-15(b) shows the remaining strengths of corroded CI pipes in full-scale bending tests conducted by Atkinson et al. (2002). CI pipes containing through-wall corrosion pits are able to sustain a bending stress up to 100 MPa (Figure 4-15(b)), which indicates that the cracked pipes have remaining strength and localised failures occur before catastrophic breaks, justifying the possibility of LBB applicability.

$$\sigma_r = \sigma_u \left(1 - \frac{c}{t_0}\right) \tag{4.19}$$

$$\sigma_b > \sigma_n \tag{4.20}$$

$$\sigma_b \geq \sigma_r \tag{4.21}$$

where, σ_u is ultimate material tensile strength, σ_r is remaining strength, σ_h is hoop stress induced by internal pressure, c is corrosion depth, and σ_b is bending stress.

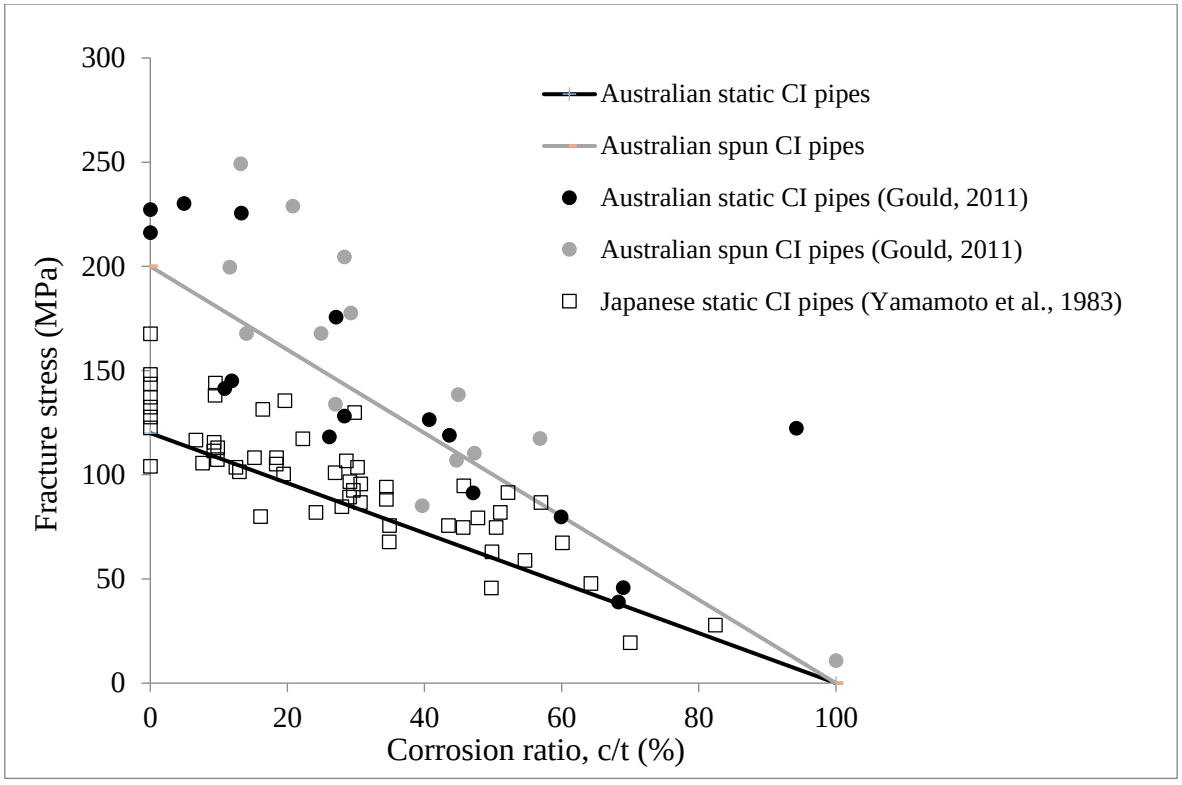

(a)

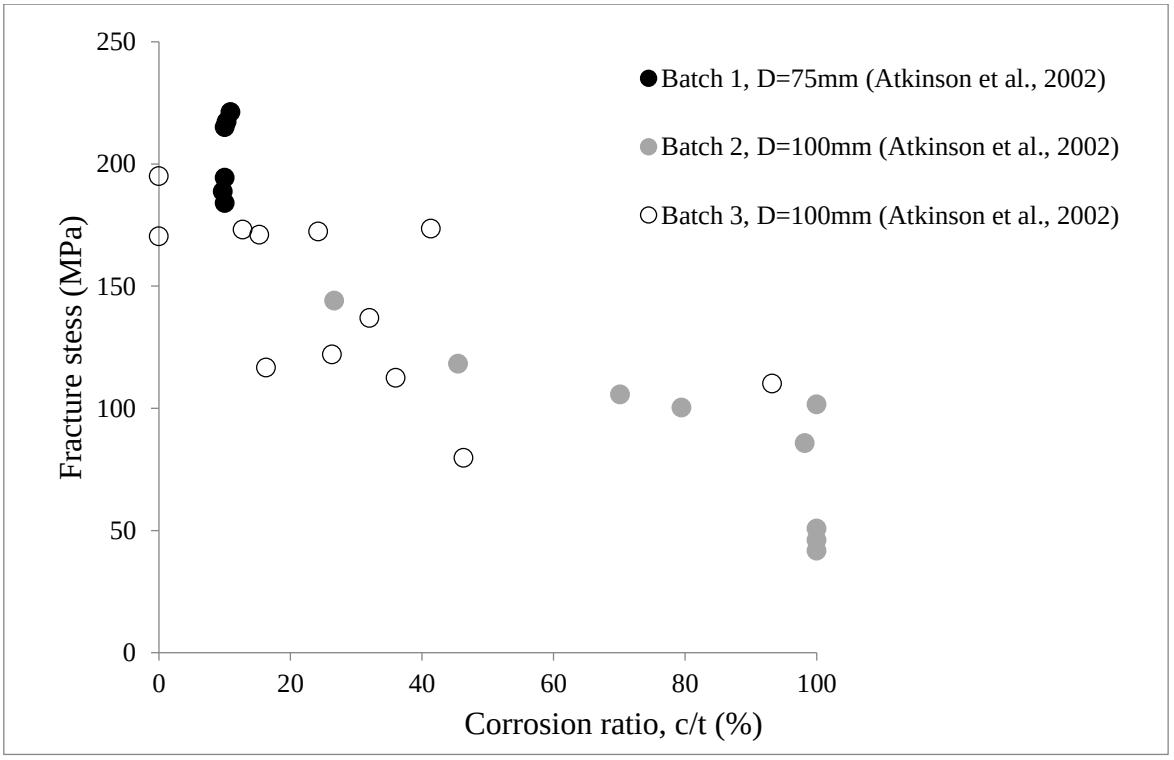

(b)

Figure 4- 15 Correlations between fracture stresses and corrosion ratios: (a) specimen tests; (b) full-scale bending tests

4.6.2.3 Break criterion

The break criterion of CI pipes containing a circumferential crack is controlled by bending stress, crack length and fracture toughness. The intensity factor is expressed in Equation 4.22, and the geometric factor is adopted from Tada et al. (2000) and Miedlar et al. (2002). The half-crack opening angle (θ) is demonstrated in Figure 4-14.

The fracture toughness of CI pipes can be determined by material and full-scale tests. The results of tests of single-edged notched-beam (SENB) specimens range from 15 to 27 MPa $m^{1/2}$ (Mohebbi et al., 2010), and full-scale bending tests provide higher values between 22 and 29 MPa $m^{1/2}$ (Conlin and Baker, 1991). Therefore, the value of 15 MPa $m^{1/2}$ is conservatively selected for evaluating the remaining strength of cracked CI pipes.

$$K_I = \sigma_s \sqrt{\pi a}\, F \tag{4.22}$$

where, K_I is intensity factor, a is half-crack length, F is geometric factor, and K_{IC} is fracture toughness.

4.6.3 Results and discussion

4.6.3.1 Failure analyses

The original wall thicknesses of the selected failure cases range from 9 to 11 mm, which match the archived standards BS-78 (1938) and AS-1724 (1975). The circumferential crack lengths account for 20- 60% of the entire perimeter when the leaking pipes were initially repaired. The cracks open to either pipe crown or base. Significant wall reduction is observed in the region of crack initiation, and the crack tips are arrested in the thick-walled areas (Figure 4-16).

Water leakage from a through-crack may be detectible when the backfill soil is fully saturated prior to a catastrophic break. A partial circumferential crack is easily repaired using screw-tightened clamps (Figure 4-13(b)). Field observations show that tightened clamps provide additional service life to leaking pipes without allowing breakages. However, corrosion rates in clamped sections are expected to rise and eventually cause breaks or capacity loss (see Cases 3, 9 and 10).

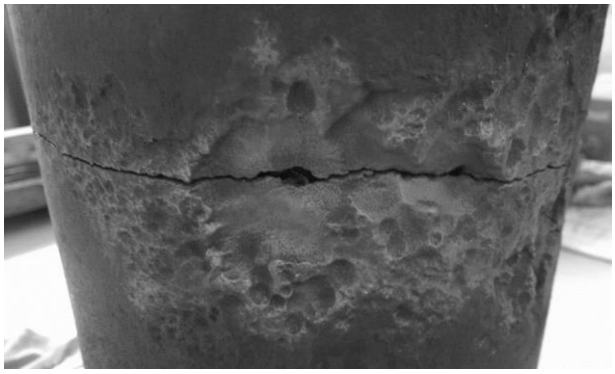

(a)

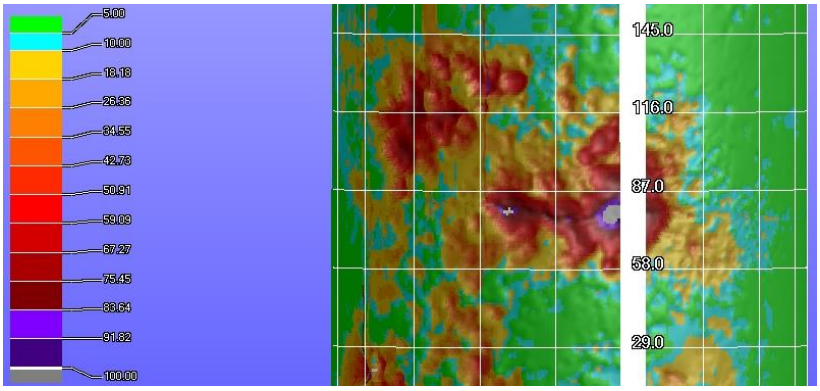

(b)

Figure 4- 16 Pipe sample 8 with a circumferential crack (a) Corrosion damage; (b) 3-D scanning image

4.6.3.2 Crack initiation

The hoop stresses induced by internal pressures for CI pipes with diameters of 100 and 150 mm were calculated using Equation 4.1 and the results are plotted in Figure 4-17 along with the typical bending stress (refer to Figure 4-12), assuming an average wall thickness of 10 mm and operating pressures ranging from 300 and 1,200 kPa. As shown in Figure 4-17, the critical hoop stress is generally less than the soil bending stress, which indicates that circumferential fracture is more critical for small-diameter CI pipes. According to the linear strength reduction correlation (Equation 4.19), circumferential crack initiation requires a corrosion depth at least 85% or more of the original wall thickness.

4.6.3.3 Remaining capacity of CI pipes containing a through circumferential crack

For CI pipes with diameters of 100 and 150 mm and with a nominal thickness of 10 mm, the remaining strengths are evaluated using Equations 4.13 and 4.22. The half-crack opening angle ranges from 10º to 110º. The geometric factors were adopted from both Tada et al. (2000) and Miedlar et al. (2002), and a lower bound fracture toughness of 15 MPa $m^{1/2}$ was selected. The results are plotted in Figure 4-18, and the remaining capacity declines with increasing crack length along the perimeter. The required bending stresses for leaking CI pipes listed in Table 4-6 are also shown in Figure 4-18.

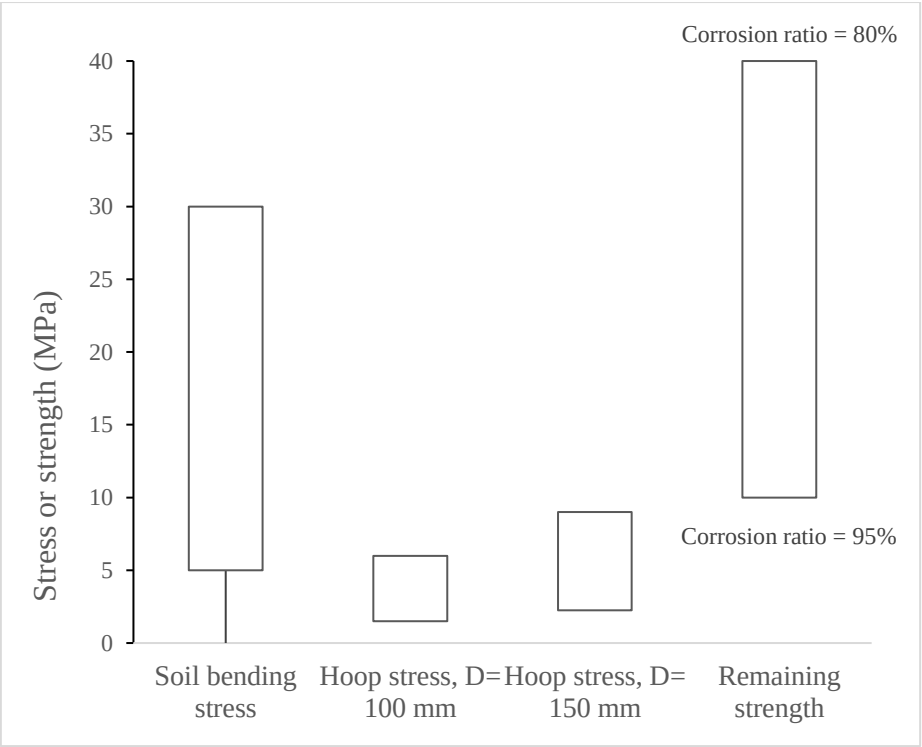

Figure 4- 17 Soil bending stress, hoop stress and remaining strength in small-diameter spun CI pipes

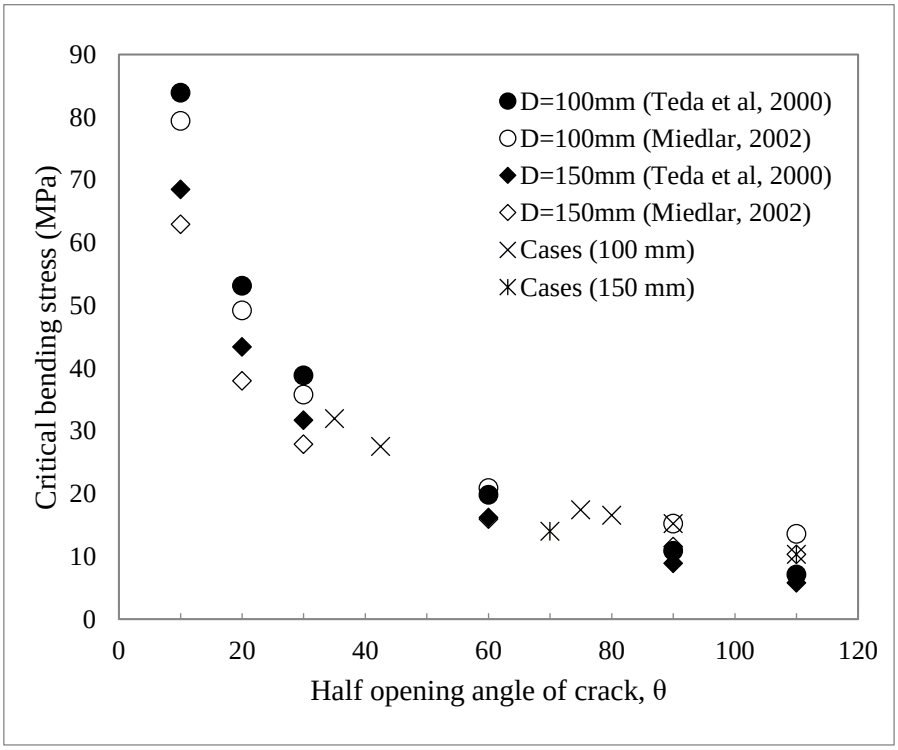

Figure 4- 18 Remaining strength of CI pipes containing a circumferential crack

4.6.4 Discussion

This study analyses the recent failure of small-diameter CI pipes. Multiple failure processes of circumferential fracture occur in CI pipes. The LBB criteria are proposed for CI pipes under bending stress using the stress criterion and the LEFM. The LBB concept is shown to be applicable to these pipes with circumferential fractures, which explains the time window between initial leak and final fracture under ordinary soil stresses. The findings of failure analysis and case studies are detailed below:

- Bending stresses from ground movements in small-diameter CI pipes are generally higher than the levels of hoop stress produced by internal pressure.
- Circumferential fracture is more commonly observed than longitudinal fracture in CI pipes with diameters of 100 and 150 mm due to the relatively higher soil bending stress than hoop stress
- Crack initiation occurs in severe corrosion pits (at least 85% of pipe wall) and leads to water leakage.
- Leaking pipes still show substantial structural capacity, and the LBB concept appears to be applicable to CI pipes under bending stress.
- The lengths of circumferential cracks normally go through 20%- 60% of the entire perimeter, which allows the easy solution of installing tightened clamps as a means of pipe repair. However, clamps may leak, leading to increased corrosion and soil moisture in local areas, which can lead to acceleration of subsequent failure. More effort is required to investigate these observations.

4.7 Conclusions

The LBB phenomenon has been observed in recent failures and full-scale bursting tests of large-diameter CI pipes. Over-designed pipe walls and coalesced pitting or patch corrosion in soil environment are the main reasons for the occurrence of LBB in CI pipes.

The LBB criteria for large-diameter CI pipes are proposed and verified by experimental results of burst tests. The procedures of LBB assessment for corroded CI pipes are proposed in accordance with LBB standards issued for other piping industries. Similarly, some findings of LBB evidence in small-diameter CI pipes which failed by circumferential fracture were summarised, and it was explained why the tightened clamp is an effective method to repair leaking small-diameter CI pipes.

From the field evidence, a detectable leak may be observed prior to a burst event, which results in a LBB time window ranging from ten days to months. However, these inferred time windows are based on the current leak detection technology, which is not geared for this purpose. Therefore, an improvement in leak detection technology and leak signatures and relating them to pipe distress levels could significantly improve the LBB time window calculation and hence the potential for pipe failure prevention. The detailed evaluation of crack growth rates and LBB time windows is shown in Chapters 6 and 7. The LBB concept is potentially applicable for corroded CI water pipes.

Chapter 5 Formation of through cracks in deteriorated cast iron pipes under cyclic pressures

5.1 Introduction

A significant portion of large-diameter (typically with diameters ≥ 300mm) water pipelines around the world including Australian water pipelines are made of cast iron (CI) (Rajeev et al., 2014). The predominant failure mode of large diameter CI mains is longitudinal barrel fracture (Makar, 2000). As identified by Makar (2000), the major factors affecting this failure mode are internal pressure and pipe corrosion. Most Australian CI water mains laid before the1980s have deteriorated by corrosion due to a number of factors, such as the absence of effective coatings, the aggressive surrounding soil environment and lack of cathodic protection. Rathnayaka et al. (2017b) found that a large corrosion patch is required to initiate failure in a large diameter pipe in order to provide sufficient stress concentration to initiate a crack. Such corrosion patches can occur by the coalescence of a number of small corrosion pits, which are very common in external pipe surfaces (Ji et al., 2015; Robert et al., 2016a). Full-scale static bursting tests conducted by Rathnayaka et al. (2017b) showed leakage through a crack in a cast iron pipe first occurs at the thinnest-walled area, typically located at the base of a corrosion patch. This phenomenon has been explained by limit load analysis as follows: a through-crack is generated when the hoop stress in the patch centre exceeds the tensile strength (Ji et al., 2015). Routine pressure transient events or any other similar loading conditions can create through-cracks in

severely corroded pipe sections. Generation of these cracks may lead to a leak or longitudinal fracture failure, depending on the corrosion patch configuration (Rathnayaka et al., 2016a).

Cyclic pressures (i.e. pressure transients) in water supply networks can be caused by routine pump and valve operations, power failures, fire hydrant operations and pipe bursts/refills (Rathnayaka et al., 2015; Sharp, 1981; Webb et al., 1978). Water pipes are normally subjected to positive pressures with relatively consistent pressure patterns, except for some extreme cases such as burst events and un-intentional power cuts to pump stations which may lower pressures even to below zero. Therefore, tension-to-tension cyclic stresses are common in water supply networks. Limited effort has been made to evaluate the fatigue resistance of CI pipes in this regard. Belmonte et al. (2009) conducted stress-controlled bending fatigue tests on beam samples cut from small-diameter CI pipes. The result of their study could not be used plot clear S-N curves due to varying corrosion damage in the specimen used for testing. Yamamoto et al. (1983) prepared both smooth and corroded fatigue test specimens from two trunk mains to conduct stress-controlled bending tests. The fatigue endurance limit (σ_e) refers to the stress level that can be applied cyclically and the material survives after 10 million cycles. The experimental results showed bending fatigue endurance limits within 10 million cycles are approximately equal to 60% of the flexural strength. A research study conducted by Brotzen and Wallace (1957) showed bending fatigue tests over-estimated the tensile fatigue endurance limit due to the presence of compressive behaviour during flexural tests.

According to ASTM-G46 (1994), elliptical (Type b) and wide shallow (Type c) pits are common shapes of corrosion pits for CI pipes. In some studies, the corrosion pits in CI pipes are described as either hemispherical or hyperbolic in shape (Brevis et al., 2015). With the exception of the studies reported by Brevis et al. (2015), Marshall (2001), Mohebbi et al. (2010) and Rajani (2000), limited data are available to quantify corrosion patch configurations in CI pipes. Grooved notches represent the common geometry of corrosion pits in CI pipes, which have lower stress concentration factors than V-shaped notches (Gilbert, 1968). The stress near a notched area of a pipe is higher than the nominal stress. The stress concentration factor of notches is defined as the ratio between the maximum stress (σ_{max}) in the vicinity of a notch and nominal stress (σ_n) in a uniform pipe section. The maximum stress with a grooved notch is calculated taking into account the net cross-sectional area of the notched specimen under static tensile load (Pilkey, 1997).

For CIs with a strength of 200 MPa or below, the effects of V-notches in reducing fatigue resistance are limited (Gilbert, 1968; Kommers, 1928; ISO-185, 1988). The notch fatigue reduction factor (K_{fn}) can be assumed to be approximately 1.0 for corroded CI pipes, based on the geometry of soil corrosion pirts or patches in CI pipes. Table 5-1 summarises the notch fatigue strength reduction factors of CI pipes reported in the research literature. The fatigue endurance limits are greatly affected by corrosive environments and the duration of the tests. The results of reversed bending fatigue tests in water and

seawater environments reported for CI pipes are also provided in Table 5-1 (Collins and Smith, 1942; Gilbert and Palmer, 1969). An equation to calculate the corrected fatigue endurance limit (σ_e'), taking into account the notch effects and corrosive environment is expressed in Equation 5.1:

$$\sigma_e' = \frac{\sigma_e}{K_{fn}\, K_{fc}} \tag{5.1}$$

where, K_{fn} and K_{fc} are respectively the reduction factors for notched and un-notched specimens, as detailed in Table 5-1.

In this chapter, the fatigue behaviour of CI water pipes is studied using the relevant research data and experimental results. Previous research outcomes are analysed and adopted where appropriate and several evaluation methods are recommended to address the effects of mean stress and notch effects on pipe performance and pipe asset life estimation. Finally, a sensitivity analysis by time-driven simulations is conducted to identify the key factors that may lead to high potential of fatigue damage.

Table 5- 1 Summary of fatigue strength reduction factors of cast irons (σ_u< 300 MPa)

Reduction factor	Item	Range	References
Notched specimens (K_{fn})	Grooved	1.00- 1.28	Gilbert (1968) Grant (1950)
	V-notch	1.00- 1.71	Gilbert (1953)
		1.00- 1.03	ISO-185 (1988)
Un-notched specimens with different corrosive mediums (K_{fc})	Water	1.29	Collins and Smith (1942)
		1.28- 1.59	Gilbert and Palmer (1969)
		1.23	Davis (1996)
	Seawater	1.55- 2.47	Gilbert and Palmer (1969)

5.2 Methodology

5.2.1 Fatigue Test Specimen Preparation Procedure

The stress-controlled fatigue tests were conducted in accordance with ASTM-E466 (2007). The corrosion products were removed by low-speed sand-blasting. The test specimens were cut from five selected ex-service CI pipe sections received from water utilities across Australia. Rectangular specimens with tangentially blending fillets were created, due to the curvatures of the sample pipes (Figure 5-1). Background information on the pipes selected for fatigue testing is provided in Table 5-2.

All fatigue tests were conducted using an Instron-8800 fatigue testing machine with a frequency of 5 Hz. Each test specimen was continuously tested until failure or the cycle count reached 20 million, when the test was terminated. The stress ratio (R), stress range ($\Delta\sigma$), alternating stress (σ_a) and mean stress (σ_m) used for fatigue analysis are defined in Equations 5.2 to 5.4. The stress ratio of 0.1 was selected to obtain the correlation between fatigue strengths and failure cycles for all pipe specimens.

$$R = \frac{\sigma_{min}}{\sigma_{max}} \tag{5.2}$$

$$\sigma_a = \frac{1}{2}\left(\sigma_{max} - \sigma_{min}\right) \tag{5.3}$$

$$\sigma_m = \frac{1}{2}\left(\sigma_{max} + \sigma_{min}\right) \tag{5.4}$$

The stress ratios of 0.3 and 0.5 were used for specimens from Pipes 1 and 5 only. The empirical equations of fatigue endurance limits proposed by Goodman (Equation 5.5) and Gerber (Equation 5.6) (Schijve, 2001) were used to verify the endurance fatigue limits obtained from fatigue tests.

$$\sigma_a = \sigma_e\left(1 - \frac{\sigma_m}{\sigma_u}\right) \tag{5.5}$$

$$\sigma_a = \sigma_e\left[1 - \left(\frac{\sigma_m}{\sigma_u}\right)^2\right] \tag{5.6}$$

Table 5- 2 Pipe sample information used for stress-controlled fatigue tests

Pipe ID	Location	Manufacturing method	Buried year	Nominal diameter (mm)	Tensile strength (MPa)
1	Sydney	Pit	1922	600	104
2	Melbourne	Spun	1938	380	151
3	Newcastle	Spun	1957	300	173
4	Sydney	Spun	1961	500	148
5	Melbourne	Spun	1976	300	214

(a)

(b)

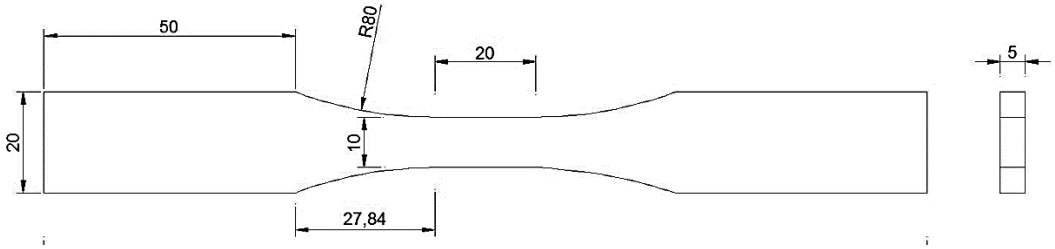

(c)

Figure 5- 1 (a) Fatigue testing, (b) Fractured cast iron specimens, (c) Sketch of fatigue test specimens (mm)

5.2.2 Effect of Corrosion

5.2.2.1 Assessment of corrosion pits/patches

Three CI pipe rings 300 mm long from Pipes 1, 2 and 3 as of Table 5-2 were examined to determine the configuration of corrosion pits/patches. The corrosion products on the external surfaces were removed by low-speed sand-blasting. The selected pipe sections were scanned using a CREAFORM 3-D laser scanner. All corrosion pits/patches over 1.0 mm in depth were recorded.

Two non-dimensional parameters, the length-depth ratio (LDR) and the aspect ratio (AR), are introduced to define a corrosion pit/patch in a CI pipe (Equations 5.7 and 5.8) and these two quantities describe the geometry of elliptically-shaped corrosion pits or patches. These two non-dimensional quantities were used to analyse the corrosion pits/patches in this study.

$$LDR = \frac{2a}{c} \tag{5.7}$$

$$AR = \frac{a}{b} \tag{5.8}$$

5.2.2.2 Pitting corrosion rate

For buried pipelines, the pitting corrosion rates of CI pipes are strongly related to the soil condition and exposure period (Petersen and Melchers, 2014; Rajani, 2000). The two-phase corrosion growth model proposed by Rajani (2000) was adopted in the present study. Equation 5.9 is rewritten from Equation 3.4:

$$c = r_s\, t + C_s\, (1 - e^{-t/\tau}) \tag{5.9}$$

where, r_s is long-term corrosion constant, C_s is corrosion scaling constant, τ is corrosion transient time, and t is exposure time.

5.2.3 Fatigue damage analysis

5.2.3.1 Pipe stress

The stress concentration factor (*SCF*) is affected by pipe internal diameter (D_i), thickness (t_o) and patch configurations (*2a*, *2b* and *c*), which has been established by the pipe stress prediction model developed in the ACAPFP project (Ji et al., 2015; Zhang et al., 2017). The stress prediction model was intended to provide guidance to the structural analysis associated with the condition assessment of pressurised CI pipelines. The model was developed to analyse the longitudinal failure mode of a pipe barrel due to a single ellipsoid like corrosion defect. The model provides a way to assess the concentrated maximum stress in the corrosion patch caused by internal pressure, as expressed in Equation 5.10.

$$\sigma_{max} = P_{max} \frac{D_i}{2t_o}\, SCF \tag{5.10}$$

5.2.3.2 Effect of cyclic pressure

Two types of cyclic pressures are considered in this analysis: (1) bursts/refills and (2) transient events. The stress ratio of a cyclic pressure event can be determined by using the minimum and maximum pressure. This is because the stress concentration factor depends only on the pipe geometry and corrosion patch configuration. Three pressure cases were considered in the analysis: Case 1: Burst/refills; Case 2: Pressure transients; and Case 3: Burst/refills and transients. Although burst/refill events are rare compared with routine pressure transients, they tend to give a low stress ratio, leading to severe fatigue damage.

5.2.3.3 Cumulative damage

The cumulative fatigue damage from cyclic pressures was quantified by the fatigue damage factor using the Miner's rule, which is given in Equation 5.11 (Schijve, 2001). With the growth of corrosion patches, the stress level and the fatigue damage in the critical locations of the pipe (typically at the base of the

patch) also increase. A through-wall crack is generally assumed to occur when the fatigue damage factor reaches 1.0. However, a critical value of 0.2 was proposed by Brevis et al. (2015) for CI pipes in corrosive soil environments. The results of a series of fatigue tests summarised by (Schijve, 2001) with variable-amplitude loading also showed the occurrence of fractures with a fatigue damage factor as low as 0.15. Therefore, a critical fatigue damage factor of 0.2 was adopted in this analysis to indicate the occurrence of a through-wall crack in the base of a corrosion patch.

$$D_{cr} = \sum_{i=1}^{k} \frac{n_i}{N_i} = 0.2 \tag{5.11}$$

where, D_{cr} is critical fatigue damage factor, N_i is the number of failure cycles for a stress amplitude to cause a fracture, n_i is the number of cycles for a stress amplitude, and *k* is different stress spectra.

5.2.3.4 Analytical method

A sensitivity analysis was conducted to identify the critical factors contributing to fatigue damage in corroded cast iron pipes. Pipe lifetime simulations on an annual basis were conducted to evaluate corrosion patch growth in the external pipe surface. The corresponding stress concentration factors (SCFs), fatigue stress spectra and cumulative damage were evaluated at the end of each year. The exponential corrosion growth (Equation 5.9) and constant length-to-depth ratio (*LDR)* and aspect ratio (*AR)* were used to describe the corrosion configurations over the exposure period for each simulation.

For the analysis conducted in this study, the fatigue strength reduction factors (K_{fn} and K_{fc}) were assumed to be 1.0; however, in practical applications the impact of these factors must be considered. The S-N curves obtained by fatigue testing were used in this simulation. Three spun CI pipe sizes (i.e. 400mm, 450mm and 500 mm) were selected for the analysis. The input parameters shown in Table 5-3 were selected on the basis of data from the research literature, experimental observations and field measurements. The influence of each parameter on fatigue performance was evaluated by changing its value within the range specified in Table 5-3 and fixing all other parameters to the base value. Using this analysis, the relative importance of various factors affecting pipe fatigue performance was identified. It is considered that a through-wall crack in a corrosion patch base forms when the maximum hoop stress exceeds the tensile strength of the pipe material. However, the fatigue mechanism may reduce the service life when D_{cr} reaches 0.2. The reduced servicing lifetime due to fatigue damage is expressed in Equation 5.12. The overall analysis procedure used in this study is provided in Figure 5-2.

$$\Delta T = T_o - T_f \tag{5.12}$$

where, T_o is the exposure time to form a through-wall crack by ignoring fatigue damage, T_f is the exposure time to form a through-wall crack by fatigue damage, and ΔT is the reduced servicing lifetime.

Table 5- 3 Input parameters used for fatigue sensitivity analysis

Variable	Base	Min	Max	References
Maximum transitent pressure, P_{max} (MPa)	0.9	0.6	1.5	Rathnayaka et al. (2015)
Burst-refills frequency, f_1 $(per\ year)$	15	0	30	
Transient frequency, f_2 $(per\ day)$	2	0	4	
Transient stress ratio, R	0.3	0.1	0.6	
Long-term corrosion constant, r_s $(mm/\ year)$	0.02	0.006	0.1	Rajani and Tesfamariam (2007)
Corrosion scaling constant, C_s (mm)	12	6	16	
Corrosion transient time, τ $(year)$	8	5	30	
Aspect ratio of corrosion patch, AR	1	0.5	2	Rajani (2000);
Length-depth ratio of corrosion patch, LDR	5	2	10	Rajani (2000); Marshall (2001)
Nominal wall thickness, t_o (mm)	Class 2	Class 1	Class 3	Jiang et al. (2017b) AS-1724 (1975); BS-78 (1938)
Tensile strength of static CI, $\sigma_{u,st}$ (MPa)	100	80	120	Jiang et al. (2017b); AS-1724 (1975)
Tensile strength of spun CI, $\sigma_{u,s}$ (MPa)	150	120	200	

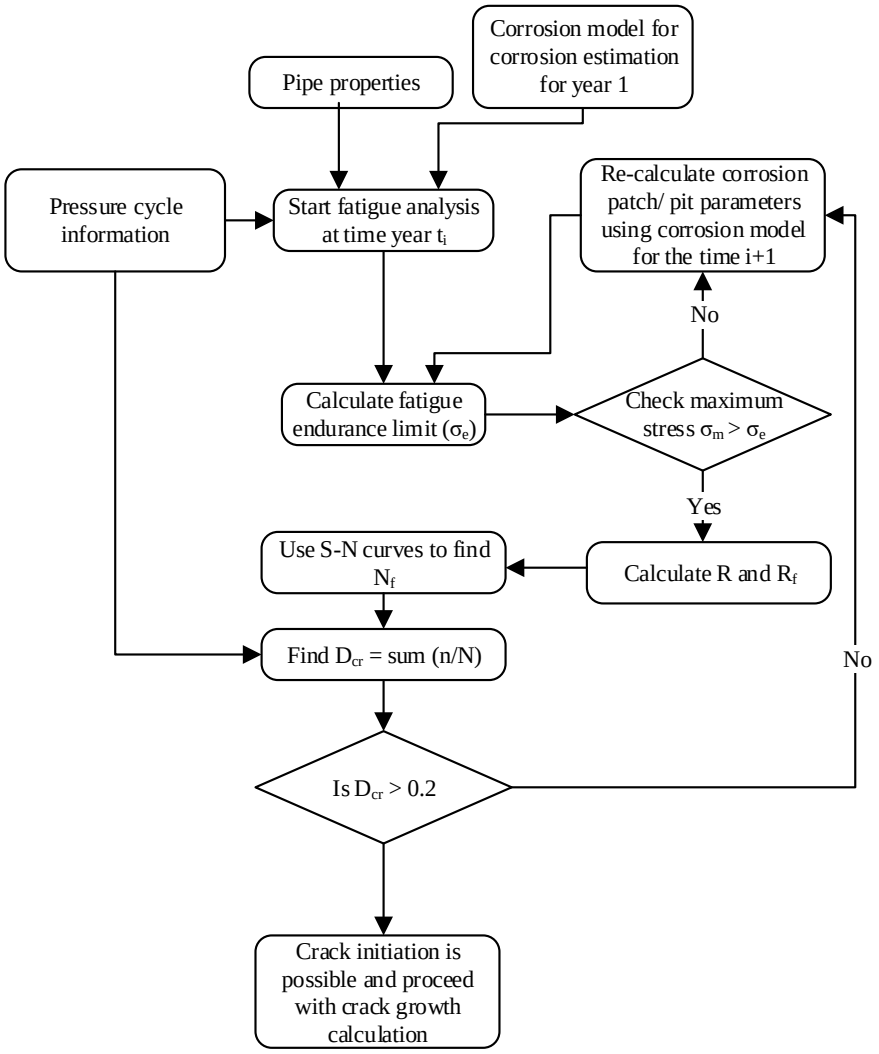

Figure 5- 2 Flowchat of the fatigue analysis

5.3 Results and discussion

5.3.1 Fatigue test results

3.1 Fatigue test results

The fatigue ration, R_f (Equation 5.13), is defined by the ratio of maximum fatigue stress in a stress cycle to ultimate tensile strength of the testing material. The fatigue rations are plotted against the fatigue loading cycles under the stress ratios of 0.1, 0.3 and 0.5 and the results are shown in Figure 5-3. The endurance ratios from empirical equations and experimental results for Pipe 1 and 5 are also shown in Figure 5-2 under the stress ratios of 0.1, 0.3 and 0.5. The fatigue lives within 1,000 and 10,000 cycles can be defined in the low cycle fatigue (LCF) regime, while the specimens surviving after this range are considered as high cycle fatigue (HCF) regime for water pipelines. The Gerber relationship (Equation 5.6) was used to predict the fatigue endurance of CI pipes under high stress ratios, and the high mean stresses tend to prolong the fatigue life for both the low cycle fatigue (LCF) and high cycle fatigue (HCF) regimes. The proposed models are plotted in Figure 5-3 to fit with the experimental results.

The results shown are for the specimens which failed within 1 million cycles or which survived at least 10 million cycles. The specimens failing between 1 million and 10 million cycles were not observed. Although the test specimens were cut from five different CI pipes, linear correlations were found between the fatigue rations and failure cycles, as shown in Figure 5-3. The power equation shown in Equation 5.14 is adopted to describe the fatigue strength of CI pipes (Bannantine et al., 1990). The fatigue ration at 1,000 cycles is approximately 0.9, which is the interception ratio ($R_{f,LCF}$, shown in Figure 5-3) between the LCF and HCF regimes for R=0.1. A preliminary version of the S-N curve is proposed based the test data (Figure 5-3). The failure cycles in both the LCF and HCF regimes can be predicted by Equation 5.14, based on the interception point and endurance ratio. The correlations between tensile strengths and tensile endurance limits are plotted in Figure 5-4, and the upper and lower limits for the endurance ratio are 0.50 and 0.25 respectively for most cases. It is clear that the tensile endurance limit rises with the increase of material tensile strength. In this study, the endurance ratios range from 0.48 to 0.55, and a conservative value of 0.5 is recommended for CI pipes under axial tension fatigue.

$$R_f = \frac{\sigma_{max}}{\sigma_u} \tag{5.13}$$

$$R_f = 10^{A_f} N^{B_f} \tag{5.14}$$

where, R_f is the fatigue ration, A_f is the fatigue ration coefficient, and B_f is the fatigue ration exponent.

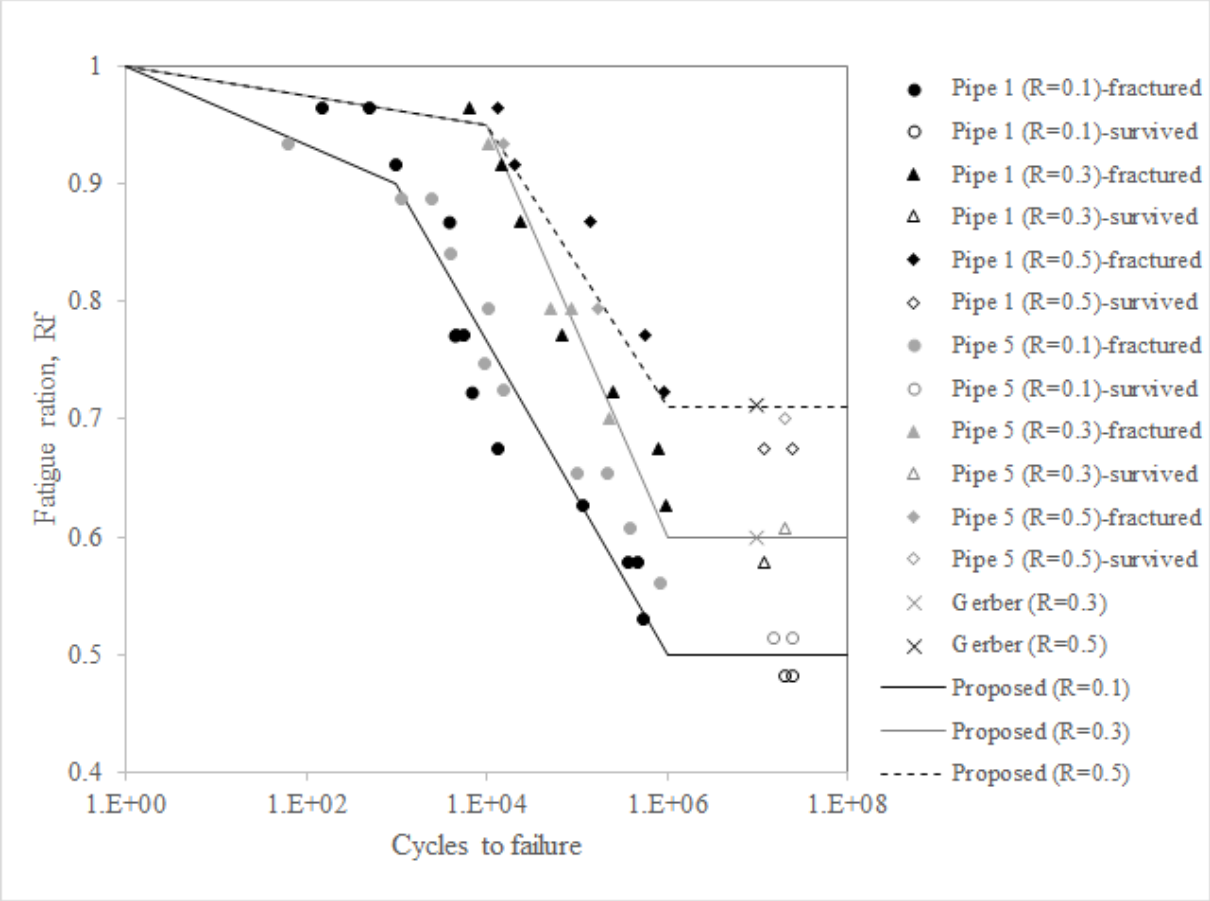

Figure 5- 3 Failure cycles vs. fatigue rations

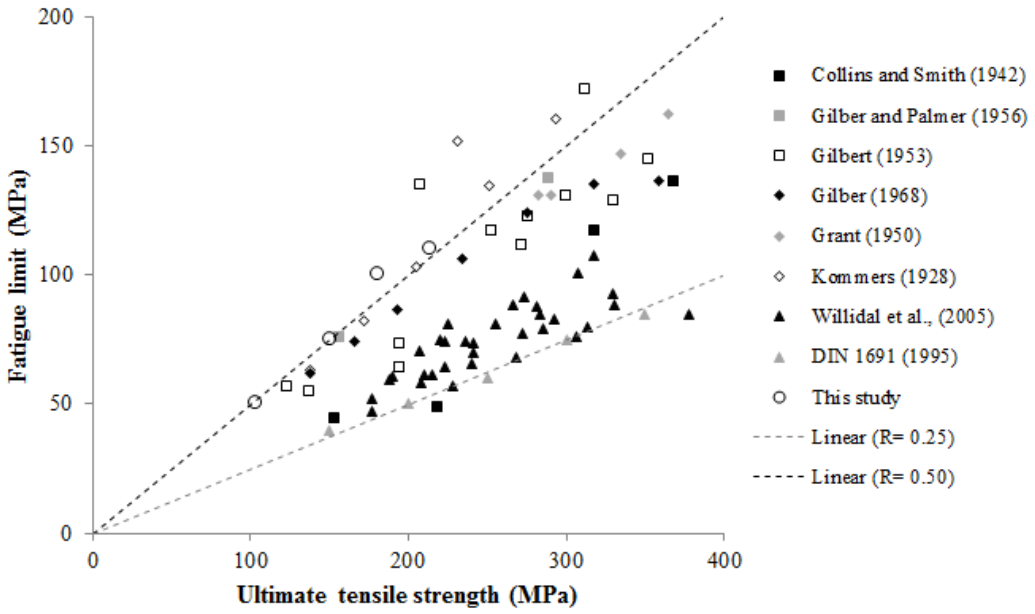

Figure 5- 4 Correlations between tensile strengths and tensile fatigue limits

5.3.2 Corrosion effects

Table 5-4 summarises the configuration of external corrosion pits/patches, which shows that circular or sub-circular pits are widely distributed and the mean of the *LDR* ranges from 6.0 to 7.0. Although some large corrosion patches may be formed by the coalescence of a number of small corrosion pits, the statistical results can still represent most of the corrosion shapes based on as-received corroded specimens.

5.3.3 Fatigue damage analysis

The pipe lifetime simulations (detailed in Section 5.2.3) using the base variables in Table 5-3 indicated that all three pressure cases (Case 1-Burst/refills, Case 2- Transients and Case 3- Burst/refills and transients) can result in an early fatigue crack compared with the no fatigue scenario for the selected pipe sizes (400mm, 450mm and 500 mm). The resulting cumulative damage factor with exposure time is shown in Figures 5-5(a), 7(b) and 7(c). The damage factors grow dramatically after reaching the critical factor of 0.2, which means the selected critical value of 0.2 is a reasonable and conservative estimate to indicate an early fracture under fatigue damage due to cyclic pressures.

Table 5- 4 Corrosion pit/patch configurations

Pipe ID	Number of pits/patches	Length to depth ratio (LDR)		Aspect Ratio (AR)	
		Mean	Standard Deviation	Mean	Standard Deviation
1	183	6.5	8.5	1.0	0.6
2	42	7.0	3.9	1.2	0.6
3	31	6.0	3.5	1.1	0.5

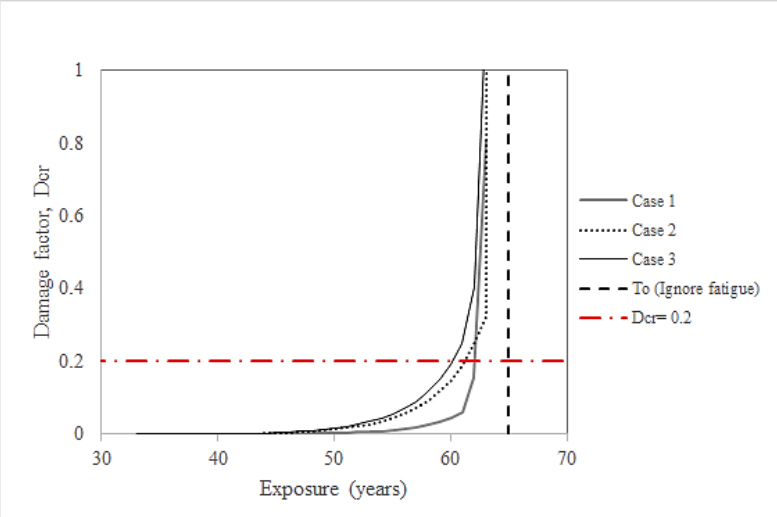

(a)

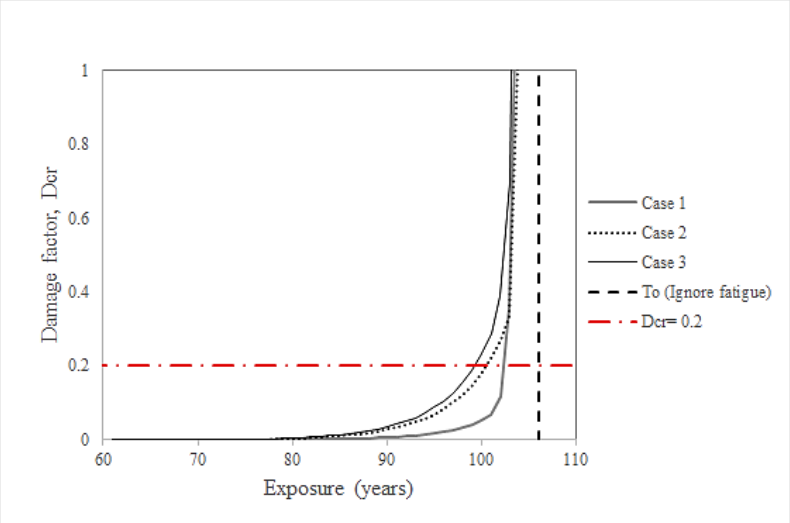

(b)

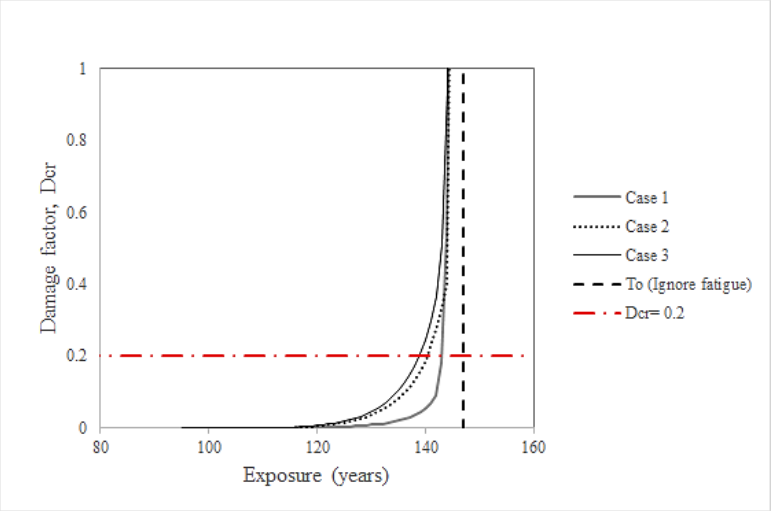

(c)

Figure 5- 5 Fatigue damage for spun cast iron pipes under base input parameters: (a) 400 mm diameter; (b) 450 mm diameter; (c) 500 mm diameter

5.3.4 Sensitivity Analysis

The reduced servicing lifetime by fatigue mechanism, ΔT (Equation 5.12), was used to identify the sensitive factors for fatigue damage. The effect of burst-refill and transient events was evaluated under pressure Case 1 and Case 2, respectively. The values of ΔT were calculated under Case 3 (critical pressure case: Transient and burst-refill) for the rest of the analyses.

CI water pipes were generally manufactured in three classes to withstand variations in operating pressures (assumed at design stage), and the wall thickness of pipes increased according to the pipe diameter and operating pressure (AIS, 1941; BS-78, 1938). As shown in Figure 5-6 (a), pipes with low wall thickness tend to have longer ΔT. Figure 5-6 (b) shows that CI pipes with high tensile strength

experience lower impact of fatigue damage resulting in higher fatigue resistance. The effect of fatigue damage may be more significant for networks operating at high pressures. This is shown in the sensitivity analysis results in Figure 5-6 (c), where ΔT increases with maximum operating pressures. The decrease of the stress ratios of transient events increases the level of fatigue damage, as shown in Figure 5-6 (d). This means the occurrence of low pressure transient events together with high pressure transient events in the same pipe or pipeline could cause more severe fatigue damage in contrast to the pipelines without transient or burst-refill events. The analysis conducted on both routine pressure transient (f_2) events and occasional burst / re-fill (f_1) events indicated routine events (Figure 5-6 (f)) can cause less fatigue damage than occasional events (Figure 5-6 (e)).

As shown in Figure 5-6 (g-i), the long-term corrosion constant (r_s) has a significant influence on fatigue damage in deteriorated CI pipes compared to the corrosion scaling constant (C_s) and corrosion transient time (τ). Medium-to-low values of the long-term corrosion rate allow longer service life with continuous fatigue damage. However, a significantly high value of the long-term corrosion rate may restrict the potential for fatigue damage and result in a through-crack mainly by corrosion. The corrosion scaling constant and corrosion transient time have relatively minor effects on the fatigue damage of CI pipes. This may be attributed to the fact that fatigue damage initiates mainly during long-term exposure and is controlled by the long-term corrosion rate.

In addition, the increase of the *LDR* and *AR* forms a longer corrosion patch in the longitudinal direction, which may result in higher stress concentration (Ji et al., 2017). The evidence that more fatigue damage would be induced in the corrosion patches as a result of high stress concentrations can be observed in Figures 5-6 (j) and (k).

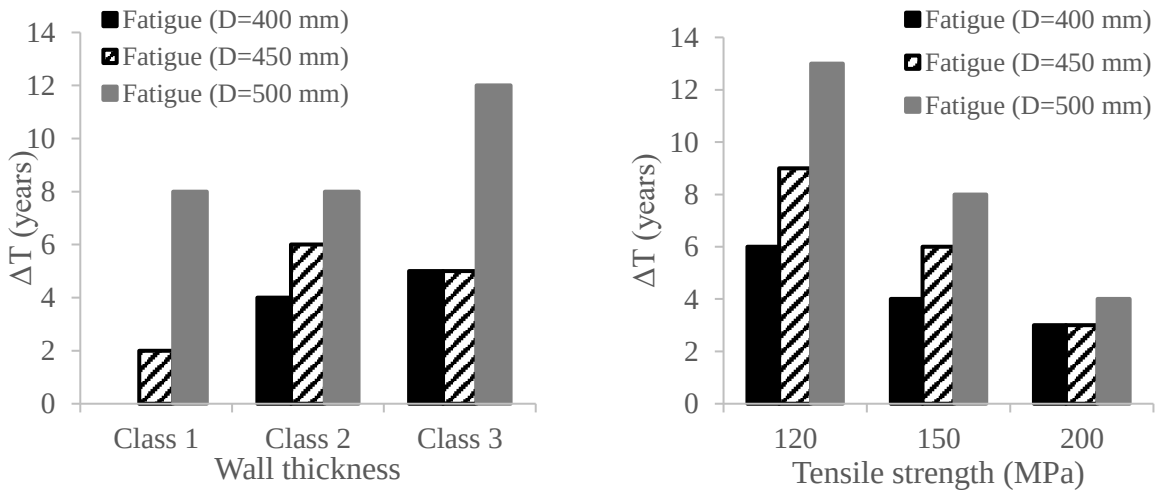

(a)

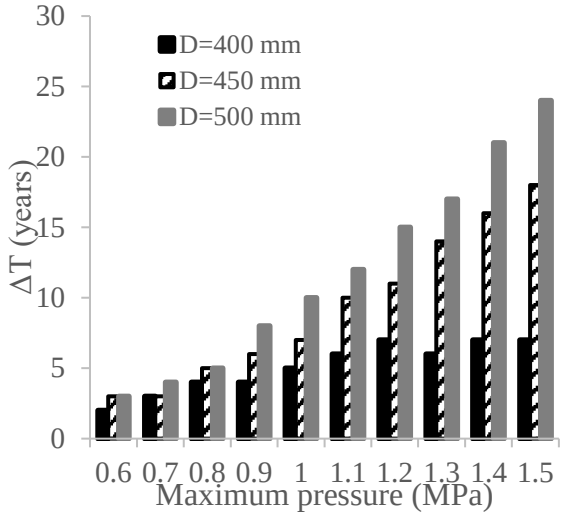
D=400 mm
D=450 mm
D=500 mm
ΔT (years)
0 5 10 15 20 25 30
0.6 0.7 0.8 0.9 1 1.1 1.2 1.3 1.4 1.5
Maximum pressure (MPa)

(b)

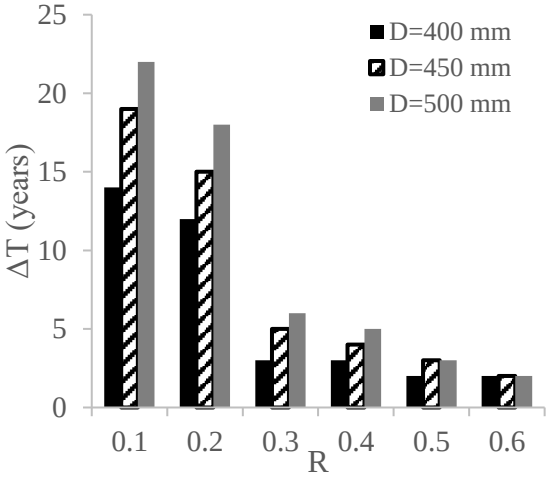
D=400 mm
D=450 mm
D=500 mm
ΔT (years)
0 5 10 15 20 25
0.1 0.2 0.3 0.4 0.5 0.6
R

(c)

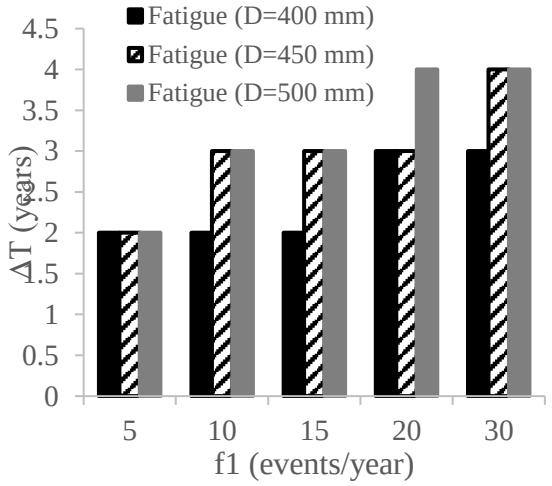
Fatigue (D=400 mm)
Fatigue (D=450 mm)
Fatigue (D=500 mm)
ΔT (years)
0 0.5 1 1.5 2 2.5 3 3.5 4 4.5
5 10 15 20 30
f1 (events/year)

(d)

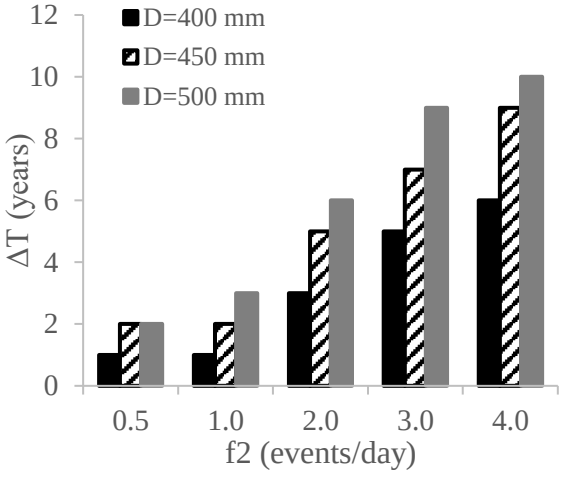
D=400 mm
D=450 mm
D=500 mm
ΔT (years)
0 2 4 6 8 10 12
0.5 1.0 2.0 3.0 4.0
f2 (events/day)

(e)

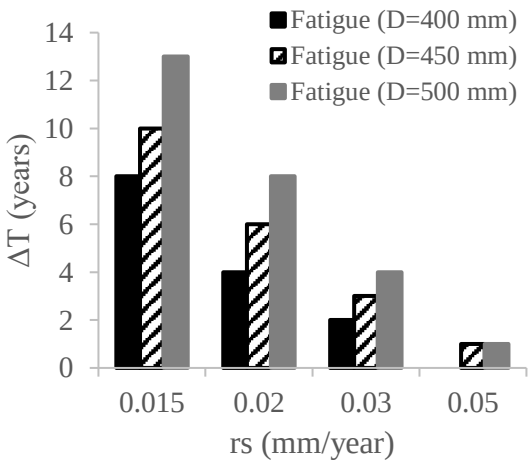
Fatigue (D=400 mm)
Fatigue (D=450 mm)
Fatigue (D=500 mm)
ΔT (years)
0 2 4 6 8 10 12 14
0.015 0.02 0.03 0.05
rs (mm/year)

(f)

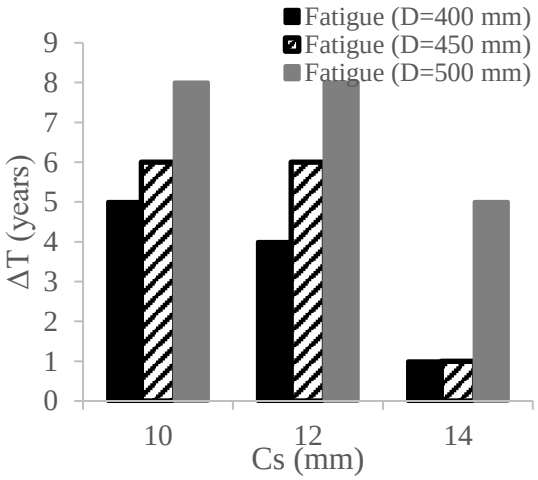
Fatigue (D=400 mm)
Fatigue (D=450 mm)
Fatigue (D=500 mm)
ΔT (years)
0 1 2 3 4 5 6 7 8 9
10 12 14
Cs (mm)

(g)

(h)

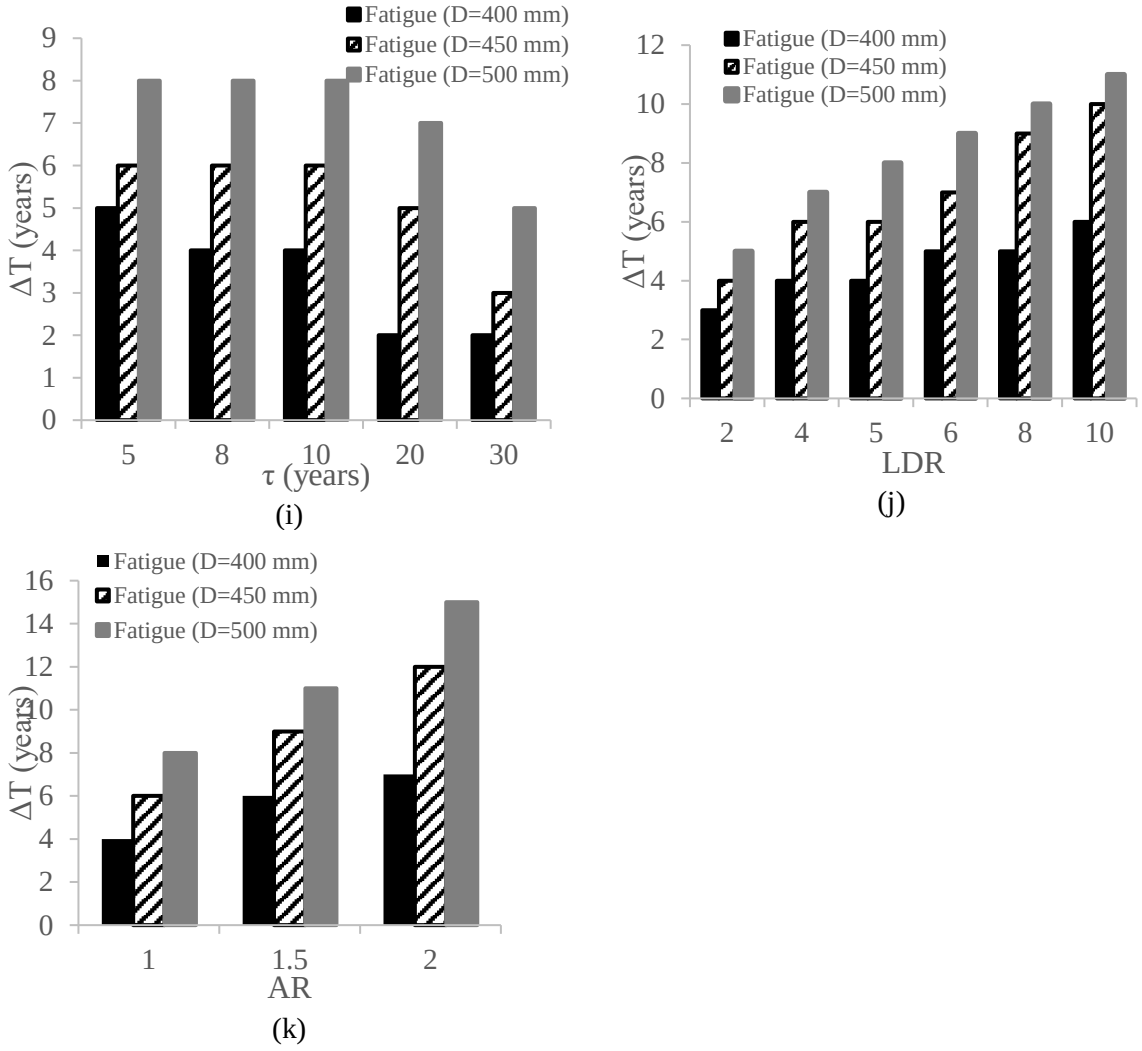

Figure 5- 6 Reduced exposure time (ΔT) by fatigue for variations in: (a) wall thickness, (b) tensile strength, (c) maximum internal pressure, (d) stress ratio, (e) frequency of burst-refill events and (f) long-term corrosion rate; (g) long-term corrosion constant; (h) corrosion scaling constant; (i) corrosion transient time; (j) length to depth ratio (LDR); (k) aspect ratio (AR)

5.4 Conclusions

In this study, S-N curves were developed by fatigue tests for CI pipe material from coupons cut from five CI pipes. Published data from the research literature were also used for comparison with the experimental results. The literature data confirmed that fatigue strengths are strongly correlated with ultimate tensile strengths. A fatigue endurance ratio of 0.5 was measured for CI pipes under a low stress ratio (less than 0.1), and Gerber's relationship enabled the evaluation of the endurance ratios for high stress ratio scenarios ($R > 0.1$). However, the analysis indicated that the increase of the stress ratio may prolong the failure cycles. The examination of corrosion pit/patch configurations indicated that most corrosion damage was either circular or elliptical in shape. Although high stress near a corrosion patch / pit affects the fatigue performance by generating high stress, the notch effects on the fatigue properties of cast iron pipes are negligible.

The results indicate that fatigue may initiate cracks at critically corroded patches prior to limit state failure (stress = tensile strength). Sensitivity analysis in conjunction with pipe lifeline simulations revealed a number of critical factors for fatigue damage in corroded CI pipes under cyclic pressures. Fatigue damage tends to be more severe in networks with high operating pressures, low stress ratios due to transient events and pipes with low tensile strength. The long-term corrosion constant was also identified as a critical variable for fatigue damage. Ageing CI pipes buried in pressure zone prone to pressure transients or /and frequent bursts may require additional condition assessment to assess the risk of fatigue damage. Further research is recommended to explore the impact of corrosive soil environments on fatigue resistance.

Chapter 6 Fatigue crack growth rates of pressurised cast iron water mains

6.1 Introduction

Corrosion is the predominant mechanism of pipe deterioration, which reduces the thickness of the pipe wall and forms stress concentrators in external pipe surfaces (Nicholas and Moore, 2009; Petersen and Melchers, 2012). Corrosion is a relatively time-consuming process as maximum long-term corrosion rates are less than 1 mm per year, even in severely corrosive environments and in many cases orders of magnitude lower (Petersen and Melchers, 2012; Rajani, 2000). Rathnayaka et al. (2017b) observed that through-wall cracks initiate approximately in the centre of corrosion patches and the crack must reach a critical length to generate a burst under normal operational pressures. Hence, pipe corrosion driven by the surrounding soil may be the main reason for stress concentration or crack initiation rather than crack propagation in CI water-pipe barrels.

Three crack growth mechanisms are possible that contribute to crack growth in CI pipe barrels: fatigue, stress corrosion cracking (SCC) and corrosion fatigue. Almost all the stresses in pipe networks, including internal pressure, thermal stress and traffic loads, are time-dependant and can be treated as cyclic stresses in fatigue analysis (Brevis et al., 2014; Doyle et al., 2003; Rajani et al., 2012). Grey CI is an alloy with high resistance to SCC, as demonstrated by experiments (Charlot and Westerman, 1981;

Miyasaka and Ogure, 1987). Therefore, fatigue is likely to be the likely fatigue crack growth mechanism for grey CI pipes.

Fatigue is a common deterioration mechanism for metallic infrastructures, including bridges and building structures (Anderson, 2005; Schijve, 2001). An existing crack may propagate under cyclic loadings, and fatigue crack growth rates (FCGRs) are generally quantified by the Paris' law (Schijve, 2001). Limited testing results of the FCGR parameters for British static CI pipes have been reported by Mohebbi et al. (2010) and Rajani et al. (2012). Corrosion fatigue is the crack growth mechanism when the structure is subjected to cyclic loads and a corrosive environment (Schijve, 2001). The corrosive medium accelerates the fatigue crack growth. However, the exact mechanism of corrosion fatigue is still debatable. The effect of corrosive environments is discussed in this chapter.

The metallic fracture surface generated by fatigue crack growth may contain macroscopic and microscopic features, depending on the material, loadings and environmental media (Forsyth, 1969). Beach (tide) marks and fatigue striations are common macroscopic and microscopic features of fatigue surfaces, respectively; however, these features are easily damaged by corrosive environments (Forsyth, 1969). Previous studies attempted to capture fatigue striations in the fracture surface of CI specimens (Belmonte et al., 2009; Mohebbi et al., 2010). Nevertheless, clear fatigue striations were not easily captured in previous studies. Different corrosion products observed in the fracture surfaces indicate the failure processes and phases of crack propagation in CI pipe barrels (Cullin et al., 2014; Makar, 2000; Rajani et al., 2012).

This chapter evaluates the FCGR parameters and threshold toughness of CI water pipes. These parameters can be used to predict the leak-before-break (LBB) time window in deteriorated CI water pipes under different operational pressures, once a fracture has initiated. The initiation of a fracture was discussed in Chapters 4 and 5.

6.2 Methodology

6.2.1 Fatigue crack growth rates (FCGR) tests

The FCGR parameters from the empirical model of Paris' law (Equation 2.12- 2.14) have been successfully used to predict fatigue failure and evaluate the remaining life of aerospace and bridge structures (Anderson, 2005; Schijve, 2001). Crack growth driven by fatigue can be divided into three phases: crack initiation, propagation, and final fracture. The FCGR parameters (Paris' constants) can be obtained from the curve of crack propagation (Figure 6-1).

$$\Delta K = K_{max} - K_{min} = Y\ \sigma_{max}\sqrt{\pi a_t} - Y\ \sigma_{min}\sqrt{\pi a_t} = Y\ \Delta\sigma\sqrt{\pi a_t} \tag{2.12}$$

$$\frac{da}{dN} = C\ \Delta K^m \tag{2.13}$$

$$R = \frac{K_{min}}{K_{max}} = \frac{\sigma_{min}}{\sigma_{max}} \tag{2.14}$$

where, a_t is through-wall crack length, N is the number of stress cycles, C and m are Paris' constants, σ_{max} is maximum nominal stress, σ_{min} is minimum nominal stress, $\Delta\sigma$ is the stress difference, K_{max} is maximum stress intensity factor, K_{min} is minimum stress intensity factor, and ΔK is the range of the stress intensity factor.

Specimens were taken from five decommissioned or fractured CI water trunk mains, and their chemical composition and microstructural features were determined. The tensile strength and fracture toughness were obtained, based on the standardised testing approaches detailed in Chapter 3. Basic information on the pipe specimens is summarised in Table 6-1.

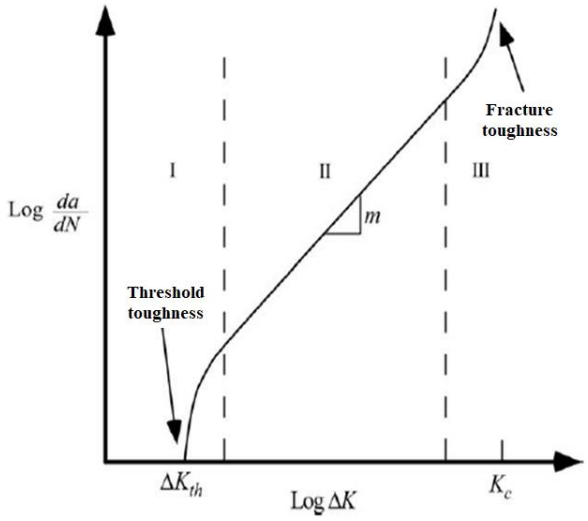

Figure 6- 1 Conceptual diagram of fatigue crack growth, modified from Anderson (2005)

The FCGR tests were conducted at a frequency of 0.5 Hz in accordance with ASTM-E647-13a (2013). Due to the restriction of pipe wall shapes, single-edge-notched beam (SENB) specimens were prepared from the five decommissioned pipes (detailed in Figure 6-2). The depth of the beam specimens was determined by the remaining wall thickness, and the bending span (*S*) was maintained at least four times the beam depth (*W*). The thickness (*B*) was half of the beam depth, and a straight-through notch of 5.0 mm was prepared by wire cutting with a tip radius of 0.5 mm. A three-point bending set-up was arranged for all fatigue tests using an Instron-4402 with a 20 kN load cell. The stress intensity factors of the SENB specimens for bending fatigue tests were calculated using Equations 2.13 and 6.1–6.3 (Anderson, 2005).

$$K_{max} = \frac{F_{max}S}{BW^{3/2}} f(\frac{a_t}{W}) \tag{6.1}$$

$$K_{min} = \frac{F_{min}S}{BW^{3/2}} f(\frac{a_t}{W}) \tag{6.2}$$

$$f\left(\frac{a}{W}\right) = \frac{3(\frac{a_t}{W})^{1/2}\left[1.99 - \left(\frac{a_t}{W}\right)\left(1 - \frac{a_t}{W}\right)^{\frac{3}{2}}\left(2.15 - \frac{3.93a_t}{W} + \frac{2.7a_t}{W} + \frac{2.7{a_t}^2}{W^2}\right)\right]}{2(1 + \frac{2a_t}{W})(1 - \frac{a_t}{W})^{3/2}} \tag{6.3}$$

where, F_{max} is maximum bending load, F_{min} is minimum bending load, S is bending span, W is beam depth, B is beam thickness, a_t is through crack length, and $f\left(\frac{a}{W}\right)$ is a geometric factor for the SENB specimen.

A digital image correlation system (Aramis) was used to record the crack growth and surface deformations until the occurrence of final fracture. As stated in ASTM-E647-13a (2013), a pre-crack was made by low-amplitude fatigue loading with a stress ratio of 0.1. The process of pre-cracking was monitored by the Aramis program, and the final length of the pre-crack was measured prior to the FCGR test. Stress ratios of 0.1, 0.3 and 0.5 were used. The FCGR testing set-up and digital image correlation system are shown in Figures 6-3 and 6-4.

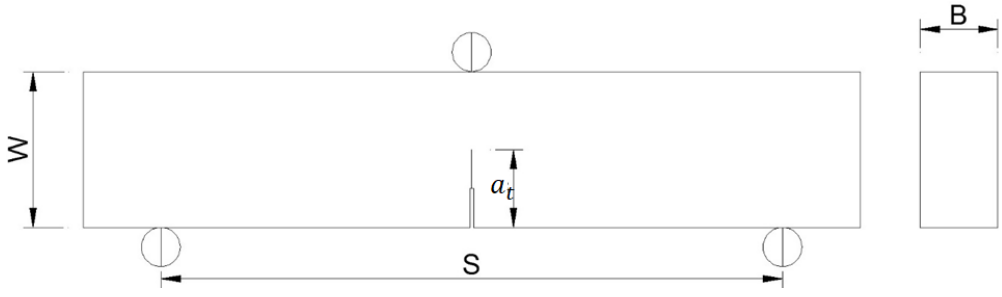

Figure 6- 2 Schematic of SENB specimen

Table 6- 1 Summary of CI pipe specimens

ID	Casting type	Burial year	Nominal pipe diameter (mm)	Tensile strength (MPa)	Fracture toughness ($MPa\sqrt{m}$)
1	Static	1922	600	104	13.8
2	Spun	1938	380	151	15.3
3	Spun	1957	300	173	14.9
4	Spun	1961	500	148	14.0
5	Spun	1976	300	214	16.8

Figure 6- 3 FCGR test set-up of CI pipe specimen during loading

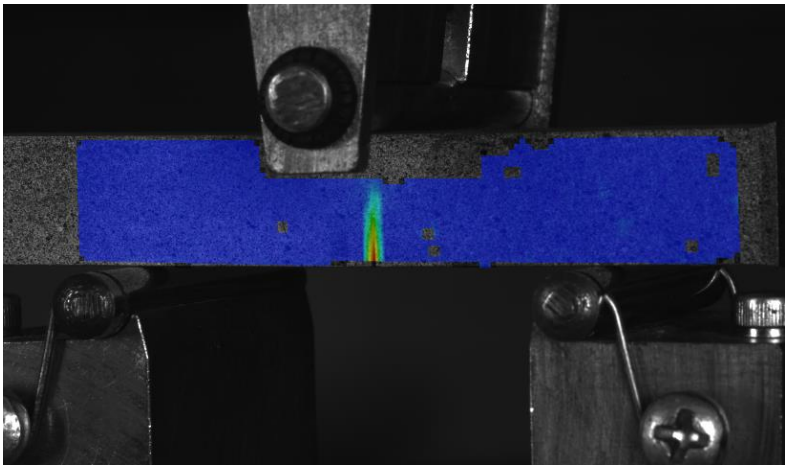

Figure 6- 4 Fatigue crack growth recorded by digital image correlation system

6.2.2 Threshold toughness

The values of threshold toughness (ΔK_{th}), expressed in Equation 6.4, represent the minimum required crack length that starts to propagate under a certain fatigue stress spectrum, which is highly dependent on the stress ratio and testing environment (Schijve, 2001). As shown in Figure 6-1, the threshold toughness can be defined as the initiation of fatigue crack propagation.

$$\Delta K_{th} = \delta\,(1 - R)^{\gamma} \tag{6.4}$$

where, ΔK_{th} is threshold toughness, R is stress ratio, and, δ and γ are the threshold parameters (Schijve, 2001).

The threshold toughness and the corresponding stress ratio of each FCGR were recorded. The research data on threshold toughness were also summarised to evaluate the threshold parameters defined in Equation 6.4.

6.2.3 Fractography examination

The fracture surface of a FCGR specimen includes two separate surfaces: the fatigue surface and the fast (instantaneous) fracture surface. Both macroscopic and microscopic features of the fracture surfaces of the FCGR specimens were examined in this study. The exact region of the fatigue fracture surface was verified by the crack growth data from the image correlation system.

The fractured specimens were stored in moisture-free containers. The macroscopic appearances of each FCGR specimen could be viewed without a microscope. A Dino-Lite digital microscope camera was used to verify the fatigue and fast fracture surfaces. A JEOL 7001F scanning electron microscope (SEM) was used to capture the microscopic features of these fracture surfaces.

6.3 Results and discussion

6.3.1 FCGR parameters

The crack growth and the corresponding cycle numbers were used to plot the crack growth curves in terms of the change of the stress intensity factor and the crack growth rate. The FCGR parameters were obtained from the crack growth curves. The fatigue crack growth rates of the Pipe 1 specimens are plotted in Figure 6-5, and the results of the FCGR parameters of five CI pipes are summarised in Table 6-2.

Data from the research literature on either SENB beams or compact tension (CT) specimens from CI pipes or other grey CI specimens were compared with the test results. Table 6-3 summarises the data from the literature on FCGR parameters.

The average results for the FCGR parameters of the static CI pipe (Pipe 1) are similar to the results for the spun CI pipes (Pipes 2 – 5). The average FCGR parameters represent the general crack propagation rate in CI pipe barrels, which indicate the remaining life of leaking CI pipes under certain spectra of operational pressures. The stress ratios have been shown to have little influence on the FCGR parameters obtained by fitting the power equation (Equation 2.13).

Table 6- 2 FCGR parameters of CI water pipes (values in brackets are the average for each pipe tested)

Pipe	Number of tests	m	C (*m/cycle*)
1	5	6.7 - 8.6 (7.5)	7.0×10^{-15} - 2.2×10^{-13} (7.4×10^{-14})
2	4	6.5 - 9.8 (8.4)	1.4×10^{-17} – 8.0×10^{-14} (2.2×10^{-14})
3	3	7.8 – 11.9 (9.9)	2.3×10^{-17} – 2.4×10^{-15} (1.1×10^{-15})
4	6	4.5 – 9.2 (6.4)	5.0×10^{-16} – 8.0×10^{-12} (2.2×10^{-12})
5	3	6.9 – 9.0 (7.8)	1.1×10^{-15} – 3.7×10^{-14} (1.9×10^{-14})
Average	-	7.8	6.5×10^{-13}

Table 6- 3 Comparison of Paris' constants from research literature data and full-scale tests

Specimen	R	Paris' constants		Reference
		m	C (*m/cycle*)	
SENB	0.1	7.4 - 8.0	2.1×10^{-16} - 4.6×10^{-15}	Mohebbi et al. (2010)
SENB	0.1	9.4 - 11.3	9.6×10^{-21} - 1.3×10^{-15}	Rajani et al. (2012)
SENB	0.1, 0.5	7.0 – 7.5	1.0×10^{-14} - 5.0×10^{-15}	Baicchi et al. (2007)
CT	0.05, 0.3, 0.7	6.2 - 6.7	6.1×10^{-16} - 2.6×10^{-12}	Bulloch (1995)
CT	0.01	5.9 - 7.2	6.0×10^{-15} - 2.0×10^{-16}	Hornbogen (1985)[1]
CT	0.1	5.5	1.8×10^{-14} - 5.1×10^{-15}	Kapadia and Imhof (1979)
SENB	0.1, 0.3, 0.5	4.5 – 11.9	1.4×10^{-17} – 8.0×10^{-12}	This study

[1] The FCGR parameters were from the best-fitting of the graphic plots.

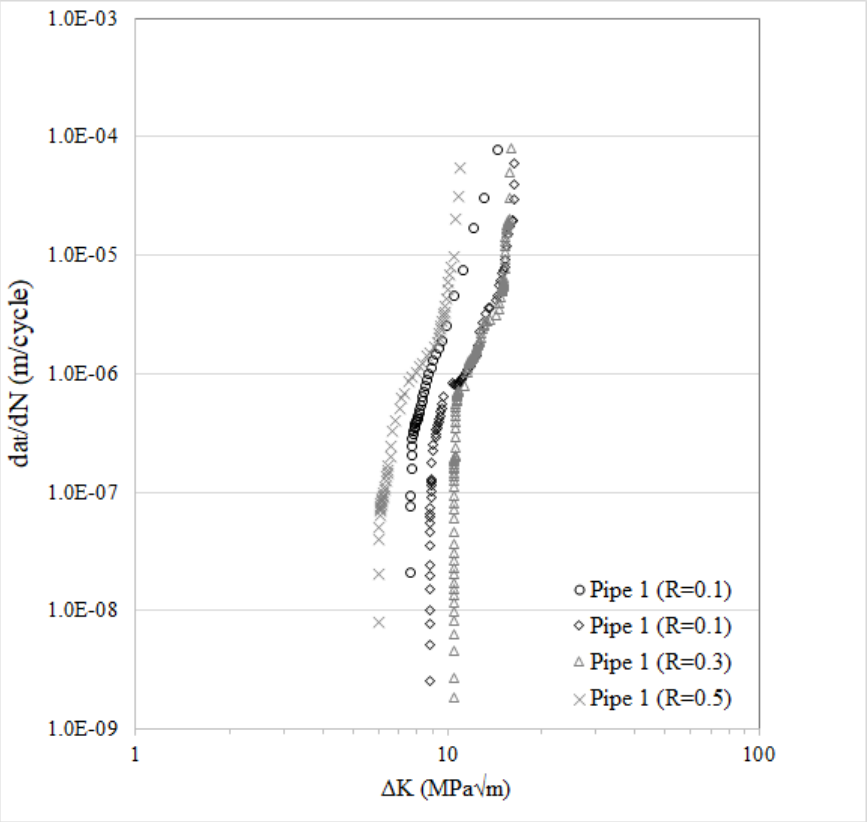

Figure 6- 5 Fatigue crack growth curves of Pipe 1 specimens

6.3.2 Threshold toughness

The values of threshold toughness obtained from the FCGR tests on five CI water trunk mains were calculated using Equation 6.4. Figure 6-6 summarises the experimental results for the threshold toughness of CI pipes with different stress ratios.

The data from the research literature on the threshold toughness of CI pipes and CI materials are also plotted in Figure 6-6 (Baicchi et al., 2007; Bulloch, 1995; Hornbogen, 1985; James and Li, 1999; Mohebbi et al., 2010; Rajani et al., 2012; Romaniv et al., 1981; Taylor et al., 1996). The threshold toughness of CI is significantly influenced by the stress ratio of the fatigue test. Furthermore, threshold toughness can be reduced or even ignored in corrosive environments, which means fatigue damage may not be restricted by limited crack length or low stress levels in a corrosive soil or water environment (Anderson, 2005; Rajani et al., 2012).

The threshold parameters of CIs, defined in Equation 6.4, δ and γ are equal to 8.6 and 0.5, respectively, based on the curve shown in Figure 6-6. These values represent the average threshold parameters of CIs subjected to cyclic loadings in an air environment, which are the upper boundary for the threshold toughness of CIs in corrosive environments.

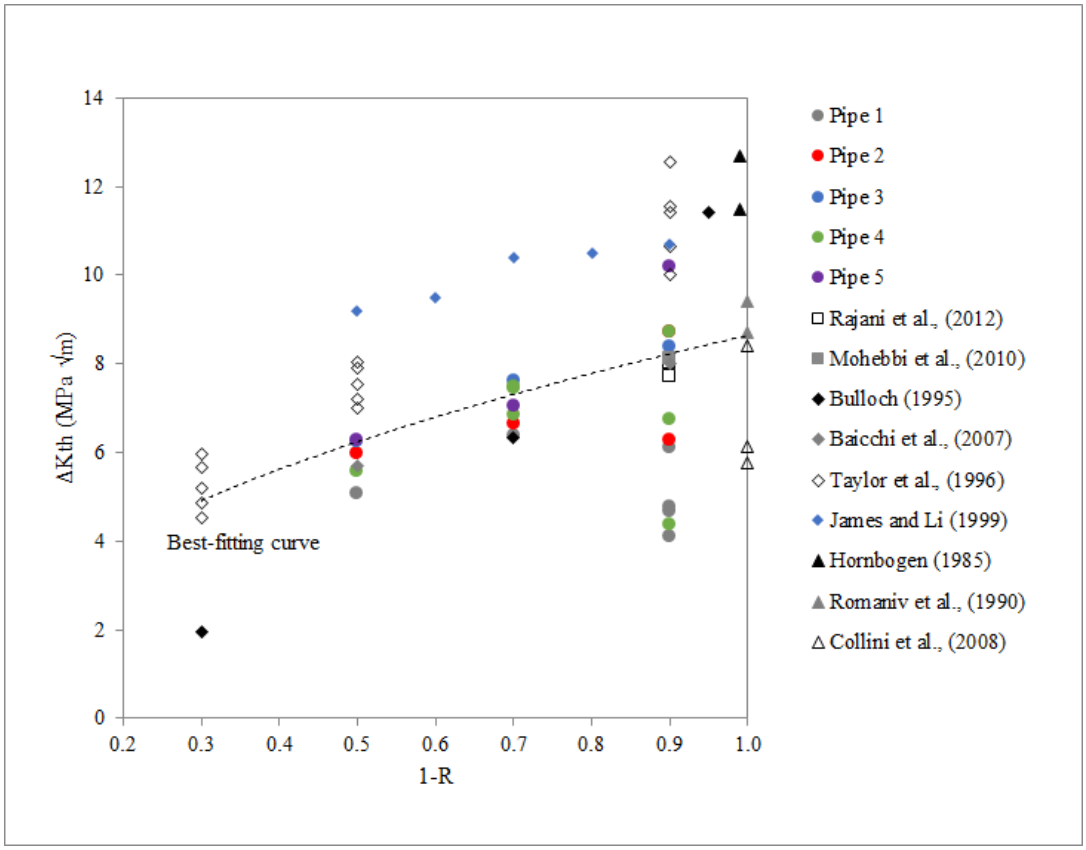

Figure 6- 6 Threshold toughness based on FCGR tests and literature data with stress ratios

6.3.3 Features of fractography

6.3.3.1 Macroscopic features

The surfaces of the failed FCGR specimens include two different regions: the fatigue surface and the final (fast) fracture surface. Figure 6-7 presents the typical fracture surfaces of specimens obtained from CI water pipes, which show distinguishable regions with different appearances. These regions are consistent with the crack growth data recorded by the digital image correlation (DIC) system. Typically, a fatigue pre-crack initiates at the edge of the straight-through notch, and the crack propagates during the FCGR test until the crack reaches the critical length, resulting in fast fracture.

The fatigue surfaces of CI pipe specimens are smoother than the surfaces of fast fractures, and the textures of the fatigue surfaces are different from the fast fracture surfaces. The colour of the fatigue surfaces of spun CI pipe specimens (Pipes 2 - 5) is generally lighter than the colour of the fast fracture surfaces (see Figure 6-7). No colour change was observed in the fracture surfaces of the static CI pipe specimen (Pipe 1), primarily due to the existence of pearlitic matrices (detailed in Chapter 3).

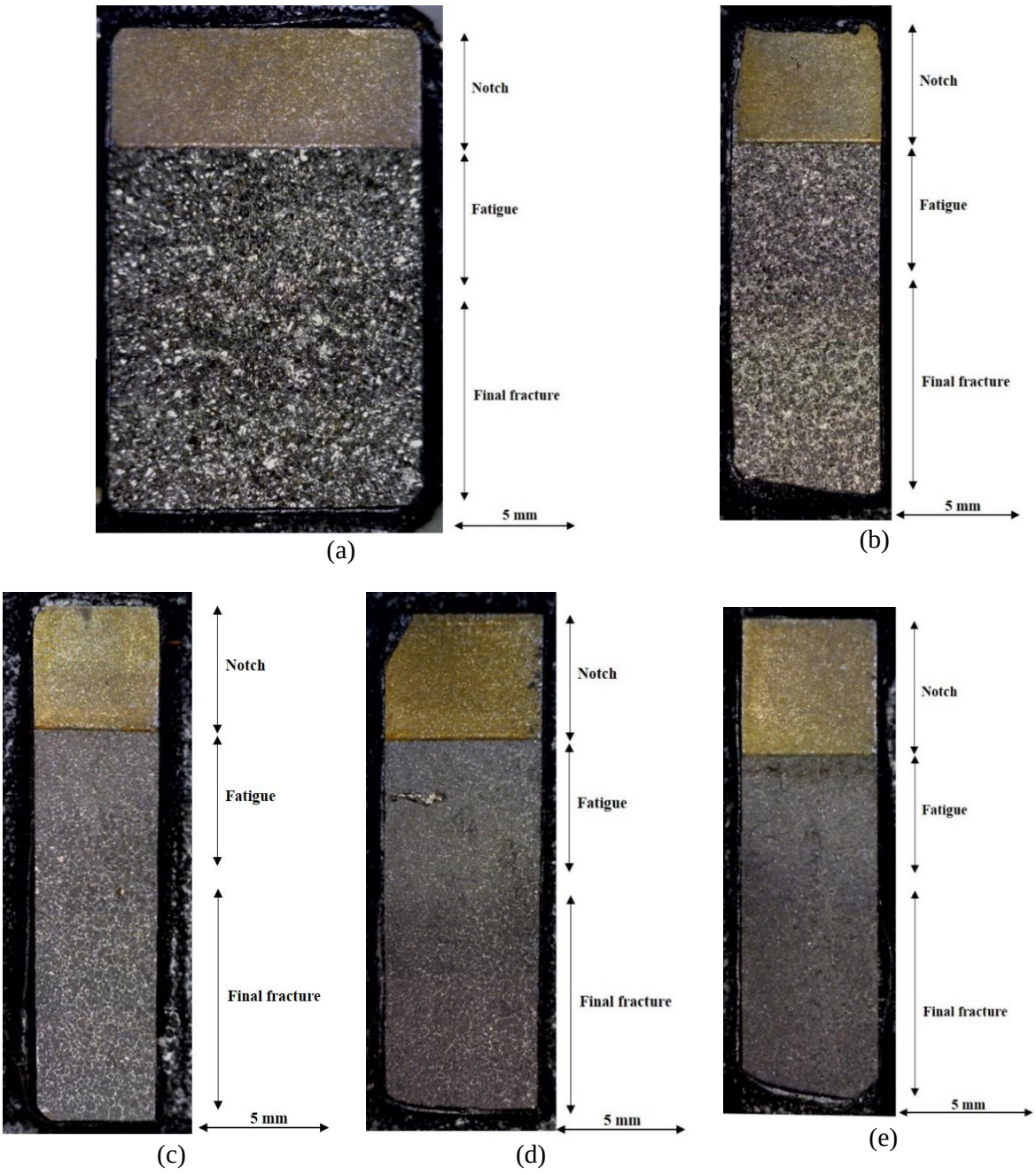

Figure 6- 7 Fracture surfaces of FCGR specimens of CI water pipes: (a) Pipe 1; (b) Pipe 2; (c) Pipe 3; (d) Pipe 4; (e) Pipe 5

6.3.3.2 Microscopic features

The tide (beach) marks captured on the fatigue surfaces of the FCGR specimens are perpendicular to the cyclic loading direction, which are visible through SEM microscopy. Figure 6-8 shows that the tide marks generated by the cyclic loads are distributed on the fatigue surface. The mode of transgranular cracking (fracturing through metallic metrices) was observed in both fatigue and fast fracture regions.

Tide marks were observed in all pipe specimens, and a comparison of fatigue and fast fracture surfaces is illustrated in Figure 6-9. Tide marks caused by cyclic loads were not observed on the fast fracture surfaces.

Fatigue striations were rarely observed on the fatigue fracture surfaces of the CI water pipes tested, and two sets of fatigue striations are shown in Figure 6-10. Due to the large distribution of graphite flakes, the fatigue striations cannot be fully generated in these scattered metallic matrices. In comparison with the tide marks, these fatigue striations cannot be considered as a common microscopic feature of the fatigue surface of the CI used in water pipes.

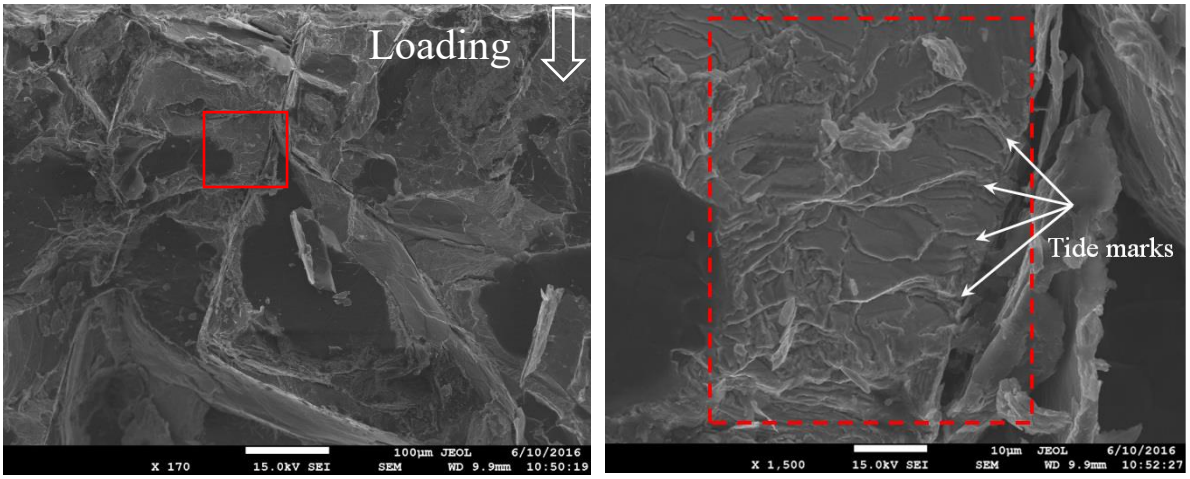

(a) (b)

Figure 6- 8 SEM images of FCGR fracture surface- fatigue surface (Pipe 1): (a) low magnification image; (b) enlarged image of the red square containing tide marks under cyclic loading

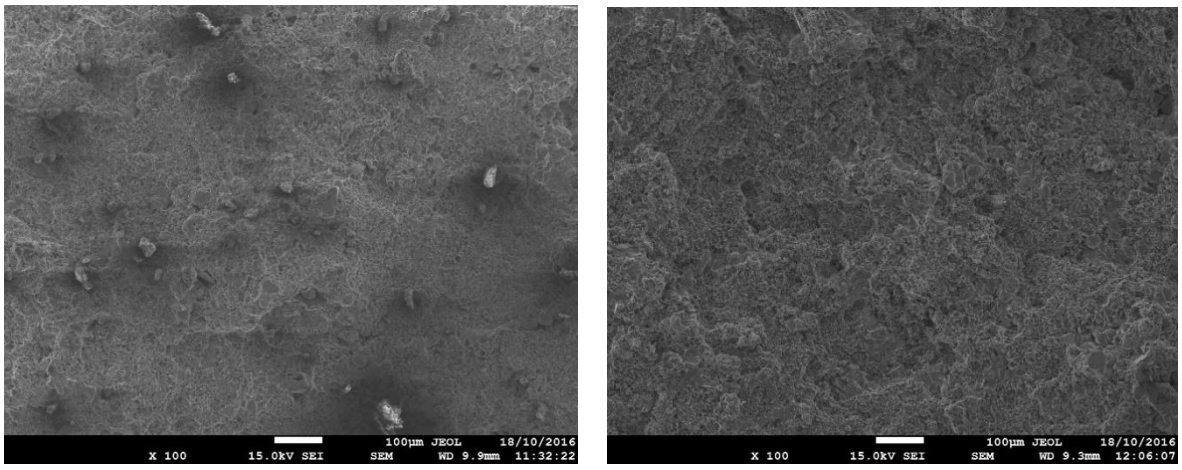

(a) (b)

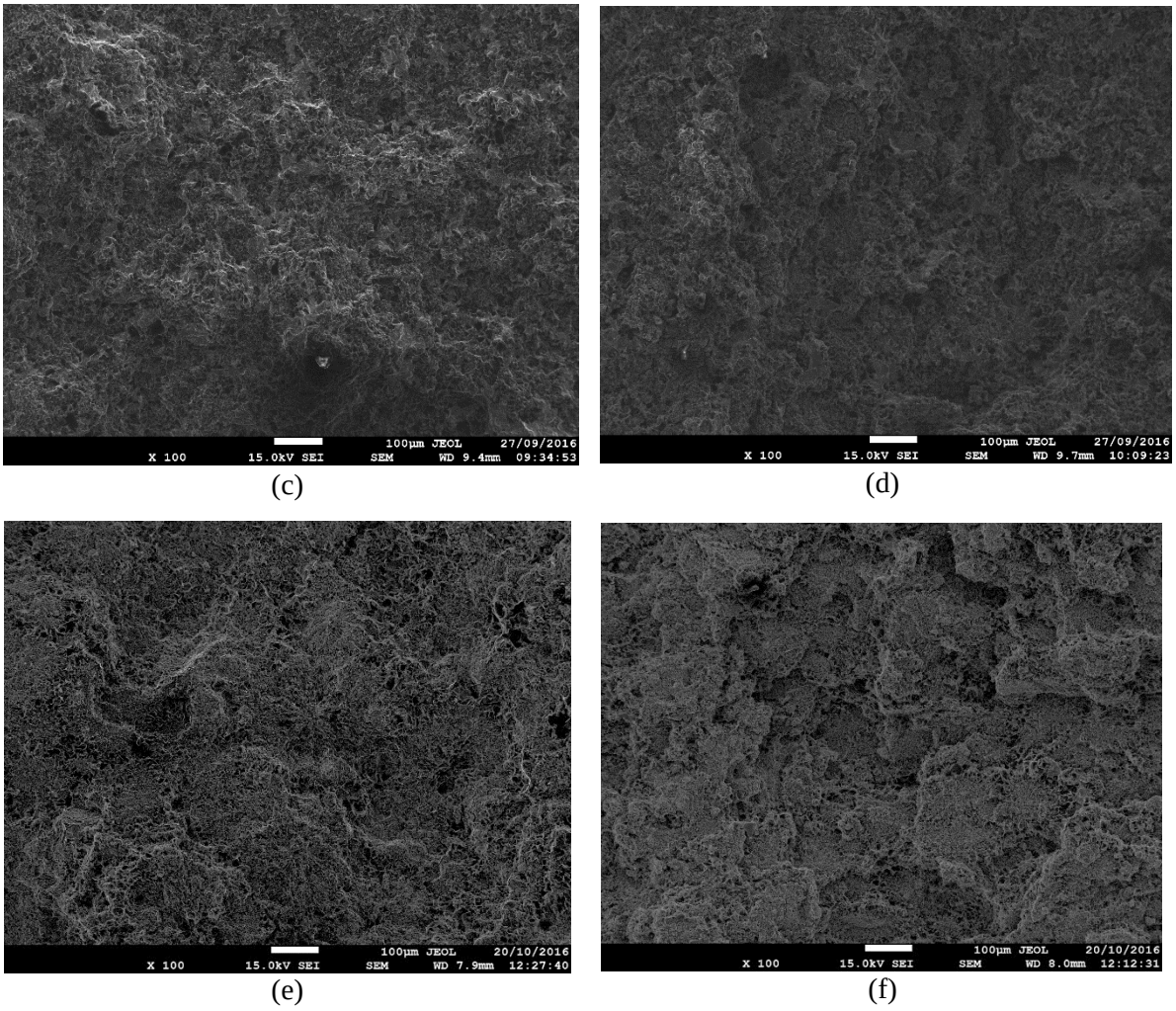

(c) (d)

(e) (f)

Figure 6- 9 SEM images of FCGR fracture surfaces: (a) Fatigue surface: Pipe 3; (b) Fast fracture surface: Pipe 3; (c) Fatigue surface: Pipe 4; (d) Fast fracture surface: Pipe 4; (e) Fatigue surface: Pipe 5; (f) Fast fracture surface: Pipe 5

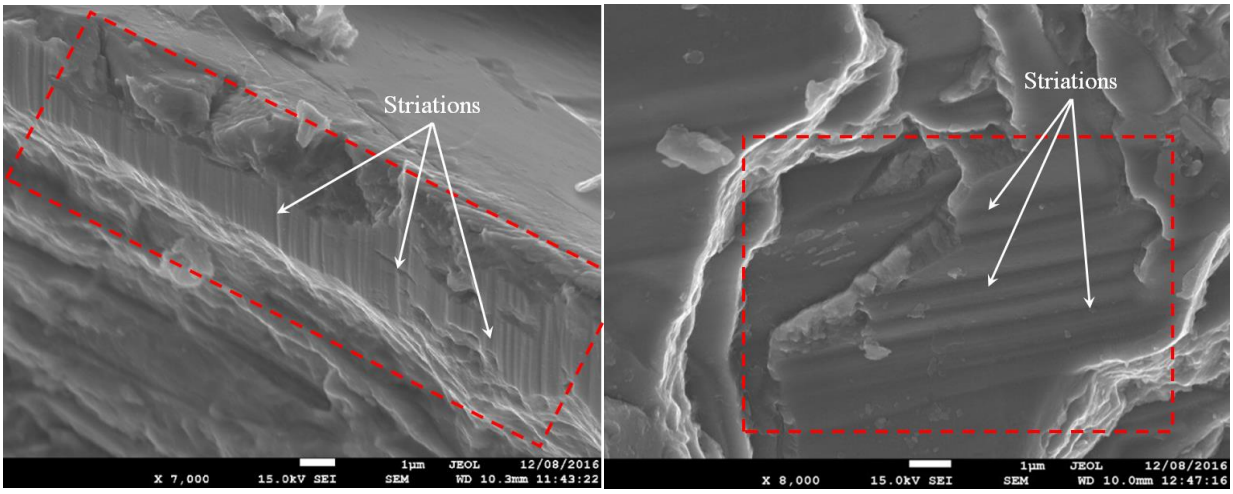

(a) (b)

Figure 6- 10 SEM images of fatigue striations in Pipe 1 specimens under FCGR testing

6.4 Conclusion

In this chapter, the fatigue crack growth in CI water pipe barrels was evaluated using the Paris' law. Fatigue crack growth rate (FCGR) parameters were reported based on a testing program of FCGR experiments on SENB specimens taken from five large-diameter CI water pipes. The stress ratios were found to have limited effects on the FCGR parameters. These test results are similar to the data in the literature on the FCGR parameters of CI water pipes and CI materials.

The values of the threshold toughness of CI water pipes were reported on the basis of the FCGR tests. The threshold toughness is significantly dependent on the stress ratios used in the fatigue tests. The threshold toughness parameters were provided from the curve of best fit of the test and the literature data. Water and corrosive soil environments may reduce the threshold toughness of CI water pipes.

The fracture surfaces of the FCGR specimens were examined to capture the features of fatigue fracture surfaces. The fatigue surface region shows a smoother texture and lighter colours, compared with the fast fracture surfaces. Furthermore, although tide marks were commonly observed in the SEM images for all pipes, fatigue striations were rarely seen on the fatigue fracture surfaces. These features of fatigue surfaces may not be visible in many pipe samples, as the fatigue surface may be damaged by the in-situ corrosive medium.

Chapter 7 Full-scale validation tests and simulation

7.1 Introduction

As detailed in Chapter 4, through-cracks initiate in the base of a corrosion patch in the CI pipe barrel, and are arrested in the ligaments of the thick remaining wall (Rathnayaka, 2016). Rajani and Kleiner (2010) and Rezaei et al. (2015) suggest that the fatigue induced by cyclic pressures may be the predominant crack growth mechanism causing pipes to fracture/burst. Full-scale pipe fatigue tests on steel and aluminium pressure pipes also show that cyclic pressure loading is capable of generating and propagating through-wall cracks in areas of high stress concentration, causing pipe failure (Alexander et al., 1997; Erdogan et al., 1969).

Controlled laboratory experiments can provide valuable information to enable understanding of the failure mechanisms of fatigue-driven failures caused by pressure variations in water pipelines. Therefore, a new pipe burst test facility has been developed at Monash University, Australia to examine the failure mechanisms of large-diameter CI pipes. In the first phase of development, the test facility was capable of continuously raising pressure inside a test pipe section to fail the test pipe section (Phase 1). The pump used to operate the burst test facility was not capable of increasing the pressure when the crack length exceeded a certain length (i.e., the pump flow rate was too low to account for water leakage

through the crack). In addition, the generation of cyclic pressure variations was not possible, as the pump in this test facility was operated manually. Therefore, possible crack growth due to fatigue could not be investigated. To investigate the effect of fatigue damage caused by cyclic pressures, the burst test facility mentioned above was upgraded to permit cyclic pressure variations. Using this upgraded facility, the research questions on fatigue crack initiation and propagation in CI pipe barrels were verified by full-scale burst tests of 600 mm diameter CI water pipes under cyclic pressures.

As a preliminary numerical simulation, the cohesive zone model (CZM) was established to simulate the fracture processes of composite and brittle materials (Barenblatt, 1962; Dugdale, 1960). The CZM of a bilinear traction-separation law was adopted to evaluate the behaviour of brittle fracture using Abaqus finite element software (Diehl, 2008).

In the present study, failures of large diameter pipes were examined for use as case studies for fatigue-driven failures. Many failures destroyed the evidence during violent bursts. However, one case study involving a failure initiated from an adjacent joint was possible to be studied. This study is presented in this section as the concluding case study in this project.

This chapter summarises the results of full-scale burst tests under cyclic pressures that validate the research questions addressed in Chapters 5 and 6. In addition to the small specimens used in Chapter 6, FCGR parameters were also obtained from these full-scale burst tests, which were used to estimate the LBB time window for preventing bursts of CI trunk mains from detectable leaks. The CZM is proposed to evaluate the leak and burst pressure of deteriorated CI trunk mains, and failures of CI trunk main bursts are analysed to demonstrate the revised approach to forensic investigation of the influence of fatigue on CI trunk main failures.

7.2 Full-scale burst tests

7.2.1 Burst facility

The burst facility was developed in two phases which are able to supply both static and cyclic pressures. The Phase 1 development of the burst test facility consisted of three sections: pipe containment, pressurisation system and instrumentation system. Detailed information about this test facility can be found in (Rathnayaka, 2016). An upgrade of the test facility (Phase 2) was required to maintain the desired internal water in a cracked pipe to overcome the leak flowing through a longitudinal crack. Two cylinders with pistons (henceforth referred to as transfer barrier cylinders (TBCs)) were incorporated to pressurise the test pipe and to store water temporarily before transferring it to the test pipe (see Figure 7-1 (b)). A minimum of two TBCs are required to conduct continuous pressure cycles (i.e., while the first cylinder is pressurising the pipe, the second cylinder is re-filled, in preparation for the cylinder to generate subsequent pressurisations). The next step in the design procedure was to calculate the size of the TBCs needed to generate the critical pressure profile shown in Figure 7-1 (a). The bore diameter of the selected TBCs was 254 mm and the rod (i.e., piston, see Figure 7-1 (b)) diameter of the selected TBCs was 228.6 mm.

The design pressure profile shown in Figure 7-1 was decided on the basis of the large-scale pressure monitoring program and represents a worst-case pressure-transient scenario (Rathnayaka et al., 2016a; Rathnayaka et al., 2016b). The effective bore length of each TBC installed is 2 m. The annulus side of each of the TBCs is connected to a standard hydraulic power unit rated to 35 MPa (see Figure 7-2). The hydraulic power unit includes a standard hydraulic pump (HP) and motor, a hydraulic oil storage tank, two electronically-operated directional control valves (DCVs) and an electro-hydraulic pressure- relief valve (PRV) (see Figure 7-2). The bore of each TBC is connected to the test pipe through a water management system. The water management system of the pipe fatigue test facility contains a water pump (WP) and several shut-off valves (SOFs). The water required for the tests is stored in the large storage tank below the test cell. The design of the TBCs (the area ratio of 5.26 between bore and annulus) allows the hydraulic oil side of the system to operate at high pressure-low flow conditions and the water side of the TBCs to operate at low pressure-high flow conditions.

The operational criteria for all valves and pumps in this test facility during a fatigue test are programmed in the Think & Do (i.e., SCADA program) computer program in such a way that the test facility is fully automated. This enables the facility to run fatigue tests for a long period of time without human interference. In addition, it is possible to run the test facility in manual mode to fill/empty the test pipe and to fill/empty the TBCs. The first step of the testing procedure is to run the water pump, keeping all SOFs identified as SOF 1 to SOF 4 in Figure 7-2 in the open position, with the exception of SOF 5. This valve arrangement enables the HP to fill the test pipe using water stored in the storage tank under

the test chamber. The test pipe is surrounded by four polycarbonate panels that capture and send the water leaking from the test pipe back into the storage tank; therefore, the water can be recirculated within the system. Once the test pipe is filled with water, SOF 1 and SOF 4 are closed and TBC 1 is filled using the same water pump through SOF3. When TBC 1 is fully filled (see Figure 7-2, pressure cycle *i*, TBC 1) the pipe fatigue test can be started. It is possible to use the water in a single stroke of one TBC to conduct several pressure cycles, depending on the leak rate through the crack (in this case, real leak flow rate < design leak flow rate). However, when explaining the operation of the test facility in the following text, it is assumed that the critical crack leaks water, and the water from one full stroke of TBC is consumed during one pressure cycle (leaking water = TBC stroke water).

A hydraulic power unit is used to run the hydraulic pump and drive TBC 1 downwards to pressurise the test pipe section and to perform the fatigue test on the test pipe with an initial pin-hole crack. To allow hydraulic oil to enter the annulus of the TBC 1, the automatic control system sets the directional control valve 1 (DCV 1) in the forward position (see Figure 7-2, pressure cycle *i*). While the TBC 1 is running to conduct pressure cycle *i*, the water pump sends water through SOF 3 to fill TBC 2 (see Figure 7-2, pressure cycle *i*). When TBC 2 is completely filled with water, the laser displacement gauge sends a signal to the control system to shut down the water pump until TBC 1 empties. During this process, DCV 2 stays in the reverse flow position to send the hydraulic oil inside the annulus of TBC 1 back to the hydraulic oil holding tank.

The combined operation of the hydraulic pump and the TBCs is only able to increase the pressure inside the test pipe. In order to decrease the pressure inside the test pipe to generate the lower half of the pressure profile shown in Figure 7-1, the test pipe should have a sufficient leak that can decrease pressure to a specified valve within a specified time. If the test pipe does not have a sufficiently large leak, an external hose is connected to the top end-plate to provide precise control of the pressure (see Figure 7-2). In a fully-automated fatigue test, the required pressure profile is inputted into the SCADA program to generate the required pressure variation in the test pipe section. The measurements taken by pressure transducers that are connected to the test pipe are used to control the operation of the pressure relief valve and to adjust the pipe pressure.

If all the water inside TBC 1 is consumed during the i^{th} pressure cycle (critical scenario), both DCV1 and DCV 2 change their status to reverse the operation of the TBCs (see Figure 7-2, pressure cycle *i*+1). This setting allows hydraulic oil to be sent to TBC 2 to generate pressure cycle *i*+1. To change the direction of water flow, SOF 1 and 4 are opened and SOF 2 and 3 are closed and the water pump is turned on to fill TBC 1 to prepare TBC 1 to conduct the next pressure cycle. The ball valve located downstream of SOF 1 and SOF 2 is used to empty the test pipe after completion of the pipe fatigue test. The pressure transducers attached to the test facility are capable of taking readings at 10 Hz. The flow rate though the crack in the pipe is calculated using the movement of the piston recorded by laser

displacement gauges (LDGs) during the fatigue test. In addition, the SCADA software automatically counts the number of pressure cycles throughout the test and displays the latest pressure profile on the computer screen. The complete fatigue test facility is shown in Figure 7-3.

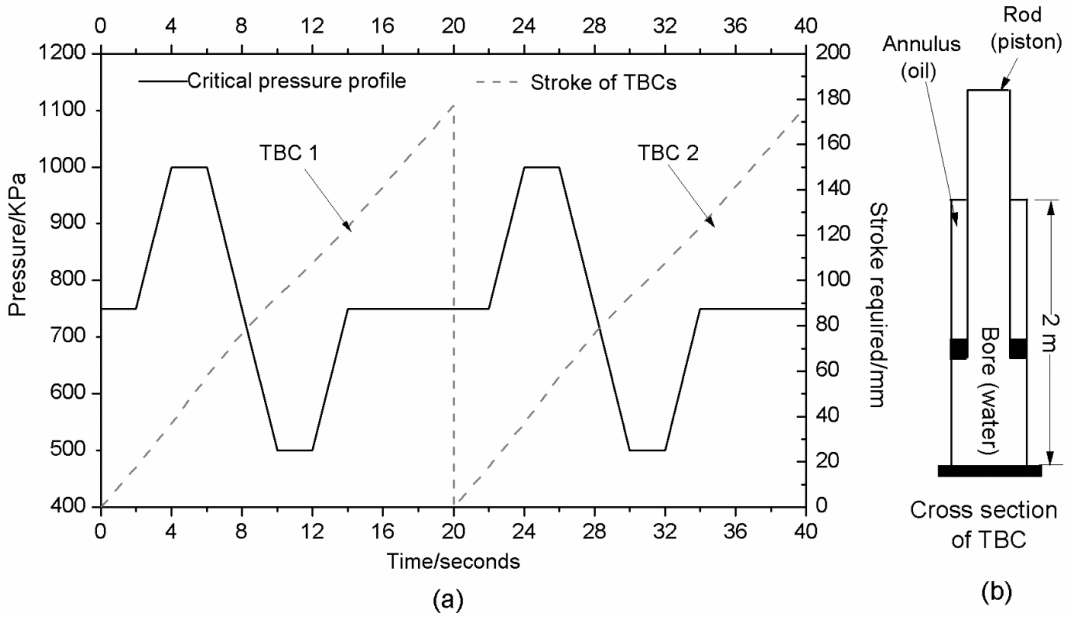

Figure 7- 1 (a) Critical design pressure profile and transfer barrier cylinders (TBCs) stroke variation when running test for critical pressure profile and (b) the cross section of TBC

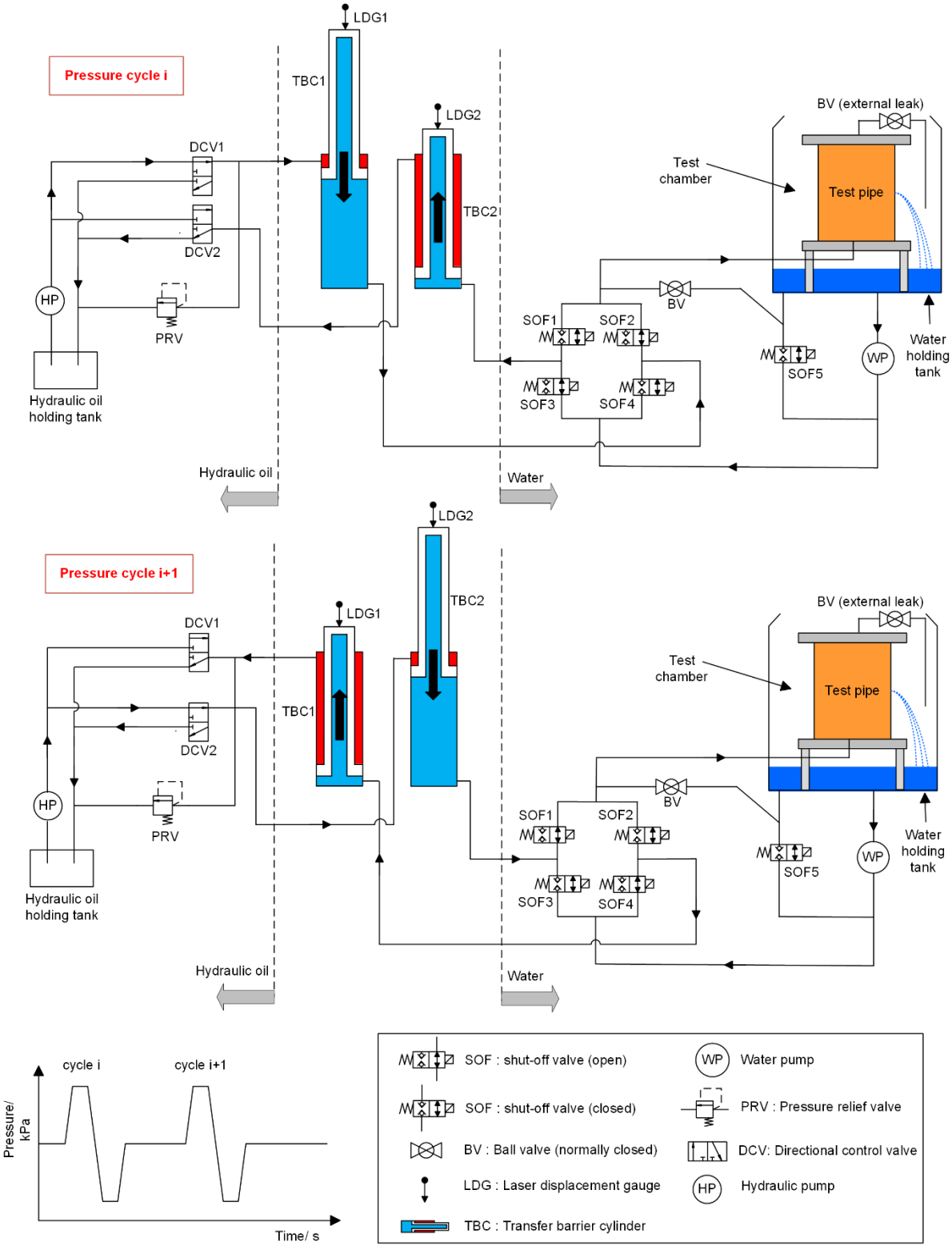

Figure 7- 2 Schematic of pipe fatigue test facility

Figure 7- 3 Components of pipe fatigue test facility

7.2.2 Pipe specimens and testing procedures

The pipe specimens used in fatigue tests were taken from a decommissioned 600 mm diameter static CI pipeline that was in service between 1922 and 2011 in the Sydney Water network. The average tensile strength and fracture toughness of the pipe material is 103 MPa (range of test results: 83–120 MPa) and 13.8 MPa√m (range of test results: 12.8–14.7 MPa√m), respectively, as detailed in Chapter 3. Moderate corrosion was found on both the internal and external pipe surfaces. The internal corrosion of the test pipe sections was removed to obtain a smooth, uniform surface free from corrosion. The dimensions of the pipe specimens and patch configurations are summarised in Table 7-1.

Two fatigue tests (F1 and F2) were carried out on the pipe specimens with a longitudinal through- crack generated by internal pressures which were part of the pipe burst test program conducted in the

ACAPFP project (detailed in Chapter 4). The aim of these tests was to evaluate fatigue crack propagation in CI pipe barrels under cyclic pressures. Fatigue test 3 (F3) was designed based on the CZMs conducted in the finite element software, Abaqus (detailed in Section 7.3). The aim of F3 was to verify the fatigue crack initiation in CI pipe barrels under cyclic pressures. Both the internal and external surfaces of these pipe specimens were scanned using a Creaform 3-D laser scanner. The patch configurations of the fatigue test specimens are shown in Figure 7-4.

Pressure cycles with a stress ratio of 0.5 were supplied by the system, which means the minimum pressure was half of the maximum pressure of a pressure cycle. The measured pressure profile during fatigue test 1 is shown in Figure 7-5. These measurements were taken at a rate of 5 Hz and the results indicated the test facility is capable of generating the required pressure profile accurately. The internal pressures and crack lengths in each test are shown in Table 7-1.

Strain gauges were attached on the external surface of test specimens to record the strain changes during the fatigue tests. The fatigue tests were recorded by two cameras. The crack lengths on the external pipe surface were measured, and these data were verified by the videos of the fatigue tests. In addition, the leak rates through the longitudinal cracks were measured for the first fatigue test to verify the analytical solution of leak rates in CI pipe barrels detailed in Chapter 4.

Table 7- 1 Summary of full-scale fatigue test specimens

Test	Length (m)	t_0 (mm)	Patch configuration (mm)			Pressure (MPa)		Crack length (mm)		Purpose
			2a	2b	c	min.	max.	initial	final	
F1	1.6	18	400	160	14.5	0.5	1.0	75	420	Crack propagation
F2	1.7	22	190	190	18.5	0.4	0.8	80	110	Crack propagation
F3	1.3	18	500	170	14.5	0.45	0.9	0	~5	Crack initiation

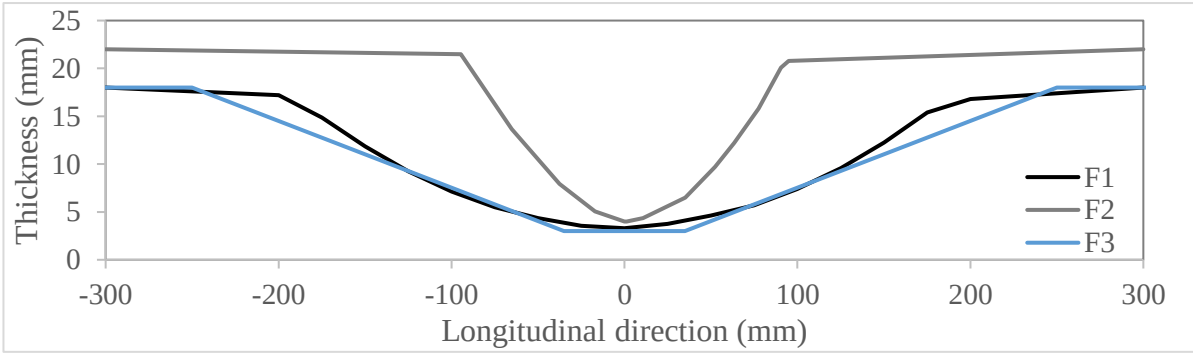

(a)

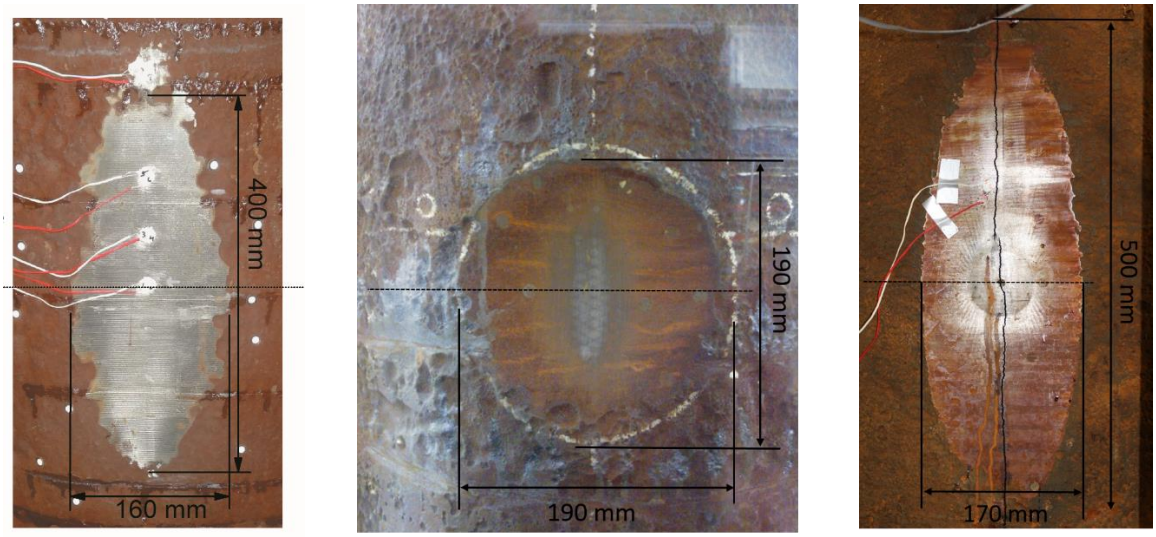

(b) (c) (d)

Figure 7- 4 Patch configurations of fatigue test specimens: (a) longitudinal thickness; (b) F1; (c) F2; (d) F3

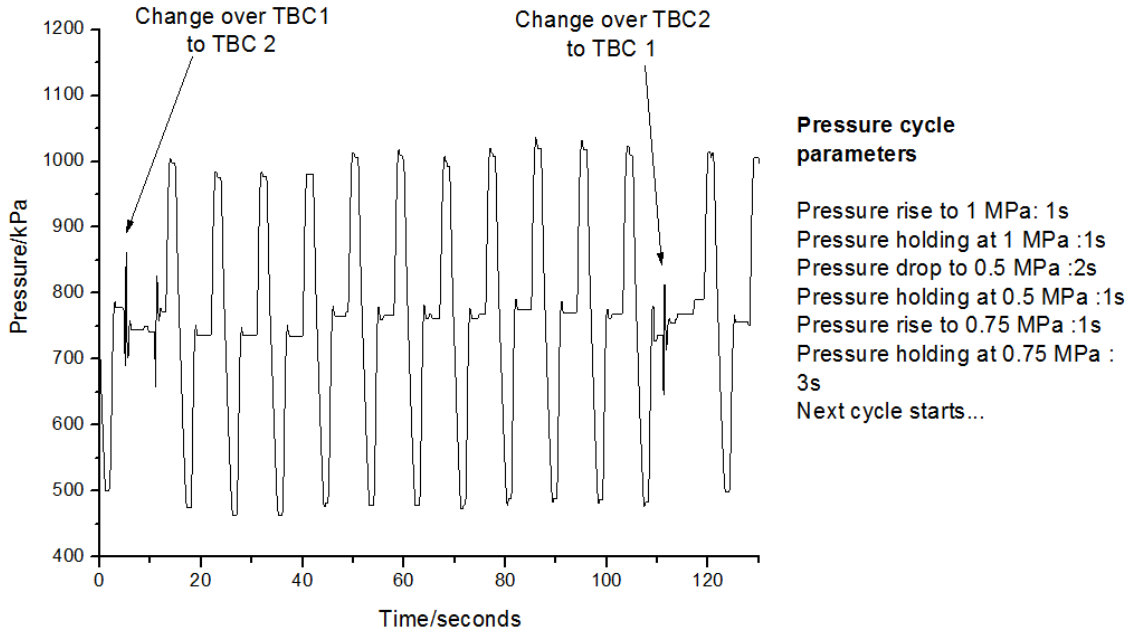

Figure 7- 5 Pressure profile in Fatigue Test 1 (i.e. simulated pressure transient)

7.2.3 Results and discussion

7.2.3.1 Propagation of a through-crack by cyclic pressure

An existing longitudinal crack enables grow under cyclic pressures. The longitudinal crack grew symmetrically in the artificial patches under the fatigue mechanism induced by cyclic internal pressures. The fatigue growth rates in the patched area are strongly affected by the patch configurations. The intensity factors and the corresponding crack growths were calculated using Equations 2.12- 2.14 and

7.1- 7.4, based on the measured crack length and operational pressures. The geometric factors for pressurised pipes containing a longitudinal crack (Equations 7.1- 7.3) are taken from Tada et al. (2000). The wall thickness in the crack tips was used to estimate the nominal stress and geometric factor with the growth of crack length.

$$K_I = \sigma_{nt} \sqrt{\pi\, a_t}\, F(\lambda) \tag{7.1}$$

$$F(\lambda') = \begin{cases} \sqrt{1 + 1.25\lambda'^2}, & 0 < \lambda \leq 1 \\ 0.6 + 0.9\lambda', & 1 \leq \lambda \leq 5 \end{cases}, \tag{7.2}$$

$$\lambda' = \frac{a_t}{\sqrt{R_i t_t}} \tag{7.3}$$

$$\sigma_{nt} = P\, \frac{R_i}{t_t} \tag{7.4}$$

where, a_t is a half of the crack length on external pipe surface, N is stress cycle, K_I is intensity factor, σ_{nt} is nominal stress for a pressurised pipe with a longitudinal crack within a corrosion patch, $F(\lambda)$ is a geometric factor for pressurised pipe containing a longitudinal crack, λ' is a dimensionless factor, R_i is internal pipe radius, and t_t is the wall thickness of the crack tip.

The data on crack growth with pressure cycles are plotted in Figure 7-6. The best fittings of the power equation (Paris's law) (Equation 2.13) provide the FCGR parameters for the full-scale fatigue tests. The average FCGR parameters are similar to the test results obtained from the SENB specimens (detailed in Chapter 6). The results for the FCGR parameters from both full-scale and specimen fatigue tests are summarised in Table 7-2.

Table 7- 2 FCGR parameters of CI water pipes from specimen and full-scale tests

Test	Number of tests	m	C (*m/cycle*)
Full scale: Static CI	2	7.9 (7.0- 8.7)	1.8×10^{-14} (4.8×10^{-15}- 3.1×10^{-14})
Specimen: Static CI	5	7.5 (6.7- 8.6)	7.4×10^{-14} (7.0×10^{-15}- 2.2×10^{-13})
Specimen: Spun CI	16	7.8 (4.5- 11.9)	8.3×10^{-13} (1.4×10^{-17}- 8.0×10^{-12})

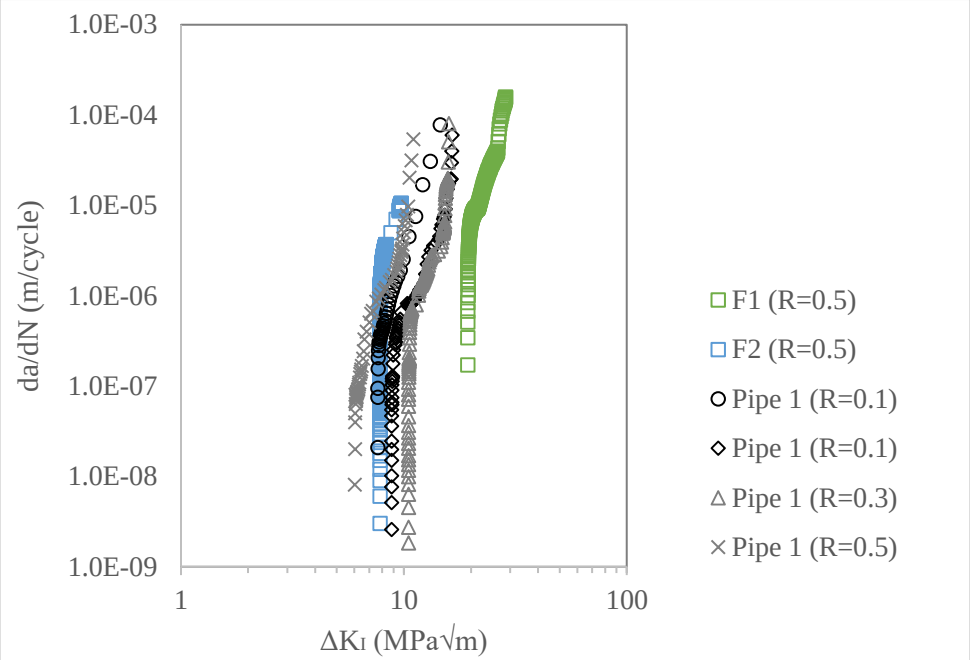

Figure 7- 6 Fatigue crack growth rates of CI water pipes from full-scale and specimen fatigue tests

7.2.3.2 LBB time window

The LBB time window can be estimated from the entire cycle numbers to propagate an initial crack to the critical length. Equation 7.5 is rephrased from the Paris' law (Equation 2.13). The initial crack length is determined by the corrosion patch configuration, and the final critical crack length is controlled by the maximum pressure, pipe dimensions and fracture toughness. An analysis and discussion of the initial and final critical length are provided in Chapter 4. The number of pressure cycles can be estimated using Equations 2.12- 2.14 and 7.1- 7.5.

$$N_f = \int_{a_i}^{a_c} \frac{1}{C(\Delta K)^m}\, da_t \tag{7.5}$$

where, N_f is failure cycle number, a_i is half of the initial crack length in pressurised pipe with a corrosion patch, and a_c is half of the final critical crack length in pressurised pipe with a corrosion patch.

The water leak rates from the longitudinal crack were estimated through the analytical solution (Equations 7.6- 7.9). The water leak and crack propagation during fatigue test 1 (F1) are shown in Figure 7-7, and a comparison of measured leak rates and the analytical solution for the F1 test is plotted in Figure 7-8. A modulus of elasticity of 100 GPa was used in this analytical solution. This analytical solution is suitable for predicting the leak rates above 25 L/min, which is the lower limit of the global leak detection method summarised in Chapter 2. Therefore, the LBB time window can be redefined as

the period between a detectable leak and the final burst event, which is shown in the failure analysis in Section 7.4.

$$\lambda = \frac{a_t}{\sqrt{R_i\, t_0}} \tag{7.6}$$

$$G(\lambda) = \begin{cases} \lambda^2 + 0.625\lambda^4 & 0 < \lambda \leq 1 \\ 0.14\lambda + 0.36\lambda^2 + 0.72\lambda^3 + 0.405\lambda^4 & 1 \leq \lambda \leq 5 \end{cases} \tag{7.7}$$

$$A = \frac{2\pi R_i^2 P\, G(\lambda)}{E} \tag{7.8}$$

$$Q = C_d A\sqrt{2P} \tag{7.9}$$

where, λ is a dimensionless factor for pressurised pipe with uniform wall thickness and a longitudinal crack, t_0 is the nominal wall thickness, $G(\lambda)$ is the geometric factor for crack opening area, A is the crack opening area, P is internal pressure, E is the modulus of elasticity, Q is leak rate, and C_d is the discharge coefficient, with 0.67 being used for a longitudinal crack in CI pipes (Cassa et al., 2010).

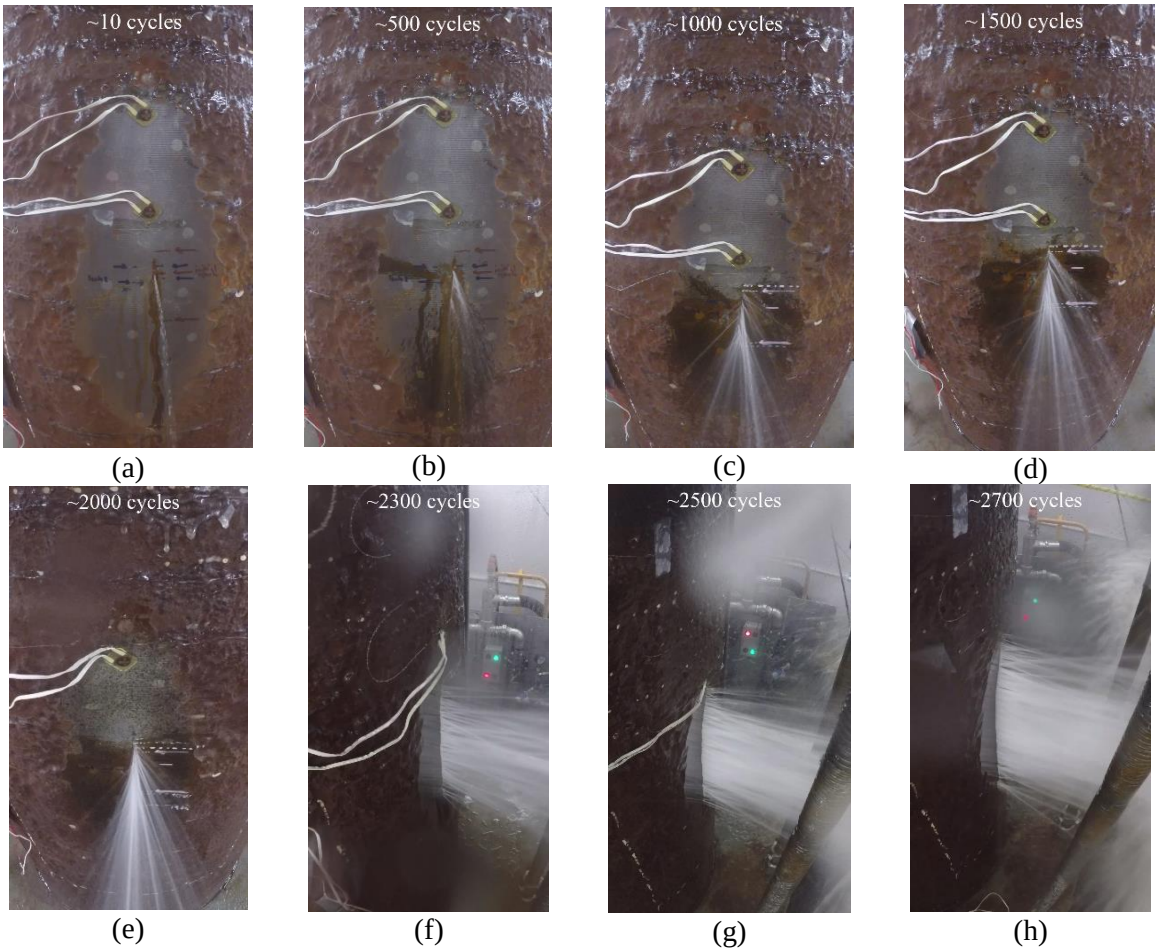

Figure 7- 7 Water leak and crack propagation of full-scale fatigue test 1 (F1)

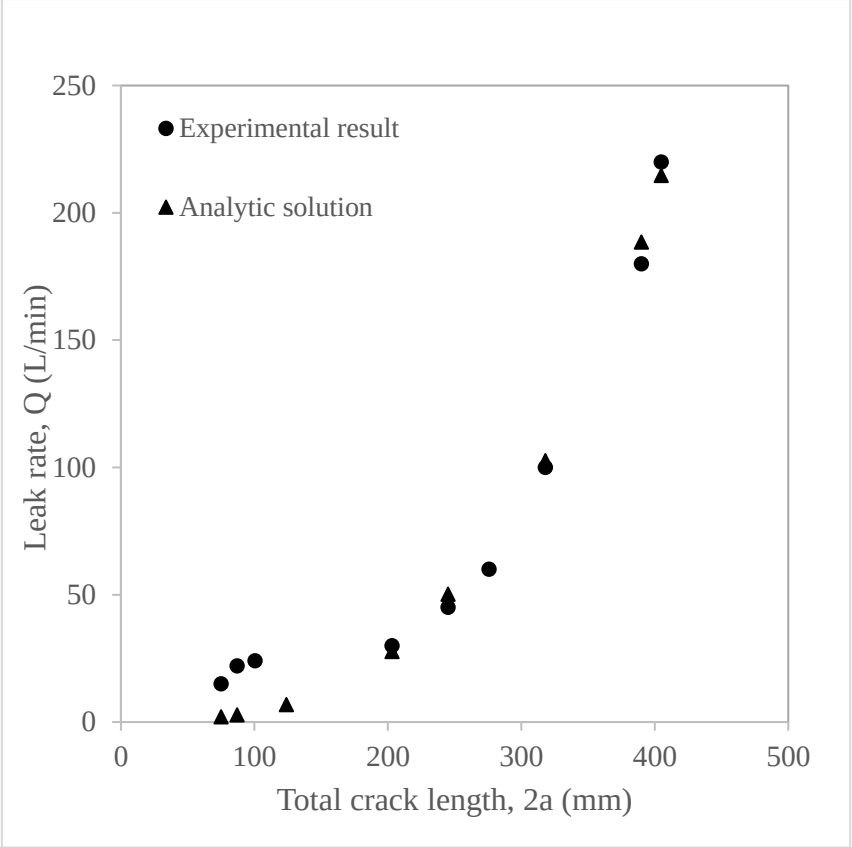

Figure 7- 8 Leak rates with crack lengths based on data and analytical solution

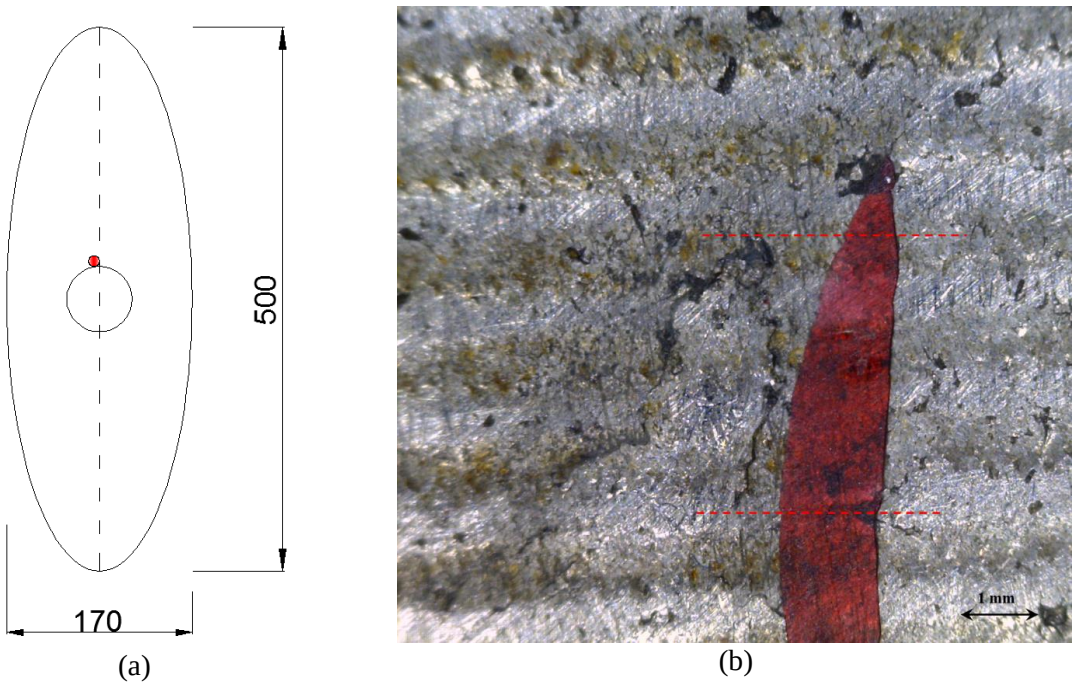

(a) (b)

Figure 7- 9 Fatigue crack initiation: (a) location of crack initiation; (b) crack initiated by cyclic pressures

7.2.3.3 Initiation of a through-crack by cyclic pressure

Fatigue crack initiation was observed in fatigue test 3 (F3). The crack initiated in the central area of an artificial patch (Figure 7-9) under cyclic pressures ranging from 0.45 to 0.9 MPa. The through-wall crack was generated after about 750 pressure cycles which were recorded by a strain gauge. The cumulative hoop strain in the artificial patch is plotted in Figure 7-10. The maximum stress in the patched area and cycle number is shown in Figure 7-11, in comparison with the stress-controlled fatigue tests obtained from specimens.

Cyclic pressures enable to generate a through-wall crack in the areas subjected to stress concentration. Local manufacturing defects or graphite flakes may also play the role of stress concentrators.

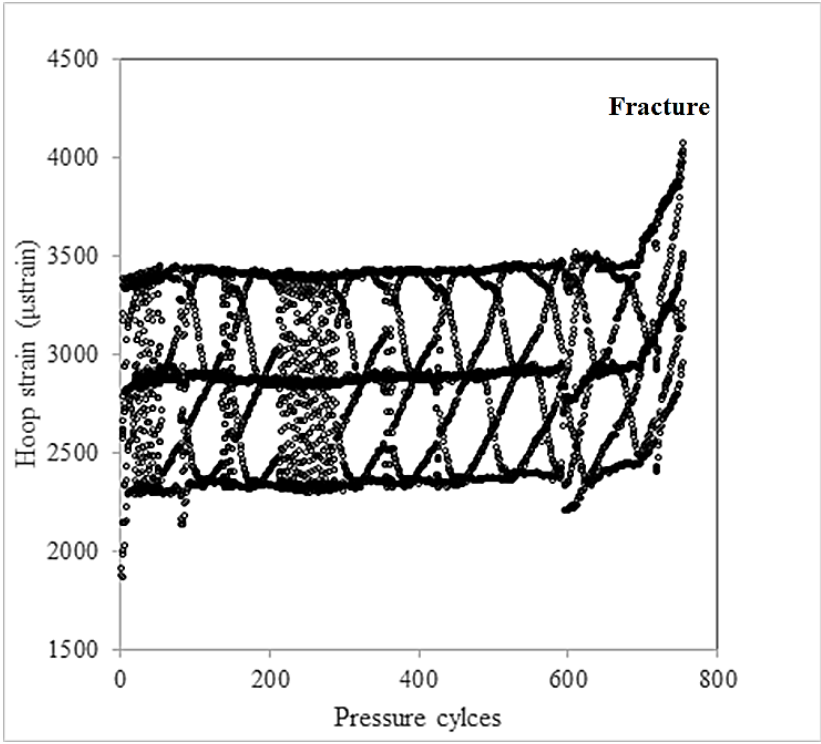

Figure 7- 10 Hoop strain recorded in area of fatigue crack initiation

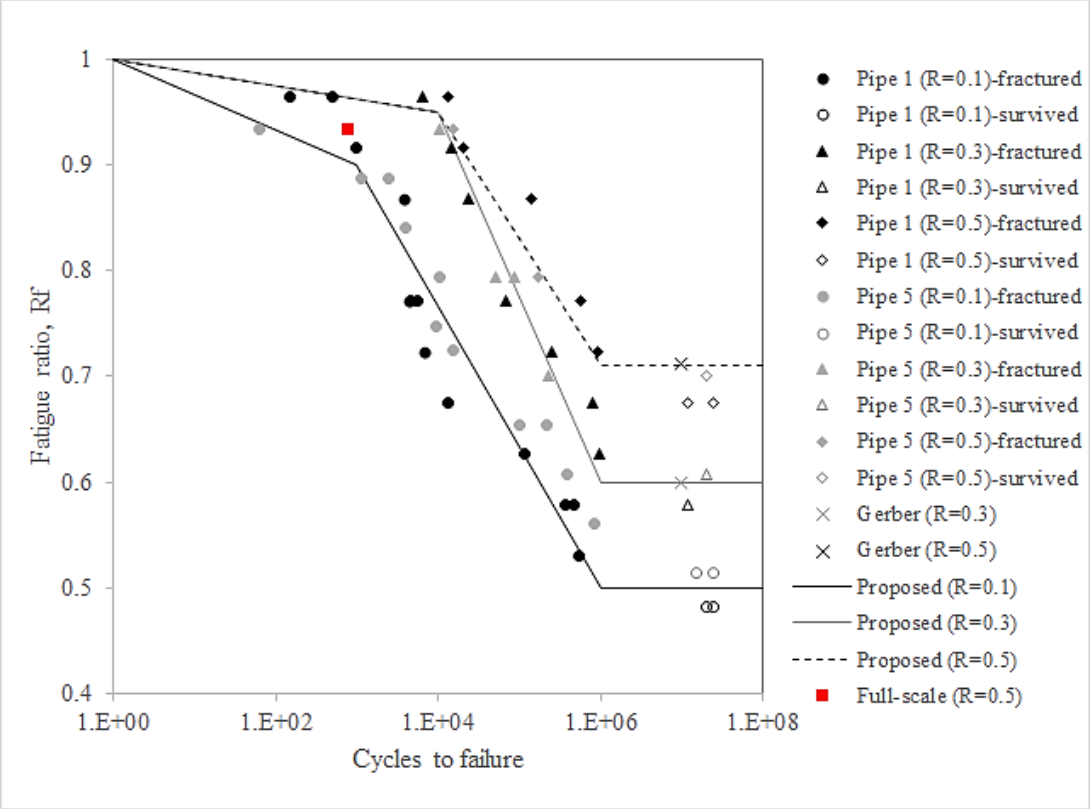

Figure 7- 11 S-N curves of CI water pipes from specimen and full-scale tests

7.3 Validation of burst tests: cohesive zone models

7.3.1 Traction separation law

The cohesive zone model was established to address the fracture of composite or brittle materials (Barenblatt, 1962; Dugdale, 1960). The finite element software Abaqus 6.13 provides a function defining the cohesive behaviour for a contacting surface.

The bilinear traction-separation law is adopted to describe the behaviour of brittle fracture. The bilinear traction-separation law (Figure 7-12) is expressed by Equations 7.10 and 7.11 (Chen and El-Hacha, 2013; Lundberg and Eliasson, 2015).

$$G_c = \frac{T_u \, \delta_f}{2} \tag{7.10}$$

$$K = \frac{T_u}{\delta_0} \tag{7.11}$$

where, G_c is the fracture energy, K is the penalty stiffness, T_u is the ultimate traction stress, δ_0 is the separation at damage initiation, and δ_f is the separation at failure.

The ultimate traction stress (T_u) is assumed to be equal to the tensile strength of CI (σ_u), and the penalty stiffness (K) is related to the modulus of elasticity (Diehl, 2008). Although the fracture energy of CIs cannot be directly measured, the relationship between fracture energy and fracture toughness (Equations 7.12- 7.14) is used to evaluate the fracture energy of CIs (Anderson, 2005).

$$G = \frac{K_I^2}{E} \tag{7.12}$$

$$G \geq G_c \tag{7.13}$$

$$K_{Ic} \geq K_I \tag{7.14}$$

where, G is the energy release rate, which is larger than or equal to the fracture energy (G_c), E is the modulus of elasticity, K_I is the intensity factor, and K_{Ic} is the fracture toughness.

The fracture toughness of CIs is greatly affected by the methods of testing and analysis (Bradley and Srinivasan, 1990). The values of fracture toughness reported for specimen tests are significantly lower than the results from the specimen tests (Conlin and Baker, 1991). The typical ranges of mechanical properties of CI pipes are summarised in Table 7-3.

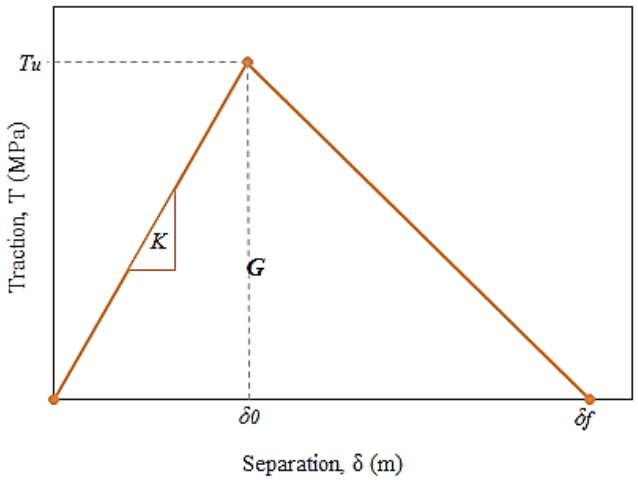

Figure 7- 12 Bilinear traction-separation model

Table 7- 3 Typical ranges of mechanical properties of static CI pipes

Mechanical properties	This study	Review data	References
Tensile strength (*MPa*)	80- 120	65- 160	Seica and Packer (2004)
Modulus of elasticity (*GPa*)	60- 100	78- 150	Rajani and Kleiner (2013b)
Fracture toughness ($MPa\sqrt{m}$)	13- 15	22- 29	Conlin and Baker (1991)
		15- 27	Mohebbi et al. (2010)

7.3.2 Methodology

7.3.2.1 Selection of cohesive zone model parameters

To simulate longitudinal fractures in CI pipe barrels, a contact surface is defined in Abaqus with the properties of cohesive behaviour and damage (Figure 7-13). The properties of the contact surface were evaluated from the ranges identified in the research literature and test results. The full-scale burst tests in corroded CI pipes were simulated using the cohesive zone model (CZM) in the finite element (FE) program in Abaqus 6.13.

The leak and burst pressures can be obtained using intact pipe models (T1, T2, T3, T4 and F3). The leak pressure is defined by the separation of elements on internal surfaces, and the burst pressure is determined by the pressure which causes the total separation of contact surfaces in the pipe segment. The simulation plan and pipe dimensions are summarised in Table 7-4.

Linear tetrahedral meshes were chosen for meshing the pipe segments with patches. Different mesh sizes were used to evaluate the cohesive behaviour of the contact surface, and the optimum mesh size of 0.4 mm for cohesive models was determined by trial analyses. The stress concentration of each pipe segment (summarised in Table 7-4) is shown in Figure 7-14.

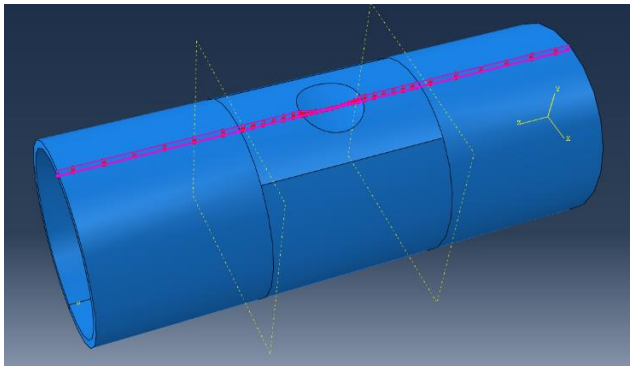

Figure 7- 13 Contact surface in pipe structure

Table 7- 4 FE simulation of pipe dimensions

Pipe sample	Length (*mm*)	t_o (*mm*)	2a (*mm*)	2b (*mm*)	c (*mm*)	Patch
T1	1.34	25	125	93	17.9	Natural
T2	1.71	25	190	190	20	Artificial
T3	1.26	17	330	100	13	Artificial
T4	1.58	18	400	160	14.5	Artificial
F3	1.5	18	500	170	15	Artificial

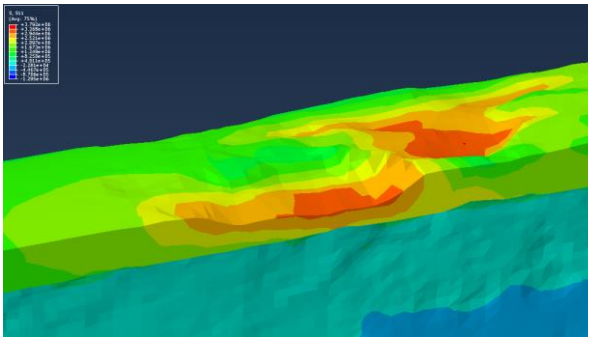

(a)

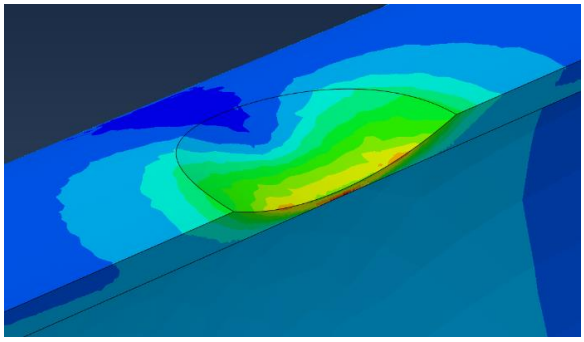

(b)

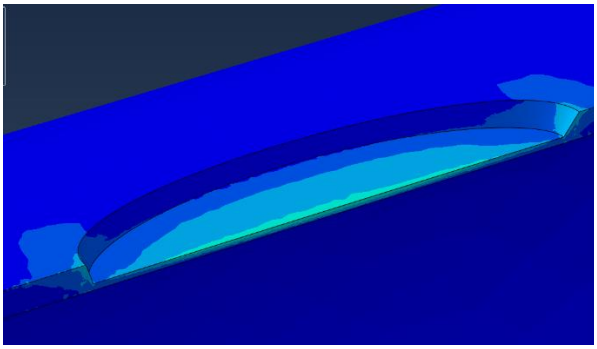

(c)

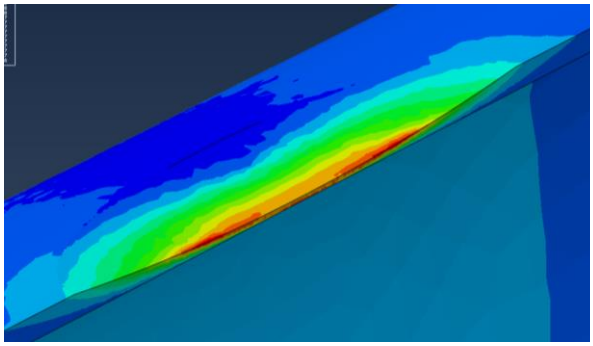

(d)

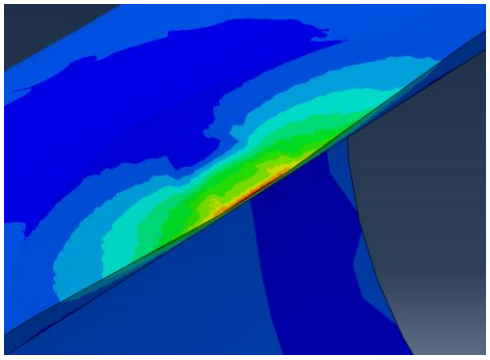

(e)

Figure 7- 14 Abaqus models: (a) T1; (b) T2; (c) T3; (d) T4; (e) F3

7.3.3.2 Evaluation of remaining capacity of leaking corroded CI pipes

The burst pressures can be analysed using the models with an existing crack (F1 and F2). The simulation plan and pipe dimensions are summarised in Table 7-5. To simulate cracked pipes, two separated contact surfaces were defined, and the crack length was controlled by the area without surface properties. It should be noted that FE-CZM does not simulate the LBB window or fatigue life of corroded CI pipes. It only computes the critical crack length at failure under monotonic loading.

Table 7- 5 FE Simulation of pipe dimensions

Pipe sample	Length (*mm*)	t_o (*mm*)	2a (*mm*)	2b (*mm*)	c (*mm*)	Patch
F1	1.58	18	400	160	14.5	Artificial
F2	1.71	18.5	190	190	15	Artificial

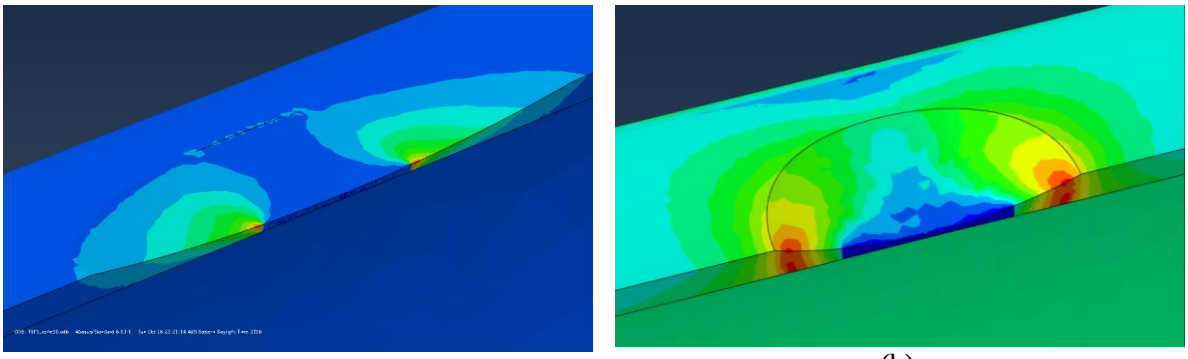

(a) (b)

Figure 7- 15 Abaqus models: (a) F1; (b) F2

7.3.3 Results and discussion

7.3.3.1 Cohesive zone parameters

The ranges of cohesive parameters, including the fracture energy (G_c), the ultimate traction stress (T_u) and the penalty stiffness (K), were calculated based on the typical values of the mechanical properties of static CI pipes (Table 7-3). Various cohesive parameters within the allowed ranges were trialled to meet the observed leak and burst pressures in full-scale burst tests. The selected cohesive parameters and mechanical properties used in the Abaqus models are shown in Table 7-6.

The simulation results of burst tests using the selected cohesive parameters are summarised in Table 7-7, which give accurate predictions of both the leak and burst pressures of these full-scale tests of CI pipe segments. A catastrophic burst was observed in T3 and F3, and these burst pressures were verified by the simulation results of the CZMs. In other tests, the maximum achieved pressures were unable to produce catastrophic bursts. The burst pressure obtained by the CZMs is above the achieved pressure, which explains why bursts did not occur in these full-scale tests.

7.3.3.2 Evaluation of remaining capacity of leaking corroded CI pipes

The burst pressures for the pipe segments containing a longitudinal crack were plotted for comparison with the maximum pressures achieved during the fatigue tests (Figure 7-16). The burst pressures from the CZMs are higher than the pressures observed during the fatigue tests. The results prove that the maximum achieved pressures in full-scale fatigue tests do not reach the burst pressures.

Table 7- 6 Input cohesive parameters and mechanical properties

Cohesive parameters and mechanical properties	Selected value	Allowed range
Fracture energy (N/m)	12,000	2,250- 14,000
Ultimate traction stress (MPa)	120	65- 160
Penalty stiffness (N/m^3)	5×10^{12}	5×10^{11}- 3×10^{13}
Young's modulus (GPa)	90	60- 100
Poisson's ratio	0.3	-

Table 7- 7 Simulation results of burst tests

Test	Full-scale tests		FE simulation		FE-CZM	
	P_{leak}	P_{burst}	P_{leak}	P_{burst}	P_{leak}	P_{burst}
T1	3.5	-[1]	3.6	-	3.7	5.3
T2	3.2	-[2]	3.0	3.55	3.2	3.8
T3	1.2	1.44	1.24	1.3	1.14	1.45
T4	0.8	-[3]	0.97	1.31	1.2	1.6
F3	0.9	1.23	-	-	1.0	1.4

1. Burst did not occur. The maximum achieved pressure was 3.5 MPa.
2. Burst did not occur. The maximum achieved pressure was 3.7 MPa.
3. Burst did not occur. The maximum achieved pressure was 1.25 MPa.

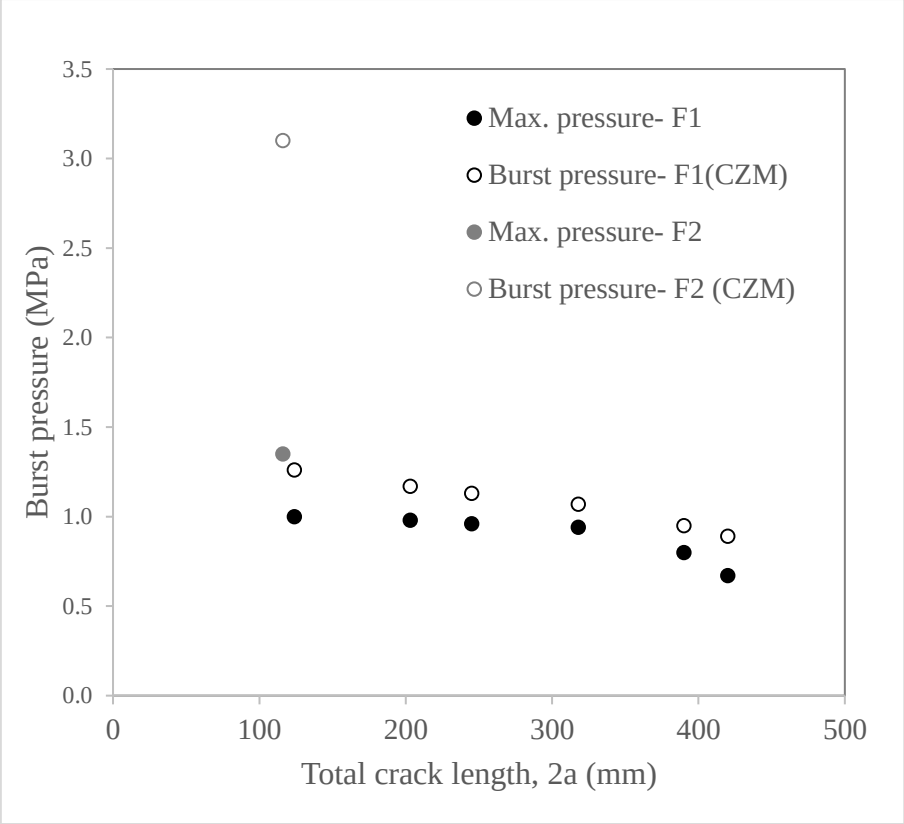

Figure 7- 16 Simulation results of burst pressures of CI pipe segments containing a longitudinal crack

7.3.4 Discussion

The preliminary analysis undertaken indicates that the fracture behaviour of CI water mains can be simulated by cohesive zone models using Abaqus. The CZM parameters were selected to evaluate the leak and burst pressures of corroded CI trunk mains. This method is potentially applicable for analysing the impacts of corrosion configurations on the remaining capacity of pressurised water pipes. The simulation results can be used in future pipeline integrity assessment and full-scale burst test design. However, the determination of the LBB time window is not simulated by Abaqus since that requires the simulation of crack growth with cyclic loading spectra.

7.4 Explanation of selected case study: Harris Street pipe burst

7.4.1 Background

A catastrophic pipe burst occurred at the intersection of Harris Street and Ultimo Street, Sydney on 10th August 2013 (see Figure 7-17), and caused substantial flooding and traffic interruption. A minor leakage was observed several weeks prior to the final failure. The fractured 500 mm diameter spun CI pipe was installed in 1961 with a nominal thickness of 15 mm, and the failure mode was identified as a longitudinal barrel fracture. The spun CI pipe was buried in a backfill sand trench with tar paint coating and factory-applied cement lining. The pavement was a 250 mm-thick bitumen-covered concrete surface, and the total burial depth was approximately 1.6 m to the pipe crown. Traffic loads tend to cause low stress on buried pipes due to the existence of concrete pavement (Robert et al., 2016b). Longitudinal barrel fracture is the predominant failure mode for large-diameter CI pipes and is caused by local stress concentrations and hoop stresses produced by internal pressures (Makar, 2000). Fatigue from cyclic internal pressures is considered as a mechanism to propagate existing cracks in pressurised pipe barrels (Cullin et al., 2014; Rathnayaka et al., 2015). Hence, the effects of internal pressures on fractured pipes require detailed analysis.

In this failure investigation, metallurgical features and mechanical properties are reported for the failed CI pipe. Modelling processes and the results of fatigue crack growth and leak rates are specified as part of the failure investigation. A significant difference between this study and previous research on large-diameter water CI pipes is that a crack growth fatigue model is proposed to predict the remaining life of leaking pressurised pipelines. A limited time window between leakage and catastrophic failure (LBB window) is identified that may be used to detect leakage incidents in order to predict or prevent future CI water-pipe bursts.

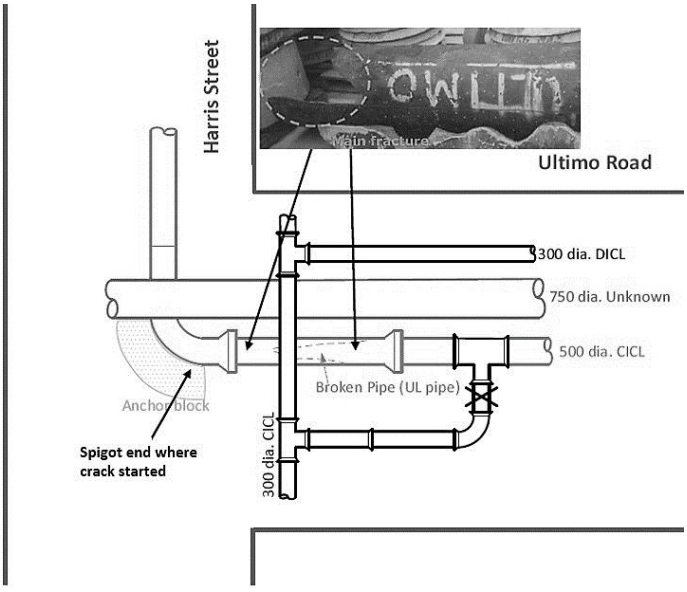

Figure 7- 17 Layout of failed pipe section and adjacent pipes

7.4.2 Methods and materials

7.4.2.1 Metallurgical analysis

The microstructure of the CI pipe material was observed using optical microscopy of a polished and etched specimen taken from the failed pipe covering the entire wall thickness. The microstructure consists of graphite flakes in a ferritic matrix. According to ASTM-A247-67 (1998), the features of graphite flakes, including type, form and size, were characterised (Table 7-7).

Two specimens taken from the major fracture surface (Figure 7-18) were prepared and examined by optical microscopy. One specimen was taken from the spigot end of the pipe section, which was inserted in an elbow joint, as shown in Figure 7-17. This specimen showed a dark grey colour that was different from the rest of the fracture surface. The second specimen contained orange brown colour corrosion products, as present in the rest of the fracture surface.

Scanning electron microscopy (SEM) using a JEOL 7001 microscope was used to produce SEM images of the fracture surfaces of tensile coupon specimens.

Figure 7- 18 Specimens from fracture surface: dark grey colour (left) and orange-brown (right)

7.4.2.2 Measurements of corrosion damage

Three-dimensional (3-D) scanning (Creamform) was conducted on remaining pipe pieces to quantify the effects of soil corrosion. Sand-blasting at slow speed was undertaken on these pipe pieces to reveal the metal surface prior to 3-D scanning.

7.4.2.3 Mechanical tests

The mechanical properties of the CI pipe material were measured following the relevant ASTM standards (Table 7-9). Specimens were taken from bare piping metal without corrosion products. Mechanical tests were conducted in an Instron 4402 with a 50 kN load cell. The Aramis digital image correlation system was used to record the deformation of the specimen surface.

7.4.2.4 Finite element analysis

3-D finite element analyses were carried out using Abaqus 6.12 to evaluate the buried pipe stresses. The model was set up on the basis of the information gathered during the site investigation. The behaviour of the CI pipes and soil was assumed to be elastic, and the parameters of piping material were obtained

from the mechanical test results. The interaction between pipe and soil interface was simulated by the Coulomb frictional model with a friction coefficient of 0.5. As can be seen in Figure 7-17, the effects of overlaid other pipelines, anchor blocks and existing cracks were evaluated separately.

7.4.2.5 Fatigue crack growth models

A numerical model was proposed to explain the fatigue crack growth behaviour using Paris' law (Equations 2.12- 2.14 and 7.1- 7.4). According to ASTM-E1049-85 (2005), internal pressure cycles were counted in order to evaluate fatigue crack growth rate. Equation 7.9 was used to estimate the leak rates throughout the service life of the target pipe (Cassa et al., 2010). The orifice area was calculated only for the crack area outside the bell joint (Tada et al., 2000), as it was assumed to be the area where the leakage occurred.

7.4.3 Results and discussion

7.4.3.1 Metallurgical analysis

Microstructural features observed by optical microscopy showed Type D graphite flakes uniformly distributed in mostly ferritic matrices (Figure 7-19 (a)). A small amount of pearlitic matrix was also observed. The average ferrite grain size was approximately 20 μm. These features were confirmed by SEM examination of the fracture surfaces of tensile coupon specimens (Figure 7-19 (b)). The graphite flakes of CI pipe samples are summarised in Table 7-8. The chemical composition of the failed pipe is shown in Table 7-9.

Images of the fracture surfaces of two specimens indicated that the crack may have been existing or initiated at the pipe spigot end where it was inserted in the bell joint. Most of the area of the fracture surface contained orange-brown coloured corrosion products that were most likely generated after the pipe burst event. The existence of dual corrosion phases in failed CI pipes has also been observed in other studies, highlighting that a fracture may grow over a period of time prior to final catastrophic fracture (Cullin et al., 2014; Makar, 2000; Rajani et al., 2012).

Table 7- 8 Graphite flakes of cast iron pipe

ASTM graphite flake	Inner surface	Centre	Outer surface
Type	A& D	D	D
Size	4	5	6
Form	VII& V	V	V

According to ASTM A247-67 (1998), size 4 (0.08- 0.16 mm); size 5 (0.04- 0.08 mm); size 6 (0.02- 0.04 mm).

Table 7- 9 Chemical composition of spun CI pipe

Specimen	C	Mn	Si	S	P	Ni	Cr	Cu	V	Ti
CI	3.60	0.51	1.52	0.05	0.49	0.01	0.01	0.01	0.01	0.06

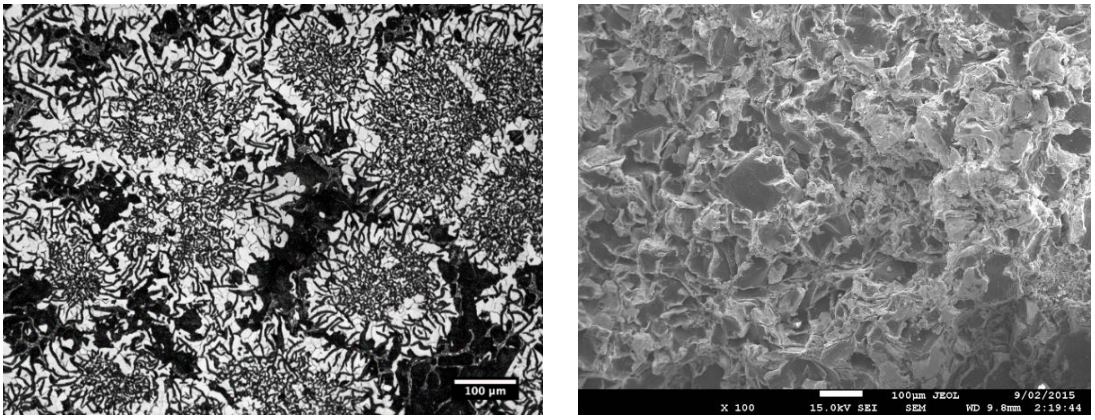

(a) (b)

Figure 7- 19 (a) Microscopic image of polished/etched specimen; (b) SEM image of fracture surface of tensile coupon specimen

7.4.3.2 Measurements of corrosion damage

After sand-blasting and 3-D scanning, the remaining pipe section (except the fracture surface discussed above) was found to be free of substantial corrosion damage. The maximum corrosion depth was less than 2.0 mm.

Table 7- 10 Summary of mechanical testing results

Property	Number of tests	Average	Standard deviation	ASTM standard	Literature reported
Tensile strength, σ_u (MPa)	8	148.1	14.1	E8- 09	137- 212 (Conlin and Baker, 1991)
Modulus of elasticity, E (GPa)	8	108.5	3.2	E8- 09	103 (AIS, 1941)
Fracture toughness, K_{max} ($MPa\sqrt{m}$)	4	14.0	1.7	E1820- 13	10.5- 15.6 (Conlin and Baker, 1991)
Paris constant, m	6	6.4	-	E647- 13a	6.2- 6.7 (Bulloch, 1995)
Paris constant, C ($m/cycle$)	6	2.2×10^{-12}	-		6.1×10^{-16}- 2.6×10^{-12} (Bulloch, 1995)

7.4.3.3 Mechanical tests

The ultimate tensile strength based on eight coupon tests yielded test results in the range from 133 to 165 MPa with an average value of 148 MPa and a standard deviation of 8 MPa. The modulus of elasticity was estimated by the initial slope of the strain-stress curves. Single-edge notched bend (SENB) specimens were adopted for both fracture toughness and fatigue crack growth rate (FCGR) tests. The results of mechanical tests from this study along with the values reported in the research literature are summarised in Table 7-10. These properties were used for subsequent FE analysis and fatigue crack growth modelling.

7.4.3.4 Finite element analysis

The results of 3-D FE analyses indicated that, as expected, pipes with a pre-crack show high stress concentration in the crack tip region. As the crack lengthens, the stress level increases significantly. The correlation between crack length and crack tip stress is shown in Figure 7-20. This indicates that pre-existing cracking is likely to be the predominant factor in the deterioration of pipe structural integrity. The critical crack length can be estimated using the limit stress criteria (Equation 7.15):

$$0.002a^2 - 0.2558a + 17.732 \leq \sigma_u \qquad (7.15)$$

The critical crack length was conservatively calculated as 300mm, since the average tensile strength of the target pipe is 148 MPa. According to the measurement, the length inserted in the bell joint was around 175 mm. FE analyses also revealed that the impact of the overlaid pipes and the supporting anchor could be ignored for the purposes of stress analysis.

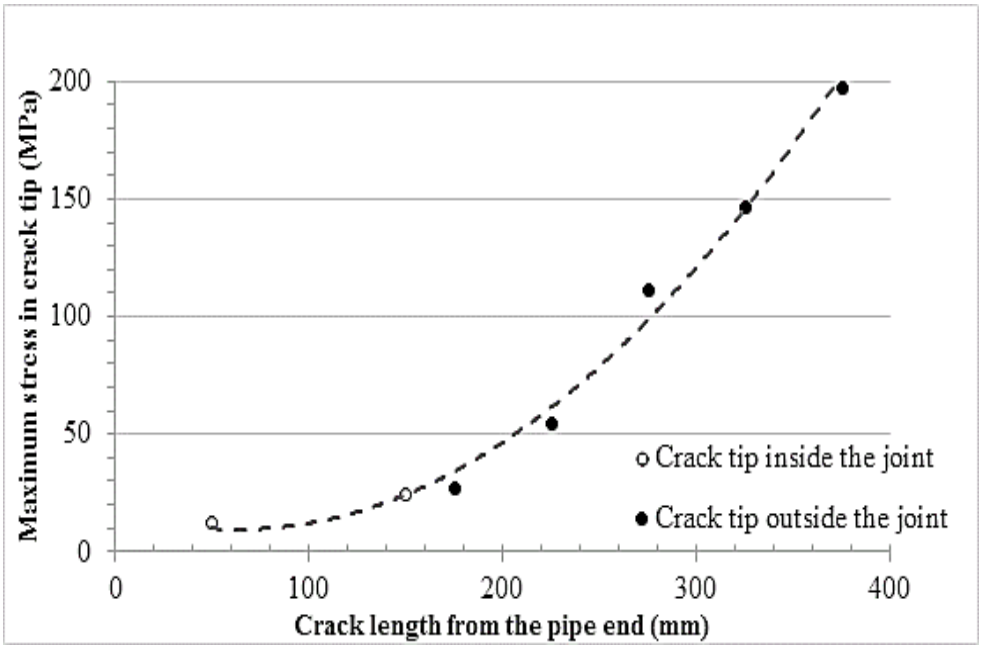

Figure 7- 20 Maximum stress in crack tip by different crack lengths

7.4.3.5 Fatigue crack growth model

It is not clear how the original crack was initiated from the spigot end. However, CI pipes with existing damage in bell joints are common, due to the high stresses introduced by installation techniques and transportation (Rajani and Abdel-Akher, 2013; Rajani et al., 2013). Figure 7-21 shows the crack growth trend between 180 and 300 mm using Equations 2.12- 2.14 and 7.1- 7.4. The measured pressure changes ranging from 390 to 520 kPa were approximately 14 events per day at the failure site. Therefore, the predicted period of crack growth is over 51 years, which matches the recorded data well.

The leak rates throughout the service life are shown in Figure 7-22 using Equation 7-9. The leak rate was relatively consistent over the majority of service life. However, a dramatic rise was expected to occur several months prior to the pipe burst. The period between significant leakage (which may have led to field observations of leakage) and pipe burst was at least one month in this case.

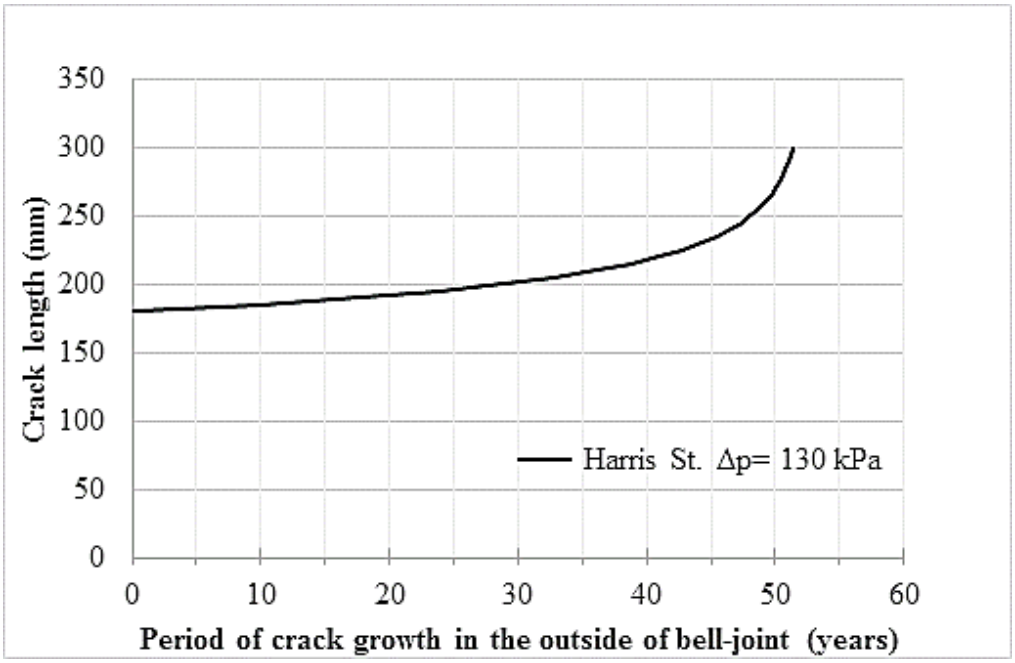

Figure 7- 21 Long-term crack growth in pipe barrel

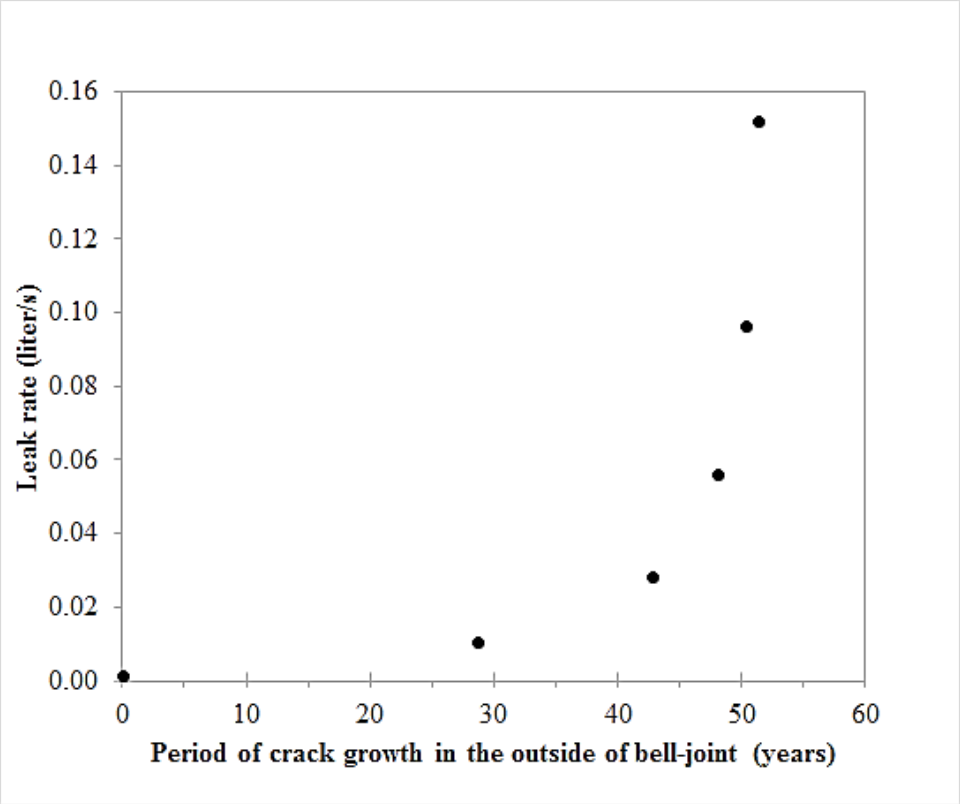

Figure 7- 22 Long-term increase of leak rate

7.4.4 Summary

This section reports the results of the failure analysis of a 500mm CI water main which burst on the 10th of August 2013 in Harris Street and Ultimo Street, Sydney. Different analysis methods were used to investigate the possible causes of the catastrophic failure. Analysis indicates that an existing crack can grow due to cyclic loading (mainly water pressure in this case) over a period and can result in major-scale bursts, even in environments with low corrosion potential. Hence, the cause of failure was identified as a combination of initial (existing) material flaws and repetitive (i.e. fatigue) loading.

Metallurgical analyses were conducted to investigate the microstructure of the failed pipe. The results revealed that a pre-crack existed a long time before final fracture, which led to the eventual burst when the crack length increased to the critical size. Correlations between crack length and crack tip stresses were calculated using 3-D FE analyses to investigate the total length of the crack (300 mm in this study) that caused the pipe to burst under high operating pressures.

Fatigue analyses were performed to identify the likely fatigue crack growth rate under cyclic internal water pressure. It was shown that the pre-crack may have stably propagated over a long period under constantly low changes of internal pressure. Unstable crack growth was expected to occur when the total crack length exceeded 250 mm in the current study.

A window in time can be identified between significant leakage and pipe burst, verifying that the LBB concept can potentially be applied to pressurized CI water pipes. For a pressurised pipe with longitudinal cracks, leakage rates are strongly related to crack lengths and internal pressures, as was shown in the present study. During the period of stable crack growth, a leakage rate less than 0.03 L/s was calculated in the current study. With unstable crack propagation, the leakage rate rises dramatically and becomes detectable weeks before catastrophic failure of the CI pipe. However, accurate LBB assessment incorporating the effects of fatigue damage in deteriorated CI pipes is required to prevent the failure of ageing pipes.

7.5 Conclusions

A burst facility established by the ACAPFP is capable of supplying cyclic pressures to large-diameter CI water pipes. The fatigue mechanism generated by cyclic internal pressures enables the initiation and propagation of through-wall cracks in CI pipe barrels. The Paris' law is able to predict the fatigue crack growth of CI pipes, and the fatigue crack growth rates (FCGR parameters) in CI pipe barrels are similar to the results of experiments conducted on SENB specimens. A LBB time window may occur in deteriorated CI pipes with corrosion patches subjected to cyclic internal pressures.

The CZM is applicable for the prediction of leak and burst pressures of longitudinal barrel fractures of CI water pipes. This method can be used to evaluate the bursting pressures of CI pipes containing a longitudinal fracture. The effects of corrosion patch configurations can be evaluated to identify critical corrosion patches for operational pressures.

The procedures of the forensic investigation of CI water pipe failures are shown in the failure analysis of a 500mm CI water main which burst on the 10th of August 2013 in Harris Street and Ultimo Street, Sydney. The analysis indicates that an existing crack can grow due to cyclic pressures over a period of time and can result in major-scale bursts, even in environments with low corrosion potential. Hence, the cause of failure was identified as a combination of initial (existing) material flaws and repetitive (i.e. fatigue) loading. Fatigue analyses were performed to identify the likely fatigue crack growth rate under cyclic internal water pressure. A window in time can be identified between a significant water leak and pipe burst, verifying that the LBB concept can potentially be applied to pressurized CI water pipes. The leak rates are strongly related to the crack lengths and internal pressures, as shown in the present study. With unstable crack propagation, the leak rate rises dramatically and becomes detectable weeks before catastrophic failure of the CI pipe. Therefore, an accurate LBB assessment incorporating the effects of fatigue damage in deteriorated CI pipes is required for better rehabilitation of ageing pipes.

Chapter 8 Conclusions and Recommendations

8.1 Conclusions

This thesis summarises the research study identifying the critical assets of CI water trunk mains in Australia and evaluating the influence of fatigue generated by cyclic pressures on CI pipe failure. This chapter presents the key findings and recommendations for future studies and for the attention of water utilities.

The results and conclusions are summarised as follows:

- CI water pipes buried between the 1860s and 1980 still account for a significant proportion of the Australian water transmission network. In Australian cities, the manufacturing methods and corrosion mitigation techniques used for CI pipes depend strongly on the burial year. In order to identify critical pipelines with high potential of longitudinal fracture in pipe barrels, an approach to summarising the remaining in-service CI trunk mains into several cohorts is proposed. Despite the various manufacturing methods used in Australian CI pipes, two major cohorts, static and spun CI pipes, are identified for the characterisation of material properties, microstructural analyses and wall thicknesses. Statistical analysis confirms that, on average,

spun CI pipes have higher burst rates and shorter life spans than statically cast pipes, due to their thinner walls. A general method of pipe cohorting for CI pipes used in Australian water utilities is developed, mainly on the basis of the pipe burial year.

- The leak-before-break (LBB) phenomenon has been observed in recent failures and full-scale bursting tests of large-diameter CI pipes. Over-designed pipe walls and pitting soil corrosion are the main reasons for the occurrence of LBB in CI pipes. Procedures for LBB assessment of corroded CI pipes are proposed in accordance with the available LBB standards issued for other piping industries. LBB criteria for large-diameter CI pipes are proposed and verified on the basis of the results of full-scale burst tests. Similarly, some findings of LBB evidence in small-diameter CI pipes which failed by circumferential fracture explain why the tightened clamp is an effective method to repair leaking small-diameter CI pipes. Based on field evidence, a detectable leak may be observed prior to a burst event, resulting in an LBB time window ranging from several days to months for intervention to prevent pipe failure.

- Most CI water trunk mains fail by the mode of longitudinal barrel fracture due to soil corrosion and internal pressure. The S-N curves obtained by fatigue testing of five CI pipes and data from the research literature confirm that fatigue strengths are strongly correlated with ultimate tensile strengths. A fatigue endurance ratio of 0.5 was observed for CI pipes under a low stress ratio (less than 0.1), and the endurance ratios under high stress ratios may be estimated based on the Gerber relationship. The increase of stress ratios prolongs the failure cycles. A sensitivity analysis was conducted using time-dependent simulations. The analysis shows that assets in transient zones or with frequent refill events may experience higher levels of fatigue damage. In addition, long-term corrosion rates and the stress ratios of transients also contribute to fatigue damage.

- The fatigue crack growth in CI water pipe barrels was evaluated using the Paris' law, and the FCGR parameters were reported based on the results of a testing program of FCGR experiments on SENB specimens taken from five large-diameter CI water pipes. The stress ratios were found to have limited effects on the FCGR parameters. The threshold toughness is significantly dependent on the stress ratios used in fatigue tests, and the threshold toughness parameters were provided from the best fitting curve of test data and data from the research literature. Water and corrosive soil environments may reduce the threshold toughness of CI water pipes. The fracture surfaces of FCGR specimens were examined to capture the features of fatigue fracture surfaces. The region of the fatigue surface shows a smoother texture and light colours, compared with the fast fracture surfaces. Furthermore, tide marks were commonly observed in SEM images, and fatigue striations were rarely seen on the fatigue fracture surfaces. However, these features

of fatigue surfaces may be damaged in corrosive media. In the field, detectable leakage may be observed prior to a burst event, resulting in an LBB time window ranging from ten days to months, depending on the leakage detection methods used.

- A burst facility established by the ACAPFP at Monash University can supply cyclic pressures to enable the understanding of the influences of repetitive/cyclic internal loading such as pressure transients on the fatigue failure of large-diameter CI water pipes. The results of laboratory pipe fatigue tests conducted using the new test facility showed fatigue as a failure mechanism in large-diameter CI water pipes. The fatigue mechanism generated by cyclic internal pressures can initiate and propagate through-wall cracks in CI pipe barrels. The Paris' law is able to predict the fatigue crack growth of CI pipes, and the fatigue crack growth rates (FCGR parameters) in CI pipe barrels are similar to the results of experiments conducted on SENB specimens. In addition, the tests also verified the possible application of the LBB concept for failure prediction and prevention in large-diameter CI pipes. The cohesive zone model (CZM) is applicable for the prediction of the leak and burst pressures of longitudinal barrel fractures of CI water pipes. This method can be used to evaluate the bursting pressures of CI pipes containing a longitudinal fracture. The effects of corrosion patch configurations can be evaluated to identify critical corrosion patches for operational pressures. The procedures of forensic investigation of CI water pipe failure are shown in the failure analysis of a 500mm CI water main which burst on the 10th of August 2013 in Harris Street and Ultimo Street, Sydney. Fatigue analyses were performed to identify the likely fatigue crack growth rate under cyclic internal water pressure. A time window can be identified between a significant water leak and pipe burst, verifying that the LBB concept can potentially be applied to pressurised CI water pipes to prevent catastrophic failures. Leak rates are strongly related to crack lengths and internal pressures, as is shown in the present study. With unstable crack propagation, the leak rate rises dramatically and becomes detectable, possibly weeks before catastrophic failure of the CI pipe.

8.2 Recommendations for future research

The failure mechanisms of CI water pipes have been explored in this research project. The findings summarised in this thesis can be implemented in the asset management and failure prediction of CI water pipes by water utilities. The following recommendations are made for future studies and for the information of water utilities:

- The cohort approach to identifying the critical assets of CI trunk mains needs to be verified and augmented with the statistical analyses of failure rates of CI trunk mains. Water utilities need to revise this approach for their pipeline assets using data on CI pipe materials, corrosion mitigation methods and pressure zones.

- The leak-before-break (LBB) concept has been verified for large-diameter CI water pipes experiencing soil pitting corrosion. The configurations of corrosion patches have significant impacts on fatigue crack propagation in CI pipe barrels. Therefore, research on the lateral growth of corrosion patches will enable the accuracy of window period predictions to be improved. In addition, suitable leak detection techniques with sufficient resolution of leak signatures need to be employed by water utilities to prevent catastrophic failures of CI water pipes. If such techniques are not available, research can be directed to develop techniques to differentiate the leak signatures and identify the severity of cracks for LBB window time analysis to enable intervention prior to catastrophic failure.

- Ageing CI mains buried in transient zones or with frequent burst rates may require additional condition assessment of fatigue damage. Future research is required to explore the impact of corrosive soil environments on fatigue resistance.

- Full-scale burst tests have been conducted in large-diameter static CI pipes. However, there are no experimental results of full-scale burst tests in large-diameter spun CI pipes. Future research should also be conducted on CI pipe specimens buried in soil environments by upgrading the Monash University burst facility. In addition, cohesive zone models can be modified to evaluate the failure analyses of small-diameter CI pipes subjected to soil bending stress.

REFERENCES

AHMAD, Z. 2006. *Principles of corrosion engineering and corrosion control,* Oxford: Butterworth-Heinemann, Elsevier.

AIS 1941. *Cast Iron Pipes, Centrifugally Cast by the Super DeLavaud Process,* Port Kembla, New South Wales, Australian Iron & Steel.

AIS 1953. *Cast Iron Pipes, Centrifugally Cast by the Super DeLavaud Process,* Port Kembla, New South Wales, Australian Iron & Steel.

AL LAHAM, S. 1998. *Stress intensity factor and limit load handbook,* UK, British Energy Generation Limited.

ALEXANDER, C. R., KIEFNER, J. & FOWLER, J. Repair of dents combined with gouges considering cyclic pressure loading. 8th Annual International Energy Week Conference and Exhibition, Houston, Texas, 1997 Houston, Texas.

ANDERSON, T. L. 2005. *Fracture mechanics: fundamentals and applications,* Boca Raton, FL : Taylor & Francis CRC press.

ANTAKI, G. A. 2003. *Piping and pipeline engineering: design, construction, maintenance, integrity, and repair,* New York, USA, CRC Press.

API-579 2016. Fitness-For-Service, API 579-1/ASME FFS-1. The American Society of Mechanical Engineers, American Petroleum Institute

AS-1724 1975. Australian Standard Specification: Cast Grey Iron Pressure Pipes and Fittings with Bolted Gland Joints. Sydney, Australia: Standards Australia.

ASME-B31G 1991. Manual for Determining the Remaining Strength of Corroded Pipelines: A Supplement to ASME B31 Code for Pressure Piping. New York, USA: American Society of Mechanical Engineers.

ASME-B31G 2009. Manual for Determining the Remaining Strength of Corroded Pipelines. *Supplement to ASME B31 Code for Pressure Piping*. New York, USA: The American Society of Mechanical Engineers.

ASTM-A247-67 1998. Standard Test Method for Evaluating the Microstructure of Graphite in Iron Castings. West Conshohocken, PA: ASTM International.

ASTM-E8 2009. Standard test method of measurement of fracture toughness. West Conshohocken, PA: ASTM International.

ASTM-E466 2007. Standard Practice for Conducting Force Controlled Constant Amplitude Axial Fatigue Tests of Metallic Materials. ASTM International.

ASTM-E647-13A 2013. Standard Test Method for Measurement of Fatigue Crack Growth Rates. ASTM International.

ASTM-E1049-85 2005. Standard practices for cycle counting in fatigue analysis, ASTM International. American Society for Testing and Materials.

ASTM-E1820 2013. Standard test method of measurement of fracture toughness. West Conshohocken, PA: ASTM International.

ASTM-G46 1994. Standard Guide for Examination and Evaluation of Pitting Corrosion. American Society of the International Association for Testing and Materials.

ATKINSON, K., WHITER, J., SMITH, P. & MULHERON, M. 2002. Failure of small diameter cast iron pipes. *Urban Water,* 4**,** 263-271.

AWWA-C100 1908. Standard Specifications for Cast-Iron Special Castings. Denver, USA: AWWA Standard.

AWWA-C102 1939. American Standard Specifications for Cast Iron Pit Cast Pipe for Water or Other Liquids. *A21.2.* Denver, USA: AWWA Standards

AWWA-C105 1972. ANSI A21.5 American National Standard for Polythylene Encasement for Gray and Ductile Cast-Iron Piping for Water and Other Liquids. Denver, USA: AWWA Standard.

AWWA-C105 2010. ANSI A21. 5 Polyethylene Encasement for Ductile-Iron Pipe Systems. *American Water Works Association.* Denver, USA: AWWA Standard.

AWWA-C106 1953. American Standard Specifications for Cast Iron Pipe Centrifugally Cast In Metal Molds, for Water or Other Liquids. Denver, USA: AWWA Standards

AWWA-C108 1962. American Standard for Cast Iron Pipe Centrifugally Cast In Sand-lined Molds, for Water or Other Liquids. Denver, USA: AWWA Standards.

BAICCHI, P., COLLINI, L. & RIVA, E. 2007. A methodology for the fatigue design of notched castings in gray cast iron. *Engineering fracture mechanics,* 74**,** 539-548.

BANNANTINE, J. A., COMER, J. J. & HANDROCK, J. L. 1990. *Fundamentals of metal fatigue analysis,* Englewood Cliffs, Prentice Hall.

BARDET, J. P., BALLANTYNE, D., G.E.C. BELL, G. E. C., DONNELLAN, A., FOSTER, S., FU, T. S., LIST, J., LITTLE, R. G., O'ROURKE, T. D. & PALMER, M. C. 2010. Expert Review of Water System Pipeline Breaks in the City of Los Angeles during Summer 2009. City of Los Angeles, USA: Report to the Steering Committee on water pipeline breaks of the City of Los Angeles, 9.

BARENBLATT, G. I. 1962. The mathematical theory of equilibrium cracks in brittle fracture. *Advances in applied mechanics,* 7**,** 55-129.

BARTHOLOME, G. & WELLEIN, R. 1995. Leak-before-break behavior of nuclear piping systems. *Theoretical and applied fracture mechanics,* 23**,** 145-149.

BELMONTE, H., MULHERON, M. & SMITH, P. 2009. Some observations on the strength and fatigue properties of samples extracted from cast iron water mains. *Fatigue & Fracture of Engineering Materials & Structures,* 32**,** 916-925.

BOND, A., MERGELAS, B. & JONES, C. Pinpointing leaks in water transmission mains. Pipeline Engineering and Construction: What's on the Horizon?, 2004 San Diego, California, United States. American Society of Civil Engineers, 1-10.

BONDS, R. W. 2005. Cement-mortar linings for ductile iron pipe. *Birmingham (AL): Ductile Iron Pipe***,** 1-7.

BONDS, R. W., BARNARD, L. M., HORTON, A. M. & OLIVER, G. L. 2005. Corrosion and corrosion control of iron pipe: 75 years of research. *Journal (American Water Works Association)***,** 88-98.

BRADLEY, W. & SRINIVASAN, M. 1990. Fracture and fracture toughness of cast irons. *International materials reviews,* 35**,** 129-161.

BREVIS, W., SUSMEL, L. & BOXALL, J. 2014. Investigating in-service failures of water pipes from a multiaxial notch fatigue point of view: A conceptual study. *Proceedings of the Institution of Mechanical Engineers, Part C: Journal of Mechanical Engineering Science*.

BREVIS, W., SUSMEL, L. & BOXALL, J. 2015. Investigating in-service failures of water pipes from a multiaxial notch fatigue point of view: A conceptual study. *Proceedings of the Institution of Mechanical Engineers, Part C: Journal of Mechanical Engineering Science,* 229**,** 1240-1259.

BROTZEN, F. R. & WALLACE, J. F. 1957. Fatigue Properties of Gray Iron. *Machine Design,* 29**,** 154-158.

BS-78 1938. British Standard Specification for Cast Iron Pipes (Vertically Cast) for Water, Gas, and Sewage and Special Castings for Use Therewith. London, UK: British Standards Institution.

BS-1211 1958. British Standard Specification: Centrifugally Cast (Spun) Iron Pressure Pipes for Water, Gas and Sweage. London, UK: British Standards Institution.

BS-7910 2005. Guidance on methods for assessing the acceptability of flaws in metallic structures. London, UK: British Standards Institution.

BS/EN-877 1999. Cast iron pipes and fittings, their joints and accessories for the evacuation of water from buildings. Requirements, test methods and quality assurance. London, UK: British Standards Institution.

BULLOCH, J. 1995. Near threshold fatigue behaviour of flake graphite cast irons microstructures. *Theoretical and applied fracture mechanics,* 24**,** 65-78.

CASSA, A., VAN ZYL, J. & LAUBSCHER, R. 2010. A numerical investigation into the effect of pressure on holes and cracks in water supply pipes. *Urban Water Journal,* 7**,** 109-120.

CASTILLO, R. & BAKER, T. The relationship between tensile strength and microstructure in flake graphite cast iron. MRS Online Proceedings Library Archive 34 (1984), 1984. Cambridge Univ Press, 487-495.

CHAN, D., GALLAGE, C. P. K., RAJEEV, P. & KODIKARA, J. 2015a. Field performance of in-service cast iron water reticulation pipe buried in reactive clay. *Canadian Geotechnical Journal,* 52**,** 1861-1873.

CHAN, D., KODIKARA, J. K., RAJEEV, P. & ROBERT, D. 2016a. Field study of large diameter cast iron water pipe buried under a roadway (in preparation).

CHAN, D., SHANNON, B. & KODIKARA, J. 2016b. Relative importance of external factors on pipe failure. *OzWater 2016.* Melbourne, Australia.

CHAN, D. C. C., GALLAGE, C., RAJEEV, P. & KODIKARA, J. 2015b. Field Performance of In-service Cast Iron Water Reticulation Pipe Buried in Reactive Clay. *Canadian Geotechnical Journal,* 52**,** 1861-1873.

CHARLOT, L. A. & WESTERMAN, R. E. 1981. Corrosion resistance of cast irons and titanium alloys as reference engineered metal barriers for use in basalt geologic storage: a literature assessment. Battelle Pacific Northwest Labs., Richland, WA (USA).

CHEN, D. & EL-HACHA, R. 2013. Cohesive fracture study of a bonded coarse silica sand aggregate bond interface subjected to mixed-mode bending conditions. *Polymers,* 6**,** 12-38.

COLLINS, W. & SMITH, J. The Notch Sensitivity of Alloyed Cast Irons Subjected to Repeated and Static Loads. Proc. Amer. Soc. Test. Mat, 1942. 639-658.

CONLIN, R. & BAKER, T. 1991. Application of fracture mechanics to the failure behaviour of buried cast iron mains. *Contractor Report-Department of Transport Transport and Road Research Laboratory.*

COVAS, D., RAMOS, H., GRAHAM, N. & MAKSIMOVIC, C. 2005. Application of hydraulic transients for leak detection in water supply systems. *Water Science and Technology: Water Supply,* 4**,** 365-374.

CULLIN, M. J., PETERSEN, T. H. & PARIS, A. 2014. Corrosion fatigue failure of a gray cast iron water main. *Journal of Pipeline Systems Engineering and Practice,* 6**,** 05014003: 1-9.

CUNAT, P.-J. Corrosion resistance of stainless steels in soils and in concrete. the Plenary Days of the Committee on the Study of Pipe Corrossion and Protection, 2001 Ceocor, Biarritz, France. 12.

DAFTER, M. & PETERSEN, R. 2013. Advanced condition assessment of Hunter Water's cast iron watermains| NOVA. The University of Newcastle's Digital Repository. *Corrosion& Materials***,** 46-49.

DAVIS, J. 1996. *ASM specialty handbook: cast irons,* Ohio, United States, ASM International.

DAVIS, P., ALLAN, I., BURN, S. & VAN DE GRAAFF, R. 2003. Identifying trends in cast iron pipe failure with GIS maps of soil environments. *Proc. Pipes.* Charles Sturt University, Wagga Wagga, N.S.W.

DE SILVA, D., MASHFORD, J. & BURN, S. 2011. Computer aided leak location and sizing in pipe networks. *Urban Water Security Research Alliance Technical Report No. 17.* Brisbane, Australia Urban Water Security Research Alliance (UWSRA).

DEB, A. K. 2002. *Prioritizing water main replacement and rehabilitation,* Denver, USA, American Water Works Association.

DIEHL, T. 2008. On using a penalty-based cohesive-zone finite element approach, Part I: Elastic solution benchmarks. *International Journal of Adhesion and Adhesives,* 28**,** 237-255.

DORN, R. 1996. Water mains: guidance on assessment and inspection techniques. *CIRIA Report.* Construction Industry Research and Information Association.

DOYLE, G. & GRABINSKY, M. 2003. Infrastructure-Applying GIS to a water main corrosion study-Geographic information systems are proving to be a valuable tool in plotting areas of water system infrastructure deterioration and how. *American Water Works Association Journal,* 95**,** 90-104.

DOYLE, G., SEICA, M. V. & GRABINSKY, M. W. 2003. The role of soil in the external corrosion of cast iron water mains in Toronto, Canada. *Canadian geotechnical journal,* 40**,** 225-236.

DUGDALE, D. S. 1960. Yielding of steel sheets containing slits. *Journal of the Mechanics and Physics of Solids,* 8**,** 100-104.

ERDOGAN, F., KIBLER, J. & ROBERTS, R. 1969. Fatigue and fracture of thin-walled tubes containing cracks. *INTERNATIONAL CONFERENCE ON PRESSURE VESSEL TECHNOLOGY, 1ST.* DELFT; NETHERLANDS: AMERICAN SOCIETY OF MECHANICAL ENGINEERS,, NEW YORK, United States.

FLETCHER, R. & CHANDRASEKARAN, M. SmartBall™: A New Approach in Pipeline Leak Detection. 2008 7th International Pipeline Conference, 2008. American Society of Mechanical Engineers, 117-133.

FORSYTH, P. J. E. 1969. The physical basis of metal fatigue. *BLACKIE AND SON LTD., LONDON, 1969, 200 P.*

FUCHS, H. & RIEHLE, R. 1991. Ten years of experience with leak detection by acoustic signal analysis. *Applied Acoustics,* 33**,** 1-19.

GILBERT, G. 1953. Fatigue Properties of Cast Iron. *British Cast Iron Research Association Journal of Research and Development,* 5**,** 94-108.

GILBERT, G. 1968. Engineering Data on Gray Cast Irons. *BRITISH CAST IRON RESEARCH ASSOCIATION, ALVECHURCH, BIRMINGHAM. 1968, 15 P.*

GILBERT, G. & PALMER, K. 1969. *Fatigue Properties of Cast Iron,* ALVECHURCH, BIRMINGHAM, UK, British Cast Iron Research Association.

GLOVER, N. & POLLARD, G. The brittle fracture of grey cast irons. ICF2, Brighton (UK) 1969, 1969. 350-359.

GOULD, S., BEALE, D., DAVIS, P., MARLOW, D. & HICKS, J. 2013. National investigation of failure rates from Australian water supply pipes. *Water Asset Management International,* 9**,** 21-24.

GOULD, S. J. F. 2011. *A study of the failure of buried reticulation pipes in reactive soils.* Dept. of Civil Engineering. Monash University. Victoria. Australia.

GRANT, J. W. 1950. Notched and Unnotched Fatigue Tests on Flake and Nodular Cast Irons. *Research British Cast Iron Association,* 3**,** 333-354.

HEATHCOTE, M. & NICHOLAS, D. 1998. *Life assessment of large cast iron watermains,* Melbourne, Australia, Melbourne: Urban Water Research Association of Australia.

HORNBOGEN, E. 1985. Fracture toughness and fatigue crack growth of grey cast irons. *Journal of materials science,* 20**,** 3897-3905.

IAEA-TECDOC-710 1993. Applicability of the Leak Before Break Concept. *Report of the IAEA Extrabudgetary Programme on the Safety of WWER-440 Model 230 Nuclear Power Plants Status report on a generic safety issue.* International Atomic Energy Agency

ISO-185 1988. International Standard- Gray cast iron- Classification Geneva, Switzerland: International Organization for Standardization.

JAKOBS, J. 1985. Underground Corrosion of Water Pipes in Canadian Cities–Case: The City of Calgary. *Final Report, Caproco Corrosion Prevention Ltd.,(CANMET Contract Report No. 0SQ81-00096, Canadian Centre for Mineral and Energy Technology, Energy, Mines and Resources Canada. Canadian Government Publishing Centre, Ottawa, Canada).*

JAMES, M. & LI, W. 1999. Fatigue crack growth in austempered ductile and grey cast irons—stress ratio effects in air and mine water. *Materials Science and Engineering: A,* 265**,** 129-139.

JESSON, D., MOHEBBI, H., FARROW, J., MULHERON, M. & SMITH, P. 2013. On the condition assessment of cast iron trunk main: The effect of microstructure and in-service graphitisation on mechanical properties in flexure. *Materials Science and Engineering: A,* 576**,** 192-201.

JI, J., ROBERT, D., ZHANG, C., ZHANG, D. & KODIKARA, J. 2017. Probabilistic physical modelling of corroded cast iron pipes for lifetime prediction. *Structural Safety,* 64**,** 62-75.

JI, J., ZHANG, C., KODIKARA, J. & YANG, S.-Q. 2015. Prediction of stress concentration factor of corrosion pits on buried pipes by least squares support vector machine. *Engineering Failure Analysis,* 55**,** 131-138.

JIANG, R., ROBERT, D., HUTCHINSON, C. R., ZHAO, X. L. & KODIKARA, J. 2017a. Leak-before-break in cast iron mains: a failure analysis of a catastrophic pipe burst on Harris Street, Sydney. *Water Practice and Technology,* 12**,** 487-494.

JIANG, R., SHANNON, B., DEO, R. N., HUTCHINSON, C. R., ZHAO, X.-L., RATHNAYAKA, S. & KODIKARA, J. 2017b. Classification of major cohorts of Australian pressurised cast iron water mains for pipe renewal (available online). *Australian Journal of Water Resources* 1-12.

JÖNSSON, L. Interaction of a hydraulic transient with a leak in a pipe flow. 14th Australasian Fluid Mechanics Conference, Adelaide University, Adelaide, Australia, 2001.

KANNAN, P., AMIRTHAGADESWARAN, K. & CHRISTOPHER, T. 2015. Validation of a Leak-Before-Break Criterion Using Limit Load Solution. *Journal of Failure Analysis and Prevention,* 15**,** 417-423.

KAPADIA, B. & IMHOF, E. 1979. Fatigue crack growth in cast irons and cast steels. *In:* SMITH, G. V. (ed.) *Cast Metals for Structural and Pressure Containment Applications.* New York: The American Society of Mechanical Engineers.

KIM, J., BAE, C., WOO, H., KIM, J. & HONG, S. Assessment of residual tensile strength on cast iron pipes. The ASCE International Conference on Pipeline Engineering and Construction, Boston, USA.[doi: 10.1061/40934 (252) 62], 2007.

KODIKARA, J., RAJEEV, P., CHAN, D. & GALLAGE, C. 2013. Soil moisture monitoring at the field scale using neutron probe. *Canadian Geotechnical Journal,* 51**,** 332-345.

KODIKARA, J., RAJEEV, P., ROBERT, D. & ZEMAN, P. 2012. Critical Review of Historical Information on Large Diameter Pipe Failure. *Advanced Condition Asessment and Pipe Failure Prediction* Monash University

KOMMERS, J. The Static and Fatigue Properties of Some Cast Irons. ASTM Proceedings, 1928. 174-204.

KROON, D. H., LINDEMUTH, D., SAMPSON, S. & VINCENZO, T. 2005. Corrosion protection of ductile iron pipe. *Materials performance,* 44**,** 24-29.

LIU, Z. & KLEINER, Y. 2013. State of the art review of inspection technologies for condition assessment of water pipes. *Measurement,* 46**,** 1-15.

LOGAN, K. H. 1945. Underground corrosion. *Transactions of the American Society of Civil Engineers,* 101**,** 811-825.

LONGMUIR, P. 1939. *Cast iron pipe: manufacture and properties, with special reference to centrifugal casting,* Charles Griffin. London, Lippincott.

LUNDBERG, A. & ELIASSON, S. 2015. Investigation and Comparison of Cohesive Zone Models for Simulation of Crack Propagation. *Division of Solid Mechanics, Lund University***,** 43.

LYONS, W. C. & PLISGA, G. J. 2005. *Standard handbook of petroleum and natural gas engineering,* Waltham, MA, Gulf Professional Publishing.

MAKAR, J. 2000. A preliminary analysis of failures in grey cast iron water pipes. *Engineering Failure Analysis,* 7**,** 43-53.

MAKAR, J. & RAJANI, B. 2000. Gray cast-iron water pipe metallurgy. *Journal of materials in civil engineering,* 12**,** 245-253.

MARSHALL, P. 2001. The Residual Structural Properties of Cast Iron Pipes: Structural and Design Criteria for Linings for Water Mains. *Report UKWIR-R-WM--01/02/14.* UK Water Industry Research Limited.

MCMULLEN, L. Advanced concepts in soil evaluation for exterior pipeline corrosion. Proceedings of the AWWA Annual Conference, 1982 Miami Beach, FL. 134-142.

MELCHERS, R. 2003. Mathematical modelling of the diffusion controlled phase in marine immersion corrosion of mild steel. *Corrosion science,* 45**,** 923-940.

MELCHERS, R. E. 2013. Long-term corrosion of cast irons and steel in marine and atmospheric environments. *Corrosion Science,* 68**,** 186-194.

MELCHERS, R. E. 2014. Long-term immersion corrosion of steels in seawaters with elevated nutrient concentration. *Corrosion Science,* 81**,** 110-116.

MELCHERS, R. E. 2015. Bi-modal trends in the long-term corrosion of copper and high copper alloys. *Corrosion Science,* 95**,** 51-61.

MIEDLAR, P. C., BERENS, A. P., GUNDERSON, A. & GALLAGHER, J. 2002. *USAF damage tolerant design handbook: guidelines for the analysis and design of damage tolerant aircraft structures*, University of Dayton Research Institute, Dayton, OH

MISIUNAS, D., VÍTKOVSKÝ, J., OLSSON, G., SIMPSON, A. & LAMBERT, M. 2005. Pipeline break detection using pressure transient monitoring. *Journal of Water Resources Planning and Management,* 131**,** 316-325.

MIYASAKA, M. & OGURE, N. 1987. Stress Corrosion Cracking of Austenitic Cast Irons in Seawater and Brine, and Its Prevention. *Corrosion,* 43**,** 582-588.

MOHEBBI, H., JESSON, D., MULHERON, M. & SMITH, P. 2010. The fracture and fatigue properties of cast irons used for trunk mains in the water industry. *Materials Science and Engineering: A,* 527**,** 5915-5923.

MOHEBBI, H. & LI, C. 2011. Experimental investigation on corrosion of cast iron pipes. *International Journal of Corrosion,* 2011**,** 1-17.

NAM, K. W., ANDO, K., YUZURU, S. & OGURA, N. 1992. LEAK-BEFORE-BREAK CONDITIONS OF PLATES AND PIPES UNDER HIGH FATIGUE STRESSES. *Fatigue & Fracture of Engineering Materials & Structures,* 15**,** 809-824.

NICHOLAS, D. & MOORE, G. 2009. Corrosion of ferrous watermains: past performance and future prediction – a review. *Corrosion and Materials* 34**,** 33-40.

PETERSEN, R., DAFTER, M. & MELCHERS, R. 2013. Long-term corrosion of buried cast iron water mains: field data collection and model calibration. *Water Asset Management International,* 9**,** 13-17.

PETERSEN, R. & MELCHERS, R. 2012. Long-Term Corrosion of Cast Iron Cement Lined Pipes. *Annual Conference of the Australasian Corrosion Association.* Melbourne, Australia.

PETERSEN, R. & MELCHERS, R. LONG TERM CORROSION OF BURIED CAST IRON PIPES IN NATIVE SOILS. Proceedings of Corrosion and Prevention 2013, 2014 Darwin, Australia 9.

PILKEY, W. D. 1997. Peterson's stress concentration factors. *John Wiley & Sons, New York*.

PILKEY, W. D. & PILKEY, D. F. 2008. *Peterson's Stress Concentration Factors,* Hoboken, N.J., John Wiley & Sons.

PRITCHARD, O. G., HALLETT, S. H. & FAREWELL, T. S. 2013. Soil Corrosivity in the UK–Impacts on Critical Infrastructure. *Infrastructure Transitions Research Consortium- Working Paper Series.* Cranfield University.

RAJANI, B. 2000. *Investigation of grey cast iron water mains to develop a methodology for estimating service life,* Denver, CO, USA, American Water Works Association.

RAJANI, B. 2012. Nonlinear stress–strain characterization of cast iron used to manufacture pipes for water supply. *Journal of Engineering Materials and Technology,* 134**,** 041005.

RAJANI, B. & ABDEL-AKHER, A. 2012. Re-assessment of resistance of cast iron pipes subjected to vertical loads and internal pressure. *Engineering Structures,* 45**,** 192-212.

RAJANI, B. & ABDEL-AKHER, A. 2013. Behavior and response of lead-caulked bell–spigot joints in cast iron water mains. *Engineering Structures,* 56**,** 2005-2013.

RAJANI, B., DICKINSON, J., XUE, H., WOODARD, P. & CANAS, R. 2013. Effect of Past Delivery Practices on Current Conditions of Cast-Iron Water Pipes. *Journal of Infrastructure Systems,* 20**,** 04013011: 1-16.

RAJANI, B. & KLEINER, Y. 2001. Comprehensive review of structural deterioration of water mains: physically based models. *Urban water,* 3**,** 151-164.

RAJANI, B. & KLEINER, Y. 2010. Fatigue failure of large-diameter cast iron mains. *Water Distribution Systems Analysis 2010.* Tucson, AZ, USA.

RAJANI, B. & KLEINER, Y. 2013a. External and internal corrosion of large-diameter cast iron mains. *Journal of Infrastructure Systems,* 19**,** 486-495.

RAJANI, B. & KLEINER, Y. 2013b. *Fracture failure of large diameter cast iron water mains,* Ottawa, Canada, Water Research Foundation.

RAJANI, B., LEWANDOWSKI, J. & MARGEVICIUS, A. 2012. Failure Analysis of Cast Iron Trunk Main in Cleveland, Ohio. *Journal of failure analysis and prevention,* 12**,** 217-236.

RAJANI, B. & MAKAR, J. 2000. A methodology to estimate remaining service life of grey cast iron water mains. *Canadian Journal of Civil Engineering,* 27**,** 1259-1272.

RAJANI, B. & TESFAMARIAM, S. Estimating time to failure of cast-iron water mains. Proceedings of the Institution of Civil Engineers-Water Management, 2007. Thomas Telford Ltd, 83-88.

RAJEEV, P., KODIKARA, J., ROBERT, D., ZEMAN, P. & RAJANI, B. 2014. Factors contributing to large diameter water pipe failure. *Water Asset Management International,* 10**,** 09-14.

RATHNAYAKA, S., KELLER, R., KODIKARA, J. & CHIK, L. 2016a. Numerical Simulation of Pressure Transients in Water Supply Networks as Applicable to Critical Water Pipe Asset Management. *Journal of Water Resources Planning and Management***,** 04016006.

RATHNAYAKA, S., SHANNON, B., RAJEEV, P. & KODIKARA, J. 2015. Monitoring of Pressure Transients in Water Supply Networks. *Water Resources Management***,** 1-15.

RATHNAYAKA, S., SHANNON, B., RAJEEV, P. & KODIKARA, J. 2016b. Monitoring of pressure transients in water supply networks. *Water Resources Management,* 30**,** 471-485.

RATHNAYAKA, S., SHANNON, B., ROBERT, D. & KODIKARA, J. 2017a. Experimental evaluation of bursting capacity of corroded grey cast iron water pipeline. *Structure and Infrastructure Engineering***,** 1-10.

RATHNAYAKA, S., SHANNON, B., ZHANG, C. & KODIKARA, J. 2017b. Introduction of the leak-before-break (LBB) concept for cast iron water pipes on the basis of laboratory experiments. *Urban Water Journal***,** 1-9.

RATHNAYAKA, S. U. P. 2016. *A study of water pressure influence on failure of large diameter water pipelines.* Monash University. Faculty of Engineering. Department of Civil Engineering.

REZAEI, H., RYAN, B. & STOIANOV, I. 2015. Pipe failure analysis and impact of dynamic hydraulic conditions in water supply networks. *Procedia Engineering,* 119**,** 253-262.

ROBERT, D., JIANG, R., RAJEEV, P. & KODIKARA, J. 2016a. Contribution of cement mortar lining to structural capacity of cast iron water mains. *ACI Materials Journal,* 113**,** 295-306.

ROBERT, D., RAJEEV, P., KODIKARA, J. & RAJANI, B. 2016b. Equation to predict maximum pipe stress incorporating internal and external loadings on buried pipes. *Canadian Geotechnical Journal,* 53**,** 1315-1331.

ROMANIV, O., SHUR, E., TKACH, A., SIMIN'KOVICH, V. & KISELEVA, T. 1981. The kinetics and mechanism of fatigue crack growth in iron. *Materials Science,* 17**,** 158-166.

ROMANOFF, M. 1957. *Underground corrosion,* Washington, DC, USA, US Government Printing Office.

ROMANOFF, M. 1964. Exterior corrosion of cast-iron pipe. *Journal (American Water Works Association)***,** 1129-1143.

ROSSUM, J. R. 1969. Prediction of pitting rates in ferrous metals from soil parameters. *Journal (American Water Works Association)***,** 305-310.

SARIN, P., CLEMENT, J. A., SNOEYINK, V. L. & KRIVEN, W. M. 2003. Iron release from corroded, unlined cast-iron pipe. *Journal (American Water Works Association)***,** 85-96.

SCHIJVE, J. 2001. *Fatigue of structures and materials*, Springer.

SCHLICK, W. 1940. Supporting strength of cast iron pipe for gas and water services. *Bulletin,* 146.

SCOTT, R. J. 1990. Water Main Renewal Study: Reticulation Water Mains 1857-1990. *An Asset Management Initiative Framework for the Future 1990.* Melbourne, Australia: Melbourne Water.

SEICA, M. V. & PACKER, J. A. 2004. Mechanical properties and strength of aged cast iron water pipes. *Journal of Materials in Civil Engineering,* 16**,** 69-77.

SHANNON, B., JIANG, R., JI, J., CHAN, D. & KODIKARA, J. 2016a. Investigation of cohort properties for Australian cast iron water mains. *IWA World Water Congress & Exhibition 2016.* Brisbane, Australia IWA.

SHANNON, B., RATHNAYAKA, S., ZHANG, C. & KODIKARA, J. 2016b. LESSONS LEARNT ON PIPE FAILURE MECHANISMS FROM OBSERVATION OF EXHUMED CAST IRON PIPES. *Oz Water* Melbourne, Australia

SHARP, B. 1981. *Water hammer: problems and solutions,* London, UK, E. Arnold.

ST. CLAIR, A. M. & SINHA, S. 2012. State-of-the-technology review on water pipe condition, deterioration and failure rate prediction models! *Urban Water Journal,* 9**,** 85-112.

SWF 2017. An innovative integrated algorithm for cost-effective management of water pipe networks. Melbourne, Australia: Milestone Report 9, Smart Water Fund.

TADA, H., PARIS, P. & IRWIN, G. 2000. *The Analysis of Cracks Handbook*, New York: ASME Press, 3 Sub edition.

TALBOT, A. N. 1926. Strength properties of cast iron pipe made by different processes as found by tests. *Journal (American Water Works Association),* 16**,** 1-44.

TAYLOR, D., HUGHES, M. & ALLEN, D. 1996. Notch fatigue behaviour in cast irons explained using a fracture mechanics approach. *International journal of fatigue,* 18**,** 439-445.

VITANAGE, D. C., KODIKARA, J. & ALLEN, G. 2014. Collaborative research on condition assessment and pipe failure prediction for critical water mains. *Water Asset Management International,* 10**,** 15- 18.

WAKELIN, R. G. & GUMMOW, R. A. 1993. A Summary of the Findings of Recent Watermain Corrosion Studies in Ontario. *Materials Performance Maintenance***,** 159-175.

WEBB, T., GOULD, B. & HARDIE, J. 1978. *Water hammer*, New South Wales University Press.

WEERASINGHE, D., KODIKARA, J. & BUI, H. 2015. Impact of Seasonal Swell/Shrink Behavior of Soil on Buried Water Pipe Failures. *International Conference on Geotechnical Engineering*

WEI, R., ADEANE, J. & HAM, J. Replacement Strategy for Cast Iron Pipes in Western Australia. CEED Seminar Proceedings 2015. 103- 108.

WILKOWSKI, G. 2000. Leak-before-break: What does it really mean? *Journal of pressure vessel technology,* 122**,** 267-272.

WILSON, D., FILION, Y. & MOORE, I. 2017. State-of-the-art review of water pipe failure prediction models and applicability to large-diameter mains. *Urban Water Journal,* 14**,** 173-184.

WILSON, D., MOORE, I. & FILION, Y. 2016. Using sensitivity analysis to identify the critical factors that lower the factor of safety of large-diameter cast iron mains. *Urban Water Journal***,** 1-9.

YAMAMOTO, K., MIZOGUTI, S., YOSHIMITSU, K. & KAWASAKI, J. 1983. Relation Between Graphitic Corrosion and Strength-Degradation of Cast Iron Pipe.(Retroactive Coverage). *Boshoku Gijutsu(Corros. Eng.)*, 32**,** 157-162.

ZHANG, C., RATHNAYAKA, S., SHANNON, B., JI, J. & KODIKARA, J. 2017. Numerical interpretation of pressurized corroded cast iron pipe tests. *International Journal of Mechanical Sciences***,** 116-124.

ZHANG, J. 1997. Designing a cost-effective and reliable pipeline leak-detection system. *Pipes and Pipelines International*, 42**,** 20-26.